



Investigation of the possibility of platinum-group element clusters in magmatic systems, using synthetic sulphide melts

Bianca Kennedy

For submission in accordance with the requirements for the degree Magister Scientiae in the Faculty of Natural and Agricultural Sciences, Department of Geology at the University of the Free State;

28 January 2014

Supervisor: Prof. M. Tredoux, Department of Geology, UFS

Co-supervisor: Prof. G. Steyl, Department of Chemistry, UFS



UNIVERSITEIT
STELLENBOSCH
UNIVERSITY



RHODES UNIVERSITY
Where leaders learn



Declaration

I, Bianca Kennedy, declare that the dissertation hereby handed in for the qualification Magister Scientiae in the Faculty of Natural and Agricultural Sciences, Department of Geology, at the University of the Free State, is my own independent work and that I have not previously submitted the same work for a qualification at / in another University/ faculty. I further more cede copyright of the dissertation in favour of the University of the Free State.

Signed on this day..... the of the month of the year 2014.

.....

Bianca Kennedy

Acknowledgements

I would like to thank my study leader Prof M. Tredoux, Department of Geology, my co-supervisor Prof G. Steyl, Department of Chemistry and the personnel of the Geology department, University of the Free State, for assisting me with everything from lab work, tricky analysis to travel arrangements and financial problems.

The Inkaba Ye Africa Research Fund for providing funding for the project. This is an AEON-IESSS contribution project (nr. 69).

Prof C. Ballhaus and Prof H.M. Helmy, Steinmann Institute for Mineralogy, Geology and Palaeontology, University of Bonn, Germany, for the use of the experimental petrology laboratory, their assistance, patience and hospitality during my stay in Germany.

Prof H.C. Swart, Dr E. Coetzee and Mrs. M. Duvenhage from the NNSC Facility, Department of Physics, University of the Free State, for the run of SAM and TOF-SIMS analysis.

Prof G. Stevens and Mr C. Koegelenberg from the Department of Geology, University of Stellenbosch, for their assistance and the use of the experimental petrology laboratory.

Dr G. Costin and the Geology Department of Rhodes University for the run of WDS-SEM analyses. The use of Jeol JXA 8230 Superprobe, instrument sponsored by NRF/NEP grant 40113 (UID 74464) is kindly acknowledged.

Abstract

The behaviour of platinum-group elements (PGE: Ir, Os, Rh, Ru, Pd and Pt) on a nano level may be the key to the enrichment of PGE in mafic ore bodies, like the Bushveld complex. Temperature controlled sulphide melts were used to investigate possible PGE-rich nano phases or clusters, in a magmatic environment, and the influence these structures may have on PGE enrichment.

The sulphide portion of a natural Cu-Ni-S \pm PGE system was mimicked experimentally. Sulphides are of the first minerals to form in a magmatic system and more likely to carry PGE-clusters. Samples were prepared using the dry powder silica tube technique. The starting powders consisted of a base mixture of an S, Cu and Fe. These were doped with variable concentration of PGE (either Pt or Pd or Ru) and chalcogene ligand (As). The samples were cooled at different rates to monitor the influence of environmental changes (time, chemistry, kinematic- and thermodynamic) on possible cluster formation.

A variety of primary and secondary nano structures (<100nm) were measured in the synthetic samples, using semi-quantitative scanning Auger microscopy (SAM). The size, morphology and composition of the nano entities were a function of the PGE-system (chemistry) and allowed cooling time. The structures formed irrelevant of the PGE concentration. Several of the identified nano structures were re-classified as potential PGE-clusters. These structures fall within the size range of clusters (10-100nm) and were a good indication whether clusters could form.

Although no conclusive clusters were measured evidence from time of flight secondary ion mass spectrometry (TOF-SIMS) analysis supported the notion that the PGE can form PGE-ligand agglomerations of 10-100nm. Scans showed irregular distribution of PGE-ligand ion bundles in compatible and incompatible phases. The PGE-ligand bundles were conclusive evidence that potential clusters can stay preserved in a system with changes in environment.

If this interpretation is correct, it might indicate that a physical enrichment process is at work during the early stages of crystallization in a magmatic environment. However clustering is only one of several mechanisms that may contribute to PGE enrichment of Bushveld-type deposits.

Table of Content

1. Declaration	i
2. Acknowledgements	ii
3. Abstract	iii
4. Table of Content	iv
5. List of Figures	vii
6. List of Tables	xi
7. Abbreviations	xvi
8. Mineral Compositions	xvii
9. Glossary	xviii
10. Chapter 1: Introduction	p 1-17
1.1. Literature study	p 1
1.2. Hypothesis	p 8
1.3. The cluster controversy	p 9
1.4. Outline of project	p 16
11. Chapter 2: Materials and Methods	p 18-27
2.1. Outline of experiments	p 18
2.2. Sample preparation	p 20
2.3. Analytical procedures	p 22
12. Chapter 3: Experimental Set-up	p 28-34
3.1. Kinematics of the experimental system	p 28
3.2. Phase relationships and equilibrium	p 30
3.3. Homogeneity and sample contamination	p 33
13. Chapter 4: Mineralogy	p 35-46
4.1. Phase association	p 35
4.2. Major phases	p 38
4.3. Minor- and PGE phases	p 42
4.4. Nano mineralogy	p 44

4.5. Summary	p 45
14. Chapter 5: Geochemistry	p 47-52
5.1. Sulphur fugacity	p 47
5.2. Metal:sulphur ratio	p 49
5.3. Partitioning coefficients	p 49
5.4. Summary	p 51
15. Chapter 6: Discussion on Nano Structures	p 53-72
6.1. Adapted classification scheme to distinguish between measured nano structures	p 53
6.2. Nano structures: larger than 100nm	p 55
6.3. Nano structures: smaller than 100nm	p 66
16. Chapter 7: Discussion	p 73-91
7.1. PGE-rich and poor nano structures and textures (<100nm) measured in the synthetic sulphide system; formation, distribution and relation to clusters	p 73
7.2. The influence of internal- (kinematic, mineralogical and geochemical) and external (thermodynamic) changes, in the mss host, on cluster formation	p 80
7.3. The physical and chemical behaviour of PGE, in a magmatic sulphide system, as proof of a cluster model	p 87
7.4. How does the PGE cluster model integrate with proposed chalcophile PGE-enrichment models for the Bushveld complex?	p 89
7.5. Summary	p 90
17. Chapter 8: Conclusion	p 92-93
18. References	p 94-08
19. Appendix A: Formulas	p 109-10
20. Appendix B: Data sheets: Experimental Set-up	p 111-15
XRD spectrographs on sample preparation and contamination	

21. Appendix C: Data sheets: Mineralogy	p 120-26
WDS-SEM data on major- and minor phases and related BSE images	
SAM data and related photo images on major phases	
XRD-spectrographs on major- and minor phases	
Size estimations of platinum-group element phases	
22. Appendix D: Data sheets: Geochemistry	p 127-29
Sulphur fugacity (f_{S_2}) calculations	
Measured metal:S ratios	
Calculated D^{PGE} and D^{As} between mss and melt	
23. Appendix E: Data sheets: Discussion on Nano Structures	p 130-50
Size estimation of nano structures	
SAM data and related photo images on nano phases	
TOF-SIMS spectra of ion distribution graphs	
24. Appendix F: Conference Proceedings	p 151-62
25. Appendix G: Articles, in press	p 163-64
26. Appendix H: Extended Summaries	p 163-69
27. Appendix I: Key Terms	p 170

List of Figures

Figure 1.1.:	Platinum-group element (PGE) plots illustrating the classification, chondrite normalised concentrations and partitioning trends of the PGE during melting.	p 4
Figure 1.2.:	The regional setting and simplified geological map of the western limb of the Bushveld complex, showing the layered body of the complex surrounded by the Transvaal group- and various granite suites.	p 10
Figure 1.3.:	The cluster model from Tredoux et al. (1995).	p 16
Figure 2.1.A and B:	Silica charges and epoxy mould with samples. A: Example of sealed evacuated silica charges, with sample powders and Si- and Fe-wool, to be heated. B: The finished sample bits set in an epoxy mould.	p 21
Figure 3.1.:	Change in free energy (ΔG) of the mss system, applicable to fast and slow cooled systems, as the reaction progresses over time (t).	p 29
Figure 4.1.A and B:	The ternary Fe-Cu-S phase diagrams. A: Phase diagram of the Fe-Cu-S system, at 900°C. B: Phase diagram of the Fe-CuS system, at 400°C.	p 37
Figure 4.2.A-D:	Phase association of fast cooled samples from experiment A. A: Po (Fe_{1-x}S) stringers surrounded by an amorphous Fe-melt phase ($\text{Fe}_x\text{Cu}_x\text{S}_x$). B: Cu-rich melt exsolutions trapped in mss (po). C: Backscatter electron (BSE) image of po (dark grey) surrounded by Cu-rich melt. D: BSE of an unpolished sample from experiment A, taken with scanning Auger microscope (SAM).	p 38
Figure 4.3.A-D:	Phase assemblages that formed in the slower cooled samples of experiment A.	p 39

Figure 4.3.A-D: A: Example of the phase associations of the slow cooled samples with po, bn, ccp and Pt-phases (PGM).
 B: Backscatter electron (BSE) image of the slower cooled samples, with po, bn, ccp and Pt-phases (white phase).
 C: BSE image of po with exsolution textures.
 D: BSE image, taken with scanning Auger microscopy (SAM), of unpolished samples from a slow cooled sample.

p 39

Figure 4.4.: The average composition of po, melt, ccp and bn (open figures) and several standards (solid figure) plotted on the ternary Cu-Fe-S phase diagram.

p 41

Figure 4.5.A and B: Pt-rich phases (PGM) present in the fast cooled samples of experiment A.

A: Backscatter electron (BSE) image of PtAs_2 (bright white spots) mineralisation and distribution in the Cu-rich melt.

B: BSE image of a Pt_xFe_x (bright white spot) in melt, measured in the As poor sample A2f.

p 43

Figure 4.6.A-C: The different size, shape and distribution of platinum-group minerals (PGM), measured in the slow cooled samples.

A: Backscatter electron (BSE) image of PtAs_2 crystals on the borders of ccp and bn, sample A1s (300 ppm Pt, 280 ppm As).

B: BSE image of Pt_xFe_x in ccp, sample A2s (300 ppm Pt, no As).

C: BSE image of PtAs_2 crystals in ccp, sample A3s (30 ppm Pt, 30 ppm As).

p 43

Figure 5.1.: Phase stability as a function of temperature and sulphur fugacity.

p 48

Figure 6.1.A-D: Various non-Pt structures, larger than 100nm, measured in the fast cooled samples of experiment A.

A: High relief Cu exsolution (type 2) structures on the mono-sulphide (mss or po) surface.

B: High density, low relief Fe_xS_x exsolutions (type 1) on the mss.

C: Irregular to rounded structures of $\text{Cu}_x\text{Fe}_x\text{S}_x$ phases (<500nm), on the melt surface.

D: Discs of Cu_xS_x crystallised in / on melt phase ($\text{Fe}_x\text{Cu}_x\text{S}_x$).

p 56

Figure 6.2.A and B: Bright phases of non-Pd nano structures, larger than 100nm.
 A: Cu rich structures outcropping on the same less Cu-rich Fe-Cu sulphide phase.
 B: High relief Cu-rich structures on a Fe-Cu sulphide surface.

p 58

Figure 6.3.A-D: Non-Pt nano structures, larger than 100 nm, measured in slow cooled samples of experiment A.
 A: Angular to crystal-like, high relief, Cu-rich Fe-Cu sulphide ($\text{Fe}_x\text{Cu}_x\text{S}_x$) features on a Fe-rich sulphide surface.
 B: Fe-rich needle-like entities scattered on the po (Fe_{1-x}S) surface.
 C: Medium relief Fe-rich Fe_{1-x}S (po) type 3 exsolution structures on po (Fe_{1-x}S).
 D: Mixture of diverse secondary- and primary Fe-S structures outcropping on the po (Fe_{1-x}S) surface.

p 59

Figure 6.4.A and B: Pt-rich nano structures, larger than 100nm, measured in the fast cooled samples of experiment A.
 A: Irregular blobs of Pt-rich Fe-Cu sulphide, type 3 exsolution structures ($\pm 400\text{nm}$) outcropping on the melt surface.
 B: Pt-Cu-rich, type 3 exsolution structures, similar to structures identified in Figure 6.4. A.

p 61

Figure 6.5.A-D: Various Pd-rich nano structures, larger than 100nm, measured in fast cooled samples from experiment B.
 A and B: Pd-Cu-rich structures ($\pm 200\text{nm}$) on Fe-rich Fe-Cu sulphide
 B: Magnification of Pd-rich structures identified in Figure 6.5. A.
 C: Pd-Cu-rich exsolution structures lying on a similar Fe-rich Fe-Cu sulphide.
 D: Inter-grown Pd-rich sulphides.

p 62

Figure 6.6.A-D: Ru-rich nano structures, larger than 100nm.
 A: Primary structures of Ru-rich Fe-Cu-S surrounded by various Ru-rich sulphides.
 B: An inter-grown collection of Ru-rich Fe-Cu-S structures.
 C: Ru-rich Fe-Cu sulphides crystallised in and between the melt.
 D: Ru-rich Cu-S crystal surrounded by Ru-rich Cu-S growths.

p 63

Figure 6.7.:	Pt-rich nano structures, smaller than 100nm, measured in fast cooled samples of experiment A.	p 67
Figure 6.8.A and B:	<p>Pd-rich nano structures, smaller than 100nm, measured in samples of experiment B.</p> <p>A: Pearls of Pd-rich structures, 70-45nm, on Fe-rich melt ($\text{Fe}_x\text{Cu}_x\text{S}$).</p> <p>B: High density Pd-rich nano structures (55nm) on a Fe-rich melt ($\text{Fe}_x\text{Cu}_x\text{S}$) phase.</p>	p 69
Figure 6.9. A-B:	<p>Ru-rich nano structures, ranging from 80-120nm, measured in samples of experiment C</p> <p>A: Crystal-like Ru-rich nano structures (100nm) spread on a Ru-rich Cu_xS_x surface.</p> <p>B: Enlarged image of Figure 6.9.A. The Ru-rich nano structures were clearly visible on the Cu-S surface.</p>	p 70
Figure 7.1.:	The correlation between the concentration of platinum-group element (PGE: Pt, Pd and Ru) added and the distribution of PGE between the mono-sulphide phase (mss or po) and melt.	p 81
Figure 7.2.:	Platinum-group element (PGE) distribution between the mono-sulphide- (mss or po) and melt phase as a function of the starting concentration As added, in the fast cooled samples.	p 82
Figure 7.3.:	Schematic sketch of the surface energy of a metal, with a free valence position or radical, illustrating the potential for physical adsorption.	p 89

List of Tables

Table 1.1.:	The physical and chemical properties of the platinum-group elements (PGE).	p 2
Table 1.2.:	The abundance and enrichment of the platinum-group elements (PGE), in different tectonic settings and Bushveld complex parental type magmas.	p 5
Table 1.3.:	The physical and chemical properties of the elements (S, Fe, Cu and As) that make out the mono-sulphide solid solution (mss) system.	p 7
Table 1.4.:	The abundance and enrichment of S, Fe, Cu and As, in different tectonic settings and Bushveld complex parental type magmas.	p 8
Table 1.5.:	Summary of the various proposed models responsible for the extreme platinum-group element (PGE) enrichment of the S-poor Bushveld complex.	p 12
Table 1.6.:	Comparison between nano entities (nano particles, clusters, colloids and nano crystals), smaller than 100nm.	p 14
Table 2.1.:	Outline of the compound powders used to prepare experiments A, B and C.	p 19
Table 2.2.:	Specifications of the ore microscope used in the study.	p 22
Table 2.3. A:	Detection limits and outlines of scanning electron microscopy (SEM) analysis.	p 23
Table 2.3. B:	The characteristics of standards used in wavelength x-ray spectrometry (WDS-SEM) analysis.	p 23
Table 2.4.:	Detection limits and outlines of x-ray (XRD) analysis, used for semi-quantitative phase identification.	p 24

Table 2.5.:	Detection limit and outlines of scanning auger microprobe (SAM) analysis conducted at the Nation Nano Surface Characterisation Facility (NNSCF).	p 26
Table 2.6.:	Detection limits and outlines of the time of flight secondary ion mass spectrometry (TOF-SIMS) analysis.	p 27
Table 3.1.:	Mole values and concentrations of the elements used to prepare experiments A, B and C.	p 28
Table 3.2.:	Kinematic indicators, of experiment A (Pt-As system), throughout sample preparations.	p 30
Table 3.3.:	The change in free energy (ΔG) during heating of the Fe-Cu-S powders.	p 31
Table 3.4. A:	Thermodynamic and phase transitions during quick quenching (950-25°C).	p 32
Table 3.4. B:	Thermodynamic and phase transitions during slow cooling (900-400°C).	p 32
Table 3.5. A:	Composition of the sample powders during the various preparation stages of the samples.	p 33
Table 3.5. B:	The average size of nano PGE-ligand phases (nm) present during the preparation process.	p 34
Table 4.1.:	Rounded values of starting powder composition (S, Cu and Fe) used for ternary phase diagram plots, see Figure 4.1. (A and B), to determine stable phases present at 900°C and 400°C.	p 35
Table 4.2.:	Chemical and physical properties, characteristics and occurrence of po, bn and ccp minerals, expected to form within the synthetic mss system.	p 37
Table 4.3.:	The average composition of the major phases measured in the samples of experiment A, B and C, as determined with quantitative wavelength dispersive scanning electron microscopy (WDS-SEM).	p 40

Table 4.4.:	The pyrrhotite (po) solid solution series, between 1190°C and 308°C.	p 41
Table 4.5.:	The average composition of po in the various experimental systems (PGE: Pt, Pd, Ru), as determined with semi-quantitative scanning electron microscopy (SEM).	p 42
Table 4.6.:	Characteristics of the Pt-phases (PGM) identified in the samples of experiment A, measured with x-ray (XRD) and scanning electron microscopy (SEM).	p 44
Table 4.7.:	The distribution and size of platinum-group minerals (PGM) measured in the samples of experiment A.	p 44
Table 4.8.:	Summary of the synthetic mono-sulphide solid solution (mss) system.	p 45
Table 5.1.:	Calculated sulphur fugacity (fS_2) of experiment A, B and C and reference sets.	p 48
Table 5.2.:	The average metal:S ratio measured in fast and slow cooled samples, from experiment A, B and C.	p 49
Table 5.3.:	Differentiation values ($D^{PGE}_{mss/melt}$) of the platinum-group elements (Pt, Pd and Ru) and As at 900°C, between mss and melt, taken from various literature sources.	p 50
Table 5.4.:	Summary of the geochemistry of the synthetic mono-sulphide solid solution (mss) system.	p 52
Table 6.1.:	The characteristics of the non-Pt nano structures, larger than 100nm, measured in the fast cooled samples of experiment A.	p 56
Table 6.2.:	The size, shape, classification and distribution of non-Pd nano structures, larger than 100nm, measured on the surface of samples from experiment B.	p 57
Table 6.3.:	Outline of the non-Pt nano structures, larger than 100nm, measured in the slower cooled samples of experiment A.	p 59

Table 6.4.:	The characteristics of Pt-rich nano structures, larger than 100nm, measured in fast cooled samples of experiment A.	p 60
Table 6.5.:	Summary of the Pd-rich nano structures, larger than 100nm, measured in experiment B.	p 61
Table 6.6.:	Outline of the Ru-rich nano structures, larger than 100nm, measured in experiment C.	p 63
Table 6.7.:	The distribution of nano structures, larger than 100nm, measured in the synthetic systems and the phases they occur in.	p 64
Table 6.8.:	Outline of the platinum-group element (PGE) -rich and non-PGE nano structures, larger than a 100nm, measured in samples from experiments A, B and C.	p 65
Table 6.9.:	The size, morphology (shape), classification and distribution of Pt-rich nano structures, smaller than 100nm, measured with scanning Auger microscopy (SAM) in the fast cooled samples of experiment A (Pt-As system).	p 66
Table 6.10.:	Distribution of Pt and Pt-ligand ions between phases in the fast cooled samples of experiment A.	p 68
Table 6.11.:	The size, morphology (shape), classification and distribution of Pd-rich nano structures, smaller than 100nm, measured with scanning Auger microscopy (SAM), in the fast cooled samples of experiment B (Pd-As system).	p 69
Table 6.12.:	The size, morphology (shape), classification and distribution of Ru-rich nano structures, smaller than 100nm, measured with scanning Auger microscopy (SAM), in the fast cooled samples of experiment C (Ru-As system).	p 70
Table 6.13.:	Distribution of Pt and Pt-ligand ions between phases in the slow cooled samples of experiment A.	p 71
Table 6.14.:	Summary of the measured platinum-group element (PGE) -rich nano structures, smaller than 100nm, in experiment A, B and C.	p 72

Table 7.1.:	Summary of measured nano structures.	p 75
Table 7.2.:	Parameters, adapted from various literature sources, used to classify a platinum-group element (PGE) -rich nano phase as a possible PGE cluster.	p 76
Table 7.3.:	Classification of platinum-group element (PGE) -rich nano structures (smaller than 100nm) as possible PGE clusters.	p 77
Table 7.4.:	Comparison of the micro-nugget models with the cluster model.	p 78
Table 7.5.:	Distribution of Pt and Pt-ligand ions between phases in the samples of experiment A as possible evidence of cluster formation.	p 79
Table 7.6.:	The thermodynamic properties of Bushveld complex melt system compared to the synthetic mono-sulphide solid solution (mss) system.	p 84
Table 7.7.:	Comparison of platinum-group element (PGE) phases and minerals between the different temperature windows (fast or slow cooled), to deduce the influence of thermodynamic conditions on cluster formation.	p 86
Table 7.8.:	Approximation of the ideal conditions under which nano phases, smaller than 100nm (possible clusters), are more likely to form.	p 86
Table 7.9.:	Hybridization and coordination numbers (C-nr) of S, Fe, Cu, As and the platinum-group elements (PGE: Pt, Pd and Ru) that make out the experimental sulphide melts.	p 88

Abbreviations

(aq):	aqueous solution	SEM:	scanning electron
b.d.l.:	below detection limit		microscope
BMS:	base metal sulphides	sm:	sulphide melt
BSE:	backscatter electron	temp.:	temperature
EDS:	energy dispersive x-ray detector spectrometer (SEM)	TOF-SIMS:	time of flight secondary ion mass spectrometry
f:	fast or quick quench	WDS:	wavelength dispersive x- ray spectrometer (SEM)
<i>f</i>S₂:	sulphur fugacity	XRD:	X-ray spectrometry
<i>f</i>O₂:	oxygen fugacity		
HCl:	hydrochloric acid		
HNO₃:	nitric acid		
H₂SO₄:	sulphuric acid		
iss:	intermediate solid solution		
(l):	liquid		
mss:	mono-sulphide solid solution		
n.d.:	not determined		
PGE:	platinum-group element (Pt, Pd, Ru, Rh, Os, Ir)		
PGM:	platinum-group mineral		
s:	slow cooled		
(s):	solid		
SAM:	scanning Auger microscope		

Mineral Compositions

Mineral abbreviations according to IUGS system

Yund and Kullerud (1966), Kretz (1983), Fleet (2006), Whitney and Evans (2010)

*No abbreviation available, authors' own abbreviation

apy:	arsenopyrite	FeAsS	mag:	magnetite	FeO
ars*:	arsenolite	As ₂ O ₃	mlc:	malachite	Cu ₂ CO ₃ ·(OH) ₂
az*:	azurite	Cu ₃ (CO ₃) ₂ (OH) ₂	mo:	molybdenite	MoS ₂
bn:	bornite	Cu ₅ FeS ₄	mrc:	marcasite	FeS ₂
brg*:	braggite	(Pt, Pd, Ni)S	mss:	mono-sulphide solid solution	
brt:	barite	BaSO ₄	ol:	olivine	(Fe, Mg) ₂ SiO ₄
cal:	calcite	CaCO ₃	orp:	orpiment	As ₂ O ₃
cb:	cubanite	CuFe ₂ S ₃	opx:	orthopyroxene	(X,Y) ₂ Si ₂ O ₆
ccp/ cp:	chalcocopyrite	CuFeS ₂	PGM:	platinum-group minerals	
cct/cc:	chalcocite	Cu ₂ S	pn:	pentlandite	FeNiS
chr:	chromite	CrO ₂	po:	pyrrhotite	Fe _{1-x} S
cin:	cinnabar	HgS	py:	pyrite	FeS ₂
coo*:	cooperite	(Pt, Pd, Ni)S	qtz:	quartz	SiO ₂
cov:	covelite	CuS	rlg:	realgar	As ₄ S ₄
dig*:	diginite	Cu ₉ S ₅	ttr:	tetrahedrite	Cu ₂ Sb ₄ S ₁₃
dol:	dolomite	CaMgCO ₃	tr*:	triolite	FeS
gn:	galena	PdS	sp:	sphalerite	ZnS
gp:	gypsum	CaSO ₄ ·2H ₂ O	sr*:	sperrylite	PtAs ₂
hem:	hematite	Fe ₂ O ₃	wo:	wollastonite	CaSiO ₃
id:	idaite	Cu ₃ FeS ₄			
ifp*:	isoferroplatinum	Pt ₃ Fe			
iss:	chalcopyrite derivative phases				

Glossary

Definitions adapted from: Hartley (1991), Cotton (1995, 1997), Keary (2001), Waychunas (2001), Eby (2004), Calas et al. (2006), Dingwell (2006) and Brown et al. (2009)

Adsorption: The physical bonding of molecules to a surface. Not a chemical process.

Atomic radius: The approximate size of a single atom. The atomic radius increases with an increase of electron shells.

Chemisorption: A chemical reaction between a molecule and metal surface.

Colloids: Special state of matter. The sub-microscopical particles (1-1000nm) have at least one direction in one dimension. The colloidal mixture is intermediate between a homogenous and heterogeneous mixture. The particles, molecules or poly-molecular phases are evenly dispersed throughout a substances (liquid, solid or gas) and are not easily settled or filtered out.

Differentiation values: Measures an elements' affinity for a certain phase against another phase. $D_{xy}^A = >1$ or <1 . For $D > 1$, element A is more compatible with phase x, and vice versa.

Electronegativity (Pauling): A measure of the capability of an atom, in a molecule, to attract electrons to itself. The greater the electronegativity of the atom, the greater is the possibility of attracting an electron.

Enthalpy (ΔH): A thermodynamic function that measures the change in heat energy (evolved or absorbed) in a system at constant pressure. The change in enthalpy is given as: $H=E + PV$. (E= heat energy, P= pressure, V= volume).

Entropy (ΔS): Statistical measurement of the disorder or randomness within a thermodynamic system (second law of thermodynamics).

Gibbs free energy: Thermodynamic state function that predicts the change in free energy, in a system with constant temperature and pressure. The Gibbs equation: $G=H-TS$. (H=enthalpy; T=temperature and S=entropy)

Ligand: A molecule or anion that may act as a stabilizing agent to form a complex with a metal ion or metal atom.

Magma: Multiphase, naturally occurring, high temperature melt bearing geo-material. Magma consists of a mixture of liquid (melts and fluids), solid (one or more populations of crystals and agglomerations of these) and gas (dissolved gasses, bubbles and vesicles) phases. A magma can have more than one melt phase.

Melt: A molten liquid material found in magma. It can either be in a liquid or glass state.

Metalloid: Element with chemical and physical properties intermediate between metals and non-metals. Metalloids comprise of B, Si, Ge, As, Sb, Te, Po and \pm As.

Miscible: Liquids that mix completely with one another.

Nano-crystals: Single crystals that exhibit crystalline properties and formed either from solution or due to weathering or a clay mineral. The crystals can be up to 100nm in size.

Phase: A homogenous, structurally and physically distinct entity. A phase can be either a solid (chemically and physically different), liquid (miscibility series) or gas (1 phase system).

Sigma (σ) bonds: The overlapping of s or p orbitals to form a chemical covalent bond. Orbital overlapping can be between s + s or s + p or $p_z + p_z$ or $d_z^2 + d_z^2$ orbitals. Sigma bonds occur in 1) homo-diatoms (rare) 2) diatomic molecules (typically) 3) poly-atomic compounds 4) multiple-bonded species and 5) organic molecules. If the bonding is due to p or d-orbital overlap the bond is called a pi-bond (π).

Solid solution: Elements with similar charge and size (solute) may continuously replace each other during crystallization, in a crystal structure, to form a solid solution in a phase (matrix or solvent). Solubility can either be interstitial (solute sits in interstitial sites) or substitution (solute occupies lattice spaces of solvent). Solubility can further be divided into unlimited and limited or partial solubility.

Valence electrons: Unpaired electrons found in the outermost energy fields of the atom. The empty bond orbitals overlap or is shared in chemical bonding.

Chapter 1: Introduction

The origin and genesis of the vastly platinum-group element (PGE: Ru, Rh, Pd, Os, Ir and Pt) enriched Bushveld complex, remains a controversy among authors. Most models, based on chalcophile principles (or R-model) (Campbell and Naldrett, 1979; Naldrett et al., 1987; Godel et al., 2007), cannot fully explain the over enrichment of PGM and Cr within the relatively small magma budget (Cawthorn and Walraven, 1998) of the Bushveld complex.

The Bushveld- and Stillwater complexes, although very similar to other ortho-magmatic Fe-Ni-Cu deposits like the Noril'sk, Sudbury and Great Dyke (Evans, 1993), in genesis and sulphide enrichment mechanism (S scavenged the PGE out of the silicate melt) (Naldrett et al., 1986; Barnes and Lightfoot, 2005), contains much higher platinum-group mineral (PGM) concentrations than can be predicted by chalcophile models. Pure chemical models or enrichment due to phase compatibility and secondary fluid enrichment, cannot explain the large reserves of magmatic ore bodies such as the Bushveld complex.

Alternative theories, like the cluster model (Tredoux et al., 1995) based on the physico-chemical properties of the PGE, is being incorporate with traditional models as explanation for the extreme PGE enrichment factors. The dissertation presents data on how the Bushveld complex melts could have become enriched in PGE, before early magmatic differentiation, by means of PGE clusters.

1.1. Literature study

1.1.1. The chemistry and physical character of the PGE

The PGE show overall similar chemical and physical properties for example high density, brittle, extreme melting and boiling points, chemical inertness, low coefficient of thermal-expansion and conductivity, high electrical conductivity and the ability to catalyze chemical reactions. The PGE are classified as noble metals due to their extremely high sublimation energies and high ionization potentials (Hartley, 1991). Different valence states and the available valence electrons for bonding contribute to their vastly different physical properties (Bond, 1991).

The PGE metals are soft, dense, malleable and do not oxidise easily (Hartley, 1991). Ease of oxygen attack can be expressed as Os < Ru < Ir < Rh < Pd < Pt. The PGE are generally found together and are closely associated or often found with Au and Ag ores (similar chemical and physical properties) and other base metals including Ag, Ni, Cu, Co and Fe. Pt, Pd and Ru were chosen as analogue to the PGE in the study. Their differences in physical, chemical and geochemical behaviour served as a comparison or control as to what factors control or influences PGE cluster formation. The physical and chemical properties of the PGE are summarised in Table 1.1.

Table 1.1.: The physical and chemical properties of the platinum-group elements (PGE). Pt and Pd is physically and chemically the most similar of the PGE. However Ru differs considerably from the Pd and Pt. Ru served as a comparison for what factors (physical or chemical) might influence cluster formation. Data was taken from Evans (1966) as cited in Barnes and Maier (1999), Hartley (1991), Cotton (1997), Halliday (2008), Lide (2008) and Brown et al. (2009).

PGE	Ru	Rh	Pd	Os	Ir	Pt
Atomic weight	101.07 g.mol ⁻¹	102.91 g.mol ⁻¹	106.40 g.mol ⁻¹	190.20 g.mol ⁻¹	192.22 g.mol ⁻¹	195.09 g.mol ⁻¹
Atomic number	44	45	46	76	77	78
Group	VIII transition metal	VIII transition metal	VIII transition metal	VIII transition metal	VIII transition metal	VIII transition metal
Packing	hexagonal	face centred	face centred	hexagonal	face centred	face centred
Atomic radius	0.133nm	0.134nm	0.138nm	0.134nm	0.136nm	0.139nm
Metallic radius	1.33 Å	1.34	1.37	1.35	1.35	1.38
Atomic volume	8.3 cm ³ /mol	8.3 cm ³ /mol	8.9 cm ³ /mol	8.9 cm ³ /mol	8.54 cm ³ /mol	9.10 cm ³ /mol
Valence states	0, II, III, (IV), (VI)	0, II, III, IV, (VI)	0,II, (III), IV	0, II, III, IV, (VI)	0, II, III, IV, (VI)	0, II, (III), IV, (VI)
Electronic configuration	(Kr)4f ⁰ 4d ⁷ 5s ¹	(Kr)4f ⁰ 4d ⁸ 5s ¹	(Kr)4f ⁰ 4d ¹⁰ 5s ⁰	(Xe)4f ¹⁴ 5d ⁶ 6s ²	(Xe)4f ¹⁴ 5d ⁷ 6s ²	(Xe)4f ¹⁴ 5d ⁹ 6s ¹
Electron negativity	2.20	2.20	2.20	2.20	2.20	2.28
Density 20°C	12.37 g.cm ⁻³	12.41 g.cm ⁻³	12.02 g.cm ⁻³	22.57 g.cm ⁻³	22.50 g.cm ⁻³	21.45 g.cm ⁻³
Melting point	2250°C	1963°C	1552°C	3027°C	2447°C	1769°C

1.1.1.1. The chemistry and physical character of platinum

Pt is a soft, lustrous, high density (21.45 kg.cm⁻³) and heavy precious metal. Pt is less susceptible to problems like stress corrosion or stress cracking than other PGE (Cotton, 1997). Pt is resistant to wear, tarnish and high temperatures, strong acids and does not

oxidise easily but can be corroded by halogens, cyanides, sulphides and alkali metals. The major use or application of Pt is as catalyst (nitric acid, fertilizers, synthetic fibres, and other materials), medical applications and medicines (anti-cancer drugs) (Brenan, 2008). The oxidation states of Pt are +2 and +4 and less commonly +1 and +3. Pt has 37 known isotopes, six of which are naturally occurring (^{190}Pt , ^{192}Pt , ^{194}Pt , ^{195}Pt , ^{196}Pt , and ^{198}Pt) (Cotton, 1997). The most abundant isotope is ^{195}Pt , comprising of 33.83% of all Pt. Of the naturally occurring isotopes only ^{190}Pt (0.1 % abundance) is unstable with a half-life of 6.5×10^{11} years. The atoms are arranged in closely packed hexagonal layers to form a face centred cubic pattern or cubic close packing crystal systems.

1.1.1.2. The chemistry and physical character of palladium

Pd is a ductile and malleable precious metal (Melber et al., 2002). It resembles Pt more closely in both physical and chemical properties (Cotton, 1997) than any of the other PGE. It is resistant to oxidation and attack from most reactants, except in nitric acid (HNO_3), sulphuric acid (H_2SO_4), hydrochloric acid (HCl) and aqua regia (Melber et al., 2002). Pd easily forms coordination complexes (mainly exhibits a square planar form) and organic bonds; that make it an excellent catalyst (Melber et al., 2002). The metal exists primarily in three oxidation states namely Pd^0 (metallic), Pd^{+2} (general oxidation state) and Pd^{+4} (Melber et al., 2002). Pd has six stable natural occurring isotopes and 18 radio-isotopes. Pd is mainly used in electronics, dentistry, auto-catalysts, jewellery, medicine and investment (Hartley, 1991).

1.1.1.3. The chemistry and physical character of ruthenium

Brittle, hard, lustrous and very rare Ru was the last of the PGE to be identified (Cotton, 1997). Ru can exist in various oxidation states of up to +8 (Cotton, 1997). The PGE metal is mostly found in the +2, +3 and +4 states. Ru^{102} (31.6%) is the most abundant isotope of the 26 known Ru isotopes. The metal does not easily react with acids, air or water and is generally insoluble, except in potassium chlorate rich aqua regia (Hartley, 1991). The reaction causes Ru to oxidise explosively. Ruthenium is predominately used as hardener for Pt and Pd, in electronics and electrochemical applications (Hartley, 1991).

1.1.2. The geochemistry of the PGE

The PGE are highly siderophile elements (affinity for Fe) and will therefore rather form metallic bonds than ionic bonds. They also display chalcophile behaviour (affinity for S) to form covalent bonds with S instead of ionized bonds with O (Mungall, 2005), based on Goldsmith classification of 1923 (Rösler and Lange, 1972). PGE have a strong affinity for sulphides (S^{2-}) (Ballhaus et al., 2006) and form native-, chalcosulphides or sulphide bonds (Rösler and Lange, 1972). The PGE can be divided according to their behaviour during magmatic processes or compatibility behaviour. Pt, Pd and Rh are known as PPGE (Pt group platinum metals) and is associated with the restite melt. Os, Ir, Ru or the IPGE (Ir group platinum metals) prefers to segregate into the partial melt, see Figure 1.1.

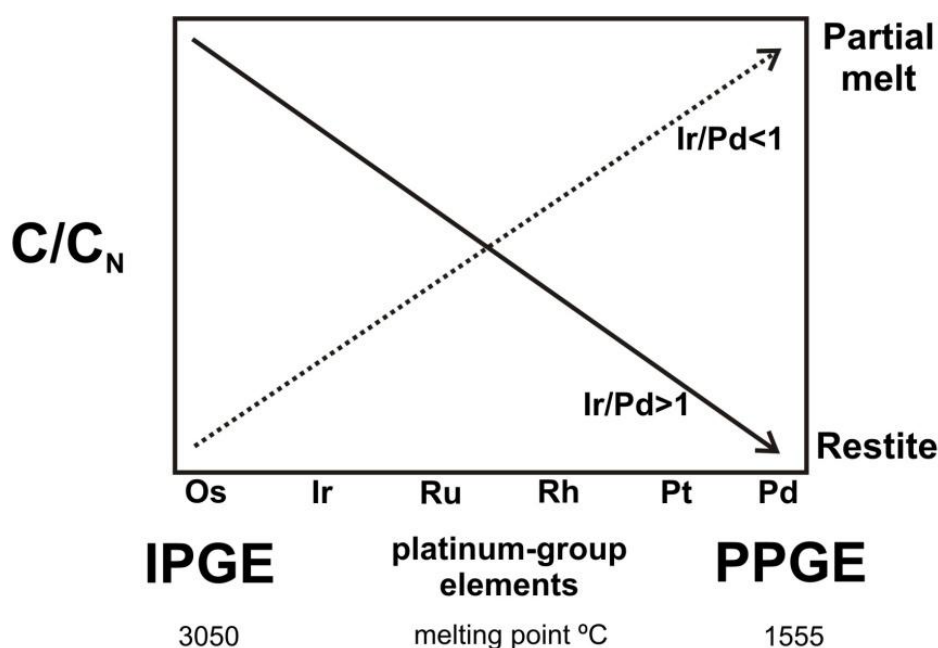


Figure 1.1.: Platinum-group element (PGE) plots illustrating the classification, chondrite normalised concentrations and partitioning trends of the PGE during melting. The Ir-group PGE (Os, Ir, Ru) tends to concentrate in the partial melt, while Pt-group PGE (Pt, Pd, Rh) segregates into the restite. Figure 1.1. was adapted from Lorand et al. (2008).

The PGE are assumed to be enriched in the crust in two main tectonic settings and environments (Von Grunewaldt, 1987 as cited in Viljoen and Schurmann, 1998). In 1) ultra-mafic to basaltic magmas, which intrude or are extruded on the surface. The magmas are from a mantle origin and 2) ophiolite complexes associated with slabs of upper mantle material. The PGE serve as outstanding tracers of mantle melt processes due to their different melting points (1555°C Pd to 3050°C Os) and fractionation character or bulk partitioning coefficient during melting. The geochemical abundance and enrichment trends of the PGE are listed in Table 1.2.

Table 1.2.: The abundance and enrichment of the platinum-group elements (PGE), in different tectonic settings and Bushveld complex parental type magmas. Values are given in parts per billion (ppb). Data was adapted from Crocket (1981), Davies and Tredoux (1985) as cited in Barnes and Maier (1999), McDonough (2003), Rudnick (2003), Mungall (2005) and Palme (2008).

PGE	Ru	Rh	Pd	Os	Ir	Pt
Silicate earth	5.0	1.0	4.0	3.0	3.0	7.0
Bulk continental crust	0.600	-	1.500	0.041	0.037	1.500
MORB	-	-	0.265	0.021	0.009	0.304
Average komatiite	4.4	1.4	10.5	1.5	1.7	10.5
Primitive mantle	4.55	0.93	3.27	3.4	3.2	6.6
CI chondrite	683	140	556	506	480	982
Bulk earth	1300	2400	1000	900	900	1900
Earth's core	4000	740	3100	2.800	2.600	5.700
PGE initial Bushveld complex magma	1.6	-	-	0.20	0.20	-
Avg. B1 Bushveld complex magma	3.0	1.7	2.9	0.4	0.33	16.0
Avg. B2 Bushveld complex magma	1.50	0.54	2.40	0.00	0.13	11.20

The average concentration of PGE in the bulk silicate earth is 1-7 ppb (Mungall, 2005). The PGE concentration of a high grade PGE ore deposit varies between 1000x to 10 000x the concentration of bulk silicate earth. The conventional mineable cut-off grade is about 2 ppm PGE (Mungall, 2005).

1.1.3. The mineralogy of the PGE

The PGE are found in more than 109 minerals (Cabri, 2002) including Ni-Cu sulphides, PGE sulphides, tellurides, antimonides and arsenides. Native Pt occurs naturally as a solid solution compound consisting of Pt, Ir, Rh, Pd, Fe and Ni (Wenk and Bulakh, 2006). They are found in high concentrations as seen in the Bushveld complex (Merensky reef and UG2), Stillwater complex, Sudbury complex, Great dyke and Penikat complexes (AP-PV reefs).

The PGE are associated with minerals like py, pn, po, ccp and bn. PGM are found as intergrowths between various base metal sulphides (BMS) (95-97 vol%), in the triple point contacts between S-, Si- and oxide phases (Godel et al., 2010). Trace quantities of PGE (Ir, Ru, Rh) can be present in oxide and silicate minerals (Lorand et al., 2008; Brennan, 2008).

About 0.7 % of PGE ore is naturally found as totally entrapped PGM in sulphides (Godel et al., 2010).

1.1.4. The chemistry and geochemistry of the mono-sulphide solid solution system

The physical, chemical and geochemical properties of the elements (S, Fe, Cu, and As) of the synthetic mono-sulphide solution system (mss) are listed in Table 1.3. and Table 1.4.

1.1.4.1. Sulphur

S is found almost everywhere from the oceans to the core (Mandeville, 2010). The nearly odourless and tasteless S prefers to form rings or chains of covalent S-S-S bonds (Brown et al., 2009), giving way to the characteristic S₈ or rhombic sulphur. S occurs as several valence states (S^{-6} up to S^{+2}) (Mandeville, 2010) enabling the element to partake in numerous organic and inorganic reactions. S has 4 natural occurring isotopes S^{32} (95.02%), S^{33} , S^{34} and S^{36} (Mandeville, 2010). It is found in a varied array of complexes, minerals and deposits as native element, sulphides, metal sulphides (py, po), sulfosalts (ttr) and sulphates (gp and brt). The majority of sulphides in nature tend to occur as metallic sulphides forming important ore minerals like cin, sp, mo and gn (Wenk and Bulakh, 2004; Mandeville, 2010). The non-metal is an important industrial and chemical commodity. It is used in the rubber industry, pulp and paper processing, fertilizer, pesticides, H_2SO_4 acid and various chemicals (Brown et al., 2009; Mandeville, 2010).

1.4.1.2. Iron

As the 4th most abundant element (4.7%) (Brown et al., 2009) in the earth's crust, Fe is an essential building block of life and industry. It is dense, malleable, ductile and ferromagnetic. The transition group metal readily forms metal and ionic bonds (Brown et al., 2009). The main oxidation states of Fe are: ferrous (Fe^{2+}) and ferric iron (Fe^{3+}) (Brown et al., 2009). Under anaerobic conditions Fe can act as an electron donor and acceptor but under aerobic conditions the element is primarily an electron donor (Coplen et al., 2002). Fe has 14 known isotopes of which 4 stable isotopes (^{54}Fe , ^{56}Fe , ^{57}Fe (91.754%) and ^{58}Fe). The metal occurs in an array of deposits and environments as primary and secondary minerals. Common minerals of Fe include py, po, hem and mag. The metal is predominately used in alloys and iron ore.

Table 1.3.: The physical and chemical properties of the elements (S, Fe, Cu and As) that make out the mono-sulphide solid solution (mss) system. Data adapted from and Evans (1966) as cited in Barnes and Maier (1999), O'Day (2006), Vauhgan (2006), Halliday (2008), Lide (2008) and Brown et al. (2009).

Parameter	S	Fe	Cu	As ^{4,5}
Atomic weight	32.065 g/mol	55.845 g/mol	63.546 g/mol	74.922 g/mol
Atomic number	16	26	29	33
Group	non-metal chalcogene	VIII transition metal	VIII transition metal	metalloid
Packing	cubic	body centre	face centre	cubic
Bonding atomic radius	1.02Å	1.25Å	1.38Å	1.19Å
Atomic radius	1.04Å	1.72Å	1.21Å	1.19Å
Metallic radius	1.09Å	1.23Å	1.28Å	-
Atomic volume	15.50 cm ³ /mol	7.10 cm ³ /mol	7.10 cm ³ /mol	12.97 cm ³ /mol
Valence states	+6,5,4,3,2,1,-1,-2	+2, +3	+2, +1	+5,3,0,-1, -3
Electronic configuration	(Ne)3s ² 3p ⁴	(Ar)3d ⁶ 4s ²	(Ar)3d ¹⁰ 4s ¹	(Ar)3d ¹⁰ 4s ² 4p ³
Electron negativity	2.58	1.83	1.95	2.18
Density, 20°C	2.07 g.cm ³	9.90 g.cm ³	8.90 g.cm ³	5.78 g.cm ³
Melting point	115.21°C	1537.00°C	1084.62°C	817.00°C

1.4.1.3. Copper

With the highest heat and electrical conductivity, of all the elements (Brown et al., 2009), Cu is an essential trace metal (Callender, 2003). The malleable and ductile element readily forms organic compounds, metallic bonds and solid solutions. The behaviour of Cu in a geochemical or biological system is dependent on its oxidation state (Callender, 2003). The two primary oxidation states are cuprous (Cu⁺¹) and cupric (Cu⁺²) (Brown et al., 2009). Under alkaline conditions Cu is more insoluble than under acidic conditions (Garrels and Christ, 1965 as cited in Callender, 2003). Cu solubility also greatly decreases under more reducing conditions (Leckie and Nelson, 1975 as cited in Callender, 2003).

Cu has two stable isotopes namely ⁶³Cu (69.2%) and the less abundant ⁶⁵Cu (30.8%) (Coplen et al., 2002; Callender, 2003). Cu is found in an assortment of primary and secondary minerals including native Cu, sulphides (cc, cov, ccp), carbonates (mlc, az) and sulfo-salts (CuSO₄) (Callender, 2003; Wenk and Bulakh, 2006). Cu is predominantly used in alloys, hardware items, electrics and for coinage (Brown et al., 2009).

1.4.1.4. Arsenic

As governs its behaviour by readily changing electron configuration and oxidation states (electropositive to electronegative) (O'Day, 2006). This enables the element to change its reactivity, behaviour and toxicity. The partially filled valence orbitals and excess electrons allow both electron donation (5 valence electrons for chemical bonding) and electron uptake (empty p orbitals). As has a strong affinity for O and S, forming various minerals and aqueous species, including *ars*, *rlg*, and *orp* (O'Day, 2006; Wenk and Bulakh, 2006). As readily forms covalent bonds, acting as an anion (As) or di-anion (As₂) (band gap formation, Patrick and Lutz, 1999 as cited in O'Day, 2006) to form alloys with metals such as Fe, Cu, Co, Ni or Ge (O'Day, 2006). As is found as solid solution in minerals like *py*, *mrc*, *po* and *gn*. The non-metal is used in electronics, alloys, medicine and pesticides (Vaughan, 2006).

Table 1.4.: The abundance and enrichment of S, Fe, Cu and As, in different tectonic settings and Bushveld complex parental type magmas. Values are given in ppm unless otherwise stated. Data was adapted from Barnes and Maier (2002), McDonough (2003), Palme and O'Neil (2003), Rudnick and Gao (2003) and Mungall (2005).

Tectonic setting	S	Fe	Cu	As
Silicate earth	250.00	6.26%	30.00	0.05
Bulk continental crust	404.0	6.7%	27.0	2.5
MORB	-	-	61	-
Average komatiite	-	-	64	-
Primitive mantle	200.000	6.300%	20.000	0.066
CI chondrite	54,100	18.43%	131	1.81
Bulk earth	6350.0	32.0%	60	1.7
Earth's core	1.90%	85.50%	125	5.00
Avg. B1 Bushveld complex magma	800	FeO: 9.15wt.%	58	1.1
Avg. B2 Bushveld complex magma	400	FeO: 11.61wt.%	62	<0.5

1.2. Hypothesis

Is it possible for PGE to form PGE-ligand clusters (<100nm) in a magmatic system and if so what role do these entities play in the ore enrichment process? Can clusters be responsible for enrichment of PGE in highly incompatible phases?

The enrichment of PGE in mafic ore-deposits is about 10 000 times higher than average continental crust (Mungall and Naldrett, 2008). The highly PGE enriched reserves of the S-poor Bushveld complex are higher than can be obtained from sulphide-platinum modelling (Campbell and Naldrett, 1979). Most geochemical models fail to explain the primary metal (PGE) concentration mechanism. Alternative models, like the cluster model Tredoux et al., 1995) are being incorporated with conventional models, as explanation for the extreme PGE factors in these deposits.

Deep seated mantle derived magmas, like the Bushveld complex (Rajamani and Naldrett, 1978; Francis, 1990; Barnes and Lightfoot, 2005), are dynamic, high energy, high pressure-temperature systems. Elements have elevated potential and kinetic energy. The high energy and super charged PGE may be able to bond mechanically or physico-chemically (adsorb) to ligands (As, Fe and Cu) to form stable clusters or nano phases. The clusters are semi-stable and can latch onto traditionally incompatible phases such as sulphides, silicate and oxides, causing enrichment.

The possibility of PGE clusters and their influence on ore enrichment within a magmatic system was tested. PGE nano phase smaller than 100nm measured in the incompatible mss phase of the prepared synthetic sulphide samples will inevitably prove the theory.

The paper focused on:

1. PGE-rich and poor nano structures and textures (<1000nm), measured in the synthetic systems; their formation, distribution and relation to PGE clusters.
2. The influence of internal- (kinematic, mineralogical and geochemical) and external (thermodynamic) changes, in the mss host, on cluster formation. Is there an optimum “window” or set conditions under which clusters are more likely to form?
3. The physical and chemical behaviour of PGE in a magmatic sulphide system, as proof of a possible cluster model.
4. How does the PGE cluster model integrate with chalcophile PGE-enrichment models for the Bushveld complex?

1.3. The cluster controversy

Nano technology is enabling geo-scientists to measure, track and image phase transitions on a nano-scale in natural systems. Nano phases have long been speculated to play a significant role in PGE enrichment in deposits such as the Bushveld complex.

Old models and conventional theories

Covering an area of 65000km² the Proterozoic S-poor Bushveld complex is the biggest layered mafic intrusion in the world (Cawthorn et al., 2006), see Figure 1.2. The Bushveld complex hosts an estimate of 80% of the world's PGE reserves, 75% of the world's Cr and almost 46% of the known V reserves. The Bushveld complex is also highly enriched in Cu, Co and Ni (Robb, 2005).

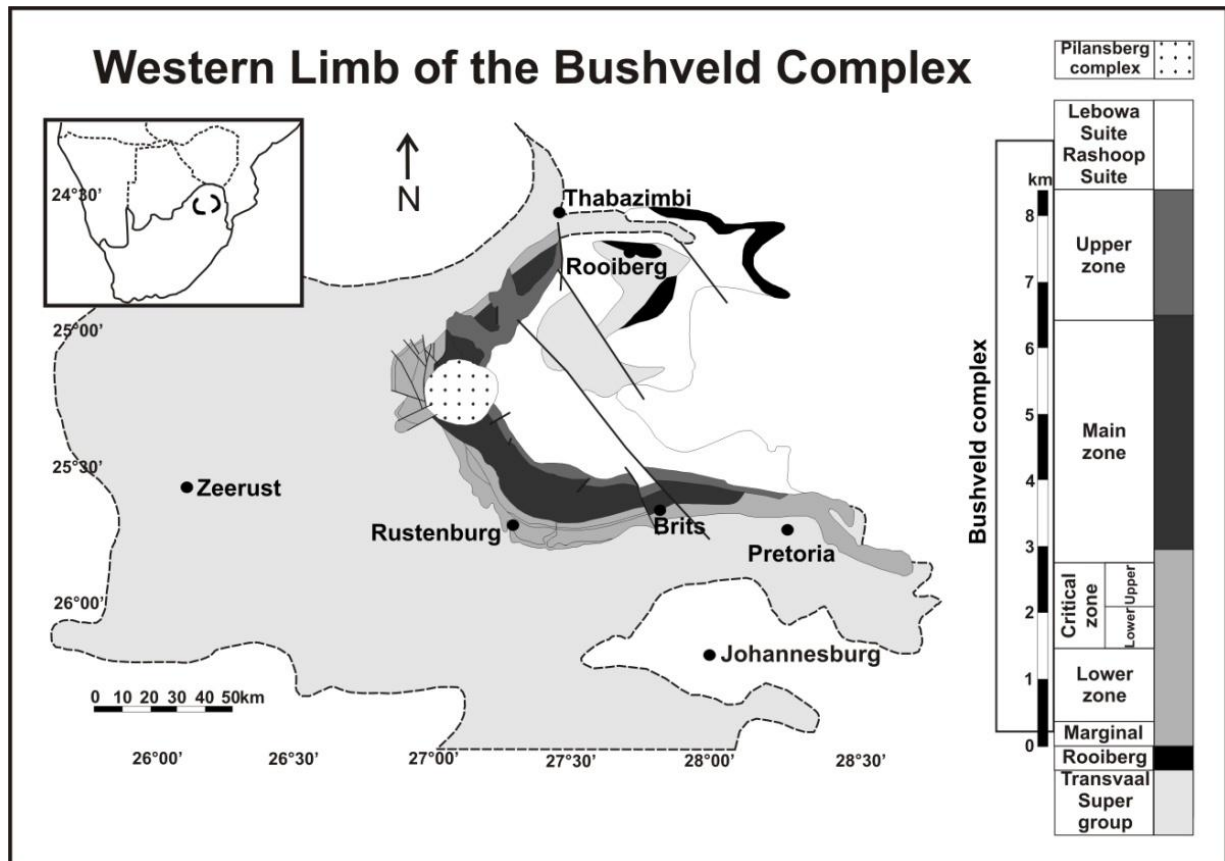


Figure 1.2.: The regional setting and simplified geological map of the western limb of the Bushveld complex, showing the layered body of the complex surrounded by the Transvaal group- and various granite suites. The Merensky- and UG2 reefs lie in the Upper critical zone. Figure was adapted from Viljoen and Schurmann (1998), Cawthorn et al. (2006), Eales and Cawthorn (1996) cited in Godel et al. (2007).

Several parental magmas have been calculated for the Bushveld complex. The parental magmas range from picritic, primitive tholeiitic basalt, a fertile mantle source (Rajamani and Naldrett 1978; Francis, 1990), a partial melt from a metasomatised sub-continental lithosphere source (Hamlyn and Keys, 1986), boninite melt (Hatton and Sharp, 1988) to crustal contaminated komatiite (Maier et al., 2000).

The parental source magmas fed into three smaller magma chambers forming the northern, eastern and western segments of the Bushveld complex (Cawthorn et al., 2006). The PGE are enriched in the chromite layers (UG, MG, and LG series), dunite pipes, Merensky- and Plat reef, see Figure 1.3. Each unit has a distinct mineralogy, enrichment and formation characteristics.

A pure chemical magma crystallisation model is used to explain the layered body of the Bushveld complex, see Figure 1.3. The model explains the layering effect of the body, due to cooling, but lack to explain the phases and enrichments within the units. The mineralisation of the Bushveld complex is believed to have been due to partial melting, crystal fractionation (the so-called Irvine model), filter pressing, liquid immiscibility, sulphide solubility (Robb, 2005).

The R-model (Campbell and Naldrett, 1979) is the leading model for enrichment of PGE in the Bushveld complex. The model is based on the chalcophile association of the PGE with S. Small amounts of sulphide magma scavenge trace elements and PGE from the very large quantity of silicate magma (Campbell and Naldrett, 1979). The PGE enriched immiscible sulphide melt globules interact with the silica magma to cause enrichment.

The concentration of trace elements in the sulphide fraction (C_{sulphide}) can be mathematically expressed as (Campbell and Naldrett, 1979):

$$C_{\text{sulphide}} = \frac{CoD(R + 1)}{(R + D)}$$

Co= original trace element concentration in host magma

R= mass ratio of silicate magma to sulphide melt, D= sulphide-silicate partitioning coefficient

The mineralisation and high enrichment of the Bushveld complex ores were probably due to repeated magma injections or pulses of different composition magmas into the chamber (Cawthorn et al., 2006). The repeated injections caused turbulence in the chamber forcing magma mixing and contamination, remineralisation and mobilization of elements and immiscible phases to form.

The ore forming processes described cannot fully explain the extreme metal concentrations of the Merensky- and UG2 reefs, from a limited magma budget (Cawthorn and Walraven, 1999). The PGE xenocryst- or nano crystal (Cawthorn and Tredoux, 2002), cluster- (Tredoux et al., 1995) and hiatus (Cawthorn, 1999) theories have been incorporated with traditional chalcophile based models (Campbell and Naldrett, 1979) as explanation to the extreme

enrichment factors. A summary of proposed enrichment models of the Bushveld complex is listed in Table 1.5.

Table 1.5.: Summary of the various proposed models responsible for the extreme platinum-group element (PGE) enrichment of the S-poor Bushveld complex. The PGE enrichment of the body cannot be limited to one event but most probably formed due to a combination of factors and mechanisms.

Model	Description	References
Parent magma	Parental magma is exceptionally enriched in PGE.	Crocket, 1981
Immiscible sulphide liquids	PGE are collected by S-droplets. The droplets segregate out into the crystals pile. Coupled with new magma injections or contamination, turbulence in the chamber and magma mixing.	Irvine, 1977 Naldrett et al., 1987 Barnes and Maier, 2002
R-factor model	Small amounts of sulphide magma scavenge PGE from the very large quantity of silicate magma causing PGE enrichment in sulphide minerals. (R-factor = mass ratio of silicate magma : mass ratio of sulphide magma)	Campbell and Naldrett, 1979
Secondary fluids	Secondary hydrothermal fluid enrichment and metal migration of PGE.	Ballhaus and Stumpfl, 1986 Li et al., 2004
Alternatively derived sulphur	The magma acquires S as it ascended to the surface from country rocks. The alternatively derived S promotes sulphur solubility and PGE can crystallize.	Leshner, 1989 Keys, 1995 Barnes and Lightfoot, 2005
Contamination by country rock	Fragments of crust or granitic material could have been incorporated into the original parental magma as it ascended causing the magma to become more siliceous.	Leshner and Arndt, 1995
Cluster model	During the early stages of magma crystallisation PGE group together to form clusters, due to strong siderophile behaviour. The PGE clusters are taken up by sulphide-, oxide- and silicate phases.	Tredoux et al., 1995 Ballhaus and Sylvester, 2000, Cawthorn and Tredoux, 2002
Oversaturated PGE micro-nugget model	Nuggets represent oversaturation of PGE in the melt or an exogenous PGE-rich phase present in the melt.	Borisov and Palme, 1997 Ertel et al., 1999 Brenan et al., 2005 Ertel et al., 2008
Hiatus theory	Mineralization is interrupted by replenishment of the magma chamber, causes mixing and a temporary hiatus.	Cawthorn, 1999
Micro-xenocryst model	The partially melted PGE stays preserved as crystals in the parental melt, due to their extreme melting points (1552°C (Pd) to 3027°C (Os)).	Cawthorn and Tredoux, 2002
Aqueous fluids and halide melts	Late deuteric melts and fluids containing higher concentrations of PGE than the co-existing silicate melt.	Hanley, 2005 Mungall and Naldrett, 2008
Dissolved PGE micro-nugget model	Nuggets represent dissolved PGE in the melt. The PGE nuggets exsolve to form solid phases upon quenching.	Cottrell and Walker, 2006

1.3.2. New models and developments

1.3.2.1. Summary on nano entities

Nano particles are zero-dimensional objects with physical dimensions that lie in the nano-meter range, of less than 100nm (Hochella, 2008). Nano phases can exhibit vastly different physical and chemical characteristics (Hochella et al., 2008), reactivity series, kinematic and thermodynamic properties (Banfield and Zang, 2001), structural and mineralogical attributes and formation mechanisms (Waychunas and Zang, 2008) from their bulk-solid counterparts.

Phases, smaller than 10nm, deviates the most from bulk materials and may be classified as entirely new phases (Hochella et al., 2008, Waychunas and Zang, 2008). Nano entities have extreme volume to surface ratios, enabling the structures to form certain bonds that are not usually possible on the micron scale. Their large surfaces also enable them to adsorb unusual and toxic elements (Hochella et al., 2008, Waychunas et al., 2008, Sen et al., 2011). The smaller the particle the greater is the interaction with the environment (Banfield and Zang, 2001).

A nano material is defined as any entity, in which half or more of the particles in a sample has dimensions in the range of 1-100nm (Reich, 2011). An array of nano objects has been defined including nano particles (clusters, colloids, nano crystals and fullerenes), nano wires and tubes, quasi-crystals and nano minerals (Sen et al., 2011, Banfield and Zang, 2001). A summary of nano particles, clusters, colloid and nano crystals is given in Table 1.6. Table 1.6. was adapted from Alonso et al. (1993), Tredoux et al. (1995), Banfield and Zang (2001), Qi et al. (2001), Ciacchi (2002), Wilson et al. (2005), Hochella (2008), Hochella et al. (2008), Waychunas et al. (2008) and Sen et al. (2011).

1.3.2.2. The cluster model

Physicist and chemists are able to synthesize a range of PGE clusters and nano phases, by either using the bottom-up or top-down approach (Sen et al., 2011). Synthetic clusters can be stabilized with 1) organic ligands (carbonyl groups) (Johnson, 1980), 2) carbonyl groups with various inorganic ligands (Johnson, 1980) 3) inorganic ligands (metals) (Cotton et al., 2005). These clusters are predominately used in medicines, catalysts and alloys. The growth, synthesising and measurement of nano phases and clusters, in a natural environment, are far more complex and are not widely described in literature.

Table 1.6.: Comparison between nano entities (nano particles, clusters, colloids and nano crystals), smaller than 100nm. The boundaries between nano phases are vague and difficult to distinguish (Banfield and Zang, 2001). A cluster is not a complex, colloid, nano mineral or nano crystal but may exhibit several properties giving it nano-particle and crystalline characteristics. Data was adapted from various literature sources, see section 1.3.2.

Parameter	Nano particles	Clusters	Colloids	Nano crystals
Definition	Natural or synthetic Organic or inorganic	Grouping of atoms. Not densely packed enough to form a particle / crystal	Molecules or poly-molecular particles dispersed in a medium	Crystals intermediate between molecular and crystalline state
Composition and types	Organic / inorganic/ synthetic primary or secondary	Semi-metallic or metallic crystalline or non crystalline	Porous solids, liquids, foams, gels, gasses and aerosols	Inorganic or Organic
Size range	1-10nm and 10-100nm Most abundant nano phase	10-100nm, can be <10nm	10-100nm, may be larger	Smaller than 100nm Depends on environment
Shape and structure	0D: clusters, colloids, nano crystals, fullerenes 1D: nano films, clay minerals 2D: nano rods 3D: particles, minerals	Zero-dimensional entities May have 3 or 4 dimensions in the nano range.	Structure must have a minimum of 1 direction in 1D 1D: thin films 2D: fibres 3D: corpuscular	Must have at least one dimension in the nanometre range.
Atomic and interior structure	Function of size and dimension.	Function of size and dimension.	Function of size and dimension.	Inhomogeneous internal strain, function of unit cells.
Stability	Function of thermodynamics of the system to predict polymorphic phase transitions, driven by size: polymorphic transition, surface- + hydration enthalpy.	Phase stability can be size dependant. Non-crystalline clusters are more stable than crystalline clusters.	May reach a critical minimum size where it is too small to settle out of suspension or solute. Large colloids (two or more colloids) take longer to settle out.	Not a function of temperature May be stable thousands of years. Life span may be too short to notice. Crystal size decreases as total energy increases.
Chemical Reactivity	Quantum characteristics The smaller the particle the greater the interaction with its environment. Bulk counterparts may become toxic on nano levels.	Function of variation in surface and near-surface atomic structure as function of size = change in chemical behaviour. Excellent absorbers due to vast surface: volume ratios.	Excellent absorbers due to vast surface: volume ratios. Particles may become electrically charged due to adsorption of anions.	Depends on environment the nano crystal is active in. Physical and chemical behaviour depends on size and shape.
Surface: volume	Function of nano particle size, greater on nano scale.	Function of nano particle size, greater on nano scale.	Extreme surface areas Surface effects predominant.	Depends on crystal size, dislocations and growths.
Crystals	May have different crystals than micron counterparts. May not exist on a larger scale.	May have different crystals than micron counterparts. May not exist on a larger scale.	Do not form crystals. Colloids can form bigger colloids, by colliding.	May act as nucleation point for crystal growth. May exist on larger scale.

In chemistry a cluster can be defined as the grouping of similar atoms or molecules of between 10-100 units. The cluster compound forms the intermediate phase between individual atoms or ions or molecules and a nano particle (Banfield and Zang, 2001) or bulk solid. Clusters contains at least one, often more, metal-metal bonding phase. Clusters can be subdivided into crystalline and non-crystalline. Non-crystalline clusters are more stable due to filled electron shells (Alonso et al., 1993).

The definition and exact size of a cluster is a controversy and dependent on a few factors:

1. The Chini “magic number” (Ciacchi, 2002), a mathematical function that predicts the stability of the cluster phase. The “magic number” places the size of a stable cluster between 10-100 atoms.
2. The stability of a cluster is a function of its atomic weight and physical character. The heavier the metal, the more likely it is to form a stable cluster phase. With reference to the PGE; Pt, Os and Ir will form relatively more stable clusters than Pd, Ru and Rh (Tredoux et al., 1995).
3. To form a stable cluster, the metal needs an appropriate ligand to form around. A semi- or non-metallic ligand shell embeds a metallic core (Ciacchi, 2002). The effect of the ligand is strongly dependent on the type of ligand used and the distribution of the particular ligand around the core of the cluster (Ciacchi, 2002). Typical ligands include organic complexes like long polymers, phenantroline, carbonyl and phosphine (Ciacchi, 2002) and semi-metals As, S, Sb, Te and Co (Tredoux et al., 1995).

During the early stages of magma differentiation, heavy metals like the PGE, can group together to form clusters. The PGE-ligand clusters form due to the physico-chemical characteristics of the PGE. The clusters’ heavy electron-clouds and huge surface areas, prompts the PGE to nucleate and form clusters.

The clusters are semi-stable to stable (Tredoux et al., 1995). A fraction of the clusters are reabsorbed into the melt, while a fraction acts as nucleation points to form nano crystals and minerals. The clusters (10-100 atoms) can easily be taken up by sulphide, spinel or silicate phases. The cluster model (Tredoux et al., 1995) focuses on the growth and the influence of PGE clusters, in a magmatic environment, see Figure 1.3.

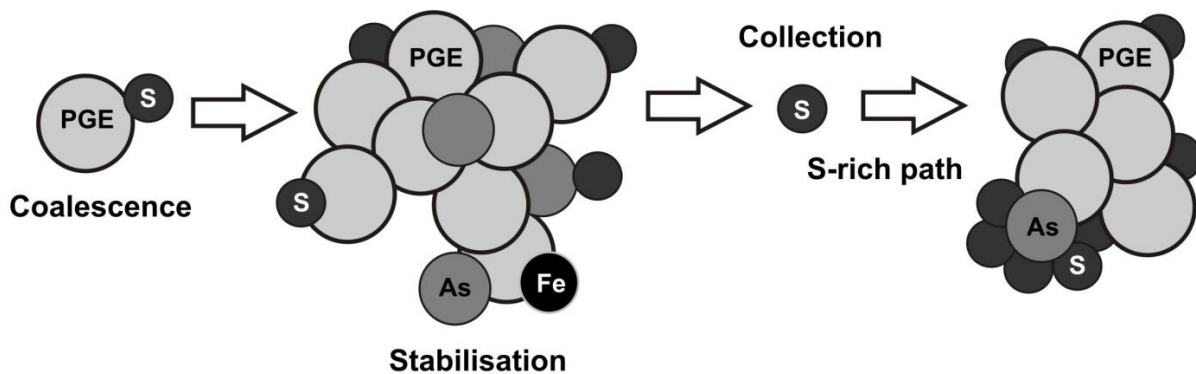


Figure 1.3.: The cluster model from Tredoux et al. (1995). Platinum-group elements (PGE) exist as poly-atomic metallic to semi-metallic clusters, smaller than 100nm, in the parental melt. The clusters either formed in the parental source or may be an artefact from the mantle. The PGE clusters formed due to the physico-chemical association of the PGE with chalcogene ligands. The clusters are further stabilised by transition metal and metalloid ligands such as Fe, Co, Cu, As, Te, Bi by means of mechanical processes. The clusters can stay preserved in the system for millions of years or alternatively be resorbed back into the melt or act as nucleation points for crystals and minerals. In an S-rich environment the clusters can be taken into the sulphide melt to form alloys, arsenides, complex sulphides and tellurides or precipitate out later as inclusions in base metal sulphides (BMS). In an S-poor environment they may stay suspended in the melt until they precipitate out to form alloys or act as nucleation points to form platinum-group minerals (PGM) in silicate and oxide phases.

The cluster model can be summarized as follows, Tredoux et al. (1995):

1. The PGE occur as metallic clusters of about 50-100 atoms (Tredoux et al., 1995) and not as individual atoms or molecules in a melt phase. The size and stability of the clusters is a function of its particular thermodynamic environment.
2. Chalcogenides like S, As, Sb and Te act as stabilizing ligands for the PGE clusters. A process of adsorption (physical process) bonds the ligands to the cluster.
3. In S rich environments the stabilized PGE clusters can now be easily taken up into sulphide melt and precipitate out as alloys, arsenides and tellurides. The fraction of PGE that is not removed will later precipitate out as sub-microscopic inclusions in BMS.
4. In S poor environments clusters will not coalesce out of the melt until they can form stable alloys and will stay suspended in the silicate melt. The PGE may also concentrate in the residual fluid.

1.4. Outline of project

Temperature controlled experiments were used to synthesise and measure possible PGE clusters, in a magmatic environment. PGE clusters (Tredoux et al., 1995), of 10-100nm, will prove that the PGE bond physically (adsorption) or physico-chemically to ligands, during the early stages of formation or before magmatic differentiation. Nano interactions, the physical

character of the elements and the holistic- and nano thermodynamic interactions have a greater influence on bonding and preservation of nano entities than speculated.

The sulphide portion of a Ni-Cu-S melt was experimentally mimicked. The experiments were manipulated in such a manner to attain optimum conditions. A constant metal/sulphide ratio (highly reducing conditions) of one was obtained throughout all experiments. Ru, Pd and Pt were used as analogue for the PGE. The chosen PGE had different physical and chemical properties. The PGE' different characteristics served as a comparison to determine if certain PGE were more probable to form clusters.

Chapter 2: Materials and Methods

Three experiments (A, B and C) were prepared using the dry reaction silica tube technique (Kullerud, 1969; Kullerud et al., 1971). The process allows for the simultaneous formation of a crystalline and a melt phase. Each sample consisted of an S, Cu and Fe powder mix doped with variable concentrations of either Pt or Pd or Ru and As.

The experiments were set-up to best represent a sulphide portion of a magmatic Ni-Cu-S system. The S-melt fraction was modelled on primitive tholeiitic basalt, from a fertile mantle source (Rajamani and Naldrett, 1978; Francis, 1990 as cited in Ballhaus et al., 2001). The samples were cooled down at different tempos and quenched to ensure that variable formation conditions were obtained. Different cooling times were essential to test if the same results (clusters) would be present in both slower and faster cooled samples.

Final sample products were made into polished sections for ore microscopy, scanning electron microscopy (SEM), x-ray spectrometry (XRD), scanning Auger microscopy (SAM) and time-of-flight secondary ion mass spectroscopy (TOF-SIMS) analysis.

2.1. Outline of experiments

The experiments were manipulated to best represent the sulphide portion of a Cu-Ni-S \pm PGE system. No Ni was used in the synthetic system. Adding Ni to the experiments would have no significant effect on the solidus and liquidus temperature of the sulphide system (Ballhaus et al., 2001). To force a broad as possible field between the liquidus of the mss phase and the subsolidus of the melt phase, high concentrations of Cu was added, as Cu lowers the solidus temperature of the sulphide system (Helmy et al., 2010). The As and PGE were added as ionic salts (ICP-MS plasma standards), to ensure that the phases were in the smallest and purest form. Adding in the ligands (PGE and As) as ionic salts was essential to ensure that system was not pre-contaminated with PGE nodules/ xenocrysts/ nano crystals.

Initial experimental runs were conducted using Pt. Pt is one of the heavier PGE (Pt, Os and Rh) and is theoretically more likely to form clusters in a magmatic system, opposed to the lighter PGE (Pd, Ru and Ir) (Tredoux et al. 1995). To test the hypothesis, similar experiments were conducted using the lighter PGE (Pd and Ru). As was used as stabilizing chalcogene

ligand. A Pd system was chosen as Pd resembles Pt more closely, in both physical and chemical properties (Cotton, 1997), than any other PGE. Pd lies in the same group as Pt and in the same period as Ru. Atomically Pd and Pt are essentially the same size, with similar atomic radius (Hartley, 1991) and volume (Lide, 2008). Theoretically Pd and Pt should act alike in the mss system, as they are chemically very similar, forming related phases and phase associations.

The Ru system was chosen as a control measure. Ru reacts geochemically different than Pt and Pd. Ru prefers to form bonds with S over ligands such as Cu, Fe and As. If Ru forms clusters, like Pd and Pt, it can be showed that the PGE form phases before sulphide saturation is achieved. Ru shows no close association physically or chemically with Pd or Pt. The outline, concentration and compound information of the starting mixtures, of experiment A, B and C, are indicated in the Table 2.1.

Table 2.1.: Outline of the compound powders used to prepare experiments A, B and C. The finest (smallest mash size) and purest powders were used to ensure that the mixtures were as homogenous and easily workable as possible. The various platinum-group elements (PGE) were added as salts, to ensure that the system was not pre-contaminated by PGE xenocrysts or nodules.

Element	Compound information	Mesh size, purity or conc.	Mix 1	Mix 2	Mix 3
S	S powder ALFA AESAR 43766 LOT: JO1W016	-325 99.5% pure	358mg	358mg	358mg
Cu	Cu powder ALFA AESAR 39682 LOT: HO3X039	-100 99.999% pure, metals basis	174mg	174mg	174mg
Fe	Fe powder ALFA AESAR 00737 LOT: A25X021	-200 99+% pure, metals basis	480mg	480mg	480mg
As	As in 5% HCl ALFA AESAR 13836 LOT: 61101004	Plasma standard solution, specpure 1000µg/ml	230ppm	0	31ppm
Exp: Pt	Pt in 20% HCl ALFA AESAR 13827 LOT: 61000229	Plasma standard solution, specpure 1000µg/ml Pt	300ppm	300ppm	40ppm
Exp: Pd	Pd in 20% HCl ALFA AESAR 13833 LOT: 61100638	Plasma standard solution, specpure 1000µg/ml Pd	300ppm	300ppm	40ppm

Table 2.1. cont.: Outline of the compound powders used to prepare experiments A, B and C.

Element	Compound information	Mesh size, purity or conc.	Mix 1	Mix 2	Mix 3
Exp: Ru	RuCl ₃ in 20% HCl ALFA AESAR 35767 LOT: 61101268	Plasma standard solution, specpure 1000µg/ml Ru	300ppm	300ppm	40ppm

Variable concentrations of PGE and As was used to test if the PGE will form clusters in:

1. **PGE and As over-saturated systems**, with a PGE-As ratio of 1: How big will the clusters be, how they are distributed, in the phases they occur and if the clusters are present do they occur in both slower and faster cooled samples?
2. **A PGE-As under saturated systems**, PGE-As ratio of 1: Will the same trends be observed as in the oversaturated samples? Test whether the PGE clusters are a function of available concentrations of PGE and a suitable anion or do they form as primary phases in any PGE system?
3. **PGE systems, no As but over saturated in PGE**: If the same trends are observed as in nr 1, it might prove that there is a physical force responsible for high enrichments in PGE systems, rather than a primarily chemical process.

2.2. Sample preparation

Step 1: Preparation of sample powders

Three main mixtures for each experiment (A, B and C) was prepared, called mix 1, 2 and 3. The relevant concentration Pt or Pd or Ru liquid (300ppm or 40ppm) was added to 358mg S-powder of each mixture. The two phases were not mixed. PGE liquids were used to ensure that the PGE stayed homogenously distributed in the system. The samples were heated in a horizontal furnace for 120 minutes at 60°C to dry out the PGE liquid. The relevant concentration of As liquid (230ppm or 31ppm) was added to the cooled powders. The samples were dried out once again, in a horizontal furnace, for 120 minutes at 60°C and homogenised. The Cu (174mg) and Fe (480mg) powders were added to the homogenised PGE-As-S powder mixtures.

Step 2: Re-homogenization of powders

The mixtures were placed in silica tubes, under a vacuum of 10^{-6} torr, and heated for 540 minutes (9 hours) to 700°C. The silica charges are illustrated in Figure 2.1. A. The samples

had to be kept at a constant temperature of between 700-800°C to ensure that the reaction do not reach a critical temperature and react exothermally. Fused silica tubes were used as they can withstand temperatures of up to 1400°C and will not react with the powders (Scott, 1974). The tubes were sealed under vacuum with an oxy-flame (Scott, 1974). The cooled powders were crushed and re-homogenised again. Re-homogenisation was critical to ensure that the samples were as homogenous as possible and that the system was not contaminated by adding PGE nodules.

Step 3: Preparation of fast and slow cooled samples

The content of the three mixtures were each split into two samples. A 150mg sample that was cooled rapidly (1000°C-0°C in a few seconds) and a 200mg sample that was cooled slowly over 10080 minutes (168 hours or 7 days) from 1000°C to 400°C. The 6 samples of each mixture (fast and slow cooled) were each placed in silica tube, under a high vacuum of 10^{-6} torr, and heated over two days to 1000°C before cooling. The fused Si tubes have low thermal expansion that allows the tubes to be cooled rapidly or quenched without shattering (Scott, 1974). Experimental conditions were manipulated to ensure that there was a free metal phase present at all times. The experiments were conducted under highly reducing conditions to force As to react as an anion with the PGE and not as a cation. The Fe, Cu and S were also controlled to form numerous Cu-Fe-S phases.

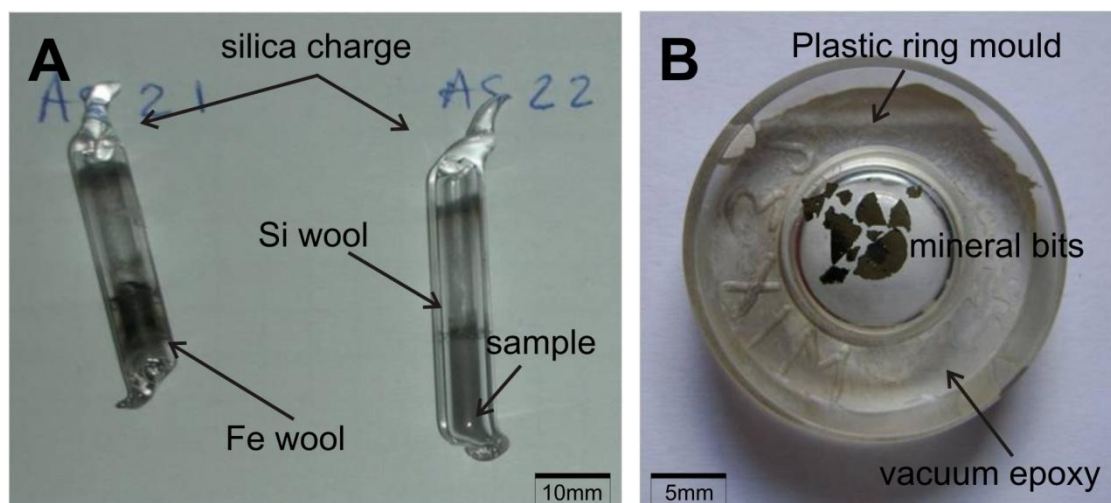


Figure 2.1. A and B: Silica charges and epoxy mould with samples. A: Example of sealed evacuated silica charges, with sample powders and Si- and Fe-wool, to be heated. The silica charges can withstand temperatures of up to 1400°C and will not react with the powders or shatter with quick quenching. B: The finished sample bits set in an epoxy mould. The epoxy moulds can be used in scanning electron microscopy (SEM) and ore microscopy measurements.

Step 5: Preparation of epoxy moulds used in analyses

The final sample bits were set in epoxy, see Figure 2.1. B. An ore-microscope was used to choose appropriate grains to set in the epoxy moulds. The finished samples were polished down to be used in ore-microscopy and SEM analyses. Whole or powdered samples bits were used in XRD and SAM analysis.

2.3. Analytical procedures

The samples were analysed using different analytical techniques to pick-up nano phases with high accuracy and precision. Methods used include ore-microscopy, SEM, SAM and XRD. The characteristics, principles and relevant sample preparation for each technique are described below.

2.3.1. Ore microscopy

The ore microscope was primarily used to qualitatively differentiate between phases, to identify textures and structures and to give a basic idea of the mineralogy of each system. The characteristics of the ore microscope used are listed in Table 2.2.

Table 2.2.: Specifications of the ore microscope used in the study. The ore microscope was used to qualitatively check the mineralogy of each system and to identify the best sample bits and areas of interest within the samples, to be used in more quantitative analytical methods.

	Ore microscope: UFS
Model	Reflective light microscope: Olympus BX51
Analyze	Non-quantitative quick analysis of opaque minerals (phases) and to identify areas of interest for SEM and SAM analyses
Sample preparation	Polished epoxy sections, sample bits
Magnification	2x, 5x, 10x, 20x, 40x magnification

A particular problem with polishing the Fe-sulphides (due to rapid quenching) is the difference in density between PGM and mss. The Fe-sulphides are particularly brittle and PGMs are easily lost during polishing. The PGM are polished out due to the broad density and hardness differences between PGM (sr=6-7) and sulphide (po=3.5-4.5, Anthony et al., 1990). Phase identification may also be hindered by problems such as fine focusing, distortions, surface effects, the thickness of the sections and quality of polishing.

2.3.2. Scanning electron microprobe: SEM

SEM analysis is a fast, reasonably precise and accurate, non-destructive analytical method with rapid data acquisition. For SEM work the samples were coated with a thin layer of C of $\pm 15\text{--}100\text{nm}$. A conducting layer is needed to produce a high energy electron beam (10–50 keV), over the sample evenly (Reed, 2005). The electron that is “excited” by the electron beam produces a characteristic fingerprint set of x-rays for each element in a phase (Reed, 2005). The outline of the EDS-SEM (energy dispersive spectrometer) work done at Geology Department, UFS and WDS-SEM (wavelength dispersive spectrometer) analyses conducted at the Geology Department of Rhodes University, is summarized in Table 2.3.A.

Table 2.3.A: Detection limits and outlines of scanning electron microscopy (SEM) analysis. Energy dispersive x-ray spectrometry (EDS-SEM) was used to identify areas of interest for nano analysis and phase identification. Quantitative wavelength dispersive x-ray spectrometry (WDS-SEM) was employed to quantify phases, elemental maps and analyses to determine metal concentrations and calculate sulphur fugacity (fS_2).

	SEM: UFS	SEM: Rhodes
Model	JOEL JSM 6610 Field Emission Scanning Electron Microscope	JOEL JXA 8230 Super Probe
Analyze	Qualitative analysis Quantitative identification of phases	Quantitative identification of phases and PGMs
Data format	Spot analysis, spectra-graphs, element and composition maps	Spot analysis, spectra-graphs, element and composition maps
Analyzers	EDS-SEM	EDS- and WDS-SEM
Sample preparation	C coated epoxy moulds with sample bits	C coated epoxy moulds with sample bits
Acc. Voltage	20kV	15kV
Probe current	20nA	20nA
Beam size	1 μm	1 μm
Detection limit	$\pm 100\text{ppm}$	$>30\text{ppm}$

The various standards employed in WDS-SEM analysis are described in Table 2.3.B.

Table 2.3.B: The characteristics of standards used in wavelength dispersive x-ray spectrometry (WDS-SEM) analysis. A po and ccp standard was used to quantify the major elements such as Cu, Fe and S. Separate standards were used for As and the platinum-group elements (Pt, Pd and Ru).

Element	Standard	Mass (%)	ZAF Fac.	Z	A	F
As	GaAs_SPI	51.8000	3.4462	9.3860	0.3672	1.0000
Cu	ccp_SPI	33.0400	0.30874	0.0899	0.9730	1.0000
	Cu_SPI	99.9990	0.0956	0.0966	0.9901	1.0000
Fe	py_SPI	46.5500	0.2107	0.2168	0.9718	1.0000

Table 2.3.B cont.: The characteristics of standards used in wavelength dispersive x-ray spectrometry (WDS-SEM) analysis.

Element	Standard	Mass (%)	ZAF Fac.	Z	A	F
S	ccp_SPI	35.7500	2.1611	2.8487	0.7584	1.0004
Pd	Pd_SPI	99.9900	1.7223	2.0070	0.8582	1.0000
Pt	Pt_SPI	99.9500	3.6070	4.9036	0.7356	1.0000
Ru	Ru_SPI	99.9000	2.0888	2.4884	0.8394	1.0000

Qualitative and semi-quantitative SEM analyses were run for the identification of

1. Major and minor phases and PGE phases (and possible clusters).
2. Chemical composition of phases.
3. Determine the phases the PGE tends to occur in and related distribution trends.

One of the biggest problems to compensate for in sulphide minerals / phases is surface imperfections caused by compositional (incomplete or partial crystallization nature of sulphides) and structural defects. Sulphides are brittle and lack cleavage or have very poor cleavage (Rosso and Vaughan, 2006). Defects include fractures, vacancies, screw and edge dislocations, terrace sites, ledges, adatoms and kinks (Rosso and Vaughan, 2006).

2.3.3. X-Ray spectrometry: XRD

XRD analysis uses the crystalline properties of solid phases to identify phases. Each mineral produces a characteristic finger print x-ray (Cullity and Stock, 2001). XRD was utilized to determine the crystalline structures of phases identified by SEM and ore-microscopy. The characteristic and trades of the XRD instruments used are given in Table 2.4.

The sulphide minerals and associations have intricate growth and exsolution structures, various morphologies and several polymorphs and solid solutions (Wuensch, 1974), making the sulphides phases difficult to quantify.

Table 2.4.: Detection limits and outlines of x-ray (XRD) analysis used for semi-quantitative phase identification. XRD measurements were used to monitor, track and quantify nano phase throughout the experimental process.

	XRD: UFS
Model	PANalytical Empyrean
Analyze	Crystal structures for qualitative chemical phase determination Line profiles for nano phase identification
Data format	Diffraction spectrum graphs
Cathode tube	Cu

Table 2.4. cont.: Detection limits and outlines of x-ray diffraction (XRD) instrument utilized for semi-quantitative phase identification.

	XRD: UFS	
Tension and current	45kV 40mA	
Filter	Ni	
Detection limit	100ppm	
Run time	Major phase determination	Nano calculations
	Step size: 0.0167113°2Th Time per step: 40s Run time: 40min	Step size: 0.0170°2Th Time per step: 40s Run time: 1h 42min

Several factors have to be taken into account when classifying and analysing sulphides, to obtain the true structural and chemical values (Wuensch, 1974):

1. Sulphides do not crystallise completely forming poor or massive crystals, making it difficult to obtain a perfect single crystal for analysis.
2. Sulphide crystals have distinct acicular habits.
3. Pseudo-symmetric and twinned crystals are common and cause the symmetry of the crystals to deviate from the norm.
4. Solid solution, polymorphism, superstructures (derivatives) and exsolution textures may cause slightly higher values of base metals Fe, Cu, Co, Ni.
5. Impurities (more applicable to natural samples).
6. The size of the unit cell. The greater the unit cell the greater the influence of external factors (Wuensch, 1974).
7. The influence of amorphous phases (melt phases in both quick quench and slow cooled samples) in samples. Amorphous and polycrystalline material may cause noise, higher background values, split peaks, overlapping peaks and doubling of peaks (Mitchell and Pérez-Ramírez, 2010). Strain and stress, due to rapid quenching, in the crystals may cause broadening- and split peaks (Klug and Alexander, 1974).

XRD analysis was in addition used to track and monitor nano phases and/or possible pre-contamination of PGE-nano entities during sample preparation. The Debye-Scherrer equation (FWHM or size calculations, crystals without strain) (Akbari et al. 2011, Dorofeev et al. 2012), see Appendix A, was used to calculate the presence, size and shape of nano phase. The method was only effective for phases with a known XRD pattern. It was possible that numerous PGE-ligand nano phases with As, Cu, Fe and S could have formed, that is not yet known or quantified, throughout the experimental process. However the PGE have extremely high melting points (1552-3027°C) making it highly unlikely that PGE-ligand nano phases could have formed during steps 1, 2 or 3 of the experimental process.

2.3.4. Scanning auger microprobe analysis: SAM or AES

Quantitative SAM analyses were run to measure and identify any nano scale entities (<1000nm) and PGE clusters (1-100nm). SAM is a near surface, fast, radiation-less analytical technique with extremely high resolution and magnification properties (Prupton et al., 2006). To produce the auger electrons an electron beam is scanned over the surface of the sample to ionize the atoms (Prupton et al., 2006). The Auger electrons are emitted from the relaxation of the electron beam. The emitted electron is immediately absorbed again making the process radiationless (Reed, 2005). The atomic number (Z) of the element in question will determine the amount of auger electrons emitted (Prupton et al., 2006). The lighter the element the more auger electrons will be emitted, as the atomic number increases the auger electron emitted decreases. The outline of the SAM work conducted at the National Nano Surface Characterization Facility (NNSCF), UFS, is given in Table 2.5.

Table 2.5.: Detection limit and outlines of scanning auger microprobe (SAM) analysis conducted at the Nation Nano Surface Characterisation Facility (NNSCF). SAM was primarily used to identify and quantify (semi-quantitative) nano entities.

	SAM: NNSCF
Model	PHI 700 Scanning Auger nano-probe
Analyze	Qualitative and semi quantitative analysis Identification and imaging of nano phases and clusters
Data format	Back-scatter images, 2D compositional maps
Standards used	No reference material needed
Sample preparation	Solid conductive material: sample grains on graphite tape
Tension and current	All AES surveys: 20kV, 10nA electron beam Depth profiles: 2kV, 2μA ion beam
Electron beam	Sputter rate of 8.5nm per min, raster area 2x2mm
Detection limit	5-50nm, only measures top ten atomic layers

The electrically conductive synthetic samples (resistivity of $\rho_0 = 2-160 \times 10^{-6} \text{ohm.m}$, Lide, 2008) were flushed with acetone (CH_3COCH_3) to remove surface contaminants of Cl, O, C and fingerprints. Contaminants are a problem (Reed, 2005) as the AES only measures the first 20 atomic layers or 10\AA (Prupton et al., 2006). The contaminants that are not removed before hand must be removed by Ar sputtering. Contaminants cause unnecessarily long run times and valuable sections of the sample may be lost or destroyed by the sputtering process. The interaction of the high energy electron beam with the surface of the sample can cause electrons to disperse, adhere to the surface, and react with the surface to form a compound or elements to diffuse in or out of the system (Prupton et al., 2006). The high energy beam may also burn or destroy nano structures.

2.3.5. Time of flight secondary ion mass spectrometry: TOF-SIMS

TOF-SIMS was used measured the distribution of As, PGE and PGE-ligand ions on the sample surface. The instrument can measure concentrations up to parts per billion (ppb). TOF-SIMS is a static, non-destructive SIMS method that measures the first few atomic layers (2-4Å) (Stephan, 2001). TOF-SIMS is of the most sensitive surface imaging techniques currently available. The molecules or ions are removed from the sample surface by a pulsed ion beam. The liberated ions are then accelerated by an electric field, under extreme vacuum conditions of 10^{-6} torr towards a detector. The ions' mass-to-charge ratio is determined by measuring the time the ions arrive at the mass detector (Stephan, 2001). TOF-SIMS is a time consuming method as each pixel of a TOF-SIMS map is a mass spectrum. However TOF-SIMS allows for detailed mapping of elements or a specific element with software manipulations. The details of the TOF-SIMS used, NNSCF, is given in Table 2.6.

Table 2.6.: Detection limits and outlines of the time of flight secondary ion mass spectrometry (TOF-SIMS) analysis. TOF-SIMS was used exclusively to identify nano structures that were not picked-up by scanning auger microscopy (SAM).

	TOF-SIMS: NNSCF	
Model	TOF SIMS 5, ionTOF	
Analyze	Qualitative to semi-quantitative surface elemental and chemical analysis	
Data format	Elemental and molecular surveys and maps, mass spectrum graphs	
Sample preparation	Samples did not need to be polished or coated Samples surfaces were cleaned with an oxygen gun and charging removed with a flood gun	
Scans	Mass range: 0-875amu Scan area: 100µm x 100µm 50 scans at 26.21 sec/scan Resolution: 512x512 pixels, final 256x256 pixels	
Tension and current	Heating: 2.9A, Emission: 0.8mA, 30keV	
Electron beam	Bi ⁺ beam, from a liquid metal ion gun	
	Spectroscopy mode	Imaging mode
	DC target: 30nA Pulsed target: 1.2pA Pulse rate: 100µs Beam size: 5µm	DC target: 0.5nA Pulsed target: 0.25pA Pulse rate: 100µs Beam size: 200nm
Detection limit	Trace elements and compounds: ppm up to ppb range Depth profiling: <10nm	

Sample preparation was an essential step in SIMS analysis. The samples were cleaned with N-gas beforehand and in the instrument the samples were cleaned with oxygen. Charge was removed with a flood gun. To compensate for edge effects an area of 300µm x 300µm was cleaned however only 100 µm x100 µm was measured.

Chapter 3: Experimental Set-up

To determine how comparable the synthetic mss system was with a sulphide portion of a natural system key experimental, kinematic and thermodynamic conditions were measured and compared. It was essential not only to monitor how successfully and reproducibly the experiments were as a whole but also to monitor samples evolution and possible pre-contamination by nano phases, that may have altered the results. XRD spectra and calculations on samples evolution and contamination are given in Appendix B.

3.1. Kinematics of the experimental process

Kinematic modelling was done to determine the 1) reaction mechanism 2) rate of the reactions and 3) optimum experimental conditions. The Pt-As system (experiment A) was used as example to model the kinematics of the experiments.

3.1.1. Reaction mechanism

The reactions of the experimental systems were overall endothermic (heating and slow cooling phases), non-spontaneous and irreversible. Mole fractions of experiment A were used to calculate the kinetics of the reactions given in Table 3.1.

The reaction can be written as:

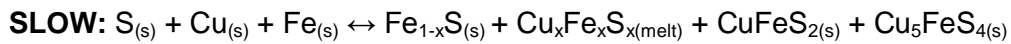
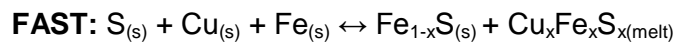


Table 3.1.: Mole values and concentrations of the elements used to prepare experiments A, B and C. The values were used to determine the rate of the reactions. Experiment A served as analogue for the experiments (A, B, C), as a basic mixture was used to prepare the mss system.

Element	S	Cu	Fe	As			PGE (Pt or Pd or Ru)		
				1	2	3	1	2	3
Mass mg	358	174	480	0.230	0.000	0.031	0.300	0.300	0.040
Mole mmole	11.10	2.70	8.60	0.0031	0.000	0.0004	0.0015	0.0015	0.0002
Conc. wt.%	35.357	17.185	47.406	230 ppm	0.000	31 ppm	300 ppm	300 ppm	40 ppm

3.1.2. Rate of reaction

The order of the reaction determines the kinematics of the system (Fergusson, 1982). The reactivity and spontaneity of the system is controlled by the thermodynamic stability of the reactants and products (Fergusson, 1982). A change in free energy (ΔG) determines if a chemical change will take place. The change in free energy, in the mss system, can be graphically expressed in Figure 3.1.

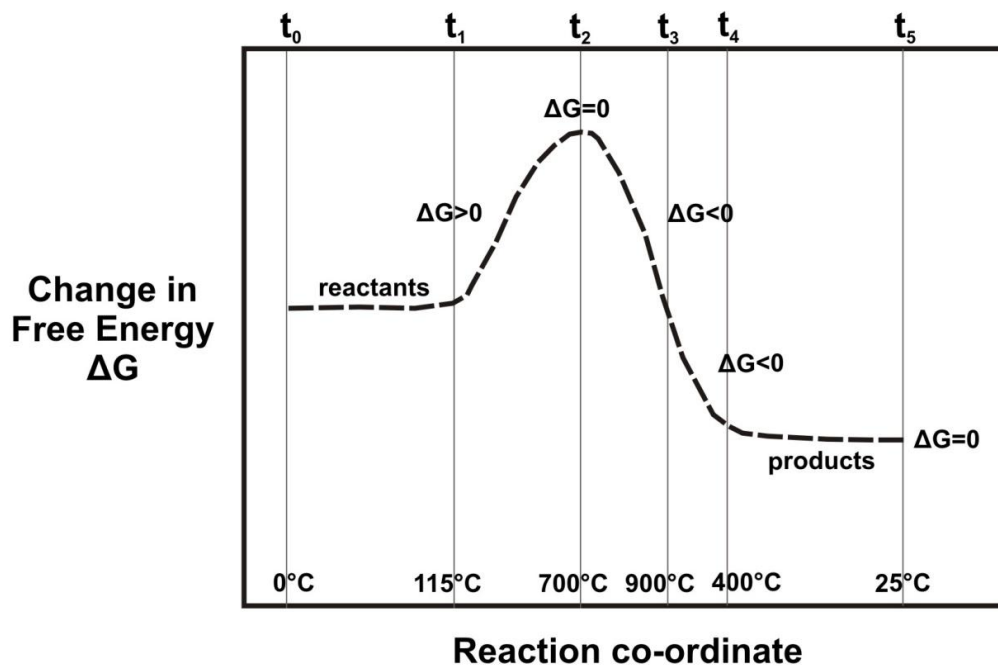


Figure 3.1.: Change in free energy (ΔG) of the mss system, applicable to fast and slow cooled systems, as the reaction progresses over time (t). The change in free energy (ΔG) for the time t_0 - t_1 was constant to negligible. As the reaction continued, with heating, there was a change in enthalpy (ΔH) and entropy (ΔS) of the system and the overall change in free energy (ΔG) was positive. At t_2 the system was completely molten and the change in free energy should have been zero (0). The system stayed at time t_2 for several hours at a constant temperature of $\pm 1000^\circ\text{C}$. As the system started to cool gradually from 1000°C to 400°C , over time t_2 - t_4 , the change in free energy (ΔG) was negative. The system as a whole became more ordered and reached equilibrium state around 400°C . From literature it is estimated that the mss is stable around 400 - 350°C . Quick cooling from t_4 - t_5 , within the stable mss phase, the change in energy in the system was negligible to zero.

The reaction rate was different for the different phases or paths of the experiment, see Table 3.2. To increase the reaction rate in the synthetic experiments high concentrations of Cu was added to the starting mix. The excess Cu lowered the sub-solidus temperature of the system, enabling melting at lower temperatures. Additional Fe was added to the charges to control the overall fugacity of the system.

Table 3.2.: Kinematic indicators, of experiment A (Pt-As system), throughout sample preparations. See Table 3.5. for explanation of steps followed during experimental set-up. Experiment A was used as analogue for the mss as a whole. In steps 1 and 2 the PGE and As liquids were dried out at low temperatures (40-60°C) to evaporate the acids. The samples were then heated for several hours at constant temperature intervals. The overall reaction was endothermic. The reaction rate was thus dependent on the concentration of the reactants (first order) and heat energy of the system. Upon cooling the reaction was still dependant on the rate of cooling or the change in heat energy. The longer the samples cool, the more complex and well developed the phases will be. Larger platinum-group element phases (PGM) were expected to crystallize in the slower cooled samples.

Steps		Chemical reaction	Order	Reaction rate t (h, m, s)	Temp. °C
Step 1	t_0	$S_{(s)} + As_{(aq)} \leftrightarrow S_{(s)} + As_{(s)}$	-	Drying of aq. No reaction between S + As	<100
Step 2	t_0	$S_{(s)} + Pt_{(s)} + As_{(aq)} \leftrightarrow$ $S_{(s)} + Pt_{(s)} + As_{(s)}$	-	Drying of aq. No reaction between S + PGE + As	<100
Step 3 Heating	$t_0 - t_2$	$S_{(s)} + Pt_{(s)} + As_{(s)} + Cu_{(s)} + Fe_{(s)} \leftrightarrow$ $S_{(l)} + Pt_{(l)} + As_{(l)} + Cu_{(l)} + Fe_{(l)} \text{ (melt)}$	first	9 hours	0- 1000
Step 4 Heating	t_3	$S_{(l)} + Pt_{(l)} + As_{(l)} + Cu_{(l)} + Fe_{(l)} \text{ (melt)}$	-	Keep at constant 950° for 48 hours	900- 1000
Step 5 FAST Cooling	$t_2 - t_5$	$S_{(l)} + Pt_{(l)} + As_{(l)} + Cu_{(l)} + Fe_{(l)} \leftrightarrow$ $Fe_{1-x}S_{(s)} + Cu_xFe_xS_{x(melt)}$ $\pm Pt \pm As \pm PGM_{(s)}$	first	48 hours several seconds	950-25
Step 5 SLOW Cooling	$t_2 - t_4$	$S_{(l)} + Pt_{(l)} + As_{(l)} + Cu_{(l)} + Fe_{(l)} \leftrightarrow$ $Fe_{1-x}S_{(s)} + Cu_xFe_xS_{x(melt)} + CuFeS_{2(s)}$ $+ Cu_5FeS_{4(s)} \pm Pt \pm As \pm PGM_{(s)}$	first	48 hours 168 hours	950- 400

3.1.3. Optimum experimental conditions

Factors that may have influenced the rate and behaviour of the reactions included 1) experimental conditions (temperature and pressure) 2) the concentration of the reactants 3) the nature or physical state of the reactants. The smaller the particles the greater the surface: volume ratio 4) the presence of a catalyst (Fergusson, 1982).

3.2. Phase relationships, thermo-chemistry and equilibrium

Three phases were present in the synthetic samples; a liquid melt phase, a solid crystalline phase and a gas phase (fugacity). The evacuated silica tube system is a closed system with constant volume but exchanges heat with its surroundings. In the experiments the heating reaction was endothermic and thus produced a positive change in free energy and entropy.

As the system becomes more complex the entropy increases and upon quick cooling is reduced to zero. The opposite trends are expected for the exothermic cooling reaction or process. The change in enthalpy in the irreversible Fe-Cu-S system is greater or equal to zero. The heating process produced a complete melt phase at $\pm 700^{\circ}\text{C}$. The theoretical thermodynamic and phase (mineralogical) evolution of the mss system, during sample heating, is tabulated in Table 3.3. Phase relationships were used to determine thermodynamic entities and equilibrium state.

Chemical equilibrium is reached, at a constant temperature and pressure, when $\Delta U=0$ (total energy, entropy, thermal, mechanical or chemical) or $\Delta G=\text{minimum}$ (Richet et al., 2010). If a system is in equilibrium it will not change spontaneously from its current state (Barton et al., 1963 as cited in Scott, 1974). If there is a slight temporary change in the system it will return to its initial (equilibrium) state (Lewis and Randal, 1961 as cited in Scott, 1974). A change in energy (mechanical, chemical or free energy) signifies a change in state that causes a change in chemical equilibrium (Fergusson, 1982). If the $\Delta H < 0$ then the ΔS should be > 0 .

Table 3.3.: The change in free energy (ΔG) during heating of the Fe-Cu-S powders. The $\Delta G=0$ for t_0-t_1 or until the reaction started. The change in free energy (ΔG) was positive for the heating reaction. When the system reached an equilibrium state or melt phase at about 700°C (t_2) the change in free energy was $\Delta G=0$. Between t_2-t_3 the change in free energy was negative ($\Delta G < 0$). The system was completely melted and there was no change in chemical state but there was a constant change in heat energy, because the system was still being heated. Around $950-1000^{\circ}\text{C}$ (constant temperature) the change in free energy was zero ($\Delta G=0$).

Temp. $^{\circ}\text{C}$	Stage t	Entropy ΔS	Enthalpy H	Free energy ΔG	Phase assemblages	P
0-100	t_0	0	0	0	S As, PGE	solid liquid
0-100	$t_0 - t_1$	0	0	0	S, Fe, Cu, As, PGE	solid
100-200	t_1	+	-	+	Fe, Cu, As, PGE S melts at 115°C	solid liquid + gas
200-700	$t_1 - t_2$	+	-	+	melting	solid liquid + gas
700	t_2	0	0	0	melt	liquid + gas
700-1000	$t_2 - t_3$	+	-	-	melt	liquid + gas
950: stable	t_3	0	0	0	melt	liquid + gas

Upon heating the mss system reached a state of equilibrium or meta-stable phase for a limited time span, at about 700°C . The system was completely melted or in a liquid phase at 700°C . The system stayed in a melt phase upon further heating to 1000°C . As the temperature increased the entropy increased. The system was then kept constant at $900-1000^{\circ}\text{C}$ for several hours. The change in entropy (ΔS) decreased to zero. Po started to

crystallize. Crystallization caused a drop in the average entropy and free energy of the system. The crystalline- and thermodynamic phase changes of the synthetic system, during cooling, are given in Table 3.4. (A and B). The change in energy, as the reactions of the mss progressed, over time is given in Figure 3.1.

Table 3.4. A: Thermodynamic and phase transitions during quick quenching (950-25°C). The system stayed at 950°C for several hours. During cooling po started to crystallize. The change in free energy was negative ($\Delta G < 1$) for t_3 and decreased slowly as the first solid phases started to crystallize and the overall chemical potential of the system changed. After quick quenching (t_5) the change in free energy was zero ($\Delta G = 0$). The system was semi-stable now and the change in chemical potential and temperature was zero.

Temp. °C	Stage t	Entropy ΔS	Enthalpy H	Free E ΔG	Phase assemblages
950-1000	t_3	0	-	-	mss, Cu-rich melt and \pm PGM
1000-25	$t_3 - t_5$	-	-	-	po, Cu-rich melt and \pm PGM
25: stable	t_5	0	0	0	po, Cu-rich melt and \pm PGM

Equilibrium could not be accurately determined in the samples. Sulphide melts cannot be quenched to glass like silicate melts (Helmy et al. 2013). The quenched melt phase formed various meta-stable sulphide phases upon cooling obscuring phase relationships. Coupled with high temperature po, that segregates to 4C po and other Fe-Cu sulphides (py and violarite) upon cooling, equilibrium cannot be established without error. The slower cooled systems were stable at about 400-300°C. The system was now stable and no further major phases should form. Similar to in the quick quench system, in the slower cooled systems, the solid phases continued to segregate and exsolve until an equilibrium state was reached.

Table 3.4. B: Thermodynamic and phase transitions during slow cooling (900-400°C). The overall change in free energy was negative ($\Delta G < 1$), during the cooling and crystallization process. At t_4 the change in free energy is negligible to zero ($\Delta G = 0$), as the system reached a semi-stable state.

Temp. °C	Stage t	Entropy ΔS	Enthalpy H	Free E ΔG	Phase assemblages
1000-950	t_3	>0	-	-	mss, Cu-rich melt \pm PGE
950-900	$t_3 - t_4$	>0	-	-	iss, mss, bn \pm PGM
900	$t_3 - t_4$	>0	-	-	bn, mss, FeS, bn \pm PGM
850	$t_3 - t_4$	>0	-	-	Cu-rich liquid (iss) separates from mss
550	$t_3 - t_4$	>0	-	-	iss crystallizes as ccp and Fe-rich iss
550-400	$t_3 - t_4$	>0	-	-	iss re-equilibrates at lower temperatures to ccp and po
400: stable	t_4	0	0	0	po, bn, ccp, mss melt \pm PGM

3.3. Homogeneity and sample contamination

To illustrate homogeneity of the sample powders during the experimental procedure and the overall accuracy and precision of the experimental methods employed (that no PGE phases were formed in an earlier stage to contaminate system and alter results), the powders were analysed at various stages with XRD and WDS-SEM, see Table 3.5. (A and B). Experiment A was used as analogue for the mss system to determine possible pre-contamination of PGE- and/or PGE ligand nano entities.

Table 3.5. A: Composition of the sample powders during the various preparation stages of the samples. The powders were analysed throughout the experimental process with semi-quantitative XRD to check the accuracy and precision during preparation. XRD analysis throughout was essential to monitor when nano phases formed. If PGE nano phases formed during the initial stages, before step 4, the data cannot be used and any PGE nano structures measured might be a result of experimental artefact. No PGE nano artefacts were measured in the analyses. However the method was only semi-quantitative and it was possible that various nano structures could have formed at lower temperatures.

	Steps followed	Expected composition	XRD identified phases
Step 1	Appropriate concentration PGE liquid was added to the S powder. The powder was heated in a furnace to dry out the liquid.	S powder Pt	elemental S Pt-salt no nano phases id
Step 2	Selected concentration of As liquid was added to homogenised PGE-S powders. Powders were dried out again to evaporate the liquid.	S powder Pt As	elemental S Pt-salt As-salt no nano phases
Step 3	The powder was homogenised and relevant concentrations of Fe and Cu was added. The mixture was heated for 9 hours in silica tubes to 700°C and kept for several hours at 700°C and cooled again. The cooled samples were reground to homogenise the system again.	po bn Pt As	po bn elemental Pt elemental As no nano Pt phases
Step 4	The samples were split into smaller samples, sealed, heated to 950°C and kept between 1000-900°C for several hours	po melt	po melt
Step 5: Fast cooled	The tubes were quick quenched in a vertical furnace from 950-900°C to ambient temperatures.	po melt PGM	po polycrystalline sulphides PGM and nano Pt-phases
Step 5: Slow cooled	The samples were split into 200mg samples, sealed, heated to 950°C and cooled slowly over several days to form the final products.	po bn ccp melt pockets PGE phases	po bn ccp polycrystalline sulphides PGM and nano Pt-phases

The Scherrer equation (Akbari et al., 2011) and manual peak identification, see Chapter 2, was used to calculate the size of possible crystalline nano phases, in experiment A, that could have formed during the various experimental steps. Known phases were identified to serve as control measures including elemental Pt and As and PGE phases (sr and ifp).

From Table 3.5.B it seemed that crystalline nano platinum phases (avg. 140 nm) only formed in the final stages of sample preparations (step 5). The method was only semi-quantitative. It was thus possible that various nano structures (PGE-rich and/or non-PGE) could have formed in the experimental process. It remains a difficulty to track and monitor primary nano phase formation in the synthetic sulphide samples, as numerous structures form as a result of quenching, exsolution and segregation.

Table 3.5. B: The average size of nano PGE-ligand phases (nm), present during the preparation process. PGE-ligand phases only formed in step 5. During steps 1, 2 and 3 Pt was present as elemental Pt. The temperature during steps 1-3 was not high enough to form platinum-group element phases (PGM).

Nano XRD	Step 1	Step 2	Step 3	Step 4	Step 5: F	Step 5: S
Nano phases expected	Pt	Pt, As	Pt, As	n/a	sr, ifp	sr, ifp
Nano phases measured	Pt-salt	Pt-salt As-salt	Pt, As	n/a	sr	sr
Avg. size of nano entities	n/a		n.d.	n/a	141nm	140nm

Chapter 4: Mineralogy

The sulphide portion of a Fe-Cu-Ni \pm PGE deposit was mimicked in the experimental process. The sulphide melt, at equilibrium, contains about 10 000 times more PGE than the co-existing silicate melt (Mungall and Naldrett, 2008). The synthetic Fe-Cu sulphides were manipulated to form a po and melt phase. Po is one of the first sulphide minerals to form in a magmatic system (Mungall, 2005) and thus the more likely phase to carry PGE clusters. The outline, experimental set-up and associated processes of the PGE-As experiments are listed in Chapter 2 and 3. Please refer to Appendix C for enlarged images, WDS-SEM, SAM- and XRD data on major and minor phases.

4.1. Phase association

The ternary Fe-Cu-S system can yield three dominant high temperature solid solutions series above 400°C (Vaughan and Craig, 1978; Fleet, 2006). The three series are 1) po solid solution (mss) 2) intermediate solid solution (iss) and the 3) cct-dig-bn series (Vaughan and Craig, 1978). Experiments were manipulated to best present a mss series. Only limited phases can form within the set elemental concentration, pressure and temperature windows (Vaughan and Craig, 1978). The phase diagrams of the mss system, see Figure 4.1. (A and B), shows the possible phase associations at 900°C and 400°C. By plotting the relevant corrected concentrations of the starting mixture powders (Fe, S and Cu) used in the experiments, see Table 4.1., on the experimentally determined ternary diagrams (Kullerud et al., 1969), the possible stable phases were deduced.

Table 4.1.: Rounded values of starting powder composition (S, Cu and Fe) used for ternary phase diagram plots, see Figure 4.1. (A and B), to determine stable phases present at 900°C and 400°C.

Elements	Original values %	Rounded values %
S	35.357	35.00
Cu	17.185	17.00
Fe	47.406	48.00
Total	99.948%	100.00%

The S, Fe and Cu values are constant for experiments A, B and C. The heating procedures of the powders were essentially the same for both quick and slow cooled samples. Slow cooled samples were cooled to 400°C and quenched. The mss system is stable around

400°C (Stone et al., 1989). Phase assemblages in the synthetic samples were dependent on the temperature, sulphur fugacity (f_{S_2}) and cooling rate (quick or slow cooled) of the relevant system, as other variables (concentration, pressure, Eh-pH conditions) were constant throughout all experiments.

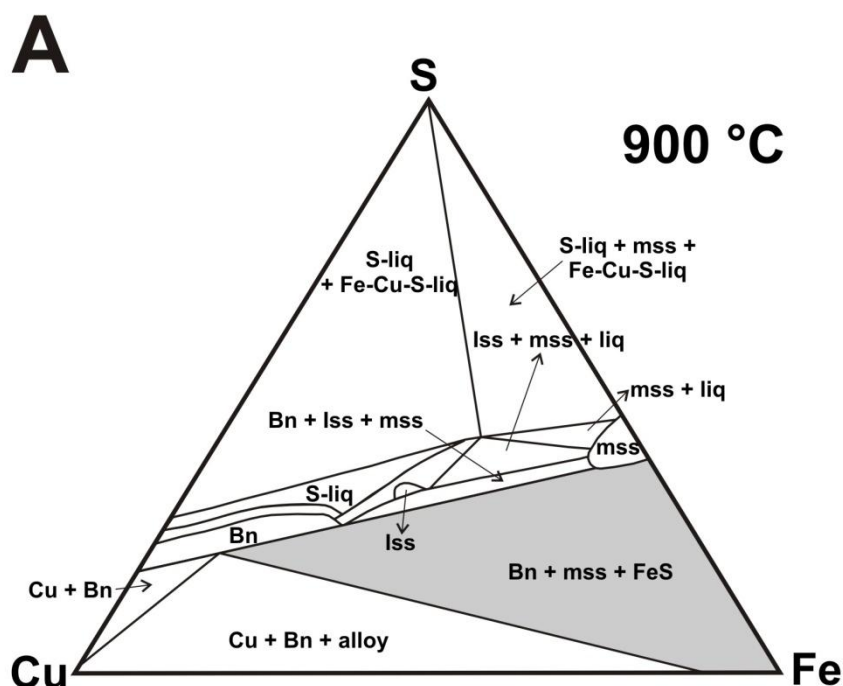


Figure 4.1. A: Phase diagram of the Fe-Cu-S system, at 900°C. The relevant system within the concentration range of the study, see Table 4.1. , is shown in grey. Bn, mss and FeS phases will form at 900°C. At 950°C the system is more simplistic with po (mss) and Cu-rich melt. Figure 4.1. A was adapted from Kullerud et al. (1969) as cited in Barnes and Lightfoot (2005). For mineral abbreviations used in Figures and Tables please refer to Mineral Compositions.

A mss or po ($Fe_{1-x}S$) and melt phase (liquid at time of quenching) should form in the quick quenched samples, around 950°C. A more complex phase assemblage was expected to form in the slower cooled samples with possible po, bn, ccp and \pm melt pockets. The characteristics of the phases expected to form in the mss system is summarised in Table 4.2.

The melt pockets in the slower cooled samples will form due to quenching from 400°C to ambient temperatures. The melt does to some extent possess a structural character on a molecular scale and a limited order (Calas et al., 2006). Changes in temperature and the chemical composition of a melt control its structural properties. The structure of a melt when cooled will rearrange as the chemistry of the melt changes (phases form). By quick quenching melts, it is possible to measure high temperature and pressure phases at ambient temperatures (Calas et al., 2006).

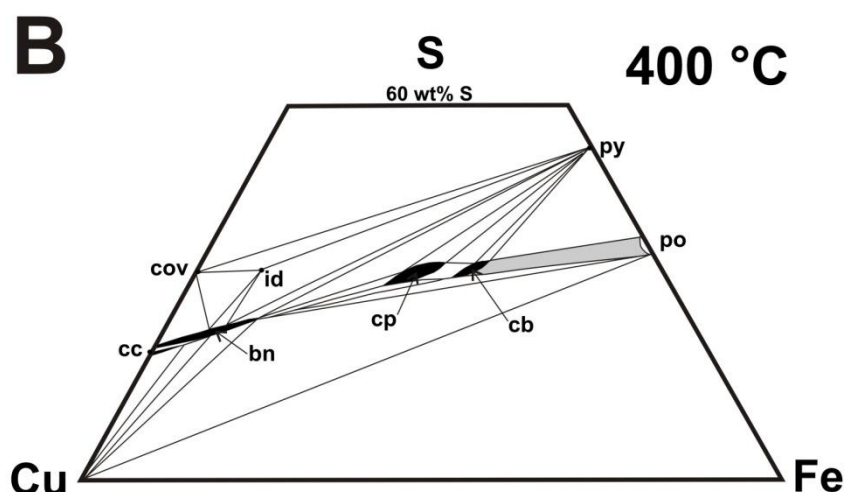


Figure 4.1. B: Phase diagram of the Fe-Cu-S system, at 400°C. The relevant system is shown in grey. With slower cooling the system has time to form more complex phase assemblages. At 400°C bn, ccp, po and melt phases are expected to form. Figure B was adapted from Yund and Kullerud (1966).

Table 4.2.: Chemical and physical properties, characteristics and occurrence of po, bn and ccp minerals, expected to form within the synthetic mss system. Po and a Cu-rich melt are expected to form in the quick quench systems. More complex phase associations were expected in the slower cooled samples with po, bn, ccp and Cu-rich melt. Data was adapted from Yund and Kullerud (1966), Craig and Scott (1974), Scott (1974), Anthony et al. (1990), Brennecke (2006), Fleet (2006), Wenk and Bulakh (2006) and Becker (2009).

	po	bn	ccp
Formula	Fe_{1-x}S $x=0$ (FeS) - 0.125 (Fe ₇ S ₈)	Cu_5FeS_4	CuFeS_2
Polymorphs	hexagonal, MC, NA, NC, 5C, 11C, 6C, monoclinic and anomalous	Low T: tetragonal High T and 2a: cubic x-bn: tetragonal	Low T: tetragonal High T (> 550°C): isometric
Wt.% elements	Fe: 62.33 Cu: up to 5.00 S: 37.67	Fe: 11.12 Cu: 63.33 S: 25.55	Fe: 30.43 Cu: 34.63 S: 34.94
Maximum Minimum thermal stability	1190°C 100°C	1100°C 228°C	557-547±5 °C
Crystal system	hexagonal or monoclinic or amorphous; depends on polymorph	tetragonal or cubic depends on polymorph orthorhombic or pseudo-cubic	tetragonal or cubic (synthetic)
Solid solutions	mss series	dig > 335°C ccp - high T bn cct-bn	iss series
Mineral association	py, mrc, ccp, pn, sulphides, mag, cal, dol	ccp, py, cal, wo, qtz and various Fe- and Cu-S	py, gn, sp and various Fe and Cu sulphides
Occurrence	High T hydrothermal, mafic igneous-, sedimentary- and contact metaphoric deposits, meteorites (tr), pegmatite	Cu-rich shales, pegmatite, mafic igneous rocks, disseminated sulphides, med-high temperature hydrothermal deposits	Cu minerals, massive and disseminated sulphides, hydrothermal veins, stockwork, exsolution product

4.2. Major phases

The experimental system behaved accordingly to form different phases (melt and crystalline) and segregation textures. The quick quench samples had more simplistic phase association in comparison with the slower cooled samples. Quick quench samples consisted of large po (Fe_{1-x}S) stringers trapped in a semi-crystalline to amorphous Cu-rich melt ($\text{Fe}_x\text{Cu}_x\text{S}_x$) matrix, see Figure 4.2. (A-D). The po (FeS) phases were poorly crystallized to massive, as observed in natural ores, due to displacement of metal atoms in the solid solution series and quenching. Cu-rich melt inclusions were measured in the po phases. The melt inclusions formed due to quick quenching, trapping incompatible elements such as PGE and Cu in the mss phase, making them the ideal place to hunt for PGE clusters.

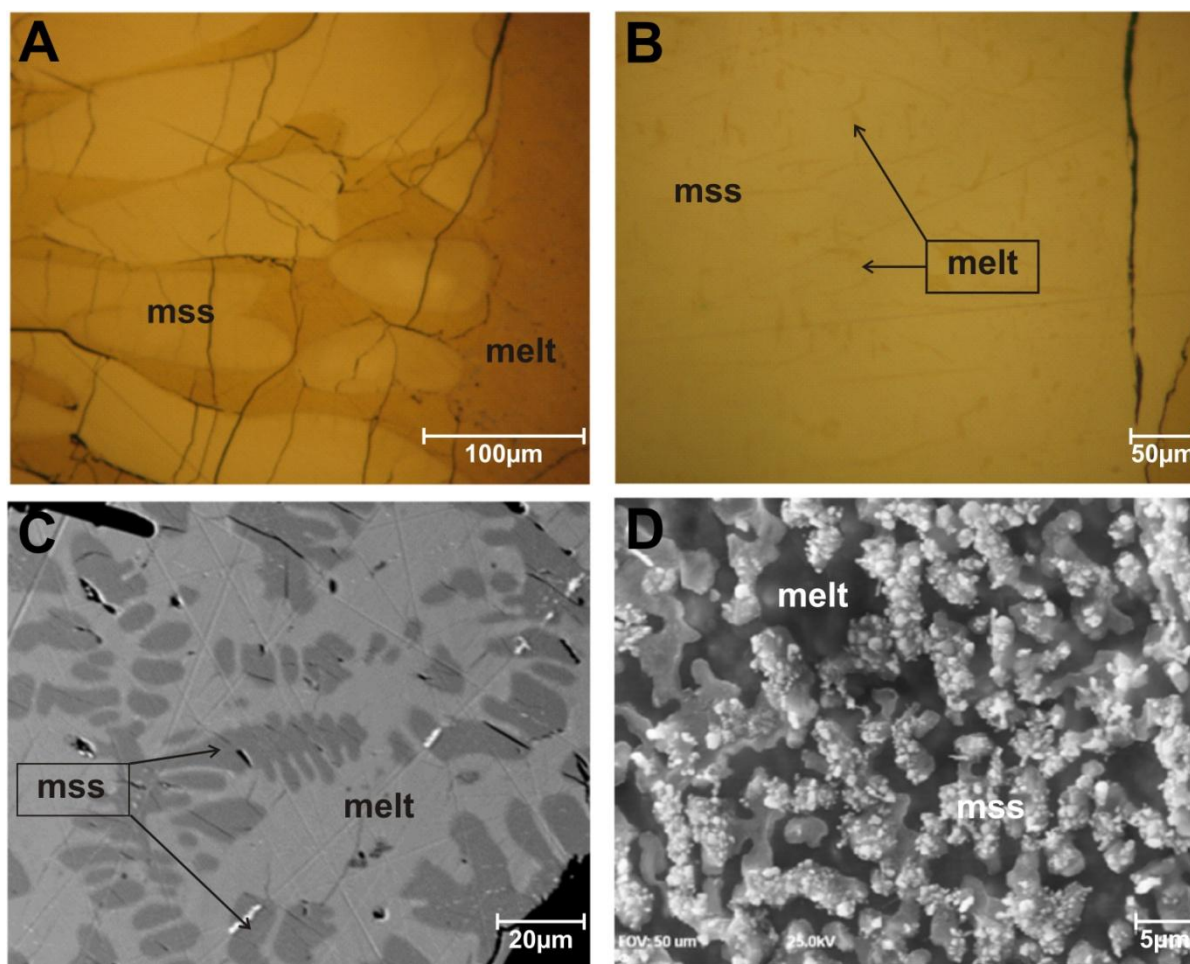


Figure 4.2. A-D: Phase association of fast cooled samples from experiment A. The samples consisted of po in a Fe-melt matrix with \pm platinum-group element (PGE) phases. A: Po (Fe_{1-x}S) stringers surrounded by an amorphous Fe-melt phase ($\text{Fe}_x\text{Cu}_x\text{S}_x$). B: Cu-rich melt exsolutions trapped in mss (po), due to quick quenching. C: Backscatter electron (BSE) image of po (dark grey) surrounded by Cu-rich melt. The white phases are Cu-rich entities. D: BSE of an unpolished sample from experiment A, taken with scanning Auger microscope (SAM). Higher resolution highlights various secondary phases and exsolutions in/on the po (light grey) phase.

The slower cooled samples formed an intricate phase association of bn, ccp, po, melt pockets and \pm PGE (PGM) phases, see Figure 4.3. A-D. Fe and Cu could be extracted, from the melt and mss during cooling, to form bn and ccp. The po phases in the slower cooled samples exhibited lower Cu values and higher concentrations of Fe. The po phases also showed Cu-rich melt exsolutions or segregations but did not measure as high concentrations of Cu as the quick cooled samples. Melt pockets were not prominent but did form in several samples. The samples were not entirely equilibrated before removal from the oven and a melt phase was thus still present. The composition of major phases measured in the experiments, as determined by WDS-SEM and XRD, is given in Table 4.3.

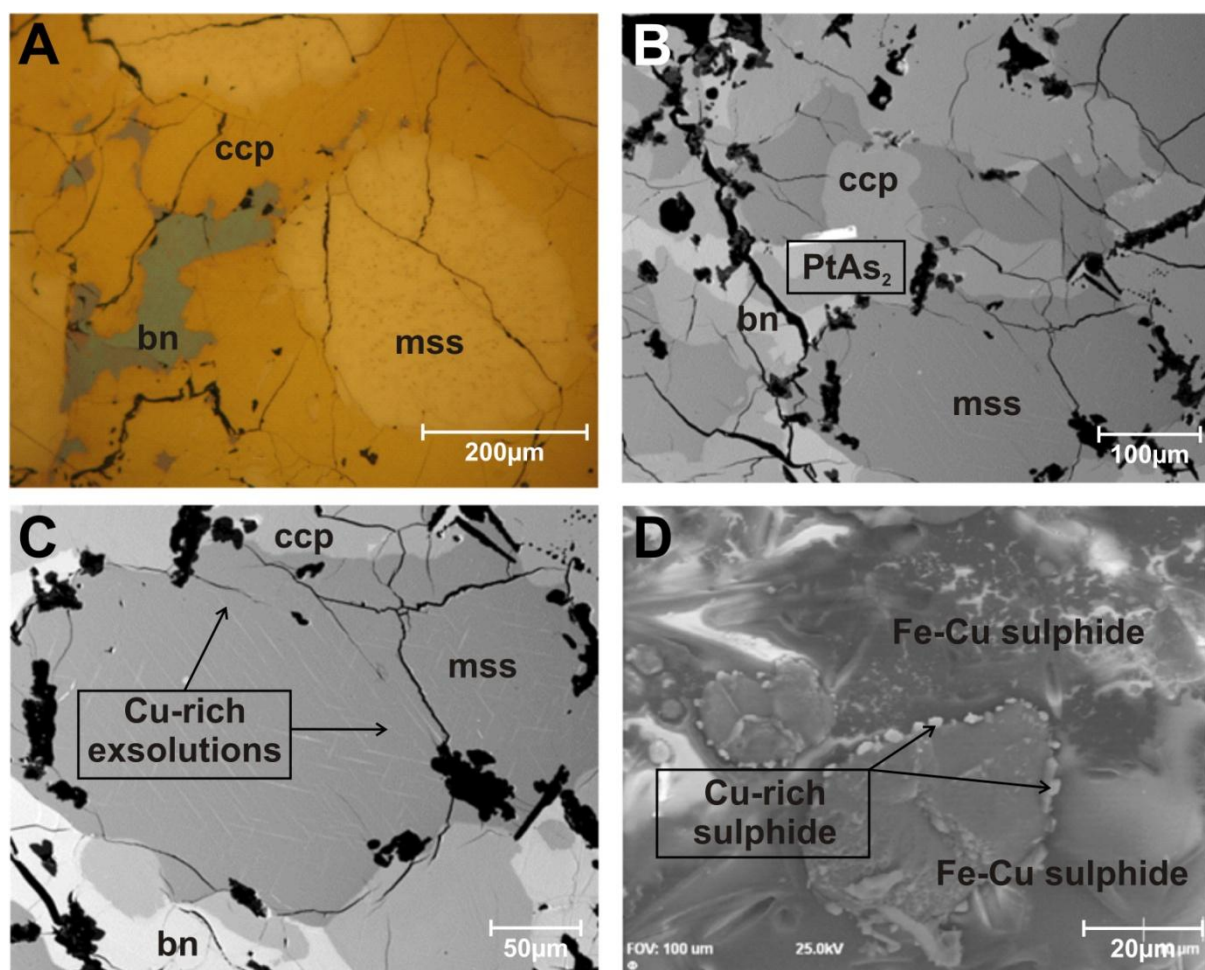


Figure 4.3. A-D: Phase assemblages that formed in the slower cooled samples of experiment A. The slower cooled samples showed more phases than the quick quench samples with po (Fe_{1-x}S), bn (CuFeS_2), ccp (Cu_5FeS_4) Cu-rich melt ($\text{Cu}_x\text{Fe}_x\text{S}_x$) and large euhedral platinum-group phases (PGM). The platinum phases included PtAs_2 and/or Pt_3Fe . The system had longer time to equilibrate to form stable phases. **A:** Example of the phase associations of the slower cooled samples with po, bn, ccp and Pt-phase (PGM). **B:** Backscatter electron (BSE) image of the slower cooled samples, with po, bn, ccp and Pt-phases (white phase). **C:** BSE image of po with exsolution textures. **D:** BSE image, taken with scanning Auger microscopy (SAM), of unpolished samples from a slow cooled sample. Large well rounded Fe-Cu sulphide phases with Cu-rich phases (possible ccp or bn) round its edges, surrounded by a sea of various Cu-Fe sulphides.

Table 4.3.: The average composition of the major phases, measured in the samples of experiment A, B and C, as determined with quantitative wavelength dispersive scanning electron microscopy (WDS-SEM), and reference sets (Anthony et al. 1990). Quick quenched samples showed two major phases; a po and Cu-rich Fe-melt with \pm platinum-group phases (PGM). The phase associations of the slower cooled systems were more complex forming po, bn, ccp and Cu-rich melt with \pm platinum-group element phases.

		melt	po	bn	ccp
Exp. A fast	wt.%	$\text{Cu}_{30}\text{Fe}_{38}\text{S}_{32}$	$\text{Cu}_5\text{Fe}_{58}\text{S}_{38}$		
	Formula	$\text{Cu}_1\text{Fe}_1\text{S}_2$	$\text{Fe}_{0.9}\text{S}_1$		
Exp. A slow	wt.%	$\text{Cu}_{26}\text{Fe}_{42}\text{S}_{32}$	$\text{Cu}_4\text{Fe}_{61}\text{S}_{37}$	$\text{Cu}_{56}\text{Fe}_{16}\text{S}_{28}$	$\text{Cu}_{27}\text{Fe}_{39}\text{S}_{35}$
	Formula	$\text{Cu}_1\text{Fe}_2\text{S}_3$	$\text{Fe}_{0.9}\text{S}_1$	$\text{Cu}_3\text{Fe}_1\text{S}_3$	$\text{Cu}_1\text{Fe}_2\text{S}_3$
Exp. B fast	wt.%	$\text{Cu}_{38}\text{Fe}_{29}\text{S}_{32}$	$\text{Cu}_2\text{Fe}_{60}\text{S}_{38}$		
	Formula	$\text{Cu}_1\text{Fe}_1\text{S}_2$	$\text{Fe}_{0.9}\text{S}_1$		
Exp. C fast	wt.%	$\text{Cu}_{22}\text{Fe}_{41}\text{S}_{36}$	$\text{Cu}_1\text{Fe}_{59}\text{S}_{39}$		
	Formula	$\text{Cu}_1\text{Fe}_2\text{S}_3$	$\text{Fe}_{0.9}\text{S}_1$		
tr	FeS wt.%		$\text{Fe}_{62.70}\text{S}_{35.40}$ $\text{Fe}_{63.0}\text{S}_{35.0}$ $\text{Fe}_{63.53}\text{S}_{36.47}$		
po	Fe_{1-x}S wt.%		$\text{Fe}_{60.18}\text{S}_{39.82}$ $\text{Fe}_{59.83}\text{S}_{39.55}$ $\text{Fe}_{61.57}\text{S}_{38.53}$		
bn	CuFeS_2 wt.%			$\text{Cu}_{62.99}\text{Fe}_{11.23}\text{S}_{25.58}$ $\text{Cu}_{63.33}\text{Fe}_{11.12}\text{S}_{25.55}$	
ccp	Cu_5FeS wt.%				$\text{Cu}_{35.03}\text{Fe}_{31.00}\text{S}_{34.96}$ $\text{Cu}_{34.63}\text{Fe}_{30.43}\text{S}_{34.94}$

The average composition of the phases measured in experiments A, B and C, as well as reference standards, were plotted on the ternary Fe-Cu-S diagram, see Figure 4.4. The synthetic phases plotted close to the reference standards indicating that the system as a whole reacted successful and that the results were representative of a natural sulphide system.

Po forms a complete solid solution series between 1190-308°C (Craig and Scott, 1974) or from 1C to lower temperature 4C po, see Table 4.4. Different types of po formed in the mss systems, see Table 4.1. Po formed in the synthetic samples and not py due to 1) the Fe:S ratio that was not high enough to form py and 2) the experiments were conducted under extreme temperatures (heated to 1050°C), py typically only forms around 800-900°C. The average Fe content of the po phases was lower than predicted by the Fe:S ratio of 1:1. This was due to high concentrations of Cu that were substitute for Fe in the po lattice (Deer et al., 1966). The Cu content of po is dependent on the temperature of the system (Vaughan and Craig, 1978). Cations such as Co and Ni exhibit similar behaviour. The high temperature po (stable between 400-1000°C) should be expressed as Fe_7S_8 or Fe_{1-x}S ($x=0-0.125$) (Deer et al., 1966).

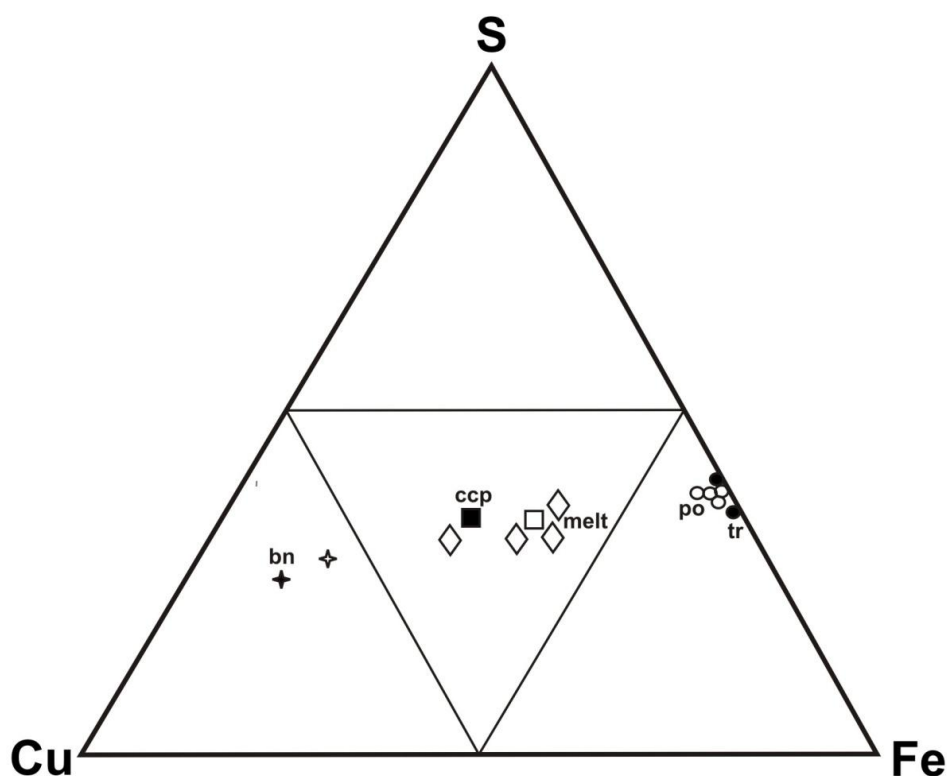


Figure 4.4.: The average composition of po, melt, ccp and bn phases (open figures) and several standards (solid figure) plotted on the ternary Cu-Fe-S phase diagram. The synthetic phases plotted in the vicinity of the corresponding reference standard. Correspondence with references samples indicated that the experiments reacted successfully and that the results were representative of a sulphide system. The synthetic po or mss had slightly higher Cu concentrations but corresponded well with the reference po and tr. The melt phase (amorphous to semi-crystalline) plotted close to ccp standard. The synthetic bn were overall less Cu-rich than the standards.

The high temperature hexagonal 1C po is the dominant po phase in the samples. However 1C po is not stable upon quenching and will segregate upon cooling to more stable monoclinic po. The quenched po will not have the same characteristic Ni-As super-structure of high temperature po ($\pm 1000^\circ\text{C}$). The quenched po exhibited structural transitions, distortions and breakdown structures due to the rapid quenching (Vaughan and Rosso, 2006).

Table 4.4.: The pyrrhotite (po) solid solution series, between 1190°C and 308°C . Hexagonal 1C po will form in the samples at 1000°C . The 1C po is not stable upon quick cooling and will segregate into more stable monoclinic po with cooling. Similar po compositions (Fe=46-47at.%) were measured in the slower cooled samples of experiment A. The data was taken from Craig and Scott (1974), Wuensch (1974), Becker (2009), Vaughan (2006) and De Villiers and Liles (2010).

Po	Formula	at.% Fe	Thermal minimum $^\circ\text{C}$	Thermal maximum $^\circ\text{C}$	Occurrence	Crystal structure
1C	Fe_{1-x}S	44.9-50.00	308~100	1190	synthetic	hexagonal
2C	FeS	49.5-50.00	-	<147	natural	hexagonal

Table 4.4. cont.: The pyrrhotite (po) solid solution series, between 1190°C and 308°C.

Po	Formula	at.% Fe	Thermal minimum °C	Thermal maximum °C	Occurrence	Crystal structure
MC	Fe _{1-x} S	47.4-44.7	262	308	synthetic	hexagonal
NA 3C	Fe _{1-x} S	47.2-47.8	209	<262	synthetic	hexagonal
5C	Fe ₉ S ₁₀	47.2-48.1	-	<209	natural	hexagonal
11C	Fe ₁₀ S ₁₁	47.2-48.1	-	<209	natural	orthorhombic
6C	Fe ₁₁ S ₁₂	47.2-48.1	-	<209	natural	monoclinic
Meta-stable	Fe _{1-x} S	0.06<x>0.03	meta-stable		natural	hexagonal
4C	Fe _{7+x} S ₈	46.4-47.3	~115	<254	natural	monoclinic
Anoma-lous	Fe _{7+x} S ₈	46.4	-	?	natural	triclinic

From the WDS-SEM results coupled with XRD analysis quick cooled samples measured monoclinic 4C and 5C po, with ± hexagonal po. The slower cooled samples in contrast measured hexagonal po. Po from faster cooled samples was more Cu-rich over slower cooled samples and measured up to 7wt.% Cu with quantitative WDS-SEM, see Table 4.5.

Table 4.5.: The average composition of po in the various experimental systems (PGE: Pt, Pd, Ru), as determined with semi-quantitative scanning electron microscopy (SEM). The po were Cu-rich, up to 7wt.% (avg. 5wt.%). Elevated Cu values are not uncommon for high temperature po (Vaughan and Craig, 1978). Monoclinic 4C and 5C po was the dominant po polymorph in the quick cooled samples. The quick cooled samples measured both monoclinic and hexagonal po. Quick quenching caused high temperature hexagonal 1C po to convert to monoclinic po. The slower cooled samples of experiment A showed hexagonal po with <3wt.% Cu (avg. 1.6wt.%).

	Exp. A: Pt fast	Exp. A: Pt slow	Exp. B: Pd fast	Exp. C: Ru fast
Composition (at.%) WDS-SEM	Cu ₄ Fe ₄₅ S ₅₁	Cu ₂ Fe ₄₈ S ₅₀	Cu ₁ Fe ₄₇ S ₅₂	Cu ₀ Fe ₄₆ S ₅₄
Composition	Fe _{1-x} S	Fe _{1-x} S	Fe _{1-x} S	Fe _{7+x} S ₈
Metal(X): S	X ₄₉ S ₅₁	X ₅₀ S ₅₀	X ₄₈ S ₅₂	X ₄₆ S ₅₄
Po polymorph	5C	4C	5C	tr, 4C

4.3. Minor- and PGE phases

PGE phases (PGM) were poorly crystallised in the fast quenched samples. No Pd-phases or Ru-phases have yet been picked-up in any fast cooled samples. Although no PGE phases were picked up with WDS-SEM high concentrations of Pd and Ru was measured in the mss and melt phases, with semi-quantitative SAM. The synthetic samples of experiment A measured Pt phases, see Figures 4.5. and 4.6. The spot-like PGE crystals, between 0.5-1µm, has thus far only been observed in the Cu-rich melt phases, see Figure 4.5. A and B.

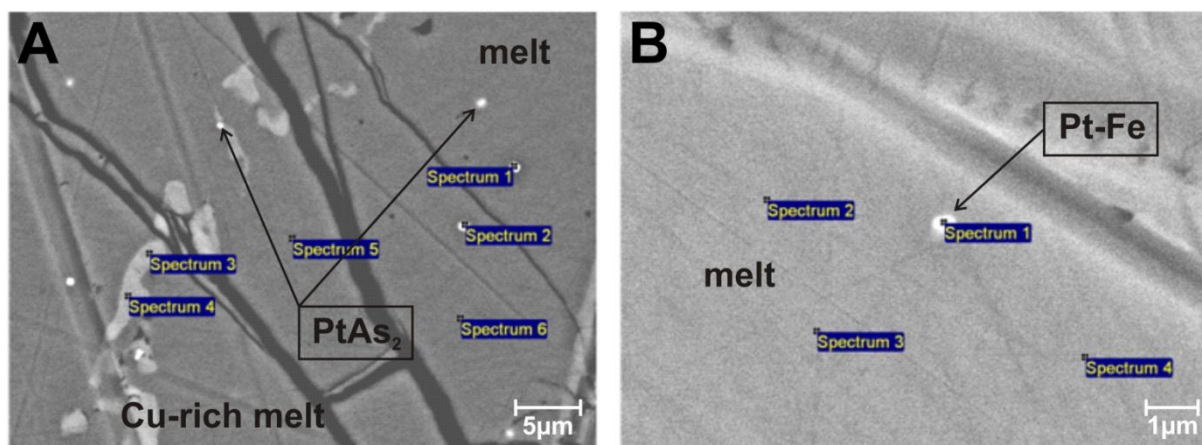


Figure 4.5. A and B: Pt-rich (PGM) phases present in the fast cooled samples of experiment A. The Pt-phases were spot-like and poorly crystallised. The phases ranged from 0.5-1µm in size, showed no distribution trends and have thus far only been measured in the Cu-rich melt phase. **A:** Backscatter electron (BSE) image of PtAs₂ (bright white spots) mineralisation and distribution in the Cu-rich melt. **B:** BSE image of a Pt_xFe_x (bright white spot) in melt, measured in the As poor sample A2f. The spot-like PGE-phases were poorly crystallized and showed no distribution trends.

The slower cooled samples of experiment A showed large Pt phases (between 0.5-30µm) and compared well with size, shape and distribution of a natural system. The Pt-phases, sr (PtAs₂) and ifp (Pt₃Fe) were measured in the ccp (FeCuS₂) and bn (Cu₅FeS₄) phases, see Figure 4.5. In the samples with no As ligand Pt-Fe PGM crystallised. The Pt-phases showed no distribution patterns and ranged from spot-, skeleton- to perfect euhedral crystals. The characteristics of the Pt-phases measured in samples from experiment A, as identified with WDS-SEM, are tabulated in Table 4.6.

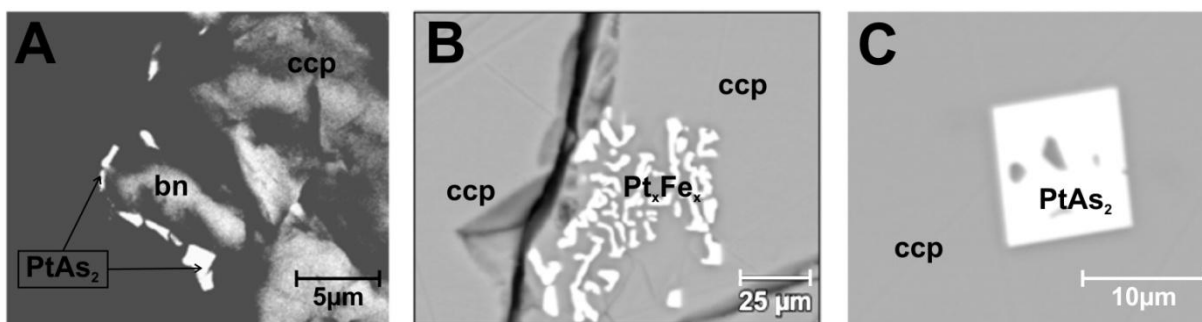


Figure 4.6. A-C: The different size, shape and distribution of Pt-phases (PGM), measured in the slow cooled samples. **A:** Backscatter electron (BSE) image of PtAs₂ crystals on the borders of ccp and bn, sample A1s (300 ppm Pt, 280 ppm As). The system showed a variety of PtAs₂ crystals, ranging from perfect euhedral to skeleton to irregular growths. The average size of the Pt-phases were between 5-50µm. **B:** BSE image of Pt_xFe_x crystals in ccp, sample A2s (300 ppm Pt, no As). The system was devoid of a chalcogene ligand (As) and used Fe to form various shaped phases with Pt (10-15µm). **C:** BSE image of PtAs₂ crystals in ccp, sample A3s (30 ppm Pt, 30 ppm As). Although the system had low concentrations of Pt and As, large cubic Pt-phases up to 10µm, were measured in the samples.

Table 4.6.: Characteristics of the Pt-phases (PGM) identified in the samples of experiment A, measured with x-ray spectrometry (XRD) and scanning electron microscopy (SEM). Measured sperrylite (PtAs₂) values conformed well to literature sources however the isoferroplatinum (Pt₃Fe) values differed considerably from cited sources. Only semi-quantitative energy dispersive scanning electron microscopy (EDS-SEM) scans were run, with in-house standards, on the samples in question. Data was adapted from Berlincourt et al. (1981), Cabri (1981, 2002) and Anthony et al. (1990).

Mineral		Sperrylite	Isoferroplatinum
Ideal formula		PtAs ₂	Pt ₃ (Fe,Cu)
General formula		(Pt,Rh)(As,Sb,S) ₂	(Pt,Pd) ₃ (Fe,Cu)
Wt.% elements literature		Pt: 56.56 As: 43.44	Pt: 91.29 Fe: 8.71
Avg. wt.% elements measured	Fast	Pt: 56 As: 44	n/a
	Slow	Pt: 52 As: 48	Pt: 84 Fe: 16
Avg. size	Fast	± 0.8µm	None measured
	Slow	± 16µm	± 12µm

The Pt-phases were phase dependent. Pt-phases have only been measured in the melt phases of quick cooled samples and more Cu-rich Fe-sulphides. The distribution is illustrated in Table 4.7.

Table 4.7.: The distribution and size of Pt-phases (PGM) measured in the samples of experiment A. A Pt-phase present in a phase is indicated with an x. In the quick quenched samples the PGM were only detected in the melt phase and were poorly mineralised. PGM was measured in the ccp and bn phases of the slower cooled samples. In systems where no As was added, Pt-Fe PGM formed instead. The size and shape of the Pt-phases were dependent on cooling time and not on the Pt concentration added.

Pt-phase distribution	sperrylite			isoferroplatinum			Avg. size µm
	po	melt		po	melt		
A1f		x					1.0
A2f	No As added				x		Poorly crystallised
A3f		x					0.6
	po	ccp	bn	po	ccp	bn	
A1s		x	x				16.7
A2s	No As added				x	x	12.0
A3s		x	x				Poorly crystallised

4.4. Nano mineralogy

It is possible that numerous PGE nano phases and crystalline entities formed in the synthetic samples. The nano phases may serve as precursors for PGM formation however precipitation directly from a melt, at magmatic temperatures, has yet to be proven

successfully experimentally (Helmy et al., 2013). XRD analysis paired with the Scherrer equation was used to calculate the average size of predetermined PGE-phases (PGM), smaller than 1000nm. The predetermined PGE phases was chosen in accordance with available ligands (S, Fe, Cu, As) and overall chemistry of the specific system. The larger scale PGE-phases, measured with WDS-SEM, was used as guide to determine which nano PGE-phases might be expected to form in the synthetic samples. The method was only effective if the nano phase was crystalline (XRD fingerprint). Unfortunately no conclusive evidence of nano phases could be derived from XRD analysis. Due to the structures' extreme small scale it could not be proven beyond a doubt that calculated PGE entities were indeed nano PGE-phases (PGM) and not an artefact of noise, strain and/or pattern shift. A detailed description of possible crystalline and non-crystalline nano features is given in Chapters 6.

4.5. Summary

Fast cooled samples showed two phases; a Cu-rich Fe-melt ($\text{Fe}_x\text{Cu}_x\text{S}_x$) and a crystalline mss (Fe_{1-x}S) phase with \pm PGE-phases (PGM). Slower cooled samples had a more complex phase association, with mss ($\text{Cu}_{0.05}\text{Fe}_{0.94}\text{S}_1$), bn ($\text{Cu}_{2.9}\text{Fe}_1\text{S}_{3.2}$), ccp ($\text{Cu}_1\text{Fe}_{1.8}\text{S}_{2.8}$), melt ($\text{Cu}_1\text{Fe}_{1.8}\text{S}_{2.6}$) and PGE phases. PGE phases have only been measured in the fast cooled samples of the Pt-As system (experiment C). No PGE-phases (PGM) has yet been picked up in the fast cooled samples of experiments B and C. The Pt-phases have thus far only been observed in the melt phase of the fast cooled samples and in the ccp and bn phases of the slower cooled samples. However a variety of nano (<1000nm) PGE phases were identified in the synthetic samples by aid of XRD. In the Pt-As and Pd-As systems As- and Fe-rich PGE were present. Ru in contrast preferred to form bonds with S and Cu over As and Fe. A summary of the phase associations of quick and slow cooled samples from experiment A, B and C is given in Tables 4.8.

Table 4.8.: Summary of the synthetic mono-sulphide solid solution (mss) system. Fast and slow cooled samples measured different phase assemblages. Slower cooled samples had a more phases and measured large platinum-group element phases (PGM) of up to 50 μm . Fast cooled samples consisted of po and melt with poorly crystallised PGE-phases.

	Fast cooled	Slow cooled
Description of sample	Elongated mss stringers in melt. Melt and exsolutions in mss.	Clearly distinguishable phases. Melt and bn exsolutions in mss.
Phases	<ul style="list-style-type: none"> mss (po): Fe_{1-x}S melt phase: $\text{Fe}_x\text{Cu}_x\text{S}_x$ \pmPGE-phases (PGM) 	<ul style="list-style-type: none"> mss (po): Fe_{1-x}S melt phase: $\text{Fe}_x\text{Cu}_x\text{S}_x$ bn: Cu_5FeS_4 ccp: CuFeS_2 \pmPGE-phases (PGM)

Table 4.8. cont.: Summary of the synthetic mono-sulphide solid solution (mss) system.

	Fast cooled			Slow cooled		
	Exp A	Exp B	Exp C	Exp A	Exp B	Exp C
PGE phases	sr: Pt₁As₂ ifp: Pt₃Fe	No Pd-PGM was picked-up in any samples thus far.	No Ru-PGM was picked-up in any samples thus far.	sr: Pt₁As₂ ifp: Pt₁Fe_{1.5}	No samples prepared.	
Shape of PGE phases	High density spots			skeleton isometric to perfect euhedral		
Avg. size of PGE phases	0.5-10µm			0.5-50µm		
Phases in which PGE phases occurred	melt phase			ccp and/ or bn		

Chapter 5: Geochemistry

Geochemistry parameters were used to check the overall accuracy and precision of the experimental process and how reproducible the results were as a whole. The monitored parameters included 1) S-fugacity (f_{S_2}) 2) metal:S ratio and 3) partitioning coefficient (D-value). Comparing and statistically modelling the entities against natural systems and set references the average deviation and precision was deduced. Tables and calculations on geochemical parameters are given in Appendix D.

5.1. Sulphur fugacity

The S-fugacity (f_{S_2}) and metal:S ratio, of the composition of the starting mix of the experimental systems, influences the chemical behaviour of chalcogens and semi-metal elements; determining whether the elements will act as electron acceptors or electron donors or both (Helmy et al., 2010). In the synthetic mss system, upon heating, the elemental S, Fe, Cu, As and PGE will change oxidation state. The metals should oxidise to cations (Fe^{2+}/Fe^{3+} , Cu^{1+}/Cu^{2+}) and S will be reduced to an anion state S^{2-} . Helmy et al., 2010 reported that with an increase in the S:metal ratio, the bulk cation ratio will increase with an increase in f_{S_2} . An increase in f_{S_2} is coupled with a fall in the atomic metal:S ratios in the sulphide phases.

Po ($Fe_{1-x}S$) was used to calculate the $-\log f_{S_2}$ of experimental and natural systems (Toulmin and Barton, 1964; Fleet 2006; Mengason et al., 2010). The S-activity (f_s) is determined by comparing set experimentally determined fugacity values of po against measured Fe:S ratios (0.910-1.000) at specific temperatures (Vaughan and Craig, 1978). High temperature po can substitute concentrations of up to 5 wt% Cu, (Vaughan and Craig, 1978) and at higher temperatures (900-1000°C) up to a maximum of 7 wt% Cu (Kullerud, 1968, as cited in Mengason et al., 2010) into its crystal lattice. The $Fe_{1-x}S$ po has empty octahedral sites that can substitute Fe^{+2} with Cu^{+1} (Mengason et al., 2010).

To compensate for the concentrations of Cu, the true metal:S ratio is given by the equation $Fe+Cu:S$. The calculated f_{S_2} (Cu-correction method of Mengason et al. 2010) of the experiments A, B and C are given in Table 5.1. The po compositions were measured using WDS-SEM, within a week of removing samples from the evacuated tubes.

Table 5.1.: Calculated sulphur fugacity (fS_2) of experiment A, B and C and reference sets. The fast cooled samples correlated well with each other and had an average $\log fS_2 \approx -2$. Slower cooled samples showed lower fugacity values of $fS_2 \approx -14$.

FAST: 950°C	Avg. Cu wt.% po	fS_2	SLOW: 400°C	Avg. Cu wt.% po	fS_2
Exp. A fast	5.40	-1.8 ± 0.55	Exp. A slow	3.54	-13.8 ± 1.30
Exp. B fast	1.80	-2.0 ± 0.70			
Exp. C fast	1.67	-0.5 ± 0.20			
Hattori (1996): 973°C	2.52	-1.5			
Hattori (1996): 856°C	6.19	-1.0			

The calculated fS_2 compared well with the reference sources and plotted against temperature, see Figure 5.1. The samples, fast and slow cooled, plotted within the $Fe_{1-x}S$ (po) stability field indicating that the system reacted sufficiently to form the desired po phase. Fugacity was constant over the different systems however it different greatly within cooling frame, see Table 5.1. A difference was expected as fugacity is a function of temperature.

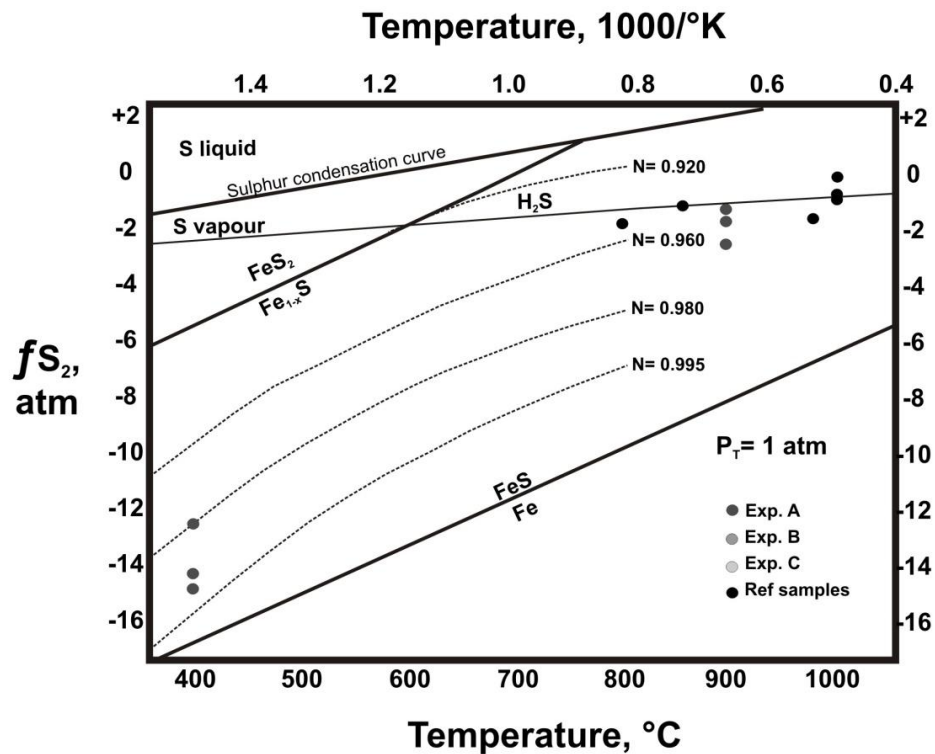


Figure 5.1.: Phase stability as a function of temperature and sulphur fugacity (fS_2). The calculated fS_2 was plotted against temperature, at 1 atm. The synthetic samples plotted in the po ($Fe_{1-x}S$ -FeS) stability field and compared well with fS_2 of reference standards from similar systems. This indicated that the overall chemistry and fugacity of the experiments reacted as anticipated to form mss (po) and associated phases. Figure and reference sets were adapted from Toulmin and Barton (1964), Barton and Skinner (1967) as cited in Popp et al. (1977), Scott (1968) as cited in Scott (1974), Lusk and Bray (2002) as cited in Fleet (2006).

The synthetic mss reacted as expected and plotted within the Fe_{1-x}S stability range. The results compared well overall with values obtained from Mengason et al. (2010), Luhr et al. (1984) and Hattori (1996) as cited in Mengason et al. (2010). The gap between the f_{S_2} of the quick- (900-1000°C) and the slower (400°C) cooled samples was expected as f_{S_2} is a function of temperature. The oxygen fugacity (f_{O_2}) and f_{S_2} increases exponentially with an increase in temperature (Barton and Skinner, 1979 as cited in Brimhall and Crerar, 1987).

5.2. The metal:S ratio

The metal:S ratio, see Table 5.2., is the sum of the measured at.% of Pt, Cu and Fe measured against the at.% S and As. The deviation was measured in the mss- and melt phases using WDS-SEM. The measured points were taken at random, see Table 5.2. The metal: sulphide ratio was used to predict how the system reacted as a whole and if chalcogene ligand As was present as anion (As^{-1}) to form phases with Pt cations (Pt^{+n}). The average measured metal:S ratios was higher than 1. This was a positive indication that As acted as anion in the melts.

Table 5.2.: The average metal:S ratio measured in fast and slow cooled samples, from experiment A, B and C. The deviation between mss and melt was on average $\pm 15\%$, with a near perfect 1:1 ratio in the majority of the samples.

Experiment		Avg. measured metal:S ratio		Average metal:S ratio
		mss	melt	
Avg. Experiment A: Pt	fast	0.9736	1.1802	1.0769
	slow	0.9840	1.0963	1.0268
Avg. Experiment B: Pd	fast	0.9263	1.1537	1.0400
Avg. Experiment C: Ru	fast	0.8611	0.9492	0.9051

5.3. Partitioning coefficients

The Nernst partitioning coefficient (D) measures the tendency a certain metal or element has for a specific phase, at a set temperature, pressure and fugacity (Palme, 2008). Ideally the metal will segregate into the more compatible phase. The D values can be used for measuring concentration or affinities for the incompatible phase. By measuring the incompatible behaviour against set values, conclusions can be drawn as how the system reacted and in certain cases where the PGE concentrated. The measured and reference sets of D^{PGE} and D^{As} between mss and sulphide melt (sm), at 900-1000°C, is given in Table 5.3.

Table 5.3.: Differentiation values ($D_{\text{mss/melt}}^{\text{PGE}}$) of the platinum-group elements (Pt, Pd and Ru) and As at 900°C, between mss and melt, taken from assorted literature sources. The reference values were used as comparison for the synthetic systems to determine how successful and representative the results were in comparison to a natural system. An absolute metal:S ratio of 1 was not achieved and not all the metal was thus in anion form to react. The D^{Pt} and D^{Pd} and tended to be more compatible in the melt phases over mss. Ru displayed opposite trends being overall more compatible in the mss than melt phase.

Element		Sample	D-value: Measured	D-value: Literature	Reference
Pt	$D_{\text{mss/sm}}^{\text{Pt}}$	A1f	0.939	~ 0.120 to 0.035-0.052	Bockrath et al. (2004) Mungall et al. (2005) as cited in Simon and Ripley (2011)
		A2f	0.330		
		A3f	0.628		
		Avg. A	0.632		
Pd	$D_{\text{mss/sm}}^{\text{Pd}}$	B1f	0.348	~0.140 to 0.072-0.120	Bockrath et al. (2004) Mungall et al. (2005) as cited in Simon and Ripley (2011)
		B2f	n.d.		
		B3f	0.333		
		Avg. B	0.341		
Ru	$D_{\text{mss/sm}}^{\text{Ru}}$	C1f	> 1	~9.000 to 8.710-17.430	Bockrath et al. (2004) Mungall et al. (2005) as cited in Simon and Ripley (2011)
		C2f	> 1		
		C3f	b.d.l.		
		Avg. C	> 1		
As	$D_{\text{mss/sm}}^{\text{As}}$	Pt	0.301	~0.400	Helmy et al. (2010)
		Pd	1.118	-	No reference
		Ru	1.596	-	

From Table 5.3. and 5.4. it was evident that Pt, Pd and Ru behaved differently in the synthetic melts. Arsenic's behaviour seemed to change depending on the PGE present. The deviation in partitioning behaviour of Pd- and Pt- vs. Ru system was likely due to the diverse chemical, physical and geochemical tendencies of the IPGE (Os, Ir, Ru) vs. PPGE (Rh, Pt, Pd). The IPGE tends to segregate into the early crystallising phases. PPGE is associated with the residual melt.

Pt and Pd showed similar distribution trends being more compatible in the Cu-rich melt phase. Pt stayed entrapped in the melt independent of sulphur fugacity or cooling window. No apparent trend with regards to Pt and Pd distribution could be distinguished. As distribution in the Pd samples were roughly equally distributed between mss and melt, being only slightly more compatible in the mss phase ($D_{\text{mss/melt}}^{\text{As}}=1.118$).

In the Pt samples As displayed different trends with a change in sulphur fugacity and cooling window. At high f_{S_2} ($\log f_{\text{S}_2}=\pm -2$) the $D_{\text{mss/melt}}^{\text{As}}=0.3$ and at lower f_{S_2} ($-\log f_{\text{S}_2}=\pm -14$) $D_{\text{mss/melt}}^{\text{As}}=1.04$. The change in As behaviour could have been due to the elements ability to

change oxidation state with a change in fugacity of the system over time as the system cooled. At higher fS_2 the system was more oxidising and As acted as an electron donor.

Similar results were reported by Helmy et al. (2010). In the study they suggested that the extreme log linear change difference in $D_{\text{mss/melt}}^{\text{As}}$ values can be attributed to As changing oxidation state. Varying oxidation states enables the element to act as both a cation or anion or both, depending on the fS_2 of the system. The Ru system on the other hand showed opposite trends. Ru and As had a greater affinity for mss phase than Pt and Pd. Ru prefer to form S dominant phases over As dominant phases and prefers to segregate out into the more incompatible early crystalline phases (Pohl, 2011).

The calculated D^{As} and D^{PGE} values were higher than the references cited due to:

1. High concentrations (ppm) of PGE added against lower (ppb) concentrations of natural systems.
2. The Measuring techniques used. Samples were analysed with semi-quantitative to quantitative WDS-SEM. A more sensitive method such as LA-ICPMS would have yielded more reliable results.
3. Experimental flaws and other mechanisms including possible PGE clusters or nodules. No real trend or phase association could be distinguished in any of the systems.

The data showed that the PGE and As was uniformly distributed in the phases, even at low concentrations. Samples with high concentrations of PGE also yielded higher concentrations of As. This leads to the idée that there must be a link between the two elements. See Chapter 8 for detailed discussion.

5.4. Summary

Measured entities (fS_2 , d-values and metal:S ratio) compared well with referenced literature sources. A summary of the geochemical parameters of experiment A, B and C is given in Table 5.4.

The average fS_2 in the quick quench samples were about $fS_2=-2$ and slower cooled samples $fS_2=-14$. The measured fugacity values were a good indication that the system reacted successfully and was comparable to a natural system. Fugacity measurements were supported by measured metal:S ratios (cation:anion). The metal:S ratios were >1 or close to

1 (2-10% variation). It seemed that the differentiation of As and PGE was dependent on the PGE added.

Table 5.4.: Summary of the geochemistry of the synthetic mono-sulphide solid solution (mss) system. Similar geochemical trends were measured in samples of the Pt- and Pd systems. Ru samples however differed considerably in metal:S, sulphur fugacity (fS_2) and differentiation trends (PGE and As). This might have been due to the influence of Ru in the system or an experimental error. The slower cooled control samples, of experiment A, also differed considerably from the fast cooled samples. Change in behaviour was expected as slower cooled samples were subjected to longer annealing and cooling times.

	Fast cooled			Slow cooled	
	Exp. A	Exp. B	Exp. C	Exp. A	
Avg. $-\log fS_2$	± -2.0	± -2.0	± 0.5	± -14.0	
Metal: S ratio	1.0769	1.0400	0.9051	1.0268	
$D^{As}_{mss/melt}$	A1f: 0.30	1.12	1.60	A1s: 1.04	
$D^{PGE}_{mss/melt}$	A1f: 0.94	0.34	>1	A1s: 0.23	

In the Pd- and Ru systems As was more compatible in the mss phase. Opposite trends were seen in the quick cooled samples of the Pt system. The PGE however displayed different distribution trends. Pt (slow and fast cooled) and Pd were concentrated in the melt phase as oppose to Ru that was more compatible with the mss phase. Change in geochemical behaviour was expected as the Ru is more compatible with the crystalline phase. Partitioning behaviour is strongly dependent on fugacity, metal:S ratio and the temperature of the system (Ballhaus et al., 2001, Mungall et al., 2005).

Chapter 6: Discussion on nano structures

An array of nano structures and textures were identified with the aid of high resolution SAM. However SAM is a semi-quantitative analytical method and because it only measures the first few atomic layers (10Å) it cannot be used to calculate or truly quantify a nano phase. Surface coatings/ contamination and oxidation have to be compensated for. Sulphur is especially a problem to determine what percentage is primary mineralisation against atmospheric contamination. The sensitivity of certain elements for SAM can also be problematic. Arsenic for example has a sensitivity of ≈ 0.4 as oppose to $S \approx 2$, making As extremely difficult to pick-up with SAM. Apart from analytical difficulties the biggest problem with quantifying and classifying nano entities is the lack of standards to measure or quantify nano entities against. There is yet no nano reference set available.

6.1. Adapted classification scheme to distinguish between measured nano structures

Nano structures were classified based on PGE content, time of formation and size of the structures. The nano entities (any phase $< 1000\text{nm}$) were primarily grouped according to PGE content; either PGE-rich or non-PGE structures. The structures were further classified or grouped according to time of formation: 1) growth structures (primary phases) and 2) nano to micro scale exsolution textures (secondary phases). The PGE-rich entities were filtered to only include phases smaller than 100nm. The PGE-rich nano structures smaller than 100nm were used to model the hypothesis on.

6.1.1. Size of nano structures

A nano entity is any nano phase smaller than 1000nm however by definition a true nano entity includes only nano phases smaller than 100nm. In the study a clear distinction was made for phases smaller than 100nm. PGE-rich nano phases, smaller than 100nm, was the key to determining whether PGE clusters can form in a magmatic system. Nevertheless nano entities larger than 100nm were also incorporated to determine whether: 1) the existence of the one might influence or contribute to the formation of the other (nucleation point or

artefact) and the 2) phase relationships and the overall chemistry of the system on a nano level.

6.1.2. PGE content

The structures, either greater or smaller than 100nm, were sub-divided according to PGE content i.e. PGE-rich and non-PGE. PGE-rich phases were essential to determine how and where the PGE formed and in what state it might be or might have been in the specific phase. Various non-PGE nano phases formed in the systems. The non-PGE structures gave a holistic view as to how the system behaved, where and how phases / minerals formed and if a link could be established between PGE content and nano shape, size and structure.

6.1.3. The type of nano structure

6.1.3.1. Primary growth structures

Primary growth structures formed in the initial melt stage before or during crystallisation at high temperatures of 900-1000°C and are more applicable to quick quench samples. The structures were PGE-rich or similar in composition to the major phases (various Fe-Cu sulphides).

6.1.3.2. Secondary nano- structures and textures

Secondary nano textures and structures in the synthetic samples formed due to: 1) Quick quenching. 2) Sample preparation and the experimental set-up. 3) As the system moved to equilibrium the incompatible elements, in the mss or melt phase, segregate out to form more stable phases.

Type 1: Exsolution textures due to quick quenching

High temperature hexagonal 1C po cannot be quenched and will on quenching exsolve or segregate to form more stable monoclinic 4C po with Fe-S phases. In the synthetic samples py, bn and melt exsolutions were measured on the surfaces of po. All the synthetic samples (slow and fast cooled) showed melt exsolutions within the mss (po) phase.

Type 2: Exsolution textures that formed due to experimental set-up procedures

High concentrations of Cu were added to the synthetic systems to lower the sub-solidus temperature. The excess Cu formed structures on the mss and melt surfaces. Several of the Cu structures measured low concentrations of PGE.

Type 3: Exsolution structures due to incompatible element segregation

The PGE used chalcophile ligands to exsolve or segregate from the mss- and melt phases. Exsolution may have occurred because of quick cooling or after cooling. After cooling, quick or slow, the phases are not in a final equilibrium state and will continue to segregate until equilibrium is reached. The equilibration process of a mineral of phase may take a few hours to several years. Exsolution textures are common in the high temperature bn-ccp solubility series (Craig and Scott, 1974). In natural systems the PGM are incompatible with the BMS and exsolve out, to sit in the triple points between incompatible phases (sulphide, oxide and silicate phases) (Gondel et al., 2010). Only 0.7% of PGM are found in BMS (Gondel et al., 2010).

6.2. Nano structures: larger than 100nm

The non-PGE nano entities were a collection of Fe-Cu sulphides or elemental Cu and Fe with no definite size, shape or distribution trends. The phases were measured on/in different Fe- and Cu- sulphides.

6.2.1. Non-PGE structures: Fast cooled samples

6.2.1.1. Pt-As system

The quick quenched samples showed medium to high relief primary and secondary structures. The nano structures were well rounded to irregular shaped to crystal-like features. On the mss surface large Cu- and Fe structures were measured. The Cu-rich phases (Figure 6.1.A) were most likely a by-product of experimental procedures. High concentrations of Cu were added to lower subsolidus temperatures of the mss system. The Cu phases ranged in size from 10nm to 1000nm and displayed no distribution pattern. They were limited to the po phase however. The Fe features (Fe-S) formed as a result of quenching of 1C po to lower 4C po, see Figure 6.1.B. Numerous Fe-S like py for examples forms in the quenching process. A

similar process was observed in the melt phase. Sulphide melts cannot be quenched to a glass. The melt thus forms various semi-crystalline to amorphous Fe-Cu-S phases, see Figure 6.1.C. Various Cu_xS_x structures (Figure 6.1.D) formed as primary structures. The structures exhibited hexagonal crystal-like features. A summary of the measured features is given in Table 6.1.

Table 6.1.: The characteristics of the non-Pt nano structures, larger than 100nm, measured in the fast cooled samples of experiment A. In contrast with the other samples the Pt system measured medium relief phases of pure Cu and Fe. Various other $\text{Fe}_x\text{Cu}_x\text{S}_x$ and Cu_xS_x structures were also crystallised in / on the melt surface. The enitites might also have formed due to quenching or as primary structures. Cu-rich phases were measured on the mss surface and may be a by-product of experimental procedures. The Fe features formed as a result of quenching of the 1C po.

Nano structure	Fig.	Pt-As system: fast cooled				
		N	Avg. size nm	Shape	Classification	Distribution
Cu_x	6.1.A	5	2000	Medium to high relief irregular to flower-like.	Type 2 exsolution	FeS (mss)
Fe_x	6.1.B	5	180	Medium relief pearls to irregular shaped	Type 1 exsolution	FeS (mss)
$\text{Fe}_x\text{Cu}_x\text{S}_x$	6.1.C	5	480	Rounded to angular and irregular shaped high relief features	Primary structure or type 1 exsolution	melt
Cu_xS_x	6.1.D	5	2280	Disc, platy to crystal-like	Primary structure or type 3 exsolution	melt
Avg. size			± 1200			

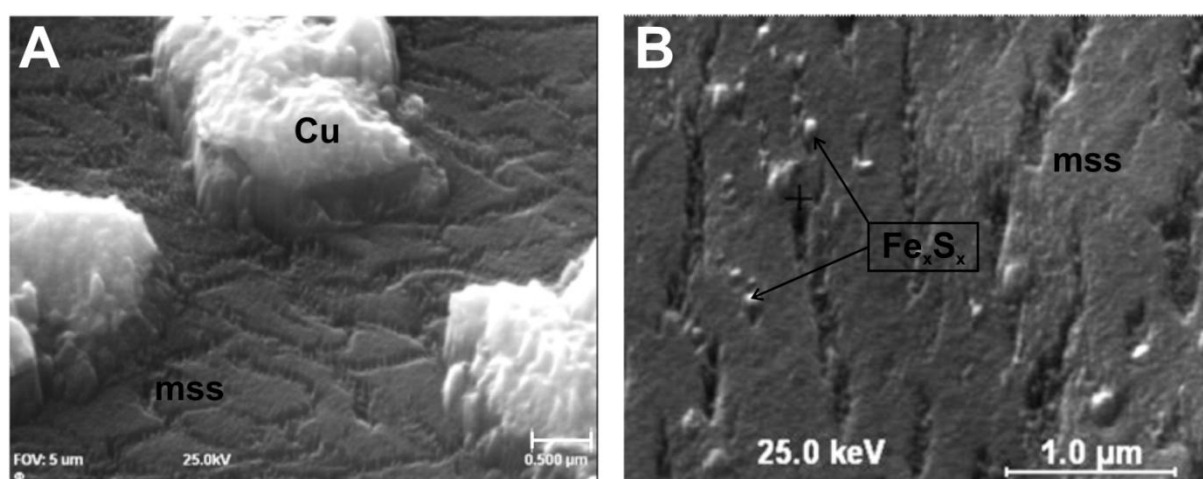


Figure 6.1. A-D: Various non-Pt structures, larger than 100nm, measured in the fast cooled samples of experiment A. A: High relief Cu exsolution (type 2) structures on the mono-sulphide (mss or po) surface. The structures most likely formed due to experimental set-up procedures. B: High density, low relief Fe_xS_x exsolutions (type 1) on the mss (po) surface.

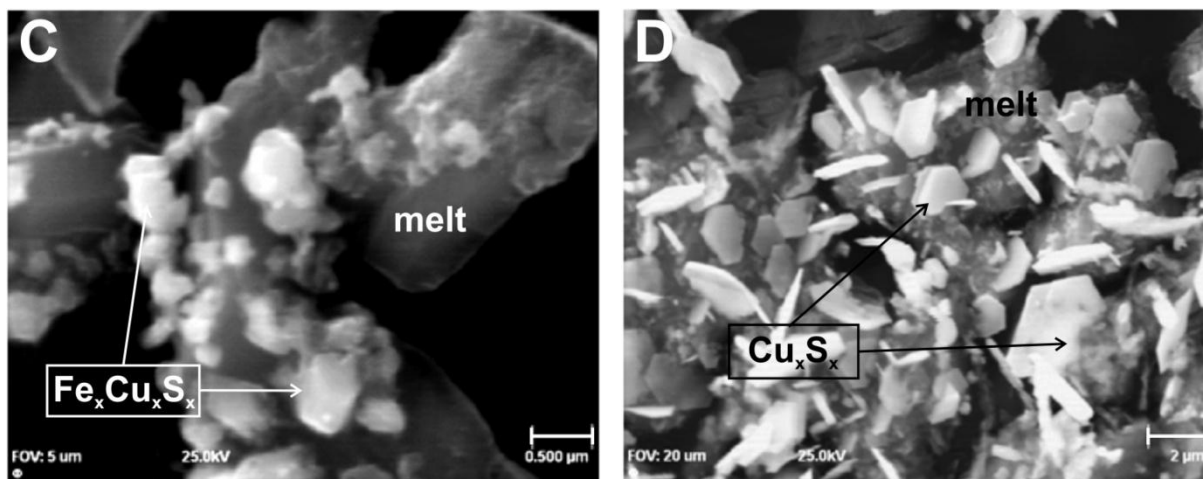


Figure 6.1. A-D cont.: Various non-Pt structures, larger than 100nm, measured in the fast cooled samples of experiment A. C: Irregular to rounded structures of $\text{Cu}_x\text{Fe}_x\text{S}_x$ phases (<500nm), on the melt surface. The structures were more Cu rich than the surrounding melt phase. D: Discs of Cu_xS_x crystallised in / on melt phase ($\text{Fe}_x\text{Cu}_x\text{S}_x$). The platy, almost hexagonal, features were up to 2000nm in diameter but only tens of nm to 500nm thick. The structures (Figure C and D) could have formed as primary growths or as exsolution type 3.

6.2.1.2. Pd-As system

The Pd-As system measured limited non-Pd structures, larger than 100nm, see Figure 6.2. A and B. The structures were overall Cu-rich. Surface features, type 2 and 3 exsolution structures, measuring only a few nano meters vertically are easily lost with polishing and will not have been picked-up by SEM. The structures formed likely due to experimental set-up procedures. The system was fairly over saturated with Cu. The non-Pd structures were low to medium relief, showed no definite distribution trends or associations and were measured on both Fe-rich mss and melt surfaces. A summary of the non-Pd features measured in the synthetic samples of experiment B is given in Table 6.2.

Table 6.2.: The size, shape, classification and distribution of non-Pd nano structures, larger than 100nm, measured on the surface of samples from experiment B. The measured structures were predominantly Cu-rich, on a Fe-Cu sulphide surface, and formed most likely due to experimental procedures.

Nano structure	Fig.	Pd-As system: fast cooled				
		N	Avg. size nm	Shape	Classification	Distribution
Cu-rich	6.2.A	5	150	Rounded to elongated irregular shaped	Type 2 or 3 exsolution	Fe-Cu sulphide
Cu sulphides	6.2.B	1	950	Well rounded to irregular patches	Type 2 or 3 exsolution	Fe-Cu sulphide
Avg. size			550			

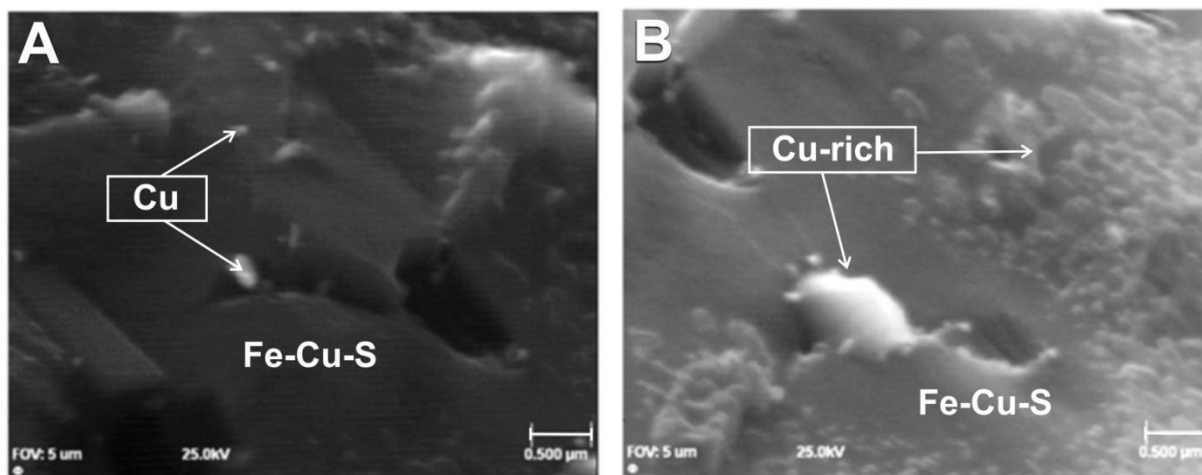


Figure 6.2. A and B: Bright phases of non-Pd nano structures, larger than 100nm. A: Cu rich structures outcropping on the same less Cu-rich Fe-Cu sulphide phase. The Cu “packets” showed no distribution trends and was most likely due to experimental set-up. High concentrations of Cu were added to lower the sub-solidus temperature of the system. B: High relief Cu-rich structures on a Fe-Cu sulphide surface. The structures formed similar to Figure 6.1. A. and were most likely experimental artefacts.

6.2.1.3. Ru-As system

No non-Ru structures were measured. The measured nano entities of the Ru system showed a clear correlation with Ru. The lowest measured Ru concentration was < 1 at.% in the Cu_xS_x phase. It seemed that a high concentration of Ru was present in the more incompatible melt phase as well as in the po phase.

6.2.2. Non-PGE structures: Slow cooled samples

6.2.2.1. Pt-As system

The nano entities measured in the slower cooled samples of experiment A differed considerably from the quick cooled samples. The faster cooled samples measured an array of elemental (Cu and Fe) and Fe-Cu sulphides. The slower cooled system however was closely associated with po (mo) and numerous Fe-sulphides. The measured Fe-Cu sulphides (460nm) in the slower cooled samples could be associated with primary crystallisation, see Figure 6.3. A. The po features were needle like to tabular to platy. The predominance of the po (Fe_{1-x}S) nano structures formed as secondary exsolution phases, see Figure 6.3. (B, C and D). However primary tabular crystal-like Fe-S were also picked-up, see Figure 6.3. D. A summary of the features is given in Table 6.3.

Table 6.3.: Outline of the non-Pt nano structures, larger than 100nm, measured in the slower cooled samples of experiment A. Structures measured in the slower cooled samples of experiment A differed vastly from the fast cooled system. The slower cooled structures consisted of primarily of po phases and various intergrowths and textures of po. The nano structures were overall platy to needle like features. Cu-rich features exhibited more crystal-like characteristics.

Nano structure	Fig.	Pt-As system: slow cooled				
		N	Avg. size nm	Shape	Classification	Distribution
$\text{Fe}_x\text{Cu}_x\text{S}_x$	6.3.A	5	460	Rounded to angular almost crystal-like structures	Primary structures	Fe-Cu sulphide
FeS (po)	6.3.B	-	n.d.	Needles to platy. Up to $3\mu\text{m}$ long and 500nm wide	Type 1 exsolution or type 3 secondary crystallisation	Fe_{1-x}S (po)
FeS (po)	6.3.C	5	1300	Angular to rounded features to elongated stringers	Type 3 secondary crystallisation	Fe_{1-x}S (po)
Fe-rich FeS (po)	6.3.D	-	n.d.	Low relief patches to needles	Type 3 exsolution	Fe-S (iron-sulphide)
Fe-S	6.3.D	-	n.d.	Needles to tubular crystals	Primary structures	Fe_{1-x}S (po)
Avg. size			n.d.			

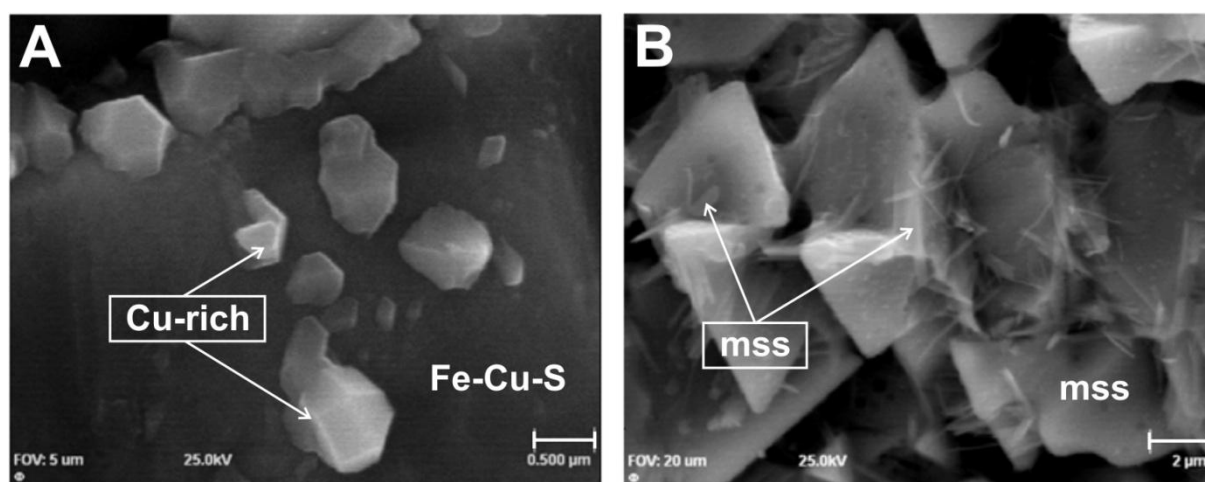


Figure 6.3. A-D: Non-Pt nano structures, larger than 100 nm, measured in slow cooled samples of experiment A. A: Angular to crystal-like, high relief, Cu-rich Fe-Cu sulphide ($\text{Fe}_x\text{Cu}_x\text{S}_x$) features on a Fe-rich sulphide surface. The structures measured about 500nm across on average. B: Fe-rich needle-like entities scattered on the po (Fe_{1-x}S) surface. The size of the structures could not be determined due to needle-like character. The structures formed most probably due to secondary mineralisation.

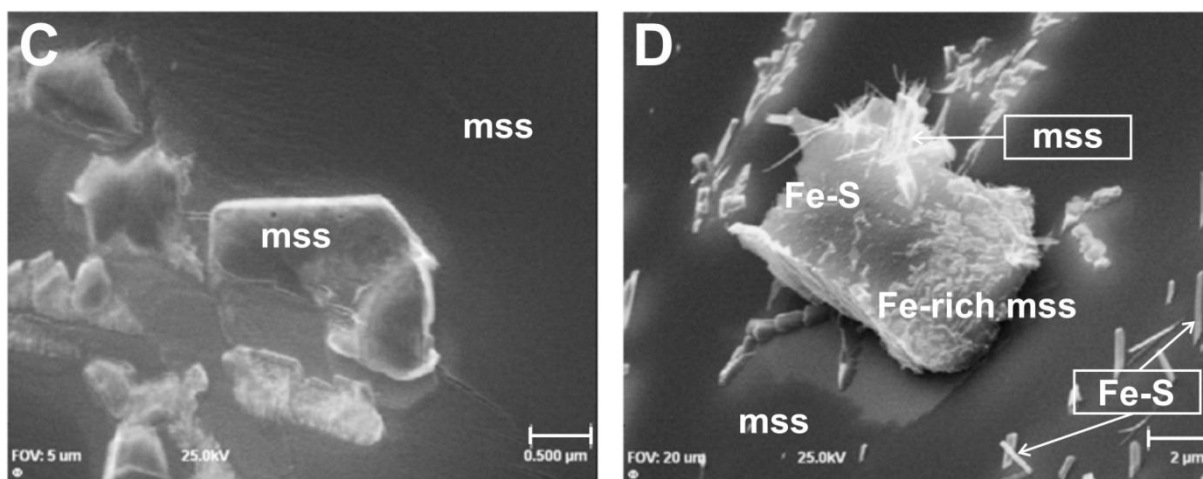


Figure 6.3. A-D cont.: Non-Pt nano structures larger than a 100nm, measured in slow cooled samples of experiment A. C: Medium relief Fe-rich Fe_{1-x}S (po) type 3 exsolution structures on po (Fe_{1-x}S). D: Assortment of secondary- and primary Fe-S structures outcropping on po (Fe_{1-x}S).

6.2.3. PGE-rich nano structures: Fast cooled samples

6.2.3.1. Pt-As system

Limited Pt-rich nano structures were identified in quick cooled samples of experiment A by aid of SAM. The type 3 exsolution structures were measured on a Pt-rich melt phase, see Figure 6.4. A and B. The structures showed a positive correlation with Cu. Some of the features showed higher concentrations of Cu. Pt might use Cu to exsolve from the melt to form a more stable phase like a PGM phases as the system evolves to an equilibrium state. Within the melt phase the Pt-rich structures no correlation or distribution pattern could be distinguished. The phases were sporadically distributed. However they were not found on all the melt surfaces. No Pt-rich entities have yet been measured on the more incompatible mss (po) surfaces of the Pt-As system. The outline of the measured Pt-rich structures in samples from experiment A is summarised in Table 6.4.

Table 6.4.: The characteristics of Pt-rich nano structures, larger than 100nm, measured in fast cooled samples of experiment A. The irregular blobs ($\pm 400\text{nm}$) found on the melt surface showed high concentrations of Pt and Cu. The structures had no distribution pattern and were found erratically on the melt surface. No PGE-rich phases have yet been measured on po.

Nano structure	Fig.	Pt-As system: slow cooled				
		N	Avg. size nm	Shape	Classification	Distribution
Pt-rich	6.4.C	5	400	Irregular blobs	Type 3 exsolution	melt
Pt-Cu-rich	6.4. B	5	390	Irregular blobs	Type 3 exsolution	melt
Average			395			

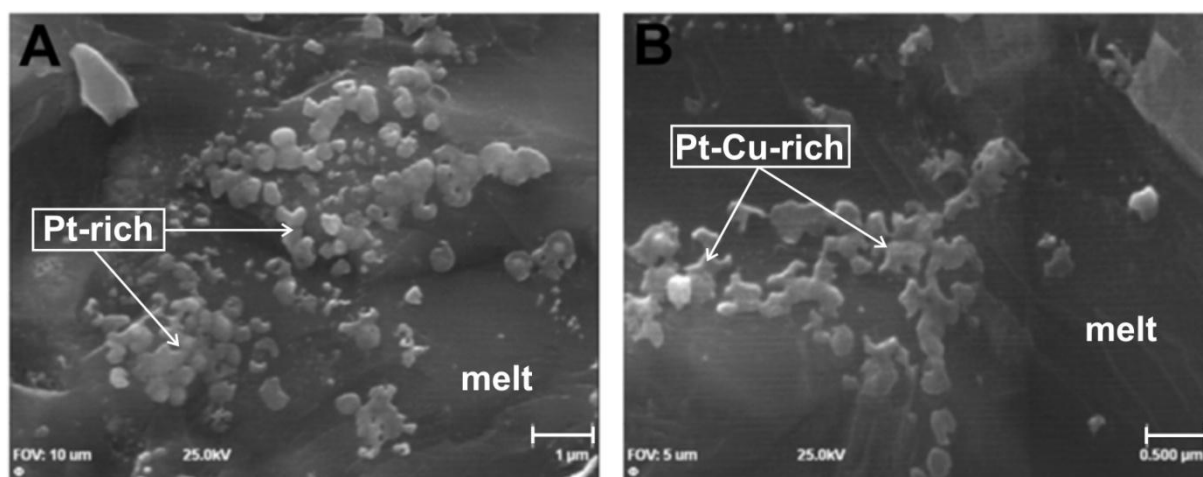


Figure 6.4. A and B: Pt-rich nano structures, larger than 100nm, measured in the fast cooled samples of experiment A. A: Irregular blobs of Pt-rich Fe-Cu sulphide, type 3 exsolution structures ($\pm 400\text{nm}$) outcropping on the melt surface. B: Pt-Cu-rich, type 3 exsolution structures, similar to structures identified in Figure 6.4. A. However the structures measured higher concentrations of Cu.

6.2.3.2. Pd-As system

Pd samples showed rounded to angular shaped extruding Pd-rich structures, see Figure 6.5. (A-D). The Pd-rich structures measured about 500nm in size and were limited to the more Cu-rich sulphides. No Pd-rich entities have yet been measured on the po (mss) surface. The Pd-rich structures were identified as possible type 3 exsolution structures. The Pd that was trapped in the Fe-Cu sulphide might have exsolved out to form PGM phases on the surface. High concentrations of Pd were measured in the surrounding Fe-Cu-S phase. An outline of the Pd-rich features is listed in Table 6.5.

Table 6.5.: Summary of Pd-rich nano structures, larger than 100nm, measured in experiment B. The structures consisted of type 1 and 3 exsolutions and were found in the Fe-rich Fe-Cu sulphide phases. The largely rounded structures measured on average about 500nm.

Nano structure	Fig.	Pd-As system: slow cooled				
		N	Avg. size nm	Shape	Classification	Distribution
Pd-Cu-rich	6.5.A 6.5.B	5	188	Angular to rounded structures	Type 3 exsolution	Fe-rich Fe-Cu-S
Pd-Cu-rich	6.5.C	5	300	Irregular shaped to roundish and elongated	Type 1 or 3 exsolution	Fe-rich Fe-Cu-S
Pd-rich sulphides	6.5.D	5	760	Rounded to angular. No definite shape could be defined	Type 1 exsolution	Fe-rich Fe-Cu-S
Avg. size			500			

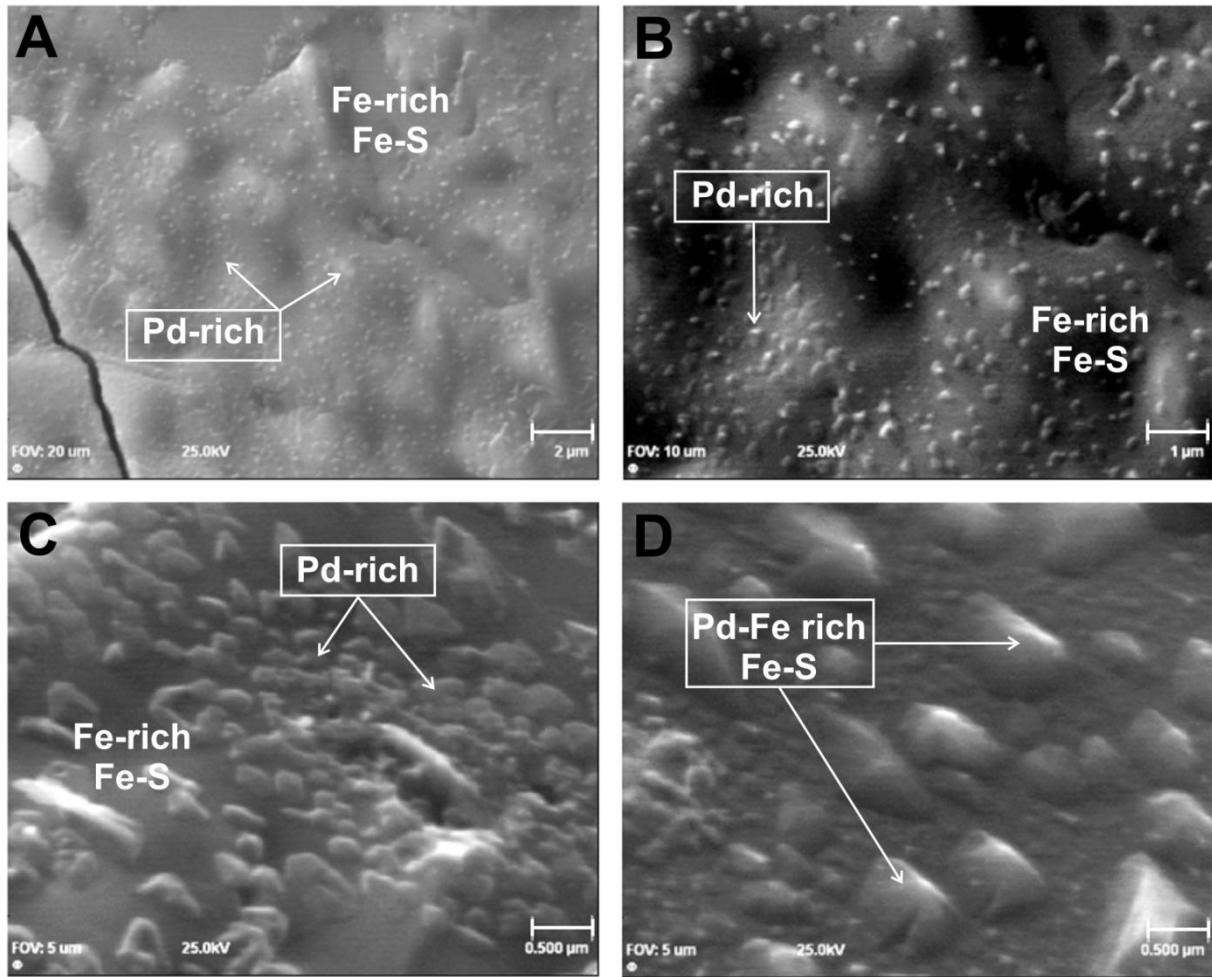


Figure 6.5. A-D: Various Pd-rich nano structures, larger than 100nm, measured in fast cooled samples from experiment B. A and B: Pd-Cu-rich structures ($\pm 200\text{nm}$) on Fe-rich Fe-Cu sulphide surface. The exsolution structures were similar in composition to their host but measured higher concentrations of Pd, Cu and $\pm\text{Fe}$. B: Magnification of Pd-rich structures identified in Figure 6.5. A. C: Pd-Cu-rich exsolution structures lying on a similar Fe-rich Fe-Cu sulphide. The structures were wide spread and densely distributed. D: Inter-grown Pd-rich sulphides. The structures formed most probably due to quenching (exsolution type 1).

6.2.3.3. Ru-As system

The Ru system displayed different nano structures than the Pt- and Pd experiments, see Figure 6.6. (A-D). Measured nano structures all showed a positive correlation with Ru. Like the Pd and Pt structures, Ru-rich entities showed a strong correlation with Cu. The Ru enriched crystal-like structures were distributed within and around a melt matrix. Most of the structures crystallised as primary phase of $\pm 650\text{nm}$ on a Fe-Cu sulphide or Cu-sulphide phase. Some of the structures could also be a result of exsolution. In the Ru system, like the Pd and Pt systems, no correlation or distribution pattern of the structures or with a specific phase could be deduced. A summary of the Ru system is set-out in Table 6.6.

Table 6.6.: Outline of the Ru-rich nano structures, larger than 100nm, measured in experiment C. The identified structures were rich in Ru and showed a positive correlation with Cu and in some cases Fe. The majority of the structures were observed on a Cu_xS_x surface and formed most likely as primary phases or type 3 exsolutions.

Nano structure	Fig.					
		N	Avg. size nm	Shape	Classification	Distribution
Ru-rich sulphide	6.6.A	5	860	Rounded to elongated	Primary structure	Cu-S in melt
Ru-Cu-rich $\text{Fe}_x\text{Cu}_x\text{S}_x$	6.6.B	3	650	Hexagonal to crystal-like	Primary structure	Ru-rich Fe-Cu-S
Ru-Fe-rich Cu_xS_x	6.6.C	5	500	Well rounded to crystal-like	Primary or type 3 exsolution	Cu-S
Ru-Fe-rich Cu_xS_x	6.6.D	1	600	Crystal-like on Cu-S inter-grown phases	Primary structure	Cu-S
Avg. size			650			

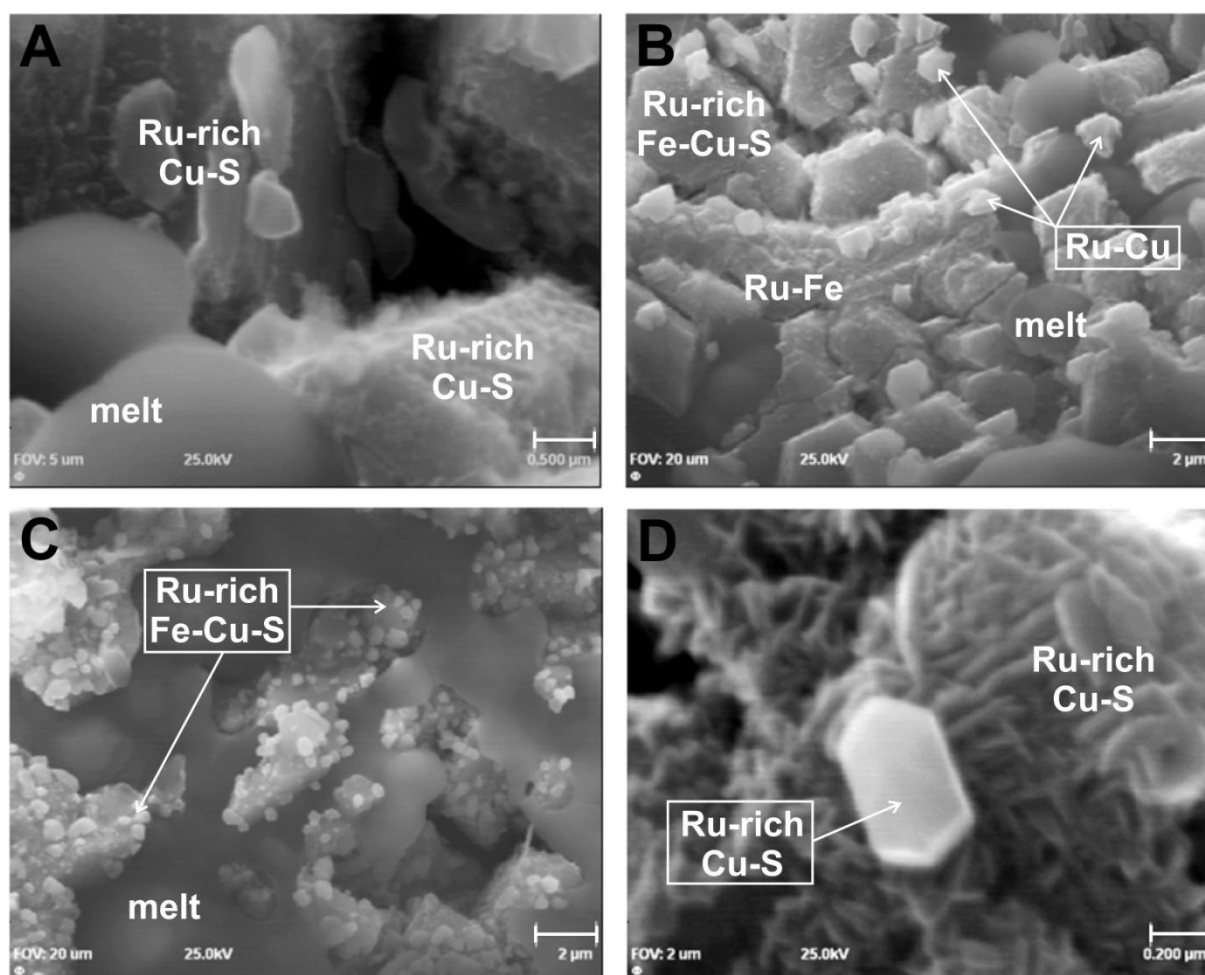


Figure 6.6. A-D: Ru-rich nano structures, larger than 100nm. A: Primary structures of Ru-rich Fe-Cu-S surrounded by Ru-rich sulphides. The structures measured high concentrations of Cu. B: An inter-grown collection of Ru-rich Fe-Cu-S structures. The structures formed most likely as primary phases. C: Ru-rich Fe-Cu sulphides in and between the semi-amorphous melt ($\text{Fe}_x\text{Cu}_x\text{S}_x$). Smaller Ru-Fe-rich Cu-S structures (white) were measured on the massive Cu-S surface (light grey). The structures most probably formed as primary phases or type 3 exsolutions. D: Ru-rich Cu-S crystal surrounded by Ru-rich Cu-S growths.

6.2.4. PGE-rich nano structures: Slow cooled samples

6.2.4.1. Pt-As system

No Pt-rich nano structures have yet been measured in the slower cooled samples. The lack of Pt-rich nano entities may have been due to slower cooling. Nano structures, which formed at higher temperatures, may have been lost or resorbed with a change in temperature and chemistry. The nano phases may also have acted as nucleation points for the formation of larger scale PGM phases. It is possible that the Pt was more evenly dispersed in the samples, bundles <100nm, making the nano phases difficult to pick-up.

6.2.5. Summary

A variety of PGE-rich and -poor nano phases, larger than 100nm, formed in the synthetic samples. The structures formed due to primary crystallisation and exsolution phases due to experimental set-up, cooling and compatibility behaviour. Non-PGE structures were a collection of Fe-Cu sulphides that formed either as primary structures or as secondary type 1 exsolution structures. The secondary features were a by-product of quenching. It is not possible to quench high temperature melt and various secondary phases will form in and on the po phase. Additionally the semi-crystalline Fe-melt phase crystallised with quenching to form numerous Fe-Cu-S. The various measured nano structures showed no phase associations or orientations. A summary of the distribution of the measured non-PGE and PGE-rich structures is given in Table 6.7.

Table 6.7.: The distribution of nano structures, larger than 100nm, measured in the synthetic systems and the phases they occur in. Non platinum-group element (PGE) structures were measured in all the phases and showed no distribution trends. Structures constituted of various Fe-Cu-S. The PGE-rich phases however were predominately primary- or type 3 exsolution structures. No PGE-rich structures have yet been measured in the mss phases. The PGE-rich structures were closely associated with Cu-rich phases.

>100nm	Exp. A:				Exp. B:		Exp. C:	
	Fast cooled		Slow cooled					
PGE content	non	PGE	non	PGE	non	PGE	non	PGE
Primary growth structures	melt							Fe-Cu sulphide Cu-S
Type 1 exsolution	mss		mss			Fe-rich Fe-Cu sulphide		
Type 2 exsolution	mss		mss		Fe-Cu sulphide			

Table 6.7. cont.: The distribution of nano structures, larger than 100nm, measured in the synthetic systems and the phases they occur in.

>100nm	Exp. A:				Exp. B:		Exp. C:	
	Fast cooled		Slow cooled					
PGE content	non	PGE	non	PGE	non	PGE	non	PGE
Type 3 exsolution	melt	melt	Fe-Cu sulphide mss		Fe-Cu sulphide	Fe-rich Fe-Cu sulphide		Cu-S

The PGE-rich phases in contrast showed strong phase associations. Pt formed irregular blobs of Pt and Pt-Cu-rich features on the melt surface. Pd-rich structures were similar to entities measured in the Pt system. The structures again showed a high correlation with Cu and crystallised as irregular shaped and sized type 3 exsolution structures on Fe-Cu sulphides. Ru structures differed vastly from Pt and Pd features. All the measured nano structures in the Ru system showed a positive correlation with Ru. The structures displayed more crystal-like features and formed as primary structures or type 3 exsolutions. The Ru-rich structures were associated with the Cu-S phases. A summary of the different type, composition, shape, size and phase associations of the measured nano structures is given in Table 6.8.

Table 6.8.: Outline of the platinum-group element (PGE) -rich and non-PGE nano structures, larger than a 100nm, measured in samples from experiments A, B and C. No definite size, shape, composition or distribution pattern could be coupled with a specific PGE or cooling system. PGE-rich phases seemed to be more rounded structures and showed a positive correlation with Cu. The PGE-rich structures measured on average 500nm.

>100nm	Exp. A: Fast cooled		Exp. A: slow cooled	
PGE content	non-Pt	Pt-rich	non-Pt	Pt-rich
Shape	Irregular, flower-like, pearls, rounded to angular	Irregular blobs	Rounded to angular to crystal. Needles, platy to tabular to patches	No Pt-rich nano entities measured Pt segregated to form larger PGM.
Composition	Cu, Fe, Cu _x S _x , Fe _x Cu _x S _x	Pt-rich and Pt-Cu-rich Fe _x Cu _x S _x	Fe _x Cu _x S _x , Fe _{1-x} S, Fe _x S _x	
Avg. size	1200nm	400nm	n.d.	
Distribution	melt mss	melt	Fe-Cu sulphide, mss, Fe-S	
>100nm	Exp. B: Fast cooled		Exp. C: Fast cooled	
PGE content	non	Pd-rich	non	Ru-rich
Shape	Rounded to irregular shaped.	Rounded, triangular to irregular shaped.	All the measured phases exhibited Ru enrichment.	Rounded to crystal-like to intergrwon
Composition	Cu _x , Fe _x , Fe _{1-x} S, Fe _x Cu _x S _x	Pd-rich Fe _x Cu _x S _x		Ru-rich Fe _x Cu _x S _x or Cu _x S _x
Avg. size	550nm	420nm		650nm
Distribution	Fe-rich sulphide phases	Fe-rich Fe-Cu sulphide		Fe-Cu sulphide and Cu-S

6.3. Nano structures: smaller than 100nm

The focus of the study was on PGE-rich nano structures smaller than 100nm. Nano entities smaller than 100nm falls within the size range of clusters (10-100nm) and served as a good indication whether clusters did form. Several of the measured PGE-rich nano structures might be reclassified as possible PGE clusters.

6.3.1. Non-PGE structures: Fast cooled samples

No distinguishable or different structures, of less than 100nm, were identified in any of the systems. The non-PGE structures coincided in composition, mainly Fe-Cu sulphides, with that of the larger measured structures as identified in Chapter 6. The structures were scarcely distributed to none existing. Most nano structures (<100nm) showed a positive correlation with PGE.

6.3.2. Non-PGE structures: Slow cooled samples

The slower cooled samples showed similar trends as the fast cooled samples. The non-PGE nano structures were smaller varieties of the larger structures and major phases. No exclusive or prominent phases were identified.

6.3.3. PGE-rich nano structures: Fast cooled samples

6.3.3.1. Pt-As system

Measurements, with SAM, of samples from experiment A yielded no definite Pt-rich nano structures. Although Pt-rich exsolution patches, of about 70nm, were picked-up on the melt surface, no cluster-like entities were directly imaged in the samples, see Figure 6.7. The exsolution textures, as with the larger structures, showed a strong correlation with Cu. A summary of the measured Pt-rich structures, smaller than 100nm, is given in Table 6.9.

Table 6.9.: The size, morphology (shape), classification and distribution of Pt-rich nano structures, smaller than 100nm, measured with scanning Auger microscopy (SAM) in the fast cooled samples of experiment A. No exclusive Pt nano structures could be defined with SAM.

Nano structure	Fig.	Pt-As system: fast cooled				
		N	Avg. size	Shape	Classification	Distribution
Pt _x Cu _x	6.7.	5	70nm	High density patches.	Type 2 or 3	melt

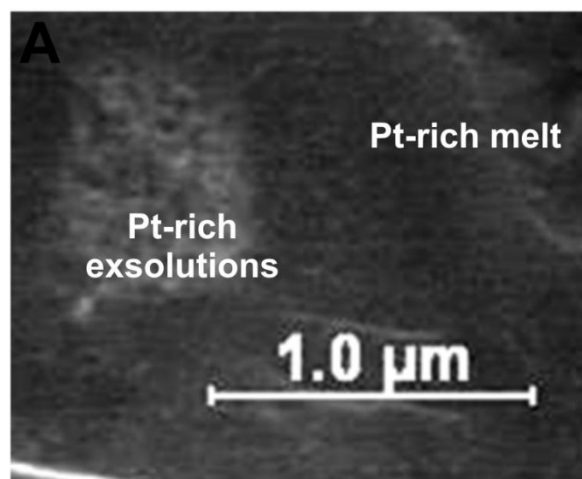


Figure 6.7.: Pt-rich nano structures, smaller than 100nm, measured in fast cooled samples of experiment A. Pt-rich patch-like features (avg. 70nm) lying on the melt surface. The structures formed most likely due to the exsolution of Pt and Cu out of the melt phase.

The Pt samples were scanned with TOF-SIMS to measure the presence and distribution of Pt, As and associated Pt-ligand ions. Sample A1f (fast cooled) and A1s (slow cooled) were used as analogue for experiment A. The samples were not polished to prevent loss of Pt and Pt-phases. Samples were additionally scanned at different resolutions to highlight surface features and to get good spectra. The samples were additionally sputtered, to remove several surface layers, to analyse deeper in the samples. The removal of surface layers was essential to distinguish primary structures from secondary surface features. The various ion scans were used to set-up a mask for phase identification. The mask was used to determine the distribution of ions between phases. Phase boundaries were estimated and not truly quantified.

Scans on the fast cooled samples showed a collection of Pt and Pt-ligand ions. The As, Pt and Pt-ligand ions were distributed in the melt- and mss phases. The ions were scattered throughout the samples and no definite trends could be determined, before or after sputtering. However Pt showed a positive correlation with the melt phase. Measurements taken before and after sputtering showed that the Pt and As ions were not products of secondary processes or surface features. Lower intensities of Pt and As ions were still picked-up after sputtering in the more incompatible phases possibly indicating that the ions were trapped by some mechanism. Whether the observed trends were due to a primary causes or a result of experimental set-up is yet to be defined.

An overview of the distribution of ions discussed above is given in Table 6.10.

Table 6.10.: Distribution of Pt and Pt-ligand ions between phases in the fast cooled samples of experiment A. The relative intensity of all the identified ions decreased after sputtering. The irregular scattering and not phases specific distributed and intensity of As and Pt ions may have been due to experimental artefact. However the ions may have collected in these phases by an external mechanism like clusters. An x indicates the presence of a ion in a phase.

		Relative intensity		Distribution of ions between phases			
				mss		melt	
		Before sputter	After sputter	Before sputter	After sputter	Before sputter	After sputter
Ions	Pt	67	11	x	x	x	x
	As	1518	39	x	x	x	x
	PtFe	<10	<10				
	PtAs	17	<10	x		x	
	PtAs₂	<10	<5				
	PtCu	10	<5	x		x	
	PtCu₂	13	<10	x		x	
	PtCu₃	28	<5	x		x	

The distribution of Pt as a function of chalcogene ligand (As, Fe and Cu) was tested by overlaying various ion scans. No trends could be distinguished. The ions were measured in both compatible and incompatible phases. However the ions showed a decrease in intensity after sputtering. It is possible that Pt may have not only used the chalcogene ligands as enrichment mechanism but also as a tool to exsolve from the sulphide phases. Similar trends were seen in Pt-rich secondary nano structures, measured on the surface of mss and melt phases with SAM, see section 6.2. and 6.3.

6.3.3.2. Pd-As system

Pd-rich nano structures, smaller than 100nm, consisted of beads or pearls of ± 55 nm. The phases formed either as primary structures or more likely type 3 exsolutions. The Pd-rich features were unevenly distributed but in high density in relation to surface are covered. The structures grouped together in sporadic clusters. The groupings ranged from less than 10 entities (± 5) to up to 50 structures, see Figure 6.8. (A and B). The structures might be indicative of an intermediate process to form PGM phases. A summary of the measured Pd-rich structures, smaller than 100nm, is given in Table 6.11.

Table 6.11.: The size, morphology (shape), classification and distribution of Pd-rich nano structures, smaller than 100nm, measured with scanning Auger microscopy (SAM), in the fast cooled samples of experiment B (Pd-As system). The pearl-like features were irregularly spread on the melt surface and sometimes grouped together to form groups of 5-50 entities.

Nano structure	Fig.	Pd-As system: fast cooled				
		N	Avg. size nm	Shape	Classification	Distribution
Pd-rich	7.3.A 7.3.B	5	55	High density pearls	Primary or type 3 exsolution	melt
Avg. size			55			

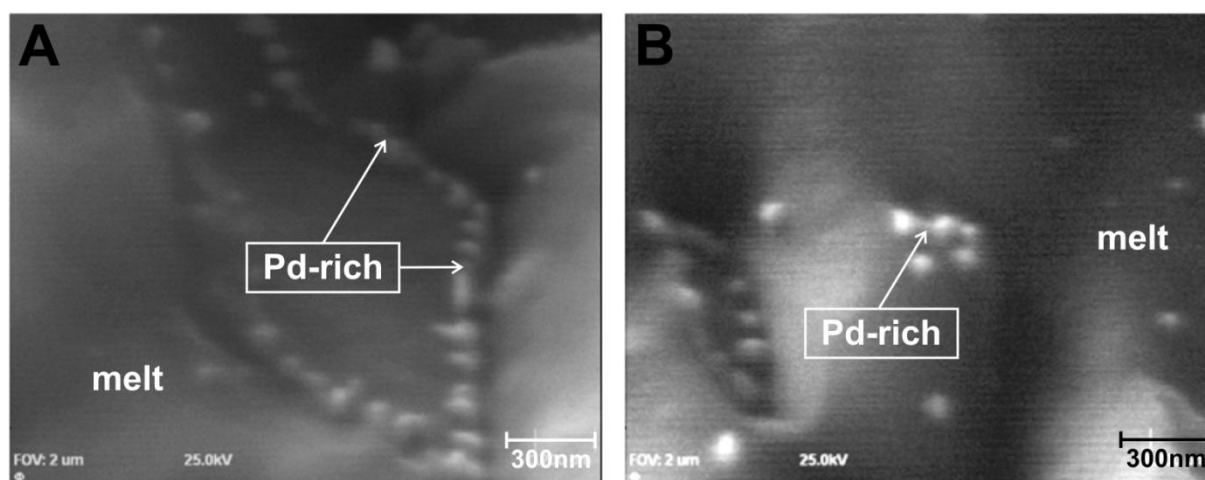


Figure 6.8. A and B: Pd-rich nano structures, smaller than 100nm, measured in samples of experiment B. A: Pearls of Pd-rich structures, 70-45nm, on Fe-rich semi-amorphous melt ($\text{Fe}_x\text{Cu}_x\text{S}_x$) phase. B: High density Pd-rich nano structures (55nm) on Fe-rich melt ($\text{Fe}_x\text{Cu}_x\text{S}_x$) phase.

6.3.3.3. Ru-As system

The phases of the Ru-As system showed a positive correlation with Ru. Various highly Ru enriched nano structures could be distinguished. The Ru-rich structures were at times higher enriched in Ru than the surrounding phase or showed similar trends. However in several cases lower Ru values were measured in the surface structures. No trend or pattern could be distinguished. The measured nano entities exhibited crystal-like features, see Figure 6.9. (A and B). The structures, about 100nm, formed most likely as primary phases on the Cu-S surface. The structures also exhibited high correlations with Cu and were scattered irregularly throughout the sample, see Table 6.12.

Table 6.12.: The size, morphology (shape), classification and distribution of Ru-rich nano structures, smaller than 100nm, measured with scanning Auger microscopy (SAM), in the fast cooled samples of experiment C (Ru-As system). The Ru entities were crystal-like and widely spread over the Ru-rich Cu_xS_x surface.

Nano structure	Fig.	Ru-As system: fast cooled				
		N	Avg. size nm	Shape	Classification	Distribution
Ru-rich Cu_xS_x	7.4.A 7.4.B	5	100	Medium relief, well rounded to crystal-like.	Primary structure	Ru-Fe-rich Cu_xS_x or $(\text{Ru,Fe})_x\text{Cu}_x\text{S}_x$
Avg. size			100			

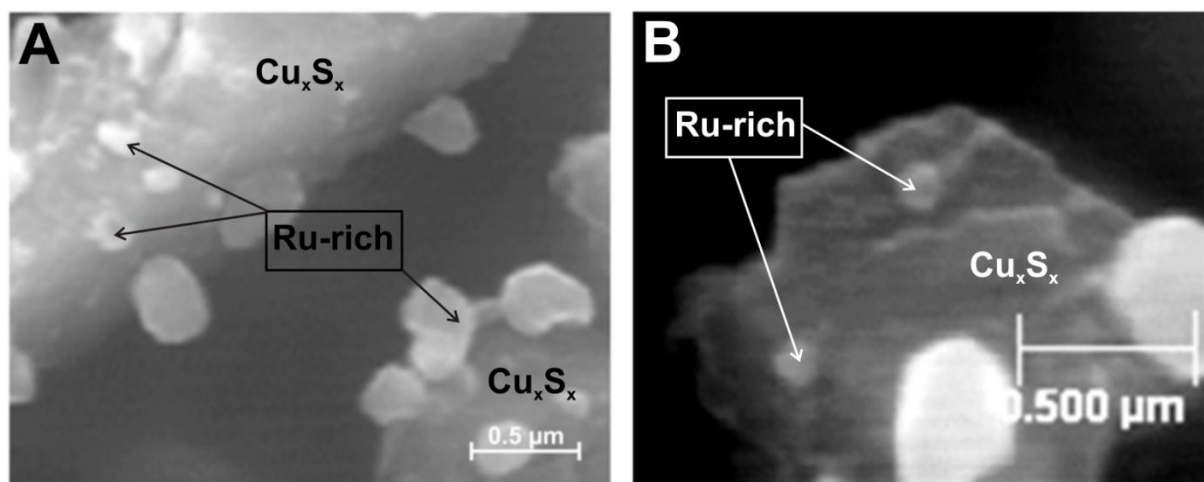


Figure 6.9. A and B: Ru-rich nano structures, ranging from 80-120nm, measured in samples of experiment C. A: Crystal-like Ru-rich nano structures ($\pm 100\text{nm}$) spread on a Ru-rich Cu_xS_x surface. B: Enlarged image of Figure 6.9.A. The Ru-rich nano structures were clearly visible on the Cu-S surface.

6.3.4. PGE-rich nano structures: Slow cooled samples

6.3.4.1. Pt-As system

No Pt-rich nano structures, smaller or larger than 100nm, were picked-up in the slower cooled samples with SAM analysis. The lack of nano structures may have been due to 1) the sensitivity of SAM for Pt and As. 2) The structure were distributed as small entities ($< 10\text{nm}$) in the samples. 3) As and Pt was extracted from the melt with longer annealing times to form PGM phases. TOF-SIMS was used to map the distribution of As, Pt and Pt-ligand ions to track the behaviour of the elements. The relative intensity of As, Pt and associated Pt-ligand ions were lower than faster cooled samples. Lower intensities of ions were expected as Pt and As were possibly extracted from the melt with prolonged cooling time to form PGM phases. Although lower intensities of Pt and As were measured the ions were spread erratically throughout the sample and measured in both compatible and incompatible phases.

The presence of Pt and As ions, in incompatible phases, after longer cooling might be an indication that a portion of nano phases / molecular agglomerations / clusters can stay preserved with a change in temperature. A summary of measured ions is given in Table 6.13.

Like the fast cooled samples the correlation between Pt and chalcogene ligand ions (Fe, Cu and As) was irregular distributed, before and after sputtering. It seemed that the Pt may not only use chalcogene ligands to latch onto, to form agglomerations, but also as a method to extract or exsolve from various phases.

Table 6.13.: Distribution of Pt and Pt-ligand ions between phases in the slow cooled samples of experiment A. The relative intensity of the identified ions decreased after sputtering and was lower than faster cooled samples. Lower intensities were expected as Pt and As could be extracted from the melt with prolonged cooling to form PGM phases. The presence of an ion (>10) is marked with an x.

		Relative intensity		Distribution of ions between phases			
				mss		melt	
		Before	After	Before	After	Before	After
Ions	Pt	31	<10	x		x	
	As	224	14	x	x	x	x
	PtFe	<10	<10				
	PtAs	<10	<10				
	PtAs ₂	<10	<10				
	PtCu	14	<10	x		x	
	PtCu ₂	<10	<10				
	PtCu ₃	<10	<10				

6.3.5. Summary

A variety of PGE-rich nano structures, smaller than 100nm, were measured in each of the PGE systems. The nano structures differed in accordance to PGE system. In the Pt experiments Pt-ligand (As, Fe, Cu) ions were measured in both compatible and incompatible phases. Similar results were seen in fast and slow cooled samples of the Pt system. The ions may serve as evidence that a vast majority of nano structures can stay preserved with a change in environment. However the intensity of the measured ions was lower in the slower cooled samples. Lower intensities were expected as the samples had longer time to anneal to form PGM phases. The fact that As and Pt were still found, even at lower levels, in all phases was an good indication that an enrichment process or possible clusters is prominent in an magmatic environment. Pd-rich features consisted of wide spread pearl-like structures on the melt surface. Ru structures in contrast closely resembled nano crystals. The structures were limited to the Cu_xS_x phase.

The distribution of the PGE-rich structures between the different phases is illustrated in Table 6.14. Pt system showed no distribution trends with regard to a specific phase. Pd and Ru structures however were only measured in the melt and Cu_xS_x phases. The Pd and Ru samples were not measured with TOF-SIMS, thus no trends could be distinguished over the PGE range.

The non-PGE nano structures correlated in composition to that of the larger phases and included nano phases of po (Fe_{1-x}S), bn (Cu_5FeS_4), ccp (CuFeS_2) and various Fe-Cu sulphides ($\text{Cu}_x\text{Fe}_x\text{S}_x$). The phases showed no distribution trends and were present in all the phase, see section 6.2. The characteristics of measured nano structures (<100nm) is given in Table 6.14.

Table 6.14.: Summary of the characteristics of the various platinum-group element (PGE) -rich nano structures, smaller than 100nm, in experiment A, B and C. The different PGE systems measured different nano structures and differed in composition, size and distribution. The Pt system showed a clear correlation with As and Cu from SIMS analysis. Pd and Ru however showed a variety of Cu-PGE structures.

<100nm	Exp. A: Fast cooled		Exp. A: slow cooled	
PGE content	non-Pt	Pt-rich	non-Pt	Pt-rich
Shape	No exclusive nano entities were picked-up. Structures resembled smaller scale versions of >100nm structures.	Patches to bundles	No exclusive nano entities were picked-up. Structures resembled smaller scale versions of >100nm structures.	Bundles
Composition		Pt-Cu Pt-ligand ions		Pt-ligand ions
Type of structure/s		Type 2 or 3 Primary and/or Type 3 exsolution		Primary and/or Type 3 exsolution
Avg. size		10-100nm		10-100nm
Distribution		Mss and melt		Mss and melt
<100nm	Exp. B: Fast cooled		Exp. C: Fast cooled	
PGE content	non-Pd	Pd-rich	non-Ru	Ru-rich
Shape	No exclusive nano entities were picked-up. Structures resembled smaller scale versions of >100nm structures.	High density pearls	No exclusive nano entities were picked-up. Structures resembled smaller scale versions of >100nm structures.	Rounded to crystal-like
Type of structure/s		Primary and/or Type 3 exsolution		Primary
Composition		Pd-Cu		Ru-Cu
Avg. size		55nm		100nm
Distribution		melt		Ru-rich Cu_xS_x

Chapter 7: Discussion

The primary enrichment of PGE in ore bodies, such as the Bushveld complex, remains a topic of controversy. Could primary enrichment of PGE have been influenced by PGE clusters? The influence of nano entities in magmas and ore-forming processes is relatively unknown. New research is showing that nano size entities (particles, crystals or clusters), driven by quantum mechanics (Johnson, 1980) play a vital role in geochemical environments. Nano structures are giving new insight into how and where minerals form or nucleate. Theoretically all minerals move through a nano stage during growth, either by inorganic or organic (biological) processes (Banfield and Zang, 2001). Nano phases can stay preserved in systems for tens of millions of years (Sen et al., 2011).

If PGE nano entities do exist, do they originate from the mantle or do they nucleate directly from a magma source, such as the Bushveld complex? The sulphide portion of a Bushveld complex type melt was experimentally mimicked to test if PGE nano clusters can form in a magmatic system and if so what influence does external factors have on formation.

Sulphides are of the first minerals to form in a magmatic system are thus more probable to carry clusters. By quick quenching the samples nano structures and phases were trapped or frozen as they were at 900-1000°C. Other samples were annealed over longer times and cooled slowly. Different cooling regimes were used to monitor the “life cycle” of possible clusters over time and temperature changes.

7.1. PGE-rich and poor nano structures and textures (<100 nm), measured in the synthetic system; formation, distribution and relation to PGE clusters

No PGE clusters were measured directly in the study. However PGE-rich nano structures, smaller than 100nm, can be reclassified as clusters or an analogues thereof. The focus of the study was on PGE-rich nano structures smaller than 100nm. The presence of nano entities in the more incompatible mss phases will serve as a good indication if clusters did form. Nano scale entities, larger than 100nm, may give insight as to how the system as a whole reacted.

The nano structures identified in the structures was classified according to size (either great than or smaller than 100nm), PGE content (PGE-rich or non-PGE) and the type of structure (primary structure or secondary exsolution). Nano-phases can 1) nucleate directly from the melt 2) form as exsolution textures 3) reactions between minerals or 4) crystallize directly from vapours (Banfield and Zang, 2001).

A collection of primary and secondary PGE-rich and non-PGE nano structures, between 100 and 1000nm, were measured in the synthetic samples. See Chapter 6 for classification scheme. The non-PGE structures, a collection of primary and secondary Fe-Cu sulphides, corresponded in composition with larger counterparts. The structures were not shape or size specific. The PGE-rich structures however differed with each system (Pt or Pd or Ru). Pt formed large $Pt_xCu_xFe_xS_x$ exsolutions of <700nm on the melt surface. The structures showed a high correlation with Cu. No Pt-rich nano structures have yet been measured in the slower cooled samples of the Pt-system. Pd structures, similar to the Pt structures, showed an association with Cu and Fe. Type 1 and 3 Pd-rich features of ± 500 nm were measured on the mss and melt surfaces.

Ru displayed different trends, geochemical properties and affinities to the Pt- and Pd-systems. Ru preferred to form stable phases with S and Cu. Ru-rich nano structures with S-, Cu. and Cu_xFe_xS of 500-900nm were measured in experiment C. The structures were more crystal-like than irregular shaped. The high density PGE-ligand structures, including Pt-, Pd and Ru system, showed no distribution trends and were measured in both incompatible and compatible phases. The structures had no definite shape or structure. Shapes ranged from flower-like structures to irregular shaped features, needle-like to high density pearls and crystal-like features.

The nano entities, smaller than 100nm, differed considerably from larger bulk counterparts. The non-PGE nano structures were smaller remnants of the larger structures described above. See also Chapters 4 and 6. Non-PGE nano structures were a collection of Fe-Cu sulphides and elemental Fe and Cu structures. However no exclusive or unique non-PGE structures, smaller than 100nm, could be distinguished in any of the systems. Nevertheless each system yielded unique PGE-ligand structures. In the fast cooled Pt samples small Pt-rich phases was measured on the melt surface as irregular patches.

In the Pd system high density Pd-rich pearls (avg. 55nm) were irregularly dispersed on the melt surface. In places the structures formed small groupings of 5-50 units of the pearl structures. The Ru-rich structures measured in samples from experiment C were more

crystal-like. The entities, of average 100nm, have thus far only been measured on Cu_xS_x surfaces. An array of PGE-rich nano structures may have been present in the samples that was not measured due to vast scale differences and working parameters. A summary of the different nano structures, non-PGE and PGE-rich, identified in the study is given in Table 7.1.

Table 7.1.: Summary of measured nano structures to illustrate the difference in structure, morphology, composition and distribution of the nano entities, as a function of size and composition. The non-PGE structures were predominately primary formed nano to micro scale phases and crystals of the measured major phases (mss or melt). Several of the structures could be attributed to experimental artefact or set-up procedures (type 1 and 2 exsolution). The PGE-rich entities however was associated with phases with high concentrations of Cu or Fe or both and formed due to primary and secondary processes.

Nano structures	PGE-rich		Non-PGE
	>100nm	<100nm	>100nm
Type of structures	Exsolution type 1, 2 and 3	Primary and exsolution type 3	Primary, exsolution type 1 and 2
Morphology (shape)	Rounded structures with irregular shapes, no specific format.	Patches High density pearls to crystal-like.	A variety of phases were measured. No definite or specific shape with relation to conc., system or cooling window
Composition	Fe-Cu sulphides \pm PGE	PGE + ligand/s (Fe, Cu, S, As)	Similar to measured major phases Fe-Cu sulphides
Avg. size	$\pm 500\text{nm}$	$\pm 75\text{nm}$	>100nm <1000nm
Distribution	melt phase Fe-(Cu)-S	mss (Fe_{1-x}S) melt phase Fe-(Cu)-S	Not restricted to a specific phase or cooling window

Banfield and Zang (2001) suggested several parameters to classify a nano phase, as no reference set is currently available to measure nano entities against. Parameters include 1) the physical character (size, shape, stability and structure), 2) chemical trades (composition, charge, and stability), 3) electronic- and magnetic properties, 4) optical character, 5) physical- and surface reactivity (adsorption tendency), 6) aggregation behaviour, 7) form (amorphous or crystalline or in-between) and 8) phase stability (stable, meta-stable or size induced). The parameters of Banfield and Zang (2001) and various literature sources were used to set-up a criteria to classify or measure the nano structures identified in the study as possible PGE-clusters, see Table 7.2.



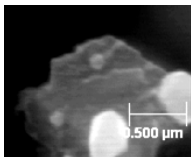
The measured PGE-rich nano structures, smaller than 100nm, identified in Chapter 7 was compared with the parameters set in Table 7.2. to verify if measured nano structures could be classified as clusters. It seemed plausible that PGE-ligand clusters did form in the synthetic Pt-As- and Pd-As experiments, see Table 7.3.

Table 7.2.: Parameters, adapted from various literature sources, used to classify a platinum-group element (PGE) -rich nano phase as a possible PGE cluster. A cluster is a zero dimensional object, of less than 100nm that can grow in dimension by nucleation. The clusters are indefinitely stable in a melt and may act as nucleation seeds for crystalloids and minerals, be taken up in the incompatible phases or may be resorbed back into the melt. Data was adapted from Tredoux et al. (1995), Jacobs and Alivisatos (2001), Cawthorn and Tredoux (2002), Hochella (2008), Hochella et al. (2008) and Waychunas et al. (2008).

Parameter		PGE clusters: Literature	Measured nano structures PGE-rich <100nm
Physical character	Size	To be defined as a nano phase, unit has to be less than 100nm.	<100nm Avg.75nm
	Shape	Zero dimensional objects. No definite structure or shape.	Various shaped were identified, see Chapter 6.
	Stability	Indefinitely stable in magma. May form and dissolve several times.	n.d.
	Structure	Do not have to adhere to crystal and internal structure of larger scale counterparts Structural defect are expected and can act as nucleation sites.	No definite or typical structure of shape could be defined for the nano structures measured.
Chemical trades	Composition	PGE–ligand bond Possible ligands: As, Fe, Cu, Bi, Te, Co	Fe-Cu-S-PGE
	Charge	Structure as a whole is uncharged	Should be uncharged.
	Stability	When cluster is incorporated in phase or mineral and equilibrates the clusters may be lost	May be stable for an undefined amount of time (few seconds to millions of years).
Electronic and magnetic character		Uncharged.	n.d.
Physical and surface reactivity		May latch onto incompatible phases such as sulphides, silicates and oxides.	PGE-rich nano structures were measured in mss and melt phases.
Aggregation behaviour		Grow in dimension to form 2D and 3D entities, minerals and crystals.	May acted as nucleation points for nano crystals and larger scale minerals.
Form		Amorphous to crystalline, depends on size.	Crystalline and non-crystalline entities were measured.
Phase stability		Size induced.	Nano phases were measured at 950-900°C but have not yet been seen at temperatures of 400°C.

Although no Ru-As clusters were measured it is not to say that they did not form. Due to the extreme scale of the nano entities and limitations of imaging techniques nano entities are easily lost if they do not outcrop on the samples surface or near surface. In a study by Helmy et al. 2013 similar experiments yielded potential Pt-ligand clusters. PGE ligand clusters cannot be conclusively proved in the study, as stipulated in Table 7.3.

Table 7.3.: Classification of platinum-group element (PGE) –rich nano structures (smaller than 100nm) as possible PGE clusters. The criteria used for classification was determined in Table 7.2. It seemed possible that nano phases, measured with scanning Auger microscopy (SAM), could semi-quantitatively be classified as PGE-clusters.

PGE system		Pt-As fast	Pt-As slow	Pd-As fast	Ru-As fast
PGE-rich nano structure, <100nm			No Pt phases were picked-up with SAM		
Physical character	Size nm	<100	-	55	100
	Shape	Patches	-	High density pearls	Rounded to almost crystal-like
	Stability	The clusters that formed at higher temperatures of 950°C stayed preserved at 400°C		n.d.	n.d.
	Structure	Non crystal-like	-	Non crystal-like	Crystal-like
Chemical trades	Comp.	Pt-Cu	-	Pd	Ru-Cu
	Charge	n.d.			
	Stability	Stable in high temp. melt	-	Stable in high temp. melt	Stable in high temp. melt
Electronic and magnetic character		n.d.			
Physical and surface reactivity		melt	-	melt	melt
Aggregation behaviour		May group together or act as nucleation point to form larger phases			
Form		Amorphous	-	Amorphous	Amorphous to possible semi-crystalline
Phase stability		Stable at 950°C	-	Stable at 950°C	Stable at 950°C
Possible cluster		Possible	-	Possible	Possible could also be nano crystals

PGE-clusters are not micro-nuggets. However is it possible that PGE micro-nuggets could have formed in the mss system? PGE nuggets, 100-1000nm, have been found to form in various synthetic PGE experiments (Borisov and Palme, 1997; Ertel et al., 1999; Blaine et al., 2005; Brenan et al., 2005; Cottrell and Walker, 2006; Ertel et al., 2008; Blaine et al., 2011 and the references therein). PGE nuggets have been interpreted to form as an effect of low oxygen fugacity in experimental systems with low PGE-solubility (Ertel et al., 1999). Several authors depict nuggets as pure experimental artefact (Blaine et al., 2005, 2011). The nuggets cause over estimation of PGE solubility in the relevant system (Blaine et al., 2005; Ertel et al., 2008).

However it has been suggested that the micro-nuggets may form as primary phases to contribute to PGE enrichment in magmatic systems such as the Bushveld complex. Studies from Ballhaus and Sylvester (2000) found micron-size, possible micro-nuggets, PGE blebs in Merensky reef samples from the Bushveld complex. Similar PGE phases have been found in meteorite samples indicating that nano-nuggets may be an important mechanism in the partitioning and solubility of highly siderophile elements (PGE) (Ertel et al., 2008).

Micro/ nano-nugget models fall within two classes 1) Oversaturated PGE melt. The nuggets represent oversaturation of PGE in the melt or an exogenous PGE-rich phase present in the melt (Borisov and Palme, 1997; Ertel et al., 1999; Brenan et al., 2005; Ertel et al., 2008; Blaine et al., 2011). 2) PGE dissolved in the melt model. PGE dissolved in the melt segregates upon thermal quenching to form solid phases (Cottrell and Walker 2006). The nuggets range from 100nm to 10000nm. The size of the nuggets is not a function of annealing time but of allowed cooling time (quenching). Nugget formation is not due to experimental artefact or low oxygen fugacity (Cottrell and Walker, 2006). A summary of the models compared to the cluster model is given in Table 7.4.

Table 7.4.: Comparison of the micro-nugget models with the cluster model. From the Table no conclusive evidence could be rendered that there is a correlation between clusters and the presence of nuggets. Data adapted from Blaine et al. (2005), Cottrell and Walker (2006), Ertel et al. (2008) Blaine et al. (2011).

Parameter		Micro nuggets	Clusters
Physical character	Size	100–1000nm	<100nm
	Shape	Not specified in literature.	No definite structure or shape.
	Stability	Not present at run conditions (melt).	Indefinitely stable in magma. May form and dissolve several times.
	Structure	Crystalline character not specified.	Do not have to adhere to crystal and internal structure of larger scale counterparts.
Chemical trades	Composition	PGE-Fe phases, more Fe rich than the bulk metal phase.	PGE–ligand bond.
	Charge	Not specified in literature.	Structure as a whole is uncharged
	Stability	Form upon thermal quench.	Clusters may be lost when incorporated in phase or mineral.
Form		Solid phases, rounded entities equally dispersed in melt.	Amorphous to crystalline, depends on size.
Phase stability		Reducing conditions Temp. up to 2500°C, 2.2GPa Low fO_2	Size induced Reducing conditions Temp. up to 1050°C fO_2 not defined

No direct correlation could be established between clusters and micro-nuggets, see Table 7.4. Clusters do not present a solid phase like nuggets and form by a physical mechanism

appose to chemical bonding. However it is possible that clusters might be precursors of nuggets or act as nucleation points for nugget formation. The correlation between clusters and micro-nuggets is yet to be determined. Due to the lack of information available on micro-nuggets it was not possible to determine without a doubt if nuggets did form in the experiment.

The measured nano entities were not conclusive evidence as proof for the formation of possible PGE clusters. TOF-SIMS was used to image the distribution of ions between phases as possible indication of clusters. A mask was used to determine the distribution of ions between the different phases (mss or melt), see Table 7.5. Numerous As, Pt and Pt-ligand ions were picked-up in mss (incompatible) and melt (more compatible) phase of both fast and slow cooled samples. The distribution of the Pt and Pt-ligand ions was a positive indication that the PGE did form agglomerations of Pt with various ligands. Furthermore several of the same Pt-ligand ions were measured in the incompatible and more compatible phases of fast and slow cooled samples. However ion agglomerations, possible clusters, can stay preserved with a change in temperature. Slower cooled samples measured lower intensities of As and Pt-ligand ions. Slower cooling and longer annealing times allowed for the extraction of PGE from the melt to form PGE phases. Ion distribution trends were also measured before and after sputtering.

The presence of Pt, As and other Pt-ligand ions, after sputtering, was evidence that the measured trends described could not only have been due to surface effects or secondary processes but that by some other mechanism the ions were trapped inside the phases. Whether the trapped ions were due to experiment artefact is yet to be determined. A summary on the distribution of measured Pt and Pt-ligand ions is given in Table 7.5.

Table 7.5.: Distribution of Pt and Pt-ligand ions between phases in the samples of experiment A as possible evidence of cluster formation. Pt-ligand (S, As, Fe, Cu) ion agglomerations, possible clusters, were measured in incompatible and compatible phases of slow and fast cooled samples. Several of the ions stayed preserved with a change in temperature. The preservation of the ions might be indicative that clusters can form in magmatic environment and a percentage may stay preserved with a change in temperature (environment).

Distribution of ions	Fast cooled		Slow cooled	
	mss	melt	mss	Fe-Cu sulphides
Ions measured, before sputter	Pt, As, PtAs, PtCu ₂ , PtCu ₃ other <10	Pt, As, PtAs, PtCu ₂ , PtCu ₃ other <10	Pt, As, PtCu other <10	Pt, As, PtCu other <5
Ions measured, after sputter	Pt, As Pt-ligand: <10, low intensities	Pt, As Pt-ligand: <10, low intensities	Pt, As other <5	Pt, As other <5

The study served as a baseline of nano structures that can possibly form in a magmatic sulphide system. Of the biggest problems with experimental work is determining whether measured structures are artefacts of the experimental setup and establishing equilibrium (Peach and Mathez, 1996; Fleet et al., 1996 as cited in Cawthorn, 1999). Nano entities and ion measurements described can thus not without a doubt be proven as primary features.

7.2. The influence of internal- (kinematic, mineralogical and geochemical) and external (thermodynamic) changes, in the mss host, on cluster formation

In a natural system the kinematics and thermodynamics of a magma chamber is dynamic and influences meso-, micro- and nano- scale activities and interactions. The kinematic, thermodynamic, mineralogy and geochemistry of the synthetic mss host system was compared to a natural magmatic Ni-Cu-S±PGE deposit to determine to what extent the factors may influence cluster formation and behaviour. Can an optimum 'window' for cluster formation be defined?

The synthetic melts were compositionally more simplistic than the Bushveld magmas with only S, Fe, Cu, As and PGE (either Pt or Pd or Ru) mimicking a sulphide portion of a Bushveld type melt or the first crystallizing phases or sulphide minerals (po, bn, ccp and a melt phase) and PGM. The parental magma of the Proterozoic Bushveld complex in contrast was possibly of picritic composition (Davies et al., 1980; Cawthorn, 2007; Mungall and Naldrett, 2008).

Studies have shown that the Bushveld complex had more than one parental source magma with repeated replenishing events (Cawthorn and Walraven, 1998; Barnes and Maier, 2002; Cawthorn, 2007). The replenishing denser magma flowed under the less dense residual magma, displacing the resident magma (Cawthorn, 2007). Cawthorn (2007) suggested that the magma of the Lower zone (Bushveld complex) was close in composition to the parental magma calculated by Davies et al. (1980) and Harmer and Sharpe (1985). The upper Critical zone may also have had a similar magma composition of Davies et al. (1980). Magma of composition proposed by Davies and Cawthorn (1984) was added and mixed with equal proportions at the pyroxenite marker (Cawthorn, 2007). Barnes and Maier (2002) suggested that the Bushveld complex formed from two main parental magmas; basaltic andesite and tholeiitic basalt. The two magmas mixed in a 60:40 ratio (Barnes and Maier, 2002).

The solubility and concentration PGE in the parental magmas of the Bushveld remains a heated topic (Davies et al., 1980, Harmer and Sharp, 1985; Barnes and Maier, 2002; Cawthorn, 2007). Research is showing that the solubility of PGE in the parental magmas may have been higher than current estimates predict (Cawthorn, 1999). Calculation made by Ballhaus and Sylvester (2000), emphasised that the PGE budget of a sulphide must be greater than the measured value. This correlates well with the “invisible platinum” concentrations, up to 0.5-2%, in sulphide phases of the Merensky reef (Bushveld complex, South Africa) (Pohl, 2011).

The $D_{mss/mss}^{PGE}$ can be used as an indication to measure the amount of PGE trapped in the mss or melt phases. High partitioning coefficients between mss and melt is not necessarily an indication of the presence of PGE clusters or PGE structures in the more incompatible mss phase. To establish if the high concentrations of PGE present in the mss phases were due to experimental flaws or possible enrichment, the $D_{mss/melt}^{PGE}$ was plotted against PGE concentration, see Figure 7.1.

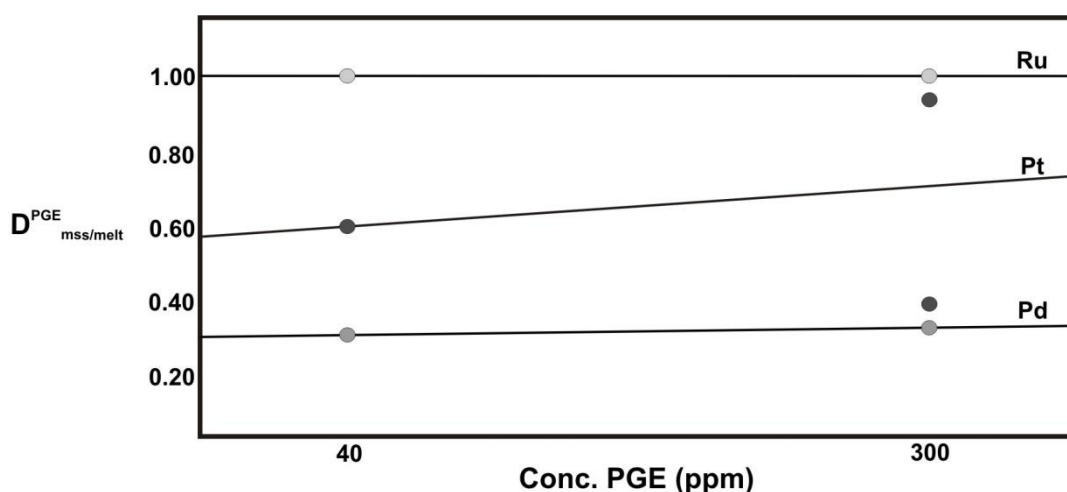


Figure 7.1.: The correlation between the concentration of platinum-group element (PGE: Pt, Pd and Ru) added and the distribution of PGE between the mono-sulphide- (mss or po) and melt phase. The fast cooled samples showed high concentrations of PGE entrapped in the mss. The samples showed a positive increase in $D_{mss/melt}^{PGE}$ with an increase in the PGE concentration added. The slower cooled samples of experiment A were not plotted. Pt was not picked-up in the majority of slower cooled samples and fell below detection limits. The slower cooled system had longer time to differentiate and the PGE could exsolve from the po into the melt and associated phases to form large PGE phases.

No direct correlation between the PGE concentration and PGE partitioning behaviour could be established without error. The high concentrations PGE measured in the mss phases must have formed by other mechanisms. The fact that high concentrations of the lighter PGE (Pd and Ru) showed similar trends to the heavier PGE (Pt) gives weight to the possibility of PGE cluster formation in the synthetic system.

It has been suggested that the presence of micro-nuggets in experimental systems as described in studies by Borisov and Palm (1997) and Ertel et al. (1999) as cited in Palme (2008), Fortenfant et al. (2003), Brenan et al., (2005), Pruseth and Palme (2004) as cited in Godel et al. (2007), influences the D values of experimental systems giving elevated D values. Micro-nuggets are not clusters or artefacts thereof. Other authors argue that high partitioning coefficients are coupled with high concentrations (ppm range) of PGE added (Fleet et al., 1999 as cited in Barnes and Maier, 2002). However sulphide droplets in magmatic systems such as ocean island basalt and mid-ocean ridge basalt (Peach et al., 1990; Helz and Rietz, 1988 as cited in Barnes and Maier, 2002) can also yield extremely high partitioning coefficients of PGE between silicate liquid and sulphide liquid, up to 20 000 and 50 000 times. The studies underline the fact that the extreme partitioning factors are a natural process and not limited to experimental artefact.

Not only was the concentration and distribution of PGE important but also available ligands. Arsenic was added as stabilising chalcogene ligand in the synthetic systems. Crystalline po phases showed higher concentrations of As. The As-rich po also measured higher concentrations of PGE. The $D_{\text{mss/melt}}^{\text{PGE}}$ was plotted against As concentration added, see Figure 7.2., to determine the influence of As on PGE distribution.

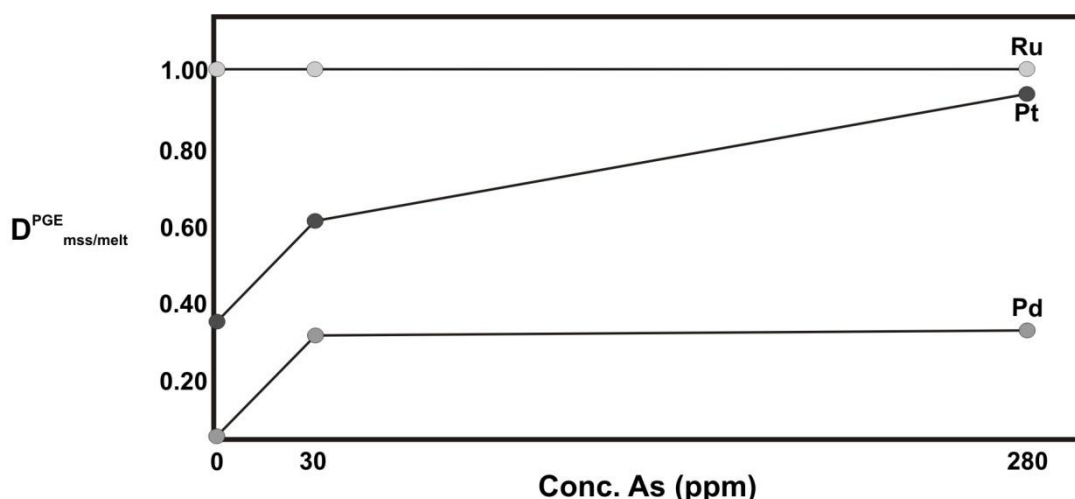


Figure 7.2.: Platinum-group element (PGE) distribution between the mono-sulphide- (mss or po) and melt phase as a function of the starting concentration As added, in the fast cooled samples. The positive correlation between PGE distribution and the available concentration of As emphasised the importance and influence of chalcogene ligands in the mss system during early magmatic processes. The D^{Pt} dropped from ± 0.9 in samples with As to ± 0.3 in As devoid samples.

The partitioning of PGE between mss and melt (Figure 7.2.) was to an extent depended on the availability of As. In a similar study by Helmy et al. (2013) they found that As had a significant influence on Pt distribution between crystalline (po) and Cu rich Fe-melts at

950°C. In samples with lower concentration of As added D^{Pt} was significantly lower than higher concentrated samples. Helmy et al. (2013) contributed the sudden drop in distribution to the presence of Pt-As poly-molecular clusters or associations. Although analysing techniques in the study was not as quantitative, it would seem that a similar scenario could have been at work in the synthetic samples.

It would thus seem that the PGE may use chalcogene ligands such as Cu, As or Fe, to form a stable phase or to serve as a nucleation points for chemical dominant reactions, enabling bonding with other incompatible phases (sulphides, oxides and silicates). Similar experiments conducted by Helmy et al. (2010, 2013), to test the partitioning of elements Se, As, Sb, Te and Bi between mss and sulphide melt in magmatic sulphide deposits, found that As anions preferred to associate with PGE in a sulphide melt by forming PGE-As molecules or possible poly metallic clusters (Helmy et al., 2010).

Sulphur plays an important role in concentrating and trapping of PGE. The reefs of the Bushveld complex hosts up to <3 vol.% S (Simon and Ripley, 2011). Various geochemical models (Simon and Ripley, 2011 and the references therein) for magmatic Ni-Cu-S PGE deposits are based on the chalcophile behaviour and affinity of the PGE for S. In a magmatic system S lowers the melting point of the system, causing elements including PGE and other metals to melt at lower temperatures. The temperature and Fe content controls the S^{2-} concentration of basalt (Metrich and Mandeville, 2010). The S-phases and oxidation state of S is dependent on the oxidation or redox (Eh-pH) state of the silicate magma (Metrich and Mandeville, 2010, Simon and Ripley, 2011). S primarily exists as S^{2-} (sulphide) and S^{+6} (sulphate) in a silicate melt (Metrich and Mandeville, 2010). The fS_2 of a magma can be an indication of the solubility of PGE and Cu in a silicate melt (Mengason et al., 2010). As magma differentiates and becomes more siliceous an immiscible S-liquid or phase forms.

Ligands or available anions influenced the nano- and micro- phases that formed in the synthetic samples. Nano phase formation did not seem to be dependent on the PGE concentration but on the availability of appropriate stabilising ligands, the chemistry of the system, ligands added, metal:S ratio, fS_2 and temperature changes (change in energy) of the system. Similar trends were observed regarding PGE phase (micro or nano) formation. The concentration of PGE added had a negligible effect on the size and shape of PGE phases that formed. The measured PGE phases showed no shape orientation and shapes ranged from spot-like, skeleton crystals to perfect euhedral isometric structures. PGE-rich nano phases in the Pt, Pd and Ru systems showed a positive correlation with Cu and Fe. TOF-SIMS measured various Pt-As structures in the Pt experiments.

If nano PGE-As entities do indeed exist or existed what was the influence of thermodynamic conditions of the host system and nano structures? Can the nano entities stay preserved over time and associated changes in temperature, fugacity and energy? A major driving force behind phase formation, in a melt environment, is the thermodynamic and kinematic constraints of a system either natural or synthetic. Melts (visco-elastic fluids) have unique geochemical and physico-chemical properties (Calas et al., 2006). High atomic mobility, a lack of long range order, extreme thermal energy and high volatile contents (Richet and Ottonello, 2010) give melts distinctive thermodynamic characteristics (Richet and Ottonello, 2010).

It is difficult to model the dynamics and physical and chemical evolution of a dynamic magmatic system such as the Bushveld complex. Although the thermodynamic changes and evolution of the closed synthetic systems were quite simplistic, it served as a good comparison of what can happen in a natural open magmatic system. PGE phase formation in the synthetic samples was highly dependent on thermodynamic changes.

A comparison between the Bushveld complex melt and the synthetic mss melts is tabulated in Table 7.6. The physical and chemical parameters of the B1 and B2 melts of Barnes and Maier (2002), was used to represent the Bushveld complex melts, in conjunction with various other references to model the possible thermodynamic conditions at time of formation.

Table 7.6.: The thermodynamic properties of Bushveld complex melt system compared to the synthetic mono-sulphide solid solution (mss) system. Data for was taken from Li et al. (2001), Barnes and Maier (2002) and Simon and Ripley (2011).The synthetic system compared fairly well to a natural system in temperature and fugacity.

Bushveld complex phase	Symbol	Bushveld complex magmas Barnes and Maier, 2002			Synthetic mss
		B1	B2	Mixed magma B1:B2	sulphide portion
Oxygen fugacity	f_{O_2}	Equal or below the nickel nickel-oxide boundary $f_{O_2} \approx -9$ (Davies et al., 1980)			n.d.
Sulphur fugacity -log f_{S_2}	f_{S_2}	Between -2 and -1			fast ≈ -2 slow ≈ -14
Redox conditions	pH-Eh	Reducing conditions			Reducing
Temperature	T	$>1358 \pm 15^\circ\text{C} - 1100$	-	-	400 - $1000 \pm 50^\circ\text{C}$
Pressure	P	300 bars-3kbar			1atm

Thermodynamic considerations on a nano scale is important to predict the stability and polymorphic transitions (Banfield and Zang, 2001; Hochella et al., 2008) of the nano entities

under set conditions, be it experimentally or in a natural system. Nano entities undergo or have severely different non-Gibbsian thermodynamic interactions and dynamics (Banfield and Zang, 2001; Rajagopal et al., 2004; Hochella et al., 2008). Nano thermodynamics is primarily driven by the change in energy (ΔG) of the system (Banfield and Zang, 2001). Nano phases may not always reach equilibrium with the rest of the system (Navrotsky, 2001). However large scale processes can still influence and control nano-particle formation, nucleation processes and stability to some extent.

Nano phases exhibit different physical and chemical properties from the bulk solid counterparts. The vast scale differences influences thermodynamic properties such as chemical potential, melting temperature, crystal-melt interfacial energy, solubility, Oswald ripening, condensation and nucleation, thermal conductivity and stability. Of the prominent differences on the nano level is the extreme surface to volume ratio (surface sites) of the particles. Nano particles have a greater interaction with the environment, than microscopic size phases, directly influencing the particles' structure and stability (Banfield and Zang, 2001). According to Hochella et al. (2008) a nano phase is stabilized by both surface enthalpy, enthalpy of polymorphic transition and enthalpy of hydration. A change in the free energy of the system (ΔG) will therefore have an effect on the nano phases (Banfield and Zang, 2001). The free energy is influenced by the temperature, external pressure, the composition of the melt, surrounding morphology and the size of the phases (Banfield and Zang, 2001).

Thermodynamic conditions and reaction kinematics will determine if a nano phase will 1) nucleate from a amorphous melt 2) be resorbed back into the melt 3) grow or change to form clusters, nano crystals or meta-stable nano particles or 4) stay preserved in the system for a few seconds to millions of years (Banfield and Zang, 2001).

From the synthetic samples it seemed that PGE clusters and/or nano phases can stay preserved in a magmatic system over temperature changes. Nano phases differed according to temperature window and annealing times (quick vs. slower cooled), see Table 7.7.

The faster cooled samples showed a variety of PGE-rich nano structures, bigger and smaller than 100nm. The samples were poorly crystallised with large PGE phases but several nano crystalline PGE phases were picked-up with XRD. Slower cooled samples showed opposite trends forming large PGE phase with \pm nano PGE structures. The missing PGE phases could have been due to PGE phase's size and/or the phase's being equally dispersed in the samples, making it difficult to pick-up with SAM. Longer annealing times may have caused the PGE to be taken up to form larger PGE phases.

Table 7.7.: Comparison of platinum-group element (PGE) phases between the different temperature windows (fast or slow cooled), to deduce the influence of thermodynamic conditions on cluster formation. Experiment A was used as analogue for the PGE-As system. Faster cooled samples showed a variety of PGE-rich nano structures, bigger and smaller than 100nm. The samples were poorly crystallised with large micron scale PGE phases. However various nano crystalline PGE phases were measured with XRD. Slower cooled samples showed opposite trends forming large PGE phases with \pm PGE nano structures.

		Experiment A: Pt-As system	
		Fast cooled	Slow cooled
Temperature		950°C	400°C
Pressure		vacuum	vacuum
Cooling time		A few seconds	Several days
PGE phases		0.5-10 μ m	0.5-50 μ m
PGE-rich nano entities	>100nm	1200nm	None measured
	<100nm	<100nm	None measured
Measured ions		As, Pt and Pt-ligand	As, Pt and Pt-ligand

TOF-SIMS however revealed that a high concentration of Pt-As bundles (possible clusters) were still present at 400°C. The presence of Pt-As ions proved that nano entities can stay preserved in the system over time and environment (temperature or free energy (ΔG)) changes. However it seemed that nano structures were being lost as the system gets more differentiated over time, with a change in temperature and chemistry. The nano phases may act as nucleation points for larger minerals / phases or are dissolved back into the melt. An approximation of favourable conditions for PGE-cluster formation determined by comparing the Bushveld complex (see section 7.3. and various references listed therein) with results from the synthetic system is proposed in Table 7.8.

Table 7.8.: Approximation of ideal conditions under which nano phases, smaller than 100nm (possible clusters), are more likely to form. Controlling factors in nano phase formation and preservation seemed to be the chemistry of the system, available ligands and the temperature, formation and cooling time of the system. Formation conditions have yet to be quantified.

		Natural system: Bushveld complex	Synthetic system: mss	Ideal conditions
Parental magma	Composition	Picritic melt	Sulphide melt mss	Fe-Ni-Cu \pm PGE type melt
	PGE content	ppb	ppm	ppb-ppm
	Ligands and other transition metals	Various, see for examples Barnes and Maier, 2002	Fe, Cu, S and As	Various chalcogene ligands such as As, Cu
	S content	ppm-wt. %	wt. %	Substantial S up to 0.08wt. %
	State of PGE in the melt	Various PGE ions PGE xenocrysts form the mantle	Uncharged PGE	Uncharged or charged ions or xenocrysts from the mantle

Table 7.8. cont.: Approximation of ideal conditions under which nano phases, smaller than 100nm (possible clusters), are more likely to form.

		Natural system: Bushveld complex	Synthetic system: mss	Ideal conditions
Kinematics	Rate of reaction	Depends on the chemistry, ΔG and ΔT	Several minutes to hours to tens of years	Depends on the chemistry, ΔG and ΔT
Thermodynamics	Temperature	$\pm 1100-1350^{\circ}\text{C}$	$400-950^{\circ}\text{C}$	Magmatic
	Pressure	Up to 3kbar	Vacuum	-
	Free Energy ΔG	Changes with ΔT . Depends on plate tectonics, thermal gradient and P	Changes with ΔT	Changes with ΔT
Geochemical restraints	fS_2	Between -1 and -2	Fast: -2 Slow: -14	Between -1 and -2. Changes with ΔT
	$D^{\text{As}}_{\text{mss/melt}}$	0.40	Pt: 0.30 Pd and Ru: >1	Ligands present As, Te, Bi
	$D^{\text{PGE}}_{\text{mss/melt}}$	Pt: 0.12-0.04 Pd: 0.14-0.07 Ru: 9.00 – 17.43	Pt: <1 Pd: <1 Ru: > 1	Not dependent on PGE concentration

7.3. The physical and chemical behaviour of PGE, in a magmatic sulphide system, as proof of a cluster model

The physical (the physical state/phase of PGE in a melt) and chemical (bonding regime) behaviour of PGE, in the synthetic sulphide system, may be the key as to how PGE is behaving and forming phases in a natural magmatic system.

Clustering can be attributed to physico-chemical interactions on the atomic level. Physical forces including large electron clouds, polarisation effects and electron negativity plays a greater role on the atomic scale. Large electron clouds and unfilled d-orbitals of the PGE, see Table 7.9., allows the formation of sigma (σ) and Pi (π) bonds with anions such as Cu, Fe and As. Sigma and Pi bonds are ranked as the strongest type of covalent bond. Chemical bonding takes place due to the linear overlapping of atomic or molecular orbitals along the relevant axis (x, y, z) (Cotton et al., 1995).

The PGE have high energy unpaired electrons that enable them to form metal-metal, metal-ligand or covalent bonds (Lorand et al., 2008). Coupled with the ability to exist in different valance states (Cotton et al., 1995) and to change hybrid state the PGE can form a vast array of bonds with other PGE and chalcogene ligands (Cu, Fe, S, Bi, Te, As). The state or

phase (individual uncharged atoms, individual ions, complex ions, molecules and collections of ions and atoms) what the elements occur, in the magma, is dependent on the chemistry, redox state (Eh-pH) and fO_2 of the system (Metrich and Mandeville, 2010). Capbianco et al., (1994) as cited in Barnes and Maier (1999) suggested that the oxidation state of the PGE, in a silicate melt, might be indicative of clustering behaviour. The model proposes that the PGE clusters break down into an ionic and metal form, upon partitioning into a phase like spinel. New PGE alloys will form in the phase. The model is similar to that of Tredoux et al., (1995).

Table 7.9.: Hybridization and coordination numbers (C-nr) of S, Fe, Cu, As and the platinum-group elements (PGE: Pt, Pd and Ru) that make out the experimental sulphide melts. The PGE can exist in various hybridization and oxidation states and coupled with empty d-orbitals it enables the PGE elements to form an array of bonds. Data adapted from Cotton et al. (1995), Makovicky (2006) and Lide (2008).

Makovicky (2000) and Eide (2000).								
Ion	C-nr	Radius Å	Hybrid orbital	Ion	C-nr	Radius Å	Hybrid orbital	
S ²⁻	6	1.84	sp ³ d ¹ sp ³ d ²	Pt ⁺²	4 (sq)	0.60	dsp ²	
					6	0.80	d ² sp ³	
				Pt ⁺⁴	6	0.63		
Fe ⁺² Fe ⁺³	4	0.63	sp ³	Ru ³⁺	6	0.68	d ² sp ³	
	6	0.61	d ² sp ³	Ru ⁴⁺	6	0.62		
	8	0.92		Ru ⁵⁺	6	0.57		
	4	0.49	dsp ²	Ru ⁷⁺	4	0.38		
	6	0.55	d ² sp ³	Ru ⁸⁺	4	0.36		
	8	0.78						
Cu ⁺ Cu ⁺²	2	0.46	sp	Pd ²⁺	4 (sq)	0.64	dsp ² d ² sp ³	
	4	0.60	sp ³		6	0.86		
	6	0.77		Pd ³⁺	6	0.76		
	2	0.60	p ²	Pd ⁴⁺	6	0.62	p ³ sp ³	
	4sq	0.57	dsp ²	As ⁺¹	3			
	6	0.73			As ⁺³	6		0.58
					As ⁺⁵	4		0.34

The PGE clusters grow by adsorption. Adsorption, see Figure 7.3., is a physical surface effect that initiates chemical bonding (Bond, 1991). An atom, ion or molecule is attracted to the surface of another molecule by means of an electromagnetic polarisation effect (physical force) (Nowak et al., 2011). The process allows sufficient time for the chemical change necessary for catalytic reactions (Bond, 1991). Adsorption is associated with exothermic reactions (negative change in enthalpy) and is more prominent at lower temperatures. Phases with extreme surface to volume ratios, including colloids (Ni, Pt and Pd), nano particles and clusters, are excellent absorbers (Banfield and Zang, 2001). Clusters can be stabilized by adsorption with inorganic or organic molecules, ions or flocculate to form colloidal particles (Banfield and Zang, 2001). Nano phases can grow, nucleate or aggregate in a system either by organic or inorganic process (Waychunas, 2001).

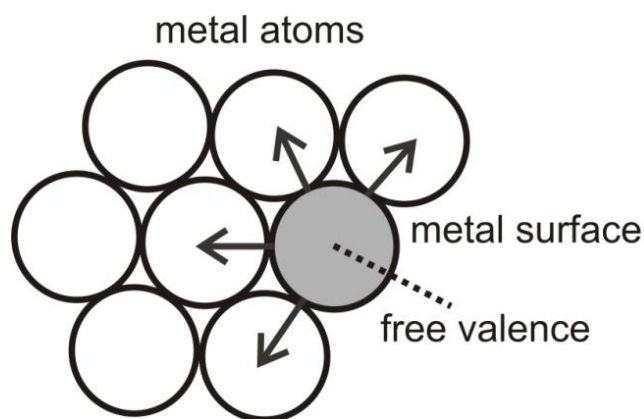


Figure 7.3.: Schematic sketch of the surface energy of a metal, with a free valence position or radical, illustrating the potential for physical adsorption. Clustering works on a similar process. The platinum-group elements (PGE) bonds physically or adsorbs ligands to form a stable phase. Nano entities have extreme surface to volume ratios making them exceptionally reactive. Figure 7.3. was adapted from Bond, 1991.

A cluster may also undergo changes throughout its life span, changing as the environment changes. The addition and loss of ligands may alter the structure, geometry and stability of the cluster, through simple addition and substitution reactions. The PGE unique physical and chemical character might enable them not to melt entirely during magma extraction (Tredoux et al., 1995). PGM micro-xenocrysts or metallic clusters may exist indefinitely in a magma chamber. The nano entities' small size implicates that they are never truly dissolved in the magma and will stay in suspension due to Brownian movement (Cawthorn and Tredoux, 2002). The entities are later removed by physical processes (Hiemstra, 1986; Tredoux et al., 1995) to cause enrichment in chromite and silicate phases.

Possible cluster formation is supported by studies from Barnes (1993), Capiobianco et al. (1994), Ballhaus et al. (1994). In the studies it was suggested that the extreme partitioning coefficients of PGE, into oxide phases, may be contributed to nucleation or trapping of PGE in the immiscible sulphide phases. González-Jiménez et al. (2009) proposed that the PGE nuggets or sub-microscopic alloys may attach to the chromite or oxide grain boundary in equilibrium with the surrounding melt.

7.4. How does the PGE cluster model integrate with proposed chalcophile PGE-enrichment models for the Bushveld complex?

Ligand-mediated PGE cluster formation, in a magmatic environment, is driven by the isochemical or siderophile (Fe-affinity) characteristics of the elements as opposed to

chemical or chalcophile (S-affinity or R-model) association with the mss. The cluster model does not work against models such as the R-model but may be incorporated with the models. The enrichment of the Bushveld cannot be limited to a single mechanism or event.

The R-model (Campbell and Naldrett, 1979) is the currently the leading model for PGE enrichment of the Bushveld complex. The model proposes that a sulphide fraction, charged with trace elements (such as PGE, Ni, Cr), interacts with an infinite silicate magma. The enriched sulphide globules move through the silicate host to cause enrichment in the silicate host. The sulphide globules may also scavenge compatible elements as the globules moves through undepleted magma. The sulphide fraction is derived from the same silicate magma host.

Results showed that PGE-rich nano entities (structures and/or clusters) can form and stay preserved, in magmatic environment, for an undefined amount of time. If the PGE-rich nano phases do form, before formal chemical bonding by means of a mechanical process, it is possible that the PGE-rich nano entities may be taken up in the sulphide melt. However in S-poor environments (oxide and silicate phases) the nano entities can stay suspended in the melt until they precipitate out as alloys or PGM (cluster model, Tredoux et al., 1995). Furthermore it might be possible that a higher fraction of the PGE-ligand nano entities (possibly clusters) may move into the sulphide portion, than the silicate fraction, due to the PGE affinity for the sulphide phase, super charging the sulphide fraction with PGE in relation to the silicate host. The charged sulphide portion, with PGE-clusters and trace metals, may interact with the silicate magma (R-model) to cause PGE enrichment or segregate out. The PGE is not only present in the immiscible sulphide portion as nano entities but also in the silicate host. The nano entities may dissolve, form bonds or segregate out to form PGM and enrich the silicate, sulphide and oxide phases.

The enrichment of PGE-rich deposits such as the Bushveld complex cannot be limited to a single enrichment mechanism but must have been a combination of various factors and processes.

7.5. Summary

It seemed probable that PGE clusters can form in a magmatic system. The PGE can form phases, on a nano level, by means of mechanical or physical processes, before pure chemical bonding takes place or without sulphide saturation having been achieved. The zero

dimensional clusters (<100nm) form due to the physico-chemical association of the PGE with chalcogene ligands.

Cluster formation is not dependent on the PGE concentration but on available chalcogene ligands. In an S-poor magmatic environment, such as the Bushveld complex, the clusters may be stabilized by Fe or other chalcogene ligands, transition metals and metalloids such as Se, Cu, As, Bi, Te and Sb, to form metallic PGM. Heavier PGE are more probable to form clusters. The probability that a PGE will cluster can be expressed as Pt > Ir > Os > Pd > Rh > Ru (Tredoux et al., 1995).

A cluster is not a crystalline phase and does not represent a mineral phase. As the cluster grows by collection, collision or nucleation the cluster may start to resemble colloidal particles, quasi-crystals, crystalloids or mineral entities. Clusters can in addition be stabilized by other clusters, metals or xenocrysts. The clusters may start to exhibit mineral- and crystalloid properties. As the clusters grow in dimension the clusters do not necessarily need to change phase.

A portion of the PGE clusters stay trapped in the incompatible phases and may exsolve out, as the highly unstable mss reaches equilibrium. A fraction of the clusters may be reabsorbed into the melt, while a fraction may act as nucleation points to form nano-crystals and minerals in the incompatible sulphide, oxide or silicate phases. The results showed that it was possible that PGE-clusters can stay persevered, in a magmatic system, with changes in environment (temperature and chemistry) over time.

No ideal parameters or conditions can yet be defined for optimum cluster formation and preservation. To truly quantify and model the kinematics and transition of the nano entities over time and temperature, control programs such as JMAK or FINEMENT can be used (Banfield and Zang, 2001). However there are certain restraints and shortcomings when applying the models to inorganic-metal bond complexes like the PGE.

Chapter 8: Conclusion

A collection PGE-rich nano structures were measured in the synthetic sulphide samples. Several structures qualified as possible clusters. If this was indeed the case, it is probable that PGE clusters can form in a natural magmatic system by means of a mechanical process.

Result showed that PGE nano phase formation did not seem to be dependent on the PGE concentration (clusters can form without the melt being over-saturated in PGE) but needed an appropriate ligand or anion (As, Cu or Fe) to form a phase. This might also hold true for clusters.

The size and morphology of the nano entities were strongly depended on the type of PGE system (either Pt or Pd or Ru). The physical and chemical interactions and properties of the PGE, on the nano level, differ vastly from bulk solid counterparts. Coupled with extreme surface to volume ratios', various bonds and structures can form on the nano level that may not be possible or exist on a larger scale.

The assortment of morphologies of measured nano structures (primary and secondary) it was evident that there are phase transitions and processes present in natural magmatic systems that have not been defined. Nano entities may have a greater influence on the geochemical behaviour of a magmatic system, than previous thought.

Nano phases can stay preserved in the system for an undefined amount of time (few seconds to several million years). Nano structures were measured in fast and slower cooled samples. The preservation and formation of nano phases and possible PGE clusters was not a function of the change in the free energy (ΔG) of the system. A change in energy and environment (thermodynamic changes) may cause of the structures to be lost (resorbed back into melt or act as nucleation points) but also prompt the formation of new phases. It seemed that nano phase formation and destruction is a continuous process over time and environment change. An ideal formation window is yet to be defined.

The PGE-rich and non-PGE nano phases showed no distribution trends and were present in all phases. The overall distribution of nano phases were irregular and not phase dependent, supporting the original hypothesis that clusters can be taken up into more incompatible phases causing enrichment in sulphide, oxide and silicate phases.

If clusters or the remnants thereof were indeed present in the synthetic samples it is possible that ligand-mediated (As, Fe and Cu) PGE-clusters can form before the exsolution of a mss melt from the magma and before formal chemical bonding. Cluster formation is driven by the isochemical (siderophile) characteristics of the elements, as appose to chemical (chalcophile) association with the mss. The primary behaviour of PGE, in a magmatic environment is dependent on the physical characteristics of the metal. Chemical behaviour may govern the secondary distribution of the phases but clustering is primarily a physical mechanism.

PGE-clusters are only one of several mechanisms that contribute to PGE enrichment in sulphide-poor deposits such as the Bushveld complex. Other mechanisms including sulphide saturation, filter pressing, hiatus and the role of secondary fluids play vital roles in ore formation, distribution and concentration of these ores.

However even if clusters did not form the variety of measured nano structures alone showed that a range of nano phases form in magmatic systems. The nano phases can form as primary and/or secondary phases, staying preserved in the system for a few seconds up to millions of years. The nano structures can act as nucleation points for minerals or are destroyed and formed several times during the lifetime of a magma chamber. The influence of nano structures on ore formation and geochemical processes is yet to be quantified.

References

- Akbari, B., Pirhadi Tavandashti, M. & Zandrahimi, M. (2011) Particle size characterization of nanoparticles - a practical guide. *Iranian Journal of Material Science and Engineering*, 8, 48-56
- Alonso, J.A., Glossman, M.D. & Iñiguez, M.P. (1993) Atomic structure of metallic clusters of medium size. In: Kumar V., Martin, T.P. & Tosatti, E (Eds.) *Proceedings of the Adriatic Research Conference Clusters and Fullerenes*, Trieste, Italy, 23-26 June 1992
- Anthony, J.W., Bideaux, R.A., Bladh, K. & Nichols, M.C. (1990) *Handbook of Mineralogy*, Vol. 1: Elements, Sulfides and Sulfosalts. Mineral Data Publishing, Arizona
- Ballhaus, C.G. & Stumpfl, E.F. (1986) Sulfide and platinum mineralization in the Merensky reef: evidence from hydrous silicates and fluid inclusions. *Contributions to Mineralogy and Petrology*, 94, 193-204
- Ballhaus, C., Ryan, C.G., Mernach, T.P. & Green, D.H. (1994) The partitioning of Fe, Ni, Cu, Pt and Au between sulphide, metal and fluid phases: a pilot study. *Geochimica et Cosmochimica Acta*, 58, 811-826
- Ballhaus, C. & Sylvester, P.J. (2000) Noble metal enrichment processes in the Merensky reef, Bushveld complex. *Journal of Petrology*, 41, 545-561
- Ballhaus, C., Tredoux, M. & Späth, A. (2001) Phase relations in the Fe–Ni–Cu–PGE–S system at magmatic temperature and application to massive sulfide ores of the Sudbury igneous complex. *Journal of Petrology*, 42, 1911–1926
- Ballhaus, C., Wohlgemuth-Euberwasser, C., Laurenz, V. & Brendt, J. (2006) Fractionation of the noble metals by physical processes. *Contributions to Mineralogy and Petrology*, 152, 667-684
- Banfield, J.F. & Zang, H. (2001) Nano-particles and the environment: Nano-particles and the environment. *Reviews in Mineralogy and Geochemistry*, 44, 1-51

- Barnes, S.J. (1993) Partitioning of the platinum-group elements and gold between silicate and sulphide magmas in the Munni Munni complex western Australia. *Geochemica et Cosmochimica Acta*, 57, 1277-1290
- Barnes, S-J. & Maier, W.D. (1999) The fractionation of Ni, Cu and the noble metals in silicate and sulfide liquids. In: Keays, R.R., Lesher, C.M. Lightfoot, P.C. & Farrow, C.E.G. (Eds.) *Dynamic processes in magmatic ore deposits and their application in mineral exploration*. Geological Association of Canada, 13, 69-106.
- Barnes, S-J. & Maier, W.D. (2002a) Platinum-group elements and microstructures in normal Merensky reef from Impala Platinum Mines, Bushveld complex. *Journal of Petrology*, 43, 103-128
- Barnes, S-J. & Maier, W.D. (2002b) Platinum-group element distribution in the Rustenburg layered suite of the Bushveld complex, South Africa. In: Cabri, L.J. (Ed.) *The Geology, Geochemistry, Mineralogy and Mineral Beneficiation of platinum-group elements*. Canadian Institute of Mining, Metallurgy and Petroleum, Spec. Vol., 54, 431-458
- Barnes, S-J. & Lightfoot, P.C. (2005) Formation of magmatic nickel-sulfide ore deposits and processes affecting their copper and platinum-group element contents. In: Hedenquist, J.W., Thompson, J.F.H., Goldfarb, R.J. & Richards, J.P. (Eds.) *Economic Geology 100th Anniversary Volume*, 179-213
- Barton, P.B., Bethke, P.M. & Toulmin, P. (1963) *Equilibrium in ore deposits*. Mineralogical Society of America, Special Paper, 1, 171-185
- Barton, P.B. & Skinner, B.J. (1967) Sulfide mineral stabilities. In: Barnes, H.L. (Ed.), *Geochemistry of hydrothermal ore deposits*. Holt, Rinehart and Winston, New York
- Barton, P.B. & Skinner, B.J. (1979) Sulfide mineral stabilities. In: Barnes, H.L. (Ed.), *Geochemistry of hydrothermal ore deposits*, 2nd edn., Wiley-Interscience, New York, 245-287
- Becker, M. (2009) The mineralogy and crystallography of pyrrhotite from selected nickel and PGE ores deposits and its effects on flotation performance. PhD thesis, University of Pretoria

- Becker, M., De Villiers, J. & Bradshaw, D. (2010) The mineralogy and crystallography of pyrrhotite from selected Nickel and PGE ore deposits. *Economic Geology*, 105, 1025-1037
- Behrens, H. & Gaillard, F. (2006) Geochemical aspects of melts: volatiles and redox behaviour. *Elements*, 2, 275-280
- Berlincourt, L.E., Hummel, H.H. & Skinner, B.J. (1981) The platinum-group minerals, platinum-group elements: Mineralogy, Geology, Recovery. The Canadian Institute of Mining and Mineralogy, 19-46
- Blaine, F.A., Linnen, R.L., Holtz, F. & Bruegmann, G.E. (2005) Platinum solubility in a haplobasaltic melt at 1250°C and 0.2Ga: the effect of water and oxygen fugacity. *Geochimica et Cosmochimica Acta*, 69, 1265-1273
- Blaine, F.A., Linnen, R.L., Holtz, F. & Bruegmann, G.E. (2011) The effect of Cl on Pt solubility in haplobasaltic melt: implications for micronugget formation and evidence for fluid transport of PGEs, *Geochimica et Cosmochimica Acta*, 75, 7792-7805
- Bockrath, C., Ballhaus, C. & Haolzhaid, A. (2004) Fractionation of the platinum-group elements during mantle melting. *Science*, 304, 1951-1953
- Bond, G.C. (1991) General introduction to catalyst platinum-group metals. In: Chemistry of the platinum-group metals, recent developments, *Studies in inorganic chemistry*, Elsevier, Amsterdam, 32-59
- Borisov, A. & Palme, H. (1997) Experimental determination of the solubility of platinum in silicate melts. *Geochemica et Cosmochimica Acta*, 61, 4349-4357
- Brenan, J.M. & Andrews, D. (2001) High-temperature stability of laurite and Ru-Os-Ir and their role in PGE fractionation in mafic magmas. *Canadian Mineralogist*, 31, 341-360
- Brenan, J.M., McDonough, W.F. & Ash, R. (2005) An experimental study of the solubility and partitioning of iridium, osmium and gold between olivine and silicate melt. *Earth and Planetary Science Letters*, 237, 855-872
- Brenan, J.M. (2008) The platinum-group elements: “Admirably adapted” for science and industry. *Elements*, 4, 227-232

- Brennecke, G.A. (2006) Origin and metal content of magmatic sulfides in Cu-Au mineralising silicic magmas: Yancocha, Peru and Yerington, NV. Master thesis, Oregon State University
- Brett, R. (1964) Experimental data from the system Cu-Fe-S and their bearing on exsolution textures in ores. *Economic Geology*, 59, 1241-1269
- Brimhall, G.H. & Crerar, D.A. (1987) Ore fluids: magmatic to supergene, *Reviews in Mineralogy*. 17, 235-321
- Brown, T.L., LeMay, H.E., Bursten, B.E. & Murphy, C.J. (2009) *Chemistry: The central science*. 11th edn., Pearson Prentice Hall, Upper Saddle River, N.J.
- Cabri, L.J. (1981) The platinum-group minerals. In Cabri, L.J. (Ed.) *Platinum-group elements: Mineralogy, Geology, Recovery*. Spec. Vol. CIMM, 23, 83-150
- Cabri, L.J. (2002) The platinum-group minerals. In: Cabri, L.J. (Ed.) *The geology, geochemistry, mineralogy and the mineral beneficiation of platinum-group elements*, Canadian Institute of Mining, Metallurgy and Petroleum, 54, 13-130
- Calas, G., Henderson, G.S. & Stebbins, J.F. (2006) Glasses and melts: linking geochemistry and material sciences. *Elements*, 2, 265-268
- Callender, E. (2003) Heavy minerals in the environment. *Treaties of Geochemistry*, 9.03, 1-39
- Campbell, I.H. & Naldrett, A.J. (1979) The influence of silicate:sulphide ratios on the geochemistry of magmatic sulphides. *Economic Geology*, 74, 1503-1505
- Capobianco, C.J., Hervig, R.L. & Drake, M.J. (1994) Experiments on crystal/liquid partitioning ruthenium, rhodium and palladium between spinel and silicate melt implications for platinum group element fractionation trends. *Chemical Geology*, 113, 23-43
- Cawthorn, R.G. & Walraven, F. (1998) Emplacement and crystallization for the Bushveld complex. *Journal of Petrology*, 39, 1669-1687
- Cawthorn, R.G. (1999) Platinum-group element mineralization in the Bushveld complex - a critical reassessment of geochemical models. *South African Journal of Geology*, 102, 268-281

- Cawthorn, R.G. & Tredoux, M. (2002) The Possibility of the Survival of PGM Micro-Xenocrysts in Mantle Melts. 9th International Platinum Symposium, Billings, USA (abstract only), viewed 20 September 2012, from:
<http://www.Nicholas.duke.edu/people/faculty/boudreau/9thPtSymposium>
- Cawthorn, R.G., Eales, H.V., Walraven, F., Uken, R. & Watkey, M.K. (2006) The Bushveld Complex. In: Johnson, M.R., Anhaeusser, C.R. and Thomas, R.J. (Eds.), The Geology of South-Africa, Johannesburg/Council for Geoscience, Pretoria, 261-299
- Cawthorn, R.G. (2007) Cr and Sr: Keys to parental magmas and processes in the Bushveld complex, South Africa. *Lithos*, 95, 381-398
- Ciacchi, L.C. (2002) Growth of Pt clusters in solid solution and on biopolymers: The microscopic mechanism. PhD thesis, Technical University of Dresden
- Coplen, T.B., Böhlke, J.K., De Bièvre, P., Ding, T., Holden, N.E., Hopple, J.A., Krouse, H.R., Lamberty, A., Peiser, H.S., Révész, K., Rieder, D.E., Rosman, K.J.R., Roth, E., Taylor P.D.P., Vocke, R.D. & Xiao, Y.K. (2002) Isotope-abundance variations of selected elements. *Pure and Applied Chemistry*, 74, 1987-2012
- Cotton, F.A., Wilkinson, G. & Gaus, P.L. (1995) Basic inorganic chemistry. 3rd edn., John Wiley and Sons Inc., Canada
- Cotton, S.A. (1997) Chemistry of precious metals. 1st edn., Blackie Academic & Professional, London
- Cotton, F.A., Murillo, C.A. & Walton, R.A. (2005) Multiple bonds between metal atoms. 3rd edn., Springer Science and Business Media Inc, New York
- Cottrell, E. & Walker, D. (2006) Constraints on core formation from Pt partitioning in mafic silicate liquids at high temperatures, *Geochimica et Cosmochimica Acta*, 70, 1565-1580
- Craig, J.R. & Scott, S.D. (1974) Sulfide mineralogy: Sulphide phase equilibria. *Reviews in Mineralogy*, 1, 1-109
- Crocket, J.H. (1981) Geochemistry of the platinum-group elements. In: Cabri, L.J., (Ed.), Platinum-group elements: Mineralogy, Geology, Recovery, Spec. Vol. CIMM, 23, 47-64

- Cullity, B.D. & Stock, S.R. (2001) Elements of x-ray diffraction. 3rd edn., Pearson Prentice Hall, Upper Saddle River, N.J.
- Davies, G., Cawthorn, R.G., Barton, J.M. & Morton, M. (1980) Parental magma of the Bushveld complex. *Nature*, 287, 33-35
- Davies, G. & Cawthorn, R.G. (1984) Mineralogical data on a multiple intrusion in the Rustenburg layered suite of the Bushveld complex. *Mineralogical Magazine*, 48, 469-480
- Davies, G. & Tredoux, M. (1985) The platinum-group element and gold contents of the marginal rocks and sill of the Bushveld complex. *Economic Geology*, 80, 838-848
- Deer, W.A., Howie, R.A. & Zussman, J. (1966) An introduction to the rock forming minerals. Wiley, New York
- De Villiers, J.P.R. & Liles, D.C. (2010) The crystal structure and vacancy distribution in 6C pyrrhotite, *American Mineralogist*, 95, 148-152
- Dingwell, D.B. (2006) Transport properties of magmas: Diffusion and rheology. *Elements*, 2, 281-286
- Dorofeev, G.A., Streletskii, A.N., Povstugar, I.V., Protasov, A.V. & Elsukov, E.P. (2012) Determination of nanoparticle size by X-ray diffraction. *Colloid Journal*, 74, 675-685
- Eales, H.V. & Cawthorn, R.G. (1996) The Bushveld complex. In: Cawthorn, R.G. (Ed.), *Layered intrusions*. Amsterdam: Elsevier, 181-230
- Eby, G.N. (2004) *Principles of environmental geochemistry*, Thomson Books/Cole, California
- Eckstrand, O.R. & Hulbert, L.J. (2007) Magmatic nickel-copper-platinum group element deposits. In: Goodfellow, W.D. (Ed.), *Mineral deposits of Canada: A synthesis of major deposit types, district metallogeny, the evolution of geological provinces and exploration methods*, Geological Association of Canada, Mineral Deposits Division, 5, 205-222
- Ertel, W., O'Neill, H.St.C., Sylvester, P.J. & Dingwell, D.B. (1999) Solubilities of Pt and Rh in a haplobasaltic silicate melt at 1300°C. *Geochimica et Cosmochimica Acta*, 63, 2439-2449

- Ertel, W., Dingwell, D.B. & Sylvester, P.J. (2008) Siderophile elements in silicate melts; a review of the mechanically assisted equilibrium techniques and the nanonugget issue. *Chemical Geology*, 248, 119-139
- Evans, A.M. (1966) *An introduction to crystal chemistry*. Cambridge University Press, Cambridge, UK
- Evans, A.M. (1993) *Ore geology and industrial minerals: An introduction*. 3rd edn., Blackwell Scientific, Oxford, UK
- Fergusson, J.E. (1982) *Inorganic chemistry and the Earth: Chemical resources, their extraction, use and environmental impact*. Pergamon Press, Oxford
- Fleet, M.E., Crocket, J.H. & Stone, W.E. (1996) Partitioning of platinum-group elements (Os, Ir, Ru, Pt, Pd) and gold between sulphide liquid and basalt melt, *Geochimica et Cosmochimica Acta*, 60, 2397-2412
- Fleet, M.E., Crocket, J.H., Liu, M. & Stone, W.E. (1999) Laboratory partitioning of platinum-group elements (PGE) and gold with application to magmatic sulphide-PGE deposits. *Lithos*, 47, 127-142
- Fleet, M.E. (2006) Phase equilibria at high temperatures in sulfide mineralogy and geochemistry, *Reviews in Mineralogy and Geochemistry*, 61, 365-419
- Fortenfant, S.S., Günther, D., Dingwell, D.B. & Rubie, D.C. (2003) Temperature dependence of Pt and Rh solubilities in a haplobasaltic melt. *Geochimica et Cosmochimica Acta*, 67, 123-131
- Francis, R.D. (1990) Sulphide globules in mid-ocean ridge basalts (MORB) and the effect of oxygen abundance in Fe-S-O liquids on the ability of those liquids to partition metals from MORB and komatitic magmas. *Chemical Geology*, 85, 199-213
- Garrels, R.J. & Christ, C.L. (1965) *Solutions, minerals and equilibria*. Harper and Row, New York
- Godel, B., Barnes, S.-J. & Maier, W.D. (2007) Platinum-group elements in sulphide minerals, platinum-group minerals, and whole rocks of the Merensky reef (Bushveld complex South Africa): Implication for the formation of the reef. *Journal of Petrology*, 48, 1569-1604

- Godel, B., Barnes, S.J., Barnes, S.-J. & Maier, W.D. (2010) Platinum ore in three dimensions: Insight from high-resolution X-Ray computed tomography, *Geology*, 38, 1127-1130
- González-Jiménez, J.M., Gervilla, F., Proenza, J.A., Kerestedjian, T., Augé, T. & Bailly, L. (2009) Zoning of laurite (Ru-S₂) erlichmanite (OsS₂): implications for the origin of PGM in ophiolite chromitites. *European Journal of Mineralogy*, 21, 419-432
- Halliday, D. (2008) *Fundamentals of physics*. 8th edn., Extended/ Halliday D, Resnick R, Walker J, John Wiley & Sons Inc., USA
- Hamlyn, P.R. & Keys, P.R. (1986) Sulphur saturation and second-stage melts: application to the Bushveld platinum metal deposits. *Economic Geology*, 81, 1431-1445
- Hanley, J.J. (2005) The aqueous geochemistry of the platinum-group elements (PGE) in surficial, low-T hydrothermal and high-T hydrothermal magmatic-hydrothermal environments. In: Mungall, J.E. (Ed.) *Exploration for platinum-group element deposits*, Mineralogical Association of Canada, Short Course Series, 35, 1-34
- Harmer, R.E. & Sharpe, M.R. (1985) Field relations and strontium isotope systematic of the marginal rocks of the eastern Bushveld complex. *Economic Geology*, 80, 813-837
- Hartley, R.F. (1991) Chemistry of the platinum-group metals: Recent developments. In: *Studies in inorganic chemistry*, Elsevier, Amsterdam
- Hatton, C.J. & Sharpe, M.R. (1988) Significance and origin of boninite-like rocks associated with the Bushveld complex. In: Crawford, A.J. (Ed.), *Boninites*, Unwyn Hyman Ltd., London, 174-207
- Hattori, K. (1996) Occurrence and origin of sulfide and sulphate in the 1991 Mount Pinatubo eruption products. In: Newhall, C.G. & Punongbayan, R.S. (Eds.), *Fire and mud: eruptions and lahars of Mount Pinatubo, Philippines*. University of Washington Press, Seattle and London, 807-824
- Helmy, H.M., Ballhaus, C., Wohlgemuth-Ueberwasser, C., Fonseca, R.O.C. & Laurenz, V. (2010) Partitioning of Se, As, Sb, Te and Bi between monosulfide solid solution and sulphide melt – Application to magmatic sulfide deposits. *Geochimica et Cosmochimica Acta*, 74, 6174–6179

- Helmy, H.M., Ballhaus, C., Fonseca, R.O.C., Wirth, H., Nagel, T. & Tredoux, M. (2013) Nanoparticles in high-temperature magmatic liquids. *Nature proceedings*, viewed 20 September 2013: www.nature.com/naturecommunications, DOI:10.1038/ncomms3405
- Hiemstra, S.A. (1979) The role of collectors in the formation of the platinum deposits in the Bushveld complex. *Canadian Mineralogist*, 17, 469-482
- Hiemstra, S.A. (1986) The distribution of chalcophile and platinum-group elements in the UG-2 chromitite layer of the Bushveld Complex. *Geology*, 81, 1080-1086
- Hochella, M.F. (2008) Nanogeoscience: from origins to cutting-edge applications. *Elements*, 4, 373-379
- Hochella, M.F., Lower, S.K., Maurice, P.A., Penn, R.L., Sahai, N., Sparks, D.L. & Twining, B.S. (2008) Nanominerals, mineral nanoparticles and earth systems, *Science*, 319, 1631-1635
- Holwell, D.A. & McDonald, I. (2010) A review of the behaviour of platinum-group elements within magmatic sulfide ore systems. *Platinum Metals Review*, 54, 26-36
- Irvine, T.N. (1977) Origin of chromitite layers in the Muskox intrusion and other stratiform intrusions: A new interpretation. *Geology*, 5, 273-277
- Jacobs, K. & Alivisatos, A.P. (2001) Nano-crystals are model systems for pressure-induced structural phase transitions. *Reviews in Mineralogy and Geochemistry*, 44, 59-72
- Johnson, B.F.G. (1980) *Transition metal clusters*. John Wiley & Sons Ltd., Great Britain
- Keary, P. (2001) *The new Penguin Dictionary of Geology*. 2nd edn., Penguin Books, London
- Keys, R.R. (1995) The role of komatiitic and picritic magmatism and S-saturation in the formation of ore deposits. *Lithos*, 34, 1-18
- Klug, H.P. & Alexander, L.E. (1974) *X-ray diffraction procedures for polycrystalline and amorphous materials*. 2nd edn., John Wiley & Sons Ltd., New York
- Kretz, R. (1983) Recommendations by the IUGS Subcommittee on the Systematics of Metamorphic Rocks. viewed 19 May 2011, from www.bgs.ac.uk/scmr/home.html

- Kullerud, G. (1968) High temperature phase relations in the Cu-Fe-S system, Carnegie Institute of Washington Yearbook 1966, Vol. 1966-1967, 404-409
- Kullerud, G., Yund, R.A. & Hoh, G.H. (1969) Phase relationships in the Cu-Fe-S, Cu-Ni-S and Fe-Ni-S system. Economic Geology Monograph, 4, 323-343
- Kullerud, G. (1971) Experimental techniques in dry sulphide research, In: Ulmer, G.C., (Ed.), Research techniques for high pressure and high temperature, Springer-Verlag, New York, 288-315
- Leckie, J.O. & Nelson, M.B. (1975) Role of natural heterogeneous sulfide systems in controlling the concentration and distribution of heavy metals. Paper presented at the Second International Symposium on Environmental Biochemistry, Ontario, Canada
- Leshner, C.M. (1989) Komatiite-associated sulphide deposits. Reviews in Economic Geology, 4, 45-101
- Leshner, C.M. & Arndt, N.T. (1995) REE and Nb isotope geochemistry, petrogenesis and volcanic evolution of contaminated komatiites at Kambalda, western Australia. Lithos, 34, 127-158
- Lewis, G.N. & Randal, M. (1961) Thermodynamics. rev. edn., McGraw-Hill Inc., New York
- Li, C., Maier, W. & De Waal, S.A. (2001) The role of magma mixing in the genesis of PGE mineralization in the Bushveld Complex: thermodynamic calculations and new interpretations. Economic Geology, 96, 653-662
- Li, C., Ripley, E.M., Merino, E. & Maier, W.D. (2004) Replacement of base metal sulphides by actinolite, epidote, calcite and magnetite in the UG2 and Merensky reef of the Bushveld complex, South Africa. Economic Geology, 99, 173-184
- Lide, D.R. (2008) CRC Handbook of chemistry and physics: 89th edn., CRC Press, USA
- Lorand, J-P., Luguet, A. & Alard, O. (2008) Platinum-group elements: A new set of key tracers for the Earth's interior. Elements, 4, 247-252
- Luhr, J.F., Carmichael, I.S.E. & Varekamp, J.C. (1984) The 1982 eruptions of El Chichón volcano, Chiapas, Mexico- mineralogy and petrology of the anhydrite-bearing pumice. Journal of Volcanology and Geothermal Research, 23, 69-108

- Lusk, J. & Bray, D.M. (2002) Phase relations and the electrochemical determination of sulphur fugacity for selected reactions in the Cu-Fe-S and FeS systems at 1 bar and temperatures between 185 and 460°C. *Chemical Geology*, 192, 227-248
- Maier, W.D., Arndt, N.T. & Curl, E.A. (2000) Progressive crustal contamination of the Bushveld complex: Evidence from Nd isotopic analyses of the cumulate rocks. *Contributions to Mineralogy and Petrology*, 140, 328-343
- Mandeville, C.W. (2010) Sulfur: A ubiquitous and useful tracer in earth and planetary science. *Elements*, 6, 75-80
- Mathez, E.A. (1999) On factors controlling the concentrations of platinum-group elements in layered intrusions and chromitites. In: Keays, R.R. (Ed.) *Dynamic processes in magmatic ore deposits and their application in mineral exploration*, Geological Association of Canada, Short Course Notes 13, 251-285
- McDonough, W.F. (2003) Compositional model for the Earth's core, *Treaties of Geochemistry*, 2.15, 547-568
- Melber, C., Detlef, K. & Mangelsdorf, I. (2002) Palladium. World Health Organisation, viewed 06 October 2012, from <http://whqlibdoc.who.int/ehc/WHOEH226.pdf>
- Mengason, M.J., Piccoli, P.M. & Candela, P. (2010) An evaluation of the effect of copper on the estimation of sulphur fugacity (fS_2) from pyrrhotite composition. *Economic Geology*, 105, 1163-1169
- Métrich, N. & Mandeville, C.W. (2010) Sulfur in magmas. *Elements*, 6, 81-86
- Mitchell, S. & Pérez-Ramírez, J. (2010) X-Ray diffraction: Surface science and methods in catalysis. 529-0611-00L, *Advanced catalysis engineering*, Institute for chemical and bioengineering, Zurich, Switzerland, viewed 22 June 2012, from: <http://cc.usst.edu.cn/Download/26da9cdf-6134-41fc-bf56-6dcccc9edd20.pdf>
- Mungall, J.E. (2005), Magmatic geochemistry of the PGE, In: Mungall, J.E. (Ed.) *Exploration for platinum-group element deposits*, Mineralogical Association of Canada, Short Course Series, 35, 1-34
- Mungall, J.E., Andrews, D.R., Cabri, L.J., Sylvester, P.J. & Tubrett, M. (2005) Partitioning of Cu, Ni, Au and platinum-group elements between monosulfide solid solution and

- sulfide melt under controlled oxygen and sulfur fugacities. *Geochemica et Cosmochimica Acta*, 69, 4349-4360
- Mungall, J.E. & Naldrett, A.J. (2008) Ore Deposits of the platinum-group elements. *Elements*, 4, 253-258
- Naldrett, A.J., Gasparri, E.C., Barnes, S.J., Von Grunewaldt, G. & Sharp, M.R. (1986) The upper critical zone of the Bushveld complex and the origin of the Merensky-type ores. Research report nr 60, Institute for Geological research on the Bushveld complex, University of Pretoria
- Naldrett, A.J., Cameron, G., Von Grunewaldt, G. & Sharp, M.R. (1987) The formation of stratiform platinum-group elements deposits in layered intrusions. Research Report no. 63, Reidel Publishing Company, Dordrecht
- Navrotsky, A. (1976) Geological applications of high temperature reaction calorimetry, In: Frasier, D.G. (Ed.) *Thermodynamics in Geology*, Reidel Publishing Company, Dordrecht
- Navrotsky, A. (2001) Thermochemistry of nanomaterials. *Reviews in Mineralogy*, 44, 73-103
- Nowak, P., Nastawny, M., Kozyra, I. & Wegrzywics, A. (2011) Controlled adsorption at the surface of copper sulphide minerals - a way to abate the problem of environmental contamination by the copper sulfide oxidation products?. *Physicochemical Problems of Mineral Processing*, 47, 131-138
- O'Day, P.A. (2006) Chemistry and mineralogy of arsenic. *Elements*, 2, 77-83
- Palme, H. & O'Neill, H.S.C. (2003) Geochemical estimates of mantle composition: *Treaties of Geochemistry*, 2.01, 1-38
- Palme, H. (2008) Platinum-group elements in cosmochemistry. *Elements*, 4, 233-238
- Patrick, M. & Lutz, H.D. (1999) Semi-empirical band structure calculations on skutterdite-type compounds. *Physics and Chemistry of Minerals*, 27, 41-46
- Peach, C.L., Mathez, E.A. & Keays, R.R. (1990) Sulfide melt-silicate melt distribution coefficients for noble metals and other chalcophile elements as deduced from MORB: implications for partial melting. *Geochemica et Cosmochimica Acta*, 54, 3379-3389

- Peach, C.L. & Mathez, E.A. (1996) Constraints on the formation of platinum-group element deposits in igneous rocks. *Economic Geology*, 91, 439-450
- Pohl, W.L. (2011) *Economic geology: Principles and practise*, Wiley and Blackwell, Oxford
- Popp, R.K., Gilbert, C.M. & Craig, J.R. (1977) Stability of Fe-Mg amphiboles with respect to sulphur fugacity. *American Mineralogist*, 62, 13-30
- Pruseth, K.L. & Palme, H. (2004) The solubility of Pt in liquid Fe-sulfides. *Chemical Geology*, 208, 233-245
- Prutton, M., Gamati, E.L. & Mohamed, M. (2006) *Scanning Auger microscopy*, Wiley, England
- Qi, Y., Tahir, C., Johnson, W.L. & Goddard, W.A. III (2001) Melting and crystallization in Ni nano-clusters: The mesoscale regime. *Journal of Chemical Physics*, 115, 385-394
- Rajagopal, A.K., Pande, C.S. & Abe, S. (2004) Nanothermodynamics- A generic approach to material properties at nano scale, Indo-US workshop on "Nanoscale materials: From Science to Technology", Puri, India (extended abstract), viewed 19 October 2012, from: <http://arxiv.org/abs/cond-mat/0403738>
- Rajamani, V. & Naldrett, A.J. (1978) Partitioning of Fe, Co Ni and Cu between sulphide liquid and basaltic melts and the composition of Ni-Cu sulphide deposits. *Economic Geology*, 73, 82-93
- Ramdohr, P. (1980) *The ore minerals and their intergrowths*. 2nd edn., Pergamon Press, Oxford
- Reed, S.J.B. (2005) *Electron microprobe analysis and scanning electron microscopy in geology*. 2nd edn., Cambridge University Press, Cambridge
- Reich, E.S. (2011) Nano rules fall foul of data gap. *Nature*, 480, 160-161
- Richet, P., Henderson, G.S. & Neuville, D.R. (2010) Thermodynamics: The oldest branch of earth sciences. *Elements*, 6, 287-292
- Richet, P. & Ottonello, G. (2010) Thermodynamics of phase equilibria in magma. *Elements*, 6, 315-320

- Robb, L. (2005) Introduction to ore-forming processes. Blackwell Publishing Ltd, Malden
- Rösler, H.J. & Lange, H. (1972) Geochemical tables. Elsevier Publishers, Amsterdam
- Rosso, K.M. & Vaughan, D.J. (2006) Sulfide mineral surfaces. Reviews in Mineralogy and Geochemistry, 61, 505-556
- Rudnick, R.L. & Gao, S. (2003) Composition of the continental crust. Treaties of Geochemistry, 3.01, 1-64
- Scott, S.D. (1968) Stöichiometry and phase changes in zinc sulfide, PhD thesis, The Pennsylvania State University
- Scott, S.D. (1974) Sulfide mineralogy: Experimental methods in sulfide synthesis. Reviews in Mineralogy, 1, 1-38
- Sen, R., Seth, D., Roy, I., Dasgupta, D. & Goswami, A. (2011) Environmental pursuits in nanomaterial system science with Indian exemplars, Nature Proceedings, 1-12, viewed 28 July 2011, from oai:nature.com:10.1038/npre.2010.4984.1
- Simon, A.C. & Ripley, E.M. (2011) The role of magmatic sulfur in the formation of ore deposits. Reviews in Mineralogy and Geochemistry, 73, 513-578
- Stephan, T. (2001) TOF-SIMS in cosmochemistry. Planetary and Space Science, 49, 859-906
- Stone, W.E., Fleet, M.E. & MacRae, N.D. (1989) Two-phase nickeliferous monosulphide solid solution (mss) in megacrysts from Mount Shasta, California: A natural laboratory for Ni-Cu sulfides. American Mineralogist, 74, 981-993
- Toulmin, P. & Barton, P.B. (1964) A thermodynamic study of pyrite and pyrrhotite. Geochimica et Cosmochimica Acta, 28, 641-671
- Tredoux, M., Lindsay, N.M., Davies, G. & McDonald, I. (1995) The fractionation of platinum-group elements in magmatic systems, with the suggestion of a novel causal mechanism. South African Journal of Geology, 98, 157-167
- Vaughan, D.J. & Craig, J.R. (1978) Mineral chemistry of metal sulphides, Cambridge University Press, Cambridge

- Vaughan, D.J. (2006) Arsenic. *Elements*, 2, 71-75
- Vaughan, D.J. & Rosso, K.M. (2006) Chemical bonding in sulfide minerals. *Reviews in Mineralogy and Geochemistry*, 61, 231-264
- Viljoen, M.J. & Schurmann, L.W. (1998) Platinum-group elements, In: Wilson, M.G.C. & Anhaeusser, C.R. (Eds.) *The mineral resources of South Africa*, Council for Geoscience, 16, 532-568
- Von Grunewaldt, G., Hatton, C.J. & Merkle, R.K.W. (1987) Platinum-group element deposits: Course notes, Institute for Geological Research on the Bushveld Complex, University of Pretoria, Pretoria
- Von Grunewaldt, G., Hulbert, C.J. & Naldrett, A.J. (1989) Contrasting platinum-group element concentration patterns in cumulus of the Bushveld complex. *Mineralium Deposita*, 24, 219-229
- Waychunas, G.A. (2001) Structure, aggregation and characteristics of nanoparticles. *Reviews in Mineralogy*, 44, 105-166
- Waychunas, G.A. & Zhang, H. (2008) Structure, chemistry and properties of mineral nanoparticles. *Elements*, 4, 381-387
- Wenk, H.R. & Bulakh, A. (2006) *Minerals: Their constitution and origin*. Cambridge University Press, Cambridge, UK
- Wilson, B., Dewers, T., Reches, Z. & Brune, J. (2005) Particle size and energetics of gouge from earthquake rupture zones. *Nature*, 434, 749
- Witney, D.L. & Evans, B.W. (2010) Abbreviations for names of rock-forming minerals. *American Mineralogist*, 95, 185-187
- Wuensch, B.J. (1974) Sulfide mineralogy: Determination, relationships and classification of sulphide minerals structures. *Reviews in Mineralogy*, 1, W1-20
- Wuensch, B.J. (1974) Sulfide mineralogy: Sulfide crystal chemistry. *Reviews in Mineralogy*, 1, W21-44
- Yund, R.A. & Kullerud, G. (1966) Thermal stability of assemblages in the Cu-Fe-S system. *Journal of Petrology*, 7, 454-88

Appendix A

Chapter 2, section 2.3.3.:

The Scherrer equation (Akbari et al., 2011):

$$D_{XRD} = \frac{K\lambda}{B \cos \theta}$$

Where D= crystallite size, K= constant (0.9), λ = diffraction wavelength,
B= FWHM ($B^2_r = B^2_0 - B^2_i$, B_0 = observed broadening B_i = instrumental broadening)

Chapter 3, section 3.2.:

Chemical equilibrium (Richet et al., 2010):

$$\Delta G = \Delta H - T\Delta S, \Delta G = -RT \ln k$$

ΔG = Gibbs free energy ΔH = change in enthalpy T = temperature ΔS = change in entropy
 R = gas constant = 8.31 k = equilibrium constant (k = products / reactant)

Chapter 5, section 5.1.:

The fS_2 (Fe:S) can be expressed as (Toulmin and Barton, 1964):

$$\text{Log } fS_2 = (70.03 - 85.83N) \left(\frac{1000}{T} - 1 \right) + 39.30\sqrt{1 - 0.9981N} - 11.91$$

Where $N = X_{FeS}^{po}$ and $N = 2 \left(\frac{nFe}{nFe+nS} \right)$, n = number of moles; T = Kelvin

The original formula from Toulmin and Barton (1964) was adapted as follows by Mengason et al., (2010) to compensate for the additional Cu in the po.

The fS_2 (Fe + Cu: S) equation:

$$\text{Log } fS_2 = (70.03 - 85.83N) \left(\frac{1000}{T} - 1 \right) + 39.30\sqrt{1 - 0.9981N} - 11.91$$

Where $N = X_{FeS}^{po}$ and $N = 2 \left(\frac{nFe+nCu}{nFe+1.5nCu+nS} \right)$, n = number of moles; T = Kelvin

And $T = T_f = 900 + 273.5 = 1173.5$ K and $T_s = 400 + 273.5 = 673.5$ K, $P = 1$ atm in all the experiments

Chapter 5, section 5.2.:

The formula for D is given as (Mungal, 2005):

$$D_{phase\ a/phase\ b}^x = \frac{x^a}{x^b}$$

x= concentration of element x, a and b are the different phases

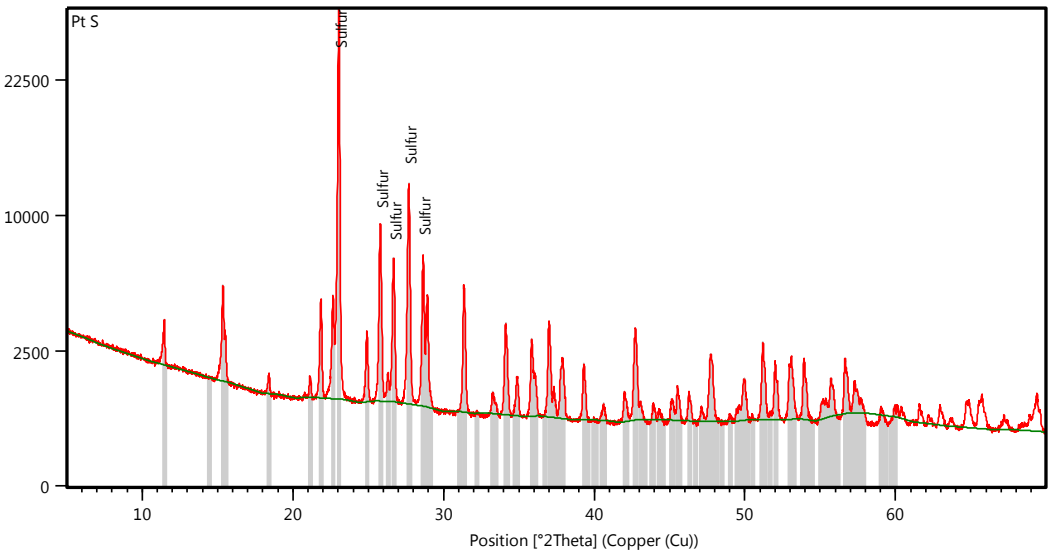
If $D > 1$, the element is more compatible in phase a, if $D < 1$ the reverse is true and the element is more compatible in phase b.

Appendix B

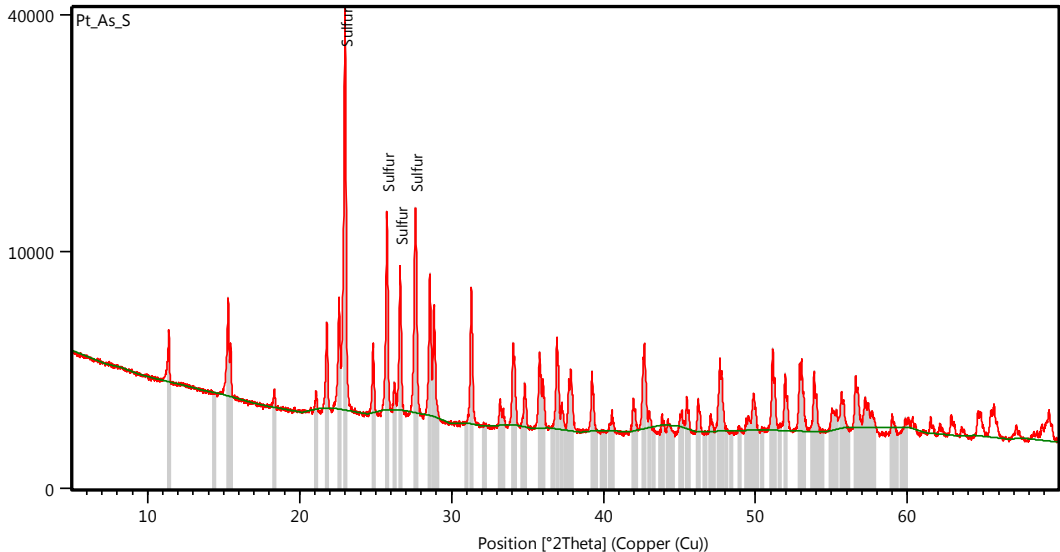
Table 3.5. A and B: XRD spectra of the evolution of synthetic system during sample preparation: See following pages.

The 5 strongest peaks were tabulated in the data sets below.

Step 1: S doped with Pt

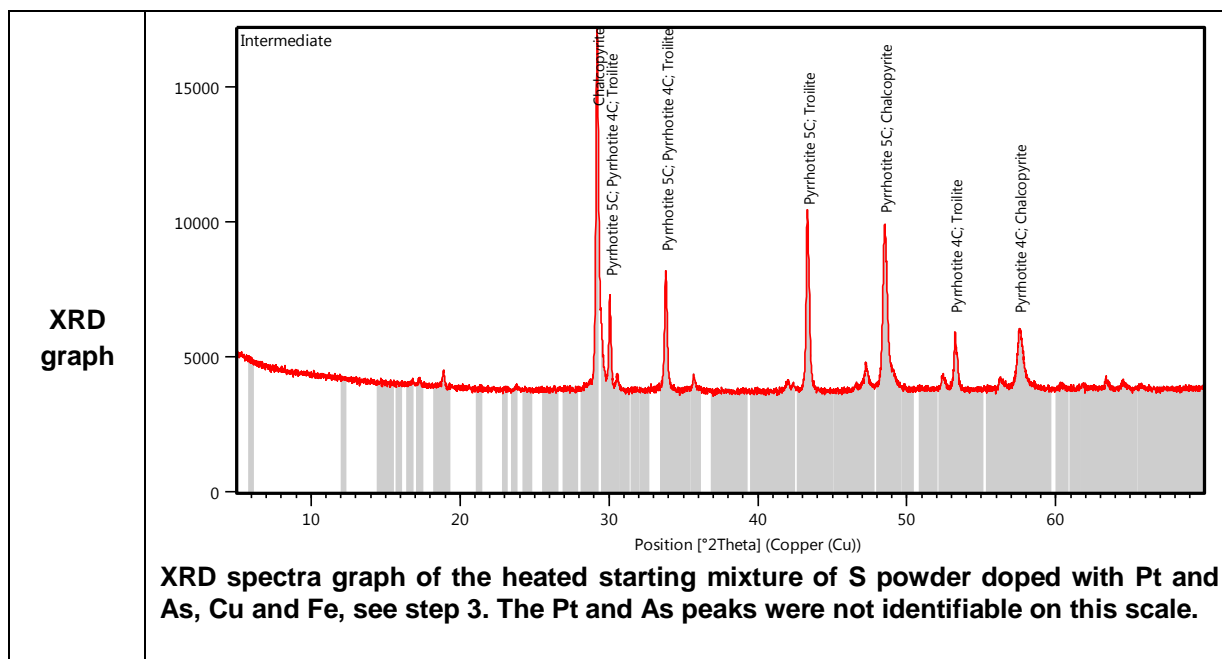
Mineral name	Position 2 Theta	Height cts	FWHM	d spacing Å	Relative intensity %	Tip width
S₁₂₈	23.1349	11197.82	0.0288	3.8510	38.62	0.0346
	25.8300	8047.32	0.1248	3.4465	27.76	0.1498
	26.7095	5887.93	0.0864	3.3349	20.31	0.1037
	27.7041	11459.56	0.1632	3.2174	39.53	0.1958
	28.6610	6338.04	0.0672	3.1121	21.86	0.0806
Pt-salt	No Pt-phases (PGM) were picked-up					
XRD graph	 <p>XRD spectra graph of S doped with Pt-salt. The Pt peaks were not identifiable on this scale.</p>					

Step 2: S + Pt doped with As

Mineral name	Position 2 Theta	Height cts	FWHM	d spacing Å	Relative intensity %	Tip width
S₁₂₈	22.9877	40455.96	0.0768	3.8658	100.00	0.0922
	23.0541	18386.40	0.0384	3.8643	45.45	0.0461
	25.7495	12567.61	0.0768	3.4570	31.06	0.0922
	26.6224	7823.50	0.0576	3.3456	19.34	0.0691
	27.6032	12547.47	0.1056	3.2290	31.02	0.1267
Pt-salt	No Pt-phases (PGM) were picked-up					
As-salt	No Pt-phases (PGM) were picked-up					
XRD graph	 <p>XRD spectra graph of S doped with Pt and As, step 2. The Pt and As peaks were not identifiable on this scale.</p>					

Step 3: Cu and Fe added to S+Pt+As and heated to 700°C

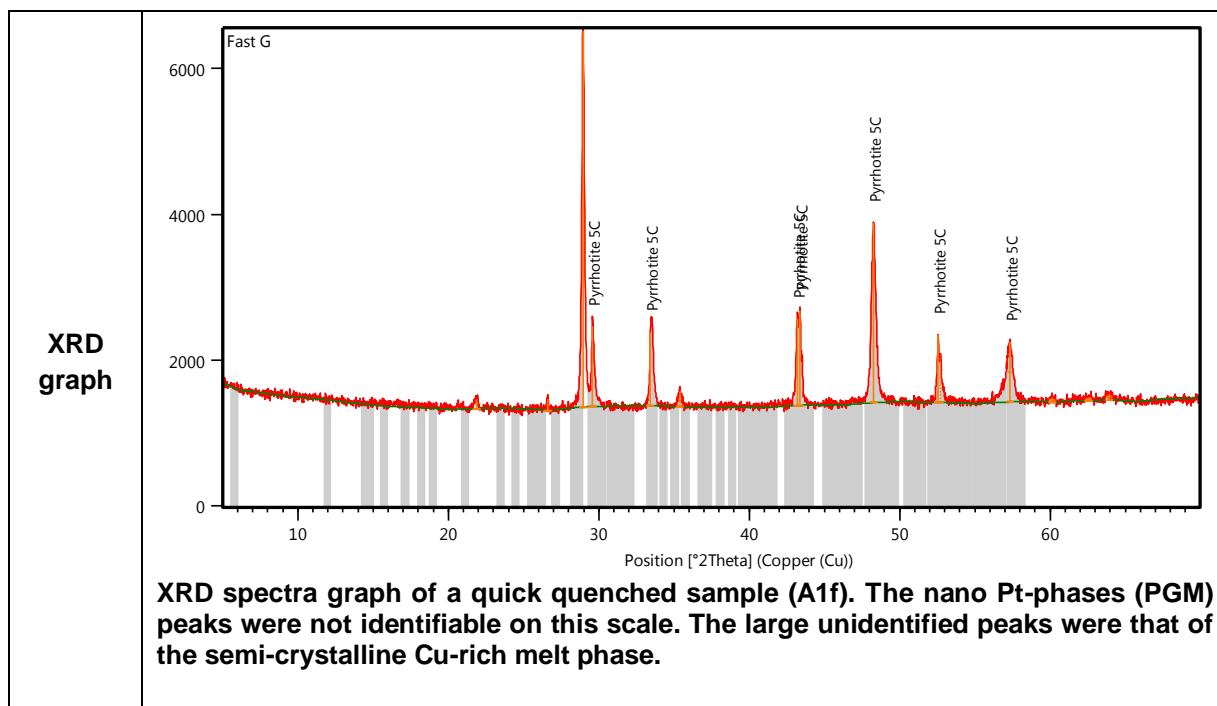
Mineral name	Position 2 Theta	Height cts	FWHM	d spacing Å	Relative intensity %	Tip width
po (tr, 4C, 5C)	30.0604	3440.89	0.0672	2.9704	26.37	0.0806
	33.7967	4389.16	0.0480	2.6500	33.64	0.0576
	43.2967	6129.53	0.0960	2.0880	46.97	0.1152
	43.4379	4356.20	0.0480	2.0868	33.38	0.0576
	53.2393	2057.75	0.0768	1.7192	15.77	0.9220
ccp	18.9197	570.05	0.0945	4.6914	4.37	0.1134
	29.1918	13049.23	0.8152	3.0548	100.00	0.1382
	48.5221	6110.23	0.0480	1.8794	46.82	0.0576
	52.4055	465.46	0.1920	1.7445	3.57	0.2304
	57.5160	2037.54	0.0480	1.6011	15.61	0.0576
Pt	No Pt-phases (PGM) were picked-up					
As	No Pt-phases (PGM) were picked-up					



Step 4: Heated homogenised powders, see step 5.

Step 5: Heated homogenised powders and quick quenched, sample A1f

Mineral name	Position 2 Theta	Height cts	FWHM	d spacing Å	Relative intensity %	Tip width
po (5C)	29.5772	1100.25	0.0669	3.0203	21.35	0.0803
	33.4500	1011.99	0.1506	2.6789	19.64	0.1807
	43.2072	1189.45	0.1020	2.0922	23.08	0.1224
	43.3884	1304.58	0.0669	2.0856	25.37	0.0803
	48.2672	2465.44	0.1338	1.8856	47.84	0.1606
melt	Several Cu-rich phases were picked-up as representative / analogue for the amorphous to semi crystalline melt phases					
PGM	No Pt-phases (PGM) were picked-up					
nano size PtAs₂	33.4500	1011.99	0.1836	2.6761		
	36.4250	13.69	0.1020	2.4646		
	43.2072	1189.45	0.1020	2.0922		
	64.0210	74.83	0.6320	1.4532		



Step 5: Heated homogenised powders and slow cooled, sample A1s

Mineral name	Position 2 Theta	Height cts	FWHM	d spacing Å	Relative intensity %	Tip width
po 4C	29.4248	700.23	0.1020	2.9933	8.45	0.1224
	33.5844	1519.15	0.1020	2.6663	18.33	0.1224
	43.1355	1391.16	0.1224	2.0956	16.79	0.1469
	53.0292	695.07	0.1224	1.7255	8.39	0.1469
	57.2467	1550.72	0.0816	1.6080	18.72	0.0979
bn	28.9169	82853.59	0.1224	3.0852	100.00	0.1469
	33.5844	1519.15	0.1020	2.6663	18.33	0.1224
	48.1573	33.87.37	0.1428	1.8803	40.88	0.1714
	57.2467	1550.72	0.0816	1.6080	18.72	0.0979
ccp	28.9169	82853.59	0.1224	3.0852	100.00	0.1469
	33.5844	1519.15	0.1020	2.6663	18.33	0.1224
	48.1573	3387.37	0.1428	1.8803	40.88	0.1714
	57.2467	1550.72	0.0816	1.6080	18.72	0.0979
SiO₂	Like the other samples fine glass, from the silica tubes, were also picked-up with XRD					
PGM	No large scale Pt-phases (PGM) were picked-up					
nano size PtAs₂	25.9576	9.43	0.1224	3.4298		
	33.5844	1519.15	0.1020	2.6663		
	43.1335	1391.16	0.1224	2.0956		
	50.8550	39.99	0.1224	1.7940		
	59.4401	16.47	0.1224	1.5576		

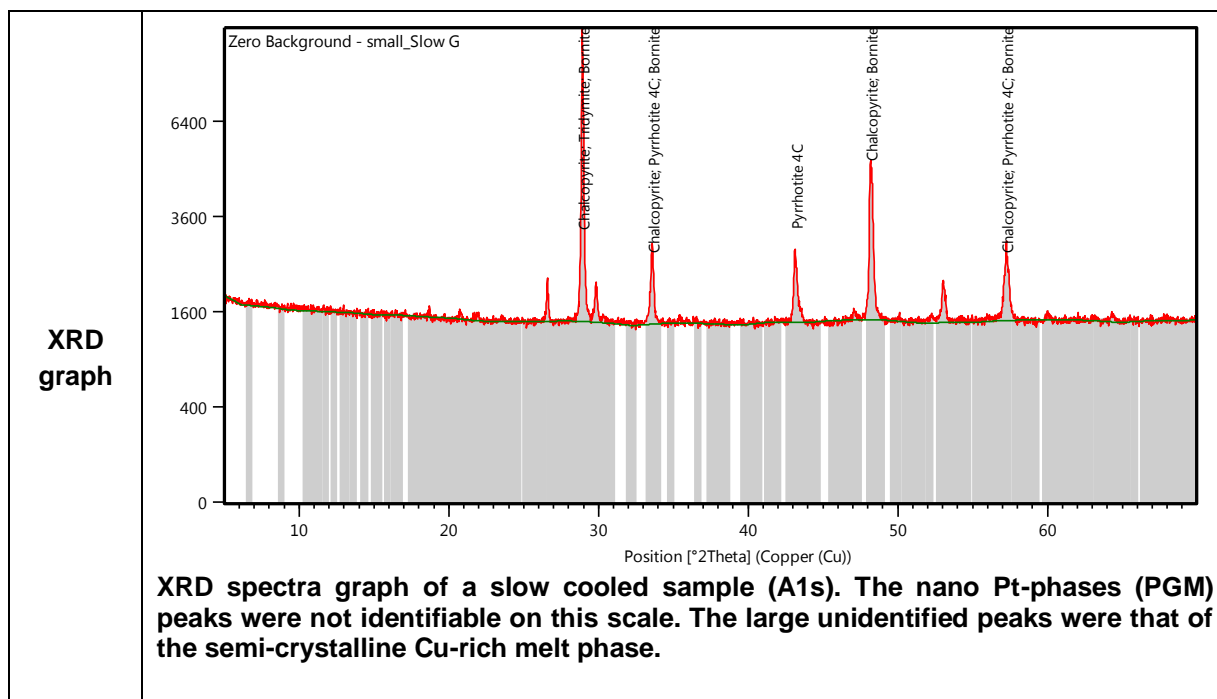


Table 3.5. B: Relative size of nano entities measured with XRD

Crystal shape correction factors for crystallite size calculations, using the Scherrer equation.

Crystallite shape	Mineral, element	Crystal system	FWHM	Integral breath
Sphere	As	hexagonal	0.89	1.07
Cube	Pt sperrylite isoferroplatinum	cubic	0.83- 0.91	1.00- 1.16
Tetrahedral	n/a	n/a	0.73- 1.03	1.94- 1.39
Octahedral	As	hexagonal	0.82- 0.94	1.04- 1.14

The average size of calculated nano Pt-phases (PGM) present during the experimental process.

		Average size (nm) of nano Pt-phases (PGM) calculated with XRD					
Step 1		No nano Pt-phases were picked up					
Step 2		No nano Pt-/As phases were picked up					
Step 3		No nano Pt-/As phases were picked up					
Step 4		n/a					
		1	2	3	4	5	Avg. nm
Step 5: fast	PtAs ₂	53	214	220	75	-	141
Step 5: slow	PtAs ₂	114	213	118	123	132	140
Avg.							141

Appendix C

Figure 4.2. A and B: Ore microscope images, no analyses

Figure 4.2. C and D: See following pages

Figure 4.3. A: Ore microscope image, no analyses

Figure 4.3. B, C and D: See following pages

Table 4.3. and 4.5.: Chemical composition of the major phases of exp. A, B and C.

Average composition (wt.%) of po (mss) present in fast and slow cooled samples of experiment A, B and C. The wt.% data was used to calculate the $\log fS_2$ of the samples.

mss	1	2	3	4	5	Average
A1f	Cu ₆ Fe ₅₈ S ₃₇	Cu ₅ Fe ₅₉ S ₃₈	Cu ₆ Fe ₅₈ S ₃₇	Cu ₆ Fe ₅₉ S ₃₈	Cu ₅ Fe ₅₈ S ₃₈	Cu ₆ Fe ₅₈ S ₃₈
A2f	Cu ₅ Fe ₅₉ S ₃₈	Cu ₅ Fe ₅₉ S ₃₈	Cu ₅ Fe ₅₈ S ₃₈	Cu ₅ Fe ₅₉ S ₃₇	Cu ₅ Fe ₅₉ S ₃₇	Cu ₅ Fe ₅₈ S ₃₇
A3f	Cu ₅ Fe ₅₇ S ₃₈	Cu ₅ Fe ₅₉ S ₃₈	Cu ₅ Fe ₅₈ S ₃₉	Cu ₆ Fe ₅₇ S ₃₇	Cu ₅ Fe ₅₈ S ₃₈	Cu ₅ Fe ₅₈ S ₃₈
						Cu₅Fe₅₈S₃₈
A1s	Cu ₃ Fe ₆₁ S ₃₇	Cu ₃ Fe ₆₂ S ₃₇	Cu ₂ Fe ₆₂ S ₃₈	Cu ₃ Fe ₆₁ S ₃₇	Cu ₃ Fe ₆₁ S ₃₆	Cu ₃ Fe ₆₁ S ₃₇
A2s	Cu ₂ Fe ₆₂ S ₃₇	Cu ₄ Fe ₆₁ S ₃₇	Cu ₃ Fe ₆₁ S ₃₆	Cu ₃ Fe ₆₁ S ₃₇	Cu ₄ Fe ₆₁ S ₃₆	Cu ₃ Fe ₆₁ S ₃₇
A3s	Cu ₂ Fe ₆₄ S ₃₈	Cu ₁ Fe ₆₃ S ₃₈	Cu ₁ Fe ₆₃ S ₃₈	Cu ₂ Fe ₆₃ S ₃₈	-	Cu ₂ Fe ₆₃ S ₃₈
						Cu₄Fe₆₁S₃₇
B1f	Cu ₃ Fe ₅₉ S ₃₆	Cu ₃ Fe ₆₀ S ₃₇	Cu ₃ Fe ₅₉ S ₃₇	Cu ₃ Fe ₅₇ S ₃₇	Cu ₃ Fe ₅₈ S ₃₇	Cu ₃ Fe ₅₉ S ₃₇
B2f	Tubes exploded: n.d.					
B3f	Cu ₁ Fe ₅₉ S ₃₈	Cu ₀ Fe ₆₁ S ₃₈	Cu ₀ Fe ₆₀ S ₃₈	Cu ₁ Fe ₆₀ S ₃₈	Cu ₁ Fe ₆₁ S ₃₉	Cu ₁ Fe ₆₀ S ₃₈
						Cu₂Fe₆₀S₃₈
C1f	Cu ₀ Fe ₆₀ S ₄₀	Cu ₀ Fe ₆₀ S ₄₀	Cu ₀ Fe ₆₀ S ₄₀	Cu ₀ Fe ₆₀ S ₄₀	Cu ₀ Fe ₆₀ S ₃₉	Cu ₀ Fe ₆₀ S ₄₀
C2f	Cu ₀ Fe ₆₀ S ₄₁	Cu ₀ Fe ₆₀ S ₄₀	Cu ₀ Fe ₅₉ S ₃₉	Cu ₀ Fe ₆₀ S ₄₀	Cu ₀ Fe ₅₉ S ₄₀	Cu ₀ Fe ₅₉ S ₄₀
C3f	Cu ₄ Fe ₅₇ S ₃₉	Cu ₅ Fe ₅₇ S ₃₉	Cu ₅ Fe ₅₇ S ₃₆	Cu ₃ Fe ₅₈ S ₃₈	Cu ₄ Fe ₅₇ S ₃₈	Cu ₄ Fe ₅₇ S ₃₈
						Cu₁Fe₅₉S₃₉

Average composition (wt.%) of melt phase present in slow and fast cooled samples of experiment A, B and C.

mss	1	2	3	4	5	Average
A1f	Cu ₃₄ Fe ₃₅ S ₃₁	Cu ₃₁ Fe ₃₇ S ₃₁	Cu ₃₃ Fe ₃₆ S ₃₁	Cu ₃₀ Fe ₄₀ S ₃₂	Cu ₃₂ Fe ₃₇ S ₃₂	Cu ₃₂ Fe ₃₇ S ₃₁
A2f	Cu ₂₉ Fe ₄₀ S ₃₂	Cu ₂₈ Fe ₄₀ S ₃₂	Cu ₃₁ Fe ₄₀ S ₃₂	Cu ₃₁ Fe ₃₇ S ₃₂	Cu ₃₂ Fe ₃₈ S ₃₂	Cu ₃₀ Fe ₃₉ S ₃₂
A3f	Cu ₃₀ Fe ₃₈ S ₃₂	Cu ₃₃ Fe ₃₈ S ₃₂	Cu ₃₀ Fe ₃₉ S ₃₂	Cu ₃₁ Fe ₃₈ S ₃₂	Cu ₃₁ Fe ₃₈ S ₃₁	Cu ₃₁ Fe ₃₈ S ₃₂
						Cu₃₁Fe₃₈S₃₂

Average composition (wt.%) of melt phase present in slow and fast cooled samples of experiment A, B ad C.

mss	1	2	3	4	5	Average
A1s	-	-	-	-	-	-
A2s	Cu ₂₄ Fe ₄₃ S ₃₄	Cu ₂₄ Fe ₄₃ S ₃₃	Cu ₂₄ Fe ₄₃ S ₃₃	Cu ₂₃ Fe ₄₂ S ₃₄	Cu ₂₄ Fe ₄₃ S ₃₄	Cu ₂₄ Fe ₄₃ S ₃₄
A3s	Cu ₂₉ Fe ₃₉ S ₃₄	Cu ₂₈ Fe ₄₀ S ₃₄	Cu ₂₈ Fe ₄₀ S ₃₃	Cu ₂₈ Fe ₄₀ S ₃₃	-	Cu ₂₈ Fe ₄₀ S ₃₄
						Cu₂₆Fe₄₂S₃₄
B1f	Cu ₅₆ Fe ₁₅ S ₂₈	Cu ₅₅ Fe ₁₅ S ₂₇	Cu ₅₇ Fe ₁₄ S ₂₇	Cu ₅₆ Fe ₁₄ S ₂₇	Cu ₃₅ Fe ₁₅ S ₂₇	Cu ₅₆ Fe ₁₅ S ₂₇
B2f	Tubes exploded: n.d.					
B3f	Cu ₂₀ Fe ₄₂ S ₃₆	Cu ₂₀ Fe ₄₂ S ₃₅	Cu ₂₀ Fe ₄₃ S ₃₇	Cu ₂₀ Fe ₄₂ S ₃₆	Cu ₁₉ Fe ₄₃ S ₃₈	Cu ₂₀ Fe ₄₂ S ₃₆
						Cu₃₈Fe₂₉S₃₂
C1f	Cu ₂₂ Fe ₄₁ S ₃₇	Cu ₂₃ Fe ₄₀ S ₃₆	Cu ₂₂ Fe ₄₁ S ₃₆	Cu ₂₁ Fe ₄₀ S ₃₆	Cu ₂₂ Fe ₄₁ S ₃₆	Cu ₂₂ Fe ₄₁ S ₃₆
C2f	Cu ₂₂ Fe ₄₁ S ₃₅	Cu ₂₂ Fe ₄₁ S ₃₆	Cu ₂₁ Fe ₄₁ S ₃₅	Cu ₂₁ Fe ₄₁ S ₃₆	Cu ₂₂ Fe ₄₁ S ₃₆	Cu ₂₂ Fe ₄₁ S ₃₆
C3f	Cu ₂₂ Fe ₄₁ S ₃₆	Cu ₂₂ Fe ₄₁ S ₃₆	Cu ₂₃ Fe ₄₀ S ₃₆	-	-	Cu ₂₂ Fe ₄₁ S ₃₆
						Cu₂₂Fe₄₁S₃₆

Average composition (wt.%) of bn phases present in slow cooled samples of experiment A.

mss	1	2	3	4	5	Average
A1s	Cu ₅₈ Fe ₁₆ S ₂₇	Cu ₅₅ Fe ₁₇ S ₂₉	Cu ₅₄ Fe ₁₆ S ₂₉	Cu ₅₅ Fe ₁₆ S ₂₉	Cu ₅₆ Fe ₁₆ S ₂₈	Cu ₅₆ Fe ₁₆ S ₂₈
A2s	-	-	-	-	-	-
A3s	-	-	-	-	-	-
						Cu₅₆Fe₁₆S₂₈

Average composition (wt.%) of ccp phases present in slow cooled samples of experiment A.

mss	1	2	3	4	5	Average
A1s	Cu ₃₀ Fe ₃₈ S ₃₂	Cu ₃₀ Fe ₃₈ S ₃₃	Cu ₃₀ Fe ₃₉ S ₃₂	Cu ₃₀ Fe ₃₈ S ₃₂	-	Cu ₃₀ Fe ₃₈ S ₃₂
A2s	Cu ₂₇ Fe ₃₈ S ₃₅	Cu ₂₇ Fe ₃₈ S ₃₆	Cu ₂₇ Fe ₃₈ S ₃₆	Cu ₂₇ Fe ₃₈ S ₃₅	Cu ₂₇ Fe ₃₈ S ₃₅	Cu ₂₇ Fe ₃₈ S ₃₅
A3s	Cu ₂₃ Fe ₄₀ S ₃₇	Cu ₂₃ Fe ₄₁ S ₃₇	Cu ₂₃ Fe ₄₀ S ₃₇	-	-	Cu ₂₃ Fe ₄₀ S ₃₈
						Cu₂₇Fe₃₉S₃₅

Figure 4.2. A and B: Ore-microscope images, no data

Figure 4.2. C:

Point	Phase	Pt	S	Fe	Cu	As	Other	Total
1	Cu-rich	0.00	30.03	36.59	30.56	0.06	0.00	97.42
2	Cu-rich	0.00	32.01	37.12	32.91	0.03	0.00	102.07
3	Cu-rich	0.00	32.36	36.09	33.86	0.00	0.00	102.31
4	po	0.01	36.70	58.18	0.00	0.02	0.00	94.91
5	po	0.07	37.22	57.52	6.91	0.02	0.00	101.74
6	po	0.00	36.87	59.05	7.39	0.04	0.00	100.36
7	melt	0.11	30.24	37.10	28.83	0.04	0.00	96.32
8	melt	0.19	30.23	35.91	29.33	0.19	0.00	95.85
Avg. error %							-	-

*Values are given in wt. %

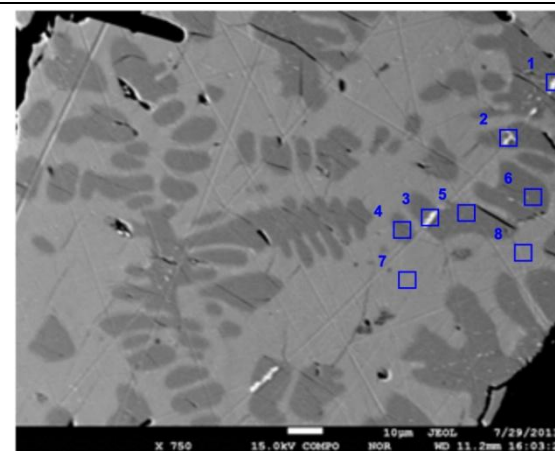


Figure 4.2.C: Backscatter electron (BSE) image of po (dark grey) surrounded by Cu-rich melt.

Figure 4.2. D:

Point	Phase	Pt	S	Fe	Cu	As	Other	Total
1	white	0.00	6.00	1.00	7.00	0.00	86.00	100.00
2	white	0.00	5.00	1.00	7.00	0.00	87.00	100.00
3	white	0.00	6.00	2.00	6.00	0.00	86.00	100.00
4	grey	0.00	3.00	4.00	5.00	0.00	88.00	100.00

*Values are given in normalized at. %

Point	Phase	Pt	S	Fe	Cu	As	Other	Total
1	Fe _x Cu _x S _x	0.00	42.86	7.14	50.00	0.00	0.00	100.00
2	Fe _x Cu _x S _x	0.00	38.46	7.69	53.85	0.00	0.00	100.00
3	Fe _x Cu _x S _x	0.00	42.86	14.29	42.86	0.00	0.00	100.00
4	Fe _x Cu _x S _x	0.00	25.00	33.33	41.67	0.00	0.00	100.00

**Surface contamination corrected values

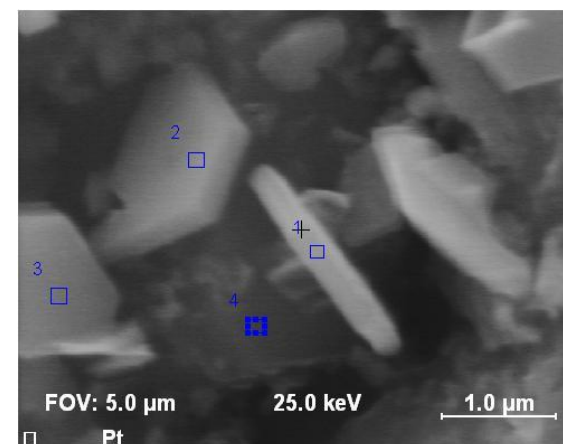


Figure 4.2.D: BSE of an unpolished sample from experiment A, taken with scanning Auger microscope (SAM).

Figure 4.3. A: Ore-microscope images, no data

Figure 4.3. B:

Point	Phase	Pt	S	Fe	Cu	As	Other	Total
1	po	0.00	37.30	61.06	3.19	0.04	0.00	101.58
2	po	0.00	35.66	53.45	10.94	0.06	0.00	101.12
3	ccp	0.09	33.08	35.99	31.03	0.03	0.00	100.23
4	po	0.04	37.41	59.77	4.56	0.04	0.00	101.84
5	ccp	0.00	32.63	35.95	30.70	0.01	0.00	99.30
6	bn	0.05	27.76	18.11	52.67	0.03	0.00	98.62
7	bn	0.04	28.59	17.42	51.95	0.04	0.00	98.04
8	ccp	0.04	33.32	34.51	30.98	0.00	0.00	98.85
9	PGM	56.66	0.24	1.00	1.00	42.09	0.00	100.985
10	po	0.06	37.37	60.37	2.75	0.00	0.00	100.55
Avg. error %		71.85	1.15	1.15	0.86	108.67	-	-

*Values are given in wt. %

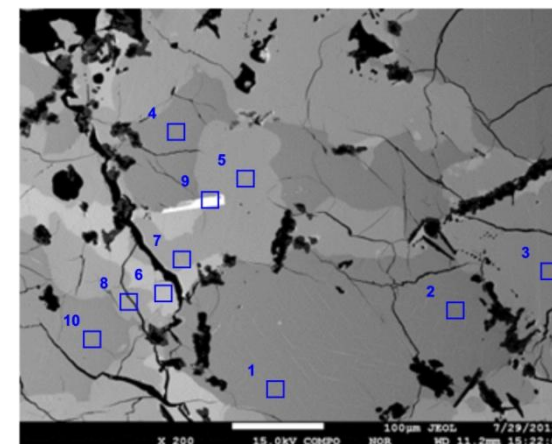


Figure 4.3.B: Backscatter electron (BSE) image of the slower cooled samples, with po, bn, ccp and Pt-phase (white phase).

Figure 4.3. C:

Point	Phase	Pt	S	Fe	Cu	As	Other	Total
1	po	0.00	37.71	62.17	2.39	0.03	0.00	102.30
2	po	0.03	37.14	61.53	2.34	0.06	0.00	101.09
3	po	0.10	36.63	58.04	6.04	0.04	0.00	100.85
4	po	0.00	36.46	59.14	4.59	0.00	0.00	100.17
5	po	0.00	35.66	53.47	10.94	0.06	0.00	100.12
Avg. error %		88.12	0.39	0.52	1.09	51.03	-	-

*Values are given in wt. %

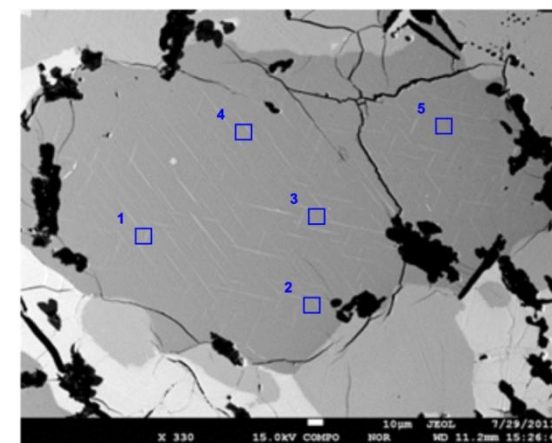


Figure 4.3.C: BSE image of po with exsolution textures.

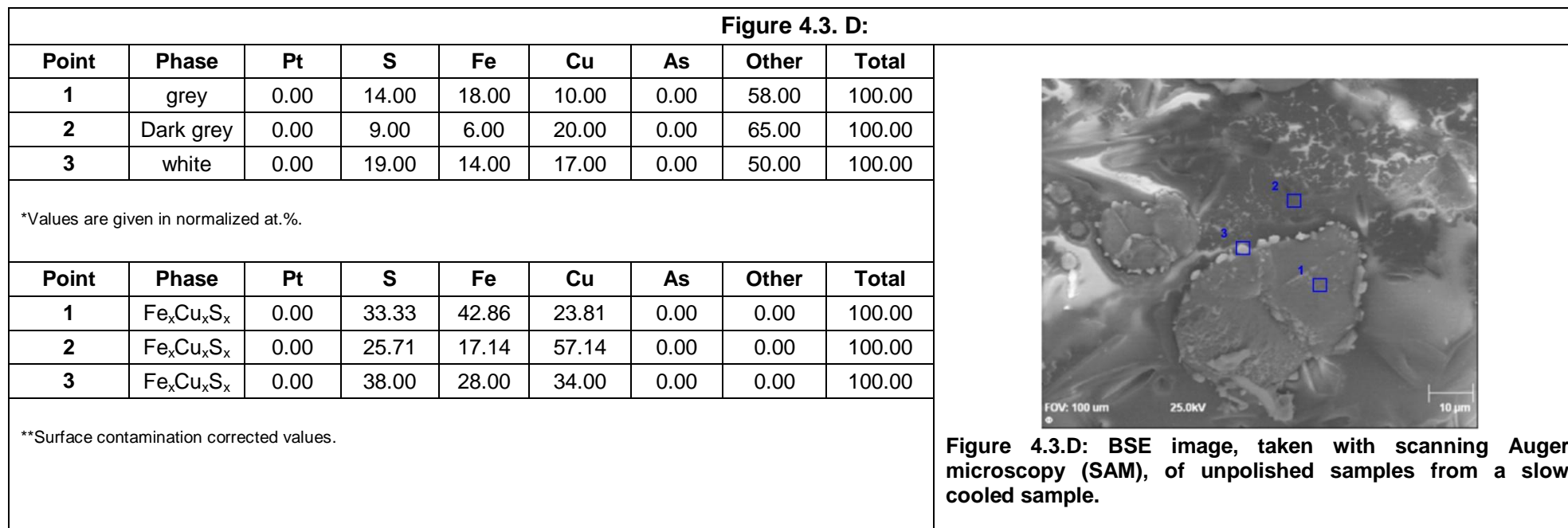


Table 4.3. and 4.5.: XRD graphs major phases: Experiment A, B and C

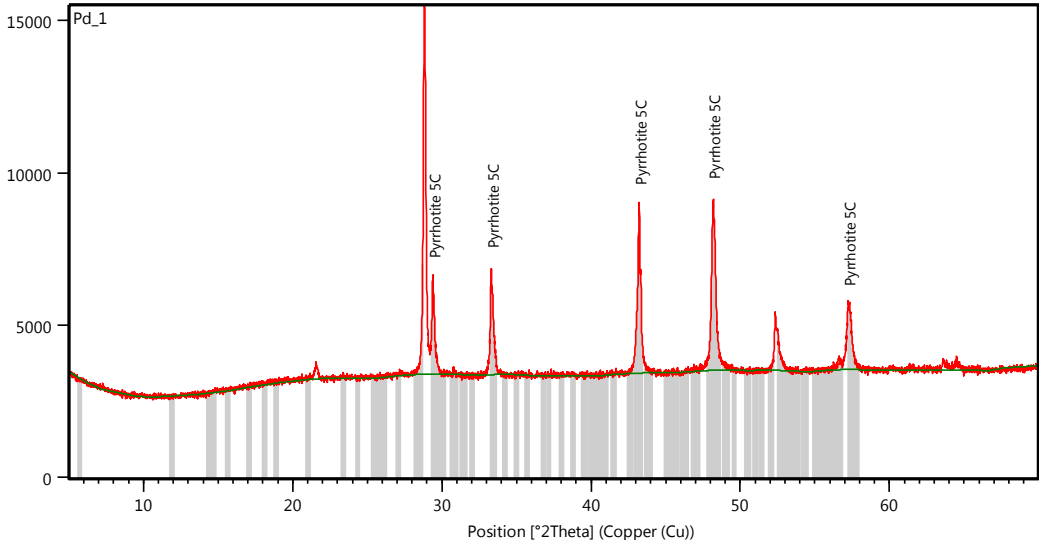
The 5 most prominent or strongest peaks were tabulated in the data sets below. The same spectra were used to calculate the size of nano crystals and phases, see section 4.1.4. Sample A1f and A1f was used as analogue for the Pt-As system and sample B1f and C1f as analogue for the Pd-As and Ru-As respectively.

Experiment A: Fast cooled, see Appendix B

Experiment A: Slow cooled, see Appendix B

Experiment B: Fast cooled

B1f

Phase name	Position 2 Theta	Height cts	FWHM	d spacing Å	Relative intensity %	Tip width
po 5C	29.4065	3137.32	0.0864	3.0349	27.80	0.1037
	33.3080	3467.78	0.0672	2.6878	30.73	0.0806
	43.2888	5522.66	0.0768	2.0909	48.94	0.9220
	48.1860	5616.49	0.0576	1.8870	49.77	0.0691
	57.2228	2083.16	0.1152	1.6086	18.46	0.1382
melt	Several Cu-rich phases were picked-up as representative / analogue for the amorphous to semi crystalline melt phases					
PGM	No Pd-phases were picked-up					
XRD graph	 <p>XRD spectra graph of sample B1f. The nano Pd-phase peaks were not identifiable on this scale. The large unidentified peaks were that of the semi-crystalline Cu-rich melt phase and silicate glass.</p>					

Experiment C: Fast cooled

C1f

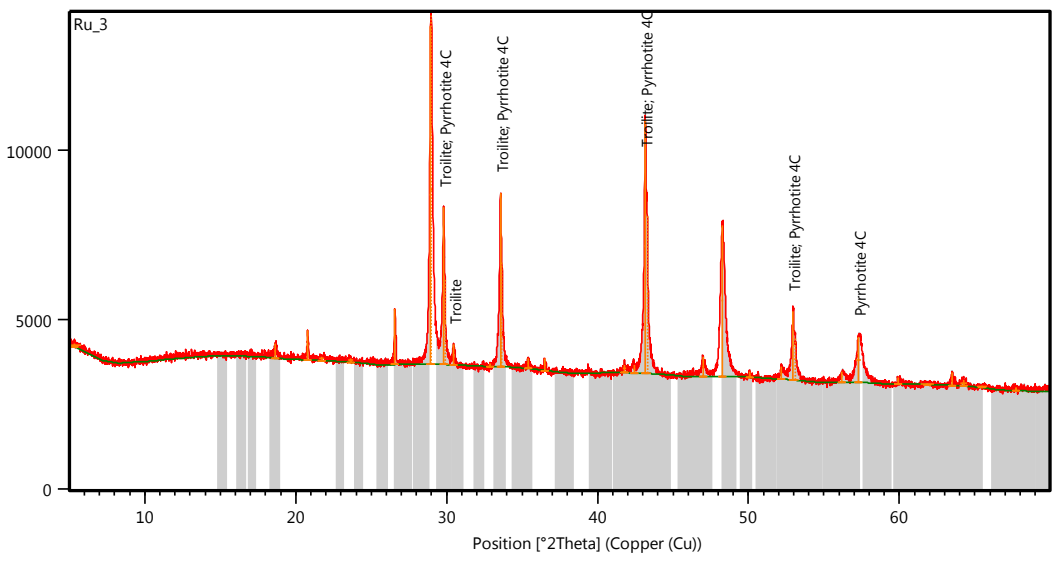
Phase name	Position 2 Theta	Height cts	FWHM	d spacing Å	Relative intensity %	Tip width
po (tr, 4C)	29.8088	4626.48	0.0672	2.9952	44.98	0.0806
	33.5726	5109.57	0.0768	2.6672	49.67	0.0922
	43.1653	7487.55	0.0768	2.0941	72.79	0.0922
	52.9411	2013.75	0.0768	1.7281	19.75	0.0922
melt	Several Cu-rich phases were picked-up as representative / analogue for the amorphous to semi crystalline melt phases					
PGM	No Ru-phases were picked-up					
XRD graph	 <p>XRD spectra graph of sample C1f. The nano Ru-phase peaks were not identifiable on this scale. The large unidentified peaks were that of the semi-crystalline Cu-rich melt and small inclusion of silica glass from the tubes.</p>					

Figure 4.4.: See data sheets on Table 4.3.

Table 4.5.: See data sheets on Table 4.1.

Figure 4.5. and 4.6.: See following pages

Table 4.6.: Characteristics of the PGE phases identified in the samples of experiment A. See following pages.

Average corrected composition (wt.%) of sr phases present in slow cooled samples of experiment A.

sperrylite	1	2	3	4	5	Avg.
A1f	Pt ₅₇ As ₄₃	Pt ₅₅ As ₄₅	-	-	-	Pt ₅₆ As ₄₄
A2f	-	-	-	-	-	-
A3f	-	-	-	-	-	-
Average fast						n/a
A1s	Pt ₅₇ As ₄₃	Pt ₅₆ As ₄₄	Pt ₅₆ As ₄₄	Pt ₃₃ As ₆₇	Pt ₃₃ As ₆₆	Pt ₄₇ As ₅₃
A2s	-	-	-	-	-	-
A3s	Pt ₅₇ As ₄₃	Pt ₅₆ As ₄₄	Pt ₅₈ As ₄₂	Pt ₅₈ As ₄₂	-	Pt ₅₈ As ₄₂
Average slow						Pt ₅₂ As ₄₈

Average corrected composition (wt.%) of ifp phases present in slow cooled samples of experiment A.

Isoferro-platinum	1	2	3	4	5	Avg.
A1f	-	-	-	-	-	-
A2f	Pt ₂₆ Fe ₇₄	Pt ₂₄ Fe ₇₆	Pt ₁₀ Fe ₉₀	-	-	Pt ₂₄ Fe ₇₆
A3f	-	-	-	-	-	-
Average fast						n/a
A1s	-	-	-	-	-	-
A2s	Pt ₈₆ Fe ₁₂	Pt ₈₅ Fe ₁₅	Pt ₈₃ Fe ₁₇	Pt ₈₃ Fe ₁₇	Pt ₈₂ Fe ₁₈	Pt ₈₄ Fe ₁₆
A3s	-	-	-	-	-	-
Average slow						n/a

Figure 4.5. A and B:

Point	Phase	Pt	S	Fe	Cu	As	Other	Total
1	Pt	32.74	18.91	13.44	9.82	25.09	0.00	100.00
2	Pt	18.47	26.97	23.20	16.44	14.92	0.00	100.00
3	po	0.00	31.34	21.88	46.78	0.00	0.00	100.00
4	po	0.00	30.06	19.79	50.15	0.00	0.00	100.00
5	melt	0.00	34.49	35.91	29.60	0.00	0.00	100.00
6	melt	0.00	34.45	35.46	30.09	0.00	0.00	100.00
Std. deviation		13.97	5.86	8.97	15.99	10.82	-	-

*Values are given in normalized wt. %

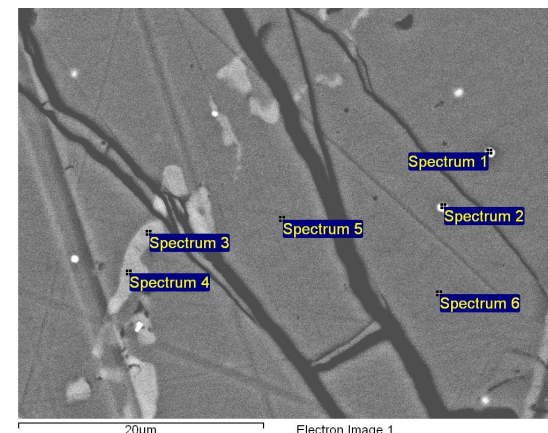


Figure 4.5.A and B: Platinum-phases (PGM) mineralisation in the fast cooled samples of experiment A. The PGM were spot-like and poorly crystallised.

Figure 4.6. A:

Point	Phase	Pt	S	Fe	Cu	As	Other	Total
1	Pt	49.46	4.66	2.06	7.30	36.52	0.00	100.00
2	Pt	48.48	3.79	2.15	7.28	38.30	0.00	100.00
3	Pt	46.61	5.99	2.70	7.99	36.71	0.00	100.00
4	bn	0.00	28.84	16.68	54.47	0.00	0.00	100.00
5	bn	0.00	29.37	16.33	54.31	0.00	0.00	100.00
6	bn	0.00	29.31	15.98	54.72	0.00	0.00	100.00
7	ccp	0.00	34.84	35.28	29.88	0.00	0.00	100.00
8	ccp	0.00	35.92	34.56	29.52	0.00	0.00	100.00
9	ccp	0.00	34.88	34.57	30.55	0.00	0.00	100.00
10	ccp	0.00	35.26	34.10	30.64	0.00	0.00	100.00
11	ccp	0.00	34.94	34.04	31.02	0.00	0.00	100.00
12	bn	0.00	28.76	15.46	55.79	0.00	0.00	100.00
Std. deviation		21.80	12.81	13.66	18.81	16.82	-	-

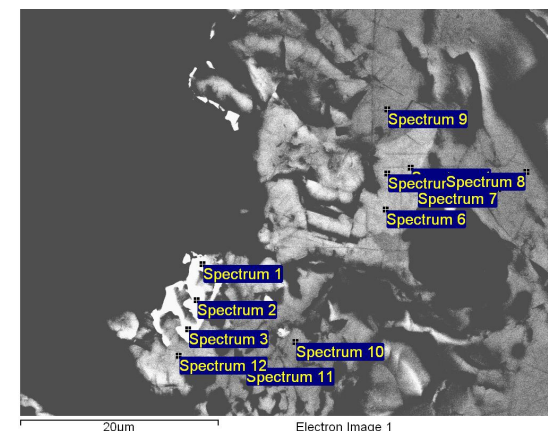


Figure 4.6. A: Backscatter electron (BSE) image of PtAs₂ crystals on the borders of ccp and bn, sample A1s (300 ppm Pt, 280 ppm As).

Figure 4.6. B:

Point	Phase	Pt	S	Fe	Cu	As	Other	Total
1	Pt	79.50	0.68	11.50	2.05	0.04	6.23	100.00
2	Pt	76.80	1.82	11.54	1.91	0.00	7.93	100.00
3	Pt	74.30	2.52	12.02	1.90	0.00	9.21	100.00
4	Pt	78.11	1.45	11.50	1.53	0.08	7.33	100.00
5	Pt	75.11	2.30	11.71	2.13	0.00	8.75	100.00
6	Pt	68.30	4.55	11.78	3.10	0.00	12.27	100.00
7	Pt	53.29	9.66	14.60	1.53	0.00	20.93	100.00
8	Pt	57.21	8.53	14.11	1.18	0.00	18.98	100.00
9	Pt	51.36	8.06	18.33	2.05	0.00	20.21	100.00
10	ccp	0.05	20.59	23.78	12.78	0.05	42.71	100.00
11	ccp	0.00	20.51	23.88	12.94	0.00	42.63	100.00
Std. deviation		N.d., no standard used EDS-SEM analysis.						

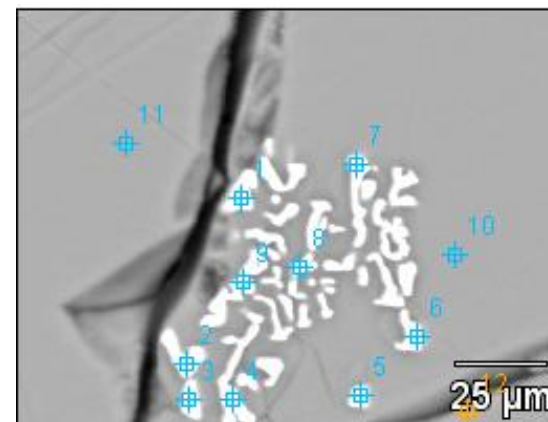


Figure 4.6. B: BSE image of Pt_xFe_x crystals in ccp, sample A2s (300 ppm Pt, no As).

Figure 4.6. C:

Point	Phase	Pt	S	Fe	Cu	As	Other	Total
1	Pt	51.53	1.86	2.99	3.41	40.21	0.00	100.00
2	Pt	49.22	2.56	6.08	4.16	37.98	0.00	100.00
3	Pt	52.59	2.16	3.18	2.95	39.11	0.00	100.00
4	Pt	52.85	1.92	3.52	2.89	38.82	0.00	100.00
5	Pt melt	14.51	21.50	38.87	23.85	11.27	0.00	100.00
6	ccp	0.00	35.43	37.58	27.00	0.00	0.00	100.00
7	ccp	0.00	35.65	37.53	26.82	0.00	0.00	100.00
8	ccp	0.00	35.65	37.71	26.64	0.00	0.00	100.00
9	ccp	0.00	35.35	37.71	26.94	0.00	0.00	100.00
10	ccp	0.00	35.45	37.69	26.86	0.00	0.00	100.00
11	ccp	0.00	35.35	37.71	26.94	0.00	0.00	100.00
Std. deviation		25.34	16.34	16.60	11.68	19.17	-	-

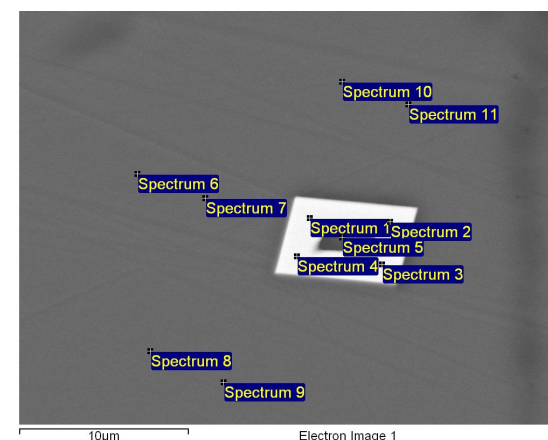


Fig. 4.6. C: BSE image of $PtAs_2$ crystals in ccp, sample A3s (30 ppm Pt, 30 ppm As).

*Values are given in normalised wt.%

Table 4.7.: The distribution and size of Pt-phases measured in samples of experiment A.

The distribution and size of measured Pt-phases in the fast cooled samples of experiment A.

Sample	Estimated size of Pt-phase (μm)					
	1	2	3	4	5	Average
	A1f					
Pt-As	1.0	1.2	0.6	1.2	1.0	1.0
Pt-Fe	No Fe phases measured					
Sample	A2f					
	No As added					
	No Pt-phases were picked up with SEM, poorly crystallised					
Sample	A3f					
	0.6	0.5	0.6	-	-	0.6
	No Fe phases measured					

The distribution and size of measured Pt-phases in the slow cooled samples of experiment A.

Sample	Estimated size of Pt-phase (μm)					
	1	2	3	4	5	Average
	A1s					
Pt-As	8.0	15.0	10.0	30.0	20.0	16.7
Pt-Fe	No Fe phases measured					
Sample	A2s					
	No As added					
	1.0	12.0	30.0	10.0	7.0	12.0
Sample	A3s					
	7	-	-	-	-	Poorly crystallised
	No Fe phases measured					

Appendix D

Table 5.1.: Sulphur fugacity (calculated)

The calculated $\log fS_2$ of po samples from experiment A, B and C, using the Cu-correction method of Mengason et al. (2010). All values are expressed in wt.%.

Fast	Formula, at.%	Cu	Fe	S	Total	N	fS_2
A1f	$XCu_{0.07}Fe_{0.89}S$	5.550	58.360	37.61	101.52	0.964	-2.4
A2f	$XCu_{0.07}Fe_{0.90}S$	5.370	58.360	37.32	101.05	0.950	-1.3
A3f	$XCu_{0.07}Fe_{0.95}S$	5.350	58.040	37.94	101.33	0.957	-1.8
Avg.	$XCu_{0.07}Fe_{0.91}S$						-1.8
A1s	$XCu_{0.04}Fe_{0.95}S$	3.00	61.23	36.84	101.07	0.987	-14.2
A2s	$XCu_{0.04}Fe_{0.96}S$	3.13	61.25	36.68	101.06	0.990	-14.9
A3s	$XCu_{0.07}Fe_{0.92}S$	4.89	59.61	37.21	101.71	0.977	-12.4
Avg.	$XCu_{0.05}Fe_{0.94}S$						-13.8
B1f	$XCu_{0.04}Fe_{0.91}S$	3.10	58.60	36.96	98.66	0.965	-2.5
B2f	Tubes exploded: n.d.						
B3f	$XCu_{0.01}Fe_{0.91}S$	0.50	60.37	38.29	99.17	0.953	-1.5
Avg.							-2.0
C1f	$XCu_{0.03}Fe_{0.9}S$	0.60	59.90	40.06	100.11	0.926	0.32
C2f	$XCu_0Fe_{0.91}S$	0.47	59.37	39.91	99.74	0.923	0.50
C3f	$XCu_0Fe_{0.91}S$	3.95	57.45	38.13	99.55	0.919	0.72
Avg.	$XCu_{0.01}Fe_{0.9}S$						0.51

Figure 5.1.: See data sheet on Table 5.1.

Table 5.2.: Metal:S ratio

The metal:S ratio of slow and fast cooled samples of experiment A, B and C.

Sample	Phase	1	2	3	4	5	Avg. metal: S	Avg.
A1f	mss	0.9938	1.0192	0.9829	1.0157	0.9953	1.0014	1.0985
	melt	1.2231	1.1815	1.2056	1.1773	1.901	1.1955	
A2f	mss	0.9697	0.9652	0.9597	0.9765	0.9796	0.9701	1.0646
	melt	1.1573	1.1454	1.1704	1.1395	1.1830	1.1591	
A3f	mss	0.9394	0.9566	0.9235	0.9740	0.9532	0.9493	1.0676
	melt	1.1486	1.2107	1.1938	1.1818	1.1945	1.1859	

The metal:S ratio cont.

Sample	Phase	1	2	3	4	5	Avg. metal: S	Avg.
A1s	mss	0.9493	0.9477	0.9629	0.9776	0.9822	0.9639	1.0310
	melt	1.0974	1.0753	1.0925	1.1178	1.1082	1.0982	
A2s	mss	0.9875	0.9730	0.9730	0.9841	1.0137	0.9863	1.0442
	melt	1.0921	1.0973	1.1146	1.1044	-	1.1021	
A3s	mss	0.9849	0.9918	1.0011	1.0029	1.0187	1.0018	1.0053
	melt	1.0812	1.1241	1.0894	1.0648	1.0863	1.0887	
B1f	mss	0.9714	0.9685	0.9431	0.9237	0.9558	0.9525	1.1537
	melt	1.34323	1.3466	1.3744	1.3464	1.3643	1.3548	
B2f	Tubes exploded: n.d.							
B3f	mss	0.9019	0.9161	0.9237	0.9080	0.9069	0.9113	0.9263
	melt	0.9415	0.9781	0.9373	0.9536	0.8956	0.9412	
C1f	mss	0.8547	0.8470	0.8564	0.8689	0.8704	0.8595	0.9040
	melt	0.9395	0.9436	0.9504	0.9465	0.9628	0.9486	
C2f	mss	0.8362	0.8646	0.8719	0.8615	0.8609	0.8589	0.9122
	melt	0.9687	0.9655	0.9793	0.9600	0.9542	0.9655	
C3f	mss	0.8455	0.8474	0.9098	0.8736	0.8477	0.8648	0.8991
	melt	0.9158	0.9366	0.9432	0.9376	0.9338	0.9334	

Table 5.3.: Calculated D-values and reference sets: $D_{mss/melt}^{As}$ and $D_{mss/melt}^{PGE}$

The distribution of As between the mss- and melt phases of slow and fast cooled samples of experiment A, B and C. Values are expressed in wt. %.

D ^{As} mss/melt		Measured conc. As, wt. %						
		1	2	3	4	5	Avg.	D value
A1f	mss	0.0120	0.0080	0.0170	0.0010	0.0150	0.0106	0.3011
	melt	0.1410	0.0090	0	0.0080	0.0180	0.0352	
A2f	No As added							
A3f	b.d.l.							
A1s	mss	0.0370	0	0.0280	0	0.0140	0.0158	2.5484
	melt	0.0100	0.0020	0.0060	0.0060	0.0070	0.0062	
A2s	No As added							
A3s	b.d.l.							
B1f	mss	0.042	0.022	0.002	0.006	0.035	0.0214	1.0700
	melt	0	0	0	0.100	0	0.0020	
B2f	No As added							

The distribution of As between the mss- and melt phases of slow and fast cooled samples of experiment A, B and C, cont.

D ^{As} _{mss/melt}		Measured conc. As, wt.%						D value
		1	2	3	4	5	Avg.	
B3f	mss	0.0380	0.0440	0	0.0300	0	0.0224	1.1667
	melt	0.0120	0.0350	0.0230	0	0.0260	0.0192	
Average fast: experiment B								1.1183
C1f	mss	0.0200	0.0420	0.0310	0.0370	0.0320	0.0324	2.0769
	melt	0.0060	0.0170	0.0210	0.0150	0.0190	0.0156	
C2f	No As added							
C3f	mss	0.0310	0.0030	0.0410	0.0440	0	0.0238	1.1553
	melt	0.0130	0.0390	0.0050	0.0210	0.0250	0.0206	
Average fast: experiment C								1.5961

PGE distribution between mss- and melt phases of slow and fast cooled samples of experiment A, B and C. Values are expressed in wt. %.

D ^{PGE} _{mss/melt}		Measured concentration PGE, wt.%						D value
		1	2	3	4	5	Avg.	
A1f	mss	0.0090	0.0080	0.0030	0.0030	0	0.0046	0.9388
	melt	0.0246	0	0	0	0	0.0049	
A2f	mss	0	0.016	0	0	0.016	0.0064	0.3299
	melt	0.022	0	0	0	0.075	0.0194	
A3f	mss	0	0	0	0	0.027	0.0054	0.6280
	melt	0	0	0	0.043	0	0.0086	
A1s	mss	0.0430	0	0	0	0	0.0086	0.2278
	melt	0	0.0590	0.0700	0	0.0220	0.0378	
A2s	b.d.l.							
A3s	b.d.l.							
B1f	mss	0	0	0.005	0	0.003	0.0016	0.3478
	melt	0	0.001	0.001	0.019	0.002	0.0046	
B2f	Tubes exploded: n.d.							
B3f	mss	0	0.0010	0	0	0	0.0002	0.3333
	melt	0	0	0.0020	0	0	0.0006	
C1f	mss	0.0500	0.0460	0.0500	0.0530	0.0410	0.048	>1
	melt	0	0	0	0	0	b.d.l.	
C2f	mss	0.0370	0.0400	0.0460	0.0220	0	0.029	>1
	melt	0	0	0	0	0	b.d.l.	
C3f	b.d.l.							

Appendix E

Figure 6.1. A-D: See following pages

Figure 6.2. A and B: See following pages

Table 6.1., 6.2. and 6.3.:

The average size, shape, classification and distribution of non PGE nano structures, larger than 100nm, measured in experiments A, B and C.

than 100nm, measured in experiments A, B and C.

Composition	Size, nm					Avg. size nm
	1	2	3	4	5	
Experiment A: FAST						
Cu _x	2000	1700	2300	2000	2000	2000
Fe _x S _x	250	150	120	250	120	180
Fe _x Cu _x S _x	300	500	650	600	350	480
Cu _x S _x	1800	2000	3000	2100	2500	2280
Average						1235
Experiment B: FAST						
Cu-rich Fe _x Cu _x S _x	300	250	200	120	110	150
Cu-rich Fe _x Cu _x S _x	950					950
Average						550
Experiment C: FAST: none measured						
Experiment A: SLOW						
Fe-rich Fe _x Cu _x S _x	950	500	300	250	300	460
po	N.d.: Long Axis measured up to 3 μm, short axis up to 500 nm					
po	1000	1500	1500	2000	500	1300
po	N.d.: Structures to densely distributed to distinguish individual features					
Fe _x S _x	N.d.: Long Axis measured up to 2.5 μm, short axis up to a max of 300 nm					
Average						n.d.
Avg. A, B and C						

Figure 6.1. A:

Point	Phase	Pt	S	Fe	Cu	other	Total
1	grey	0.00	33.00	52.00	8.00	7.00	100.00
2	white	0.00	12.00	14.00	61.00	13.00	100.00
3	grey	0.00	30.00	52.00	12.00	7.00	100.00
*Values are given in normalized at. %.							
Point	Phase	Pt	S	Fe	Cu	other	Total
1	mss	0.00	35.48	55.91	8.60	0.00	100.00
2	Cu	0.00	13.79	16.09	70.11	0.00	100.00
3	mss	0.00	32.26	55.91	12.90	0.00	100.00
**Surface contamination corrected values.							

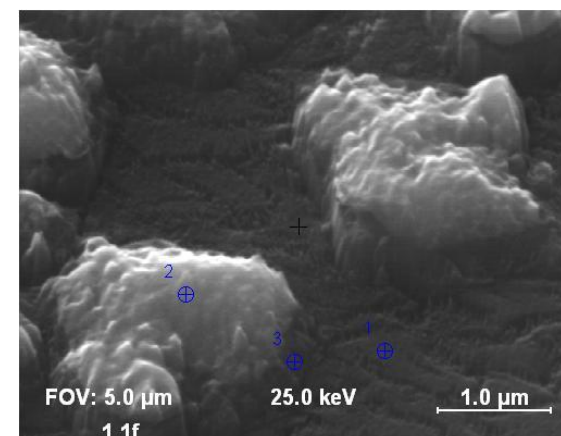


Figure 6.1. A: High relief Cu exsolution (type 2) structures on the mono-sulphide (mss or po) surface. B:

Figure 6.1. B:

Point	Phase	Pt	S	Fe	Cu	other	Total
1	white	0.00	30.00	53.00	3.00	14.00	100.00
2	grey	0.00	29.00	53.00	4.00	14.00	100.00
*Values are given in normalized at. %.							
Point	Phase	Pt	S	Fe	Cu	other	Total
1	mss	0.00	34.88	61.63	3.49	0.00	100.00
2	mss	0.00	33.72	61.63	4.65	0.00	100.00
**Surface contamination corrected values.							

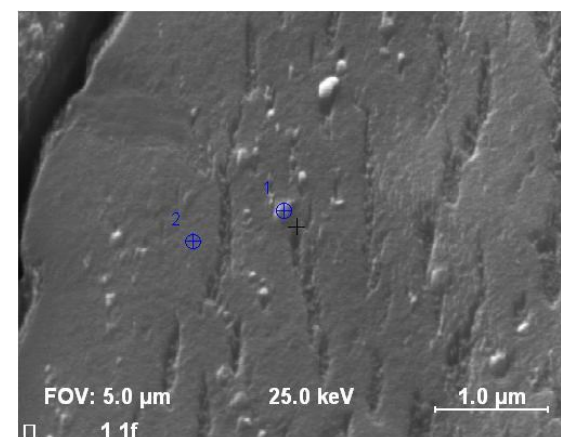
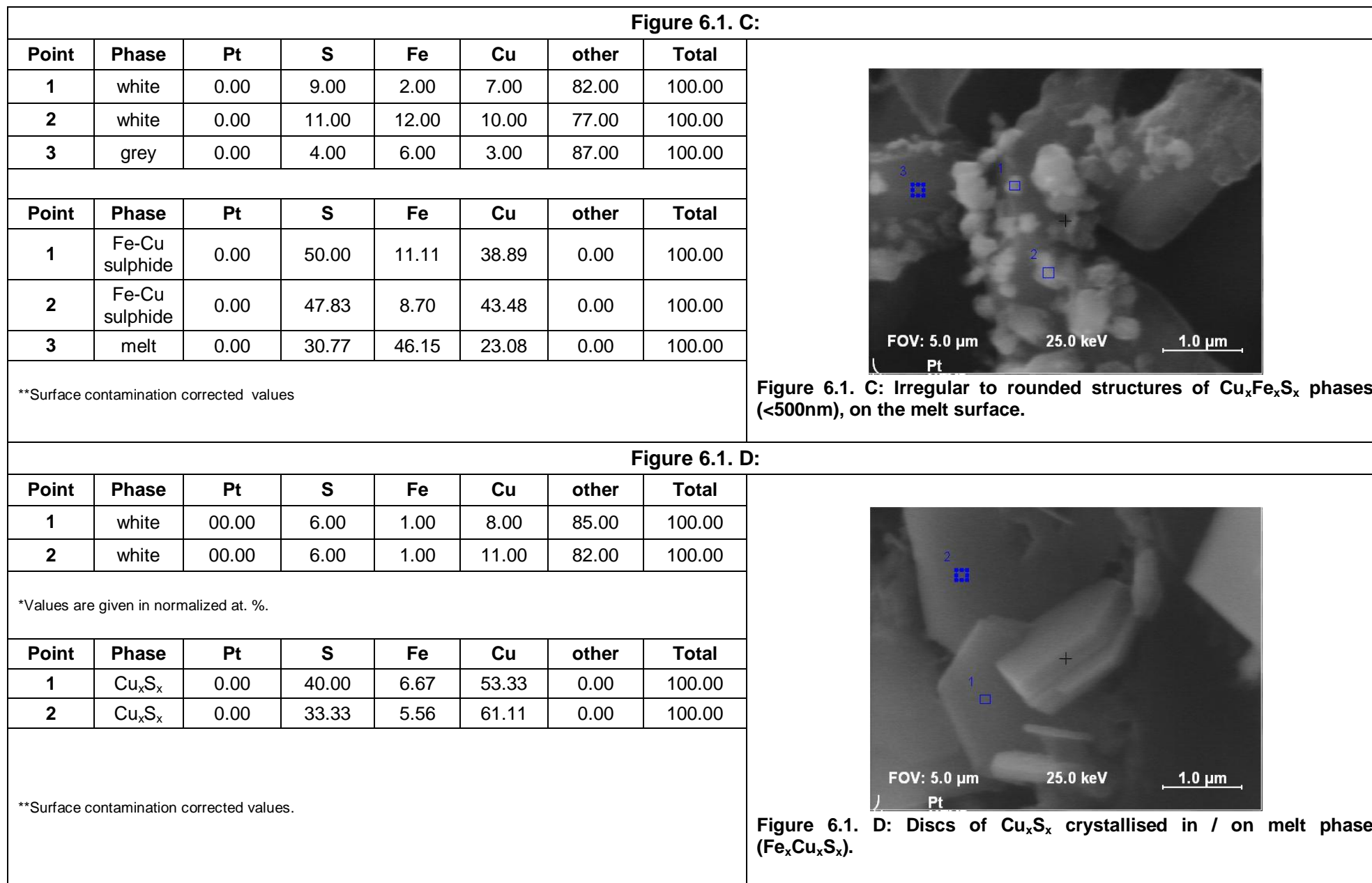
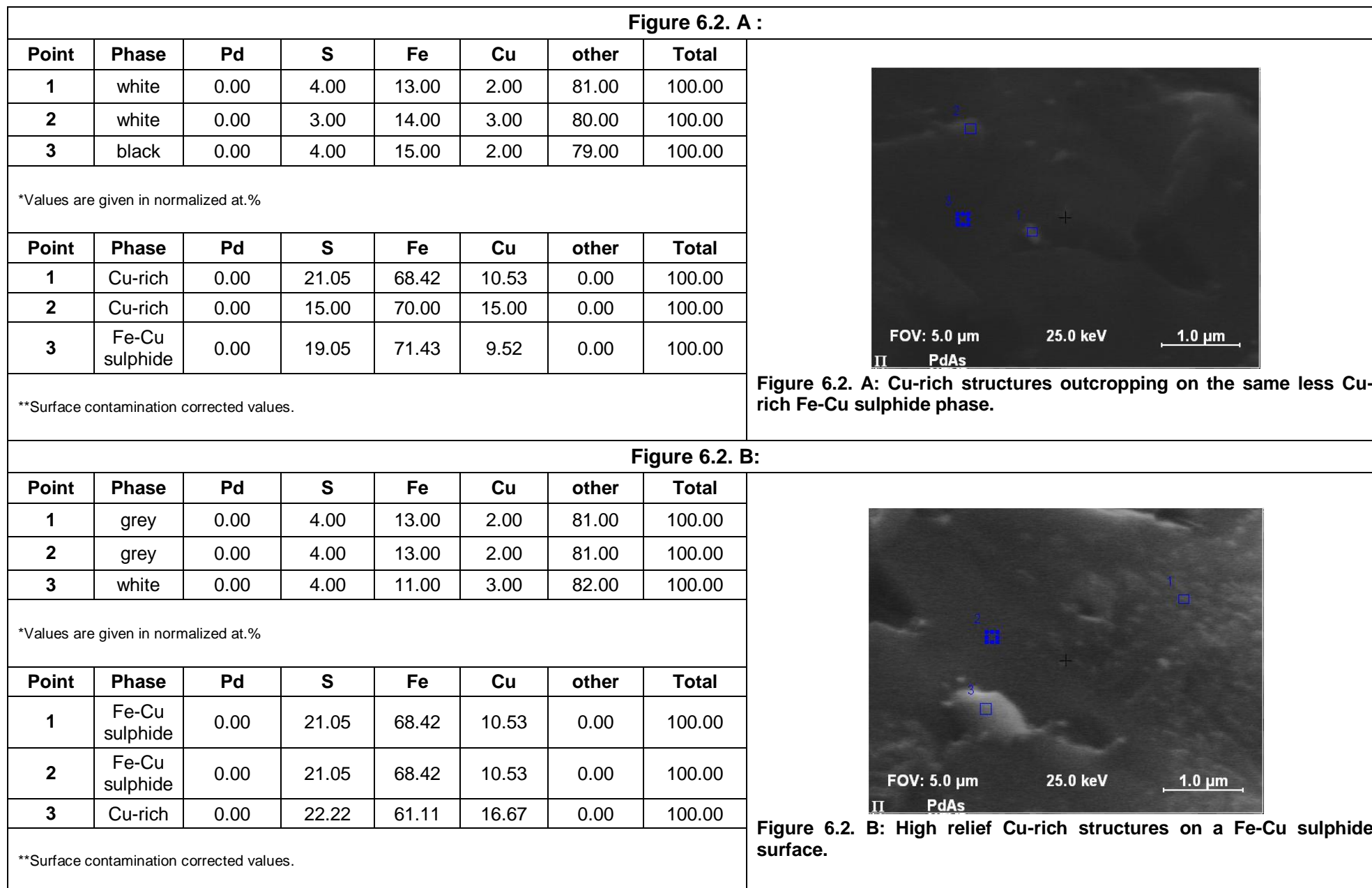
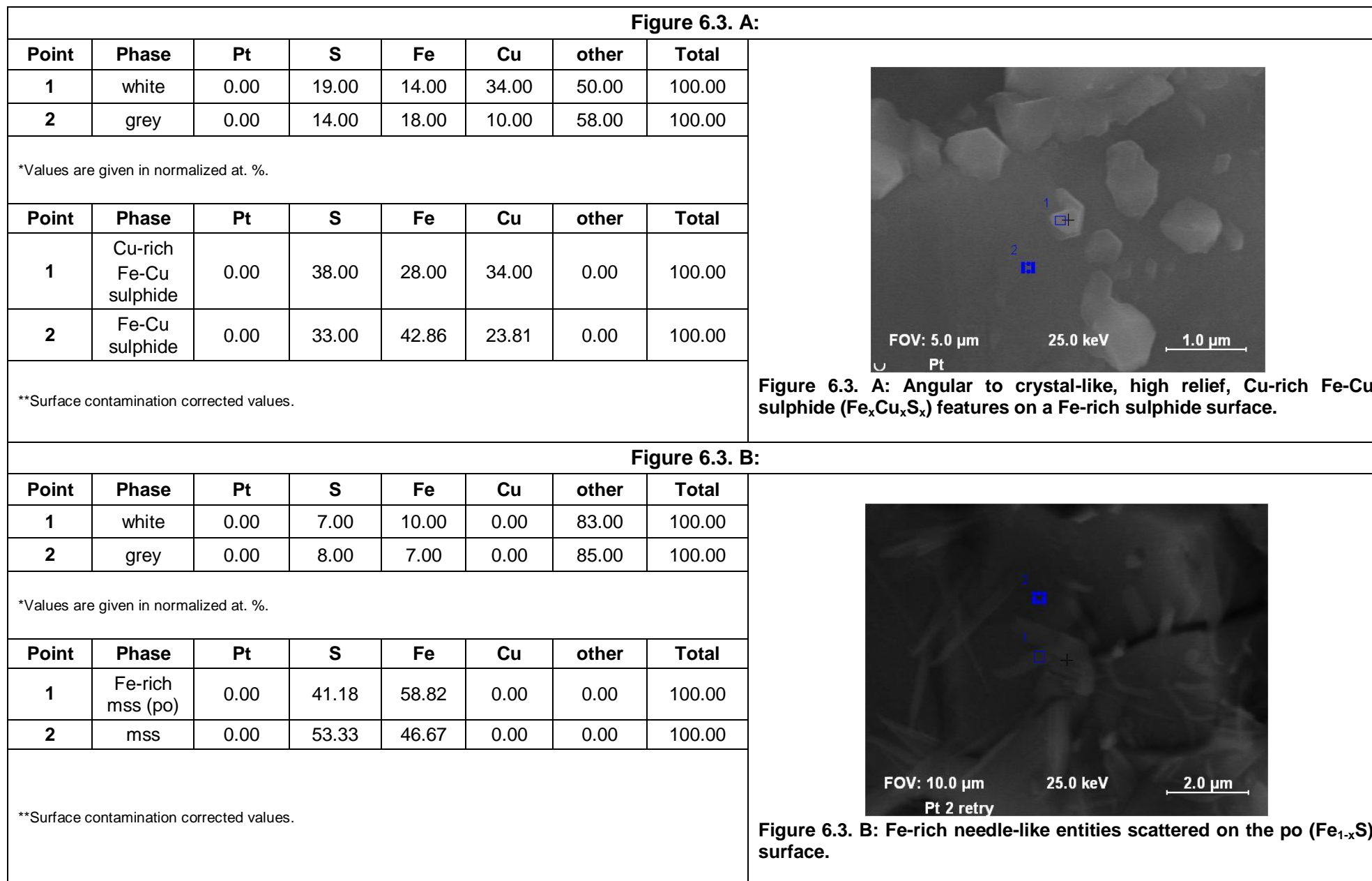


Figure 6.1. B: High density, low relief Fe_xS_x exsolutions (type 1) on the mss (po) surface.







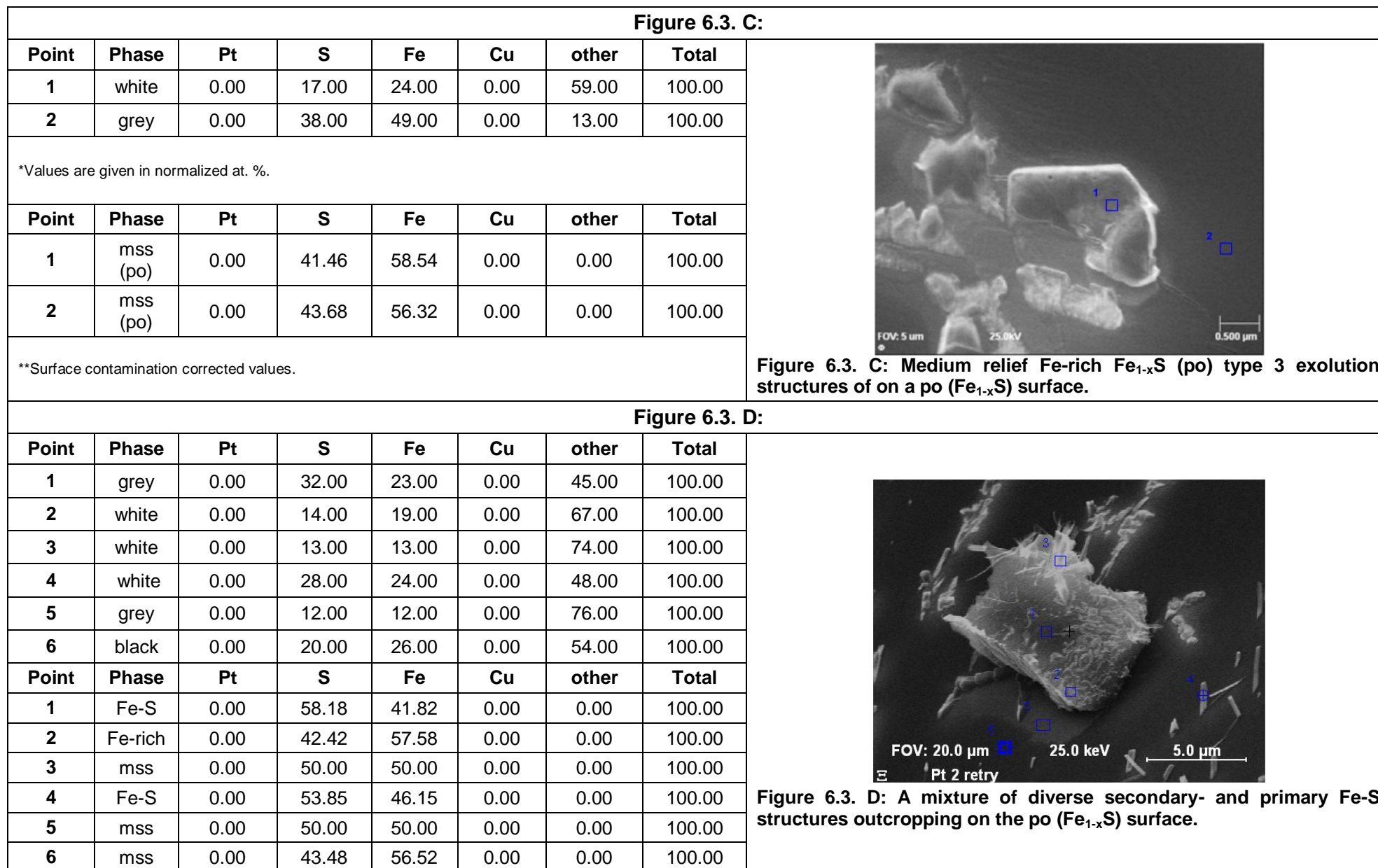


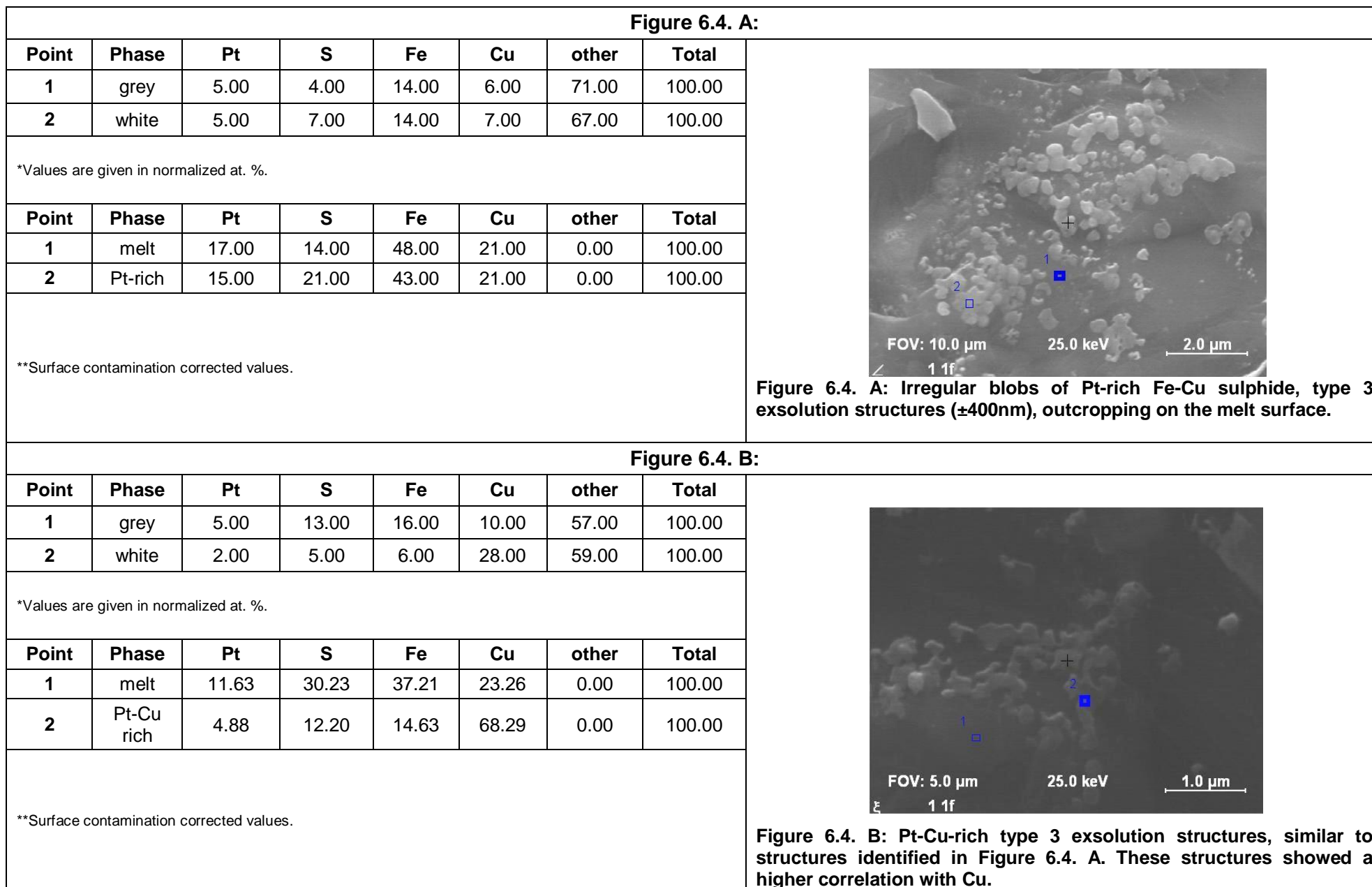
Figure 6.3. A-F: See following pages

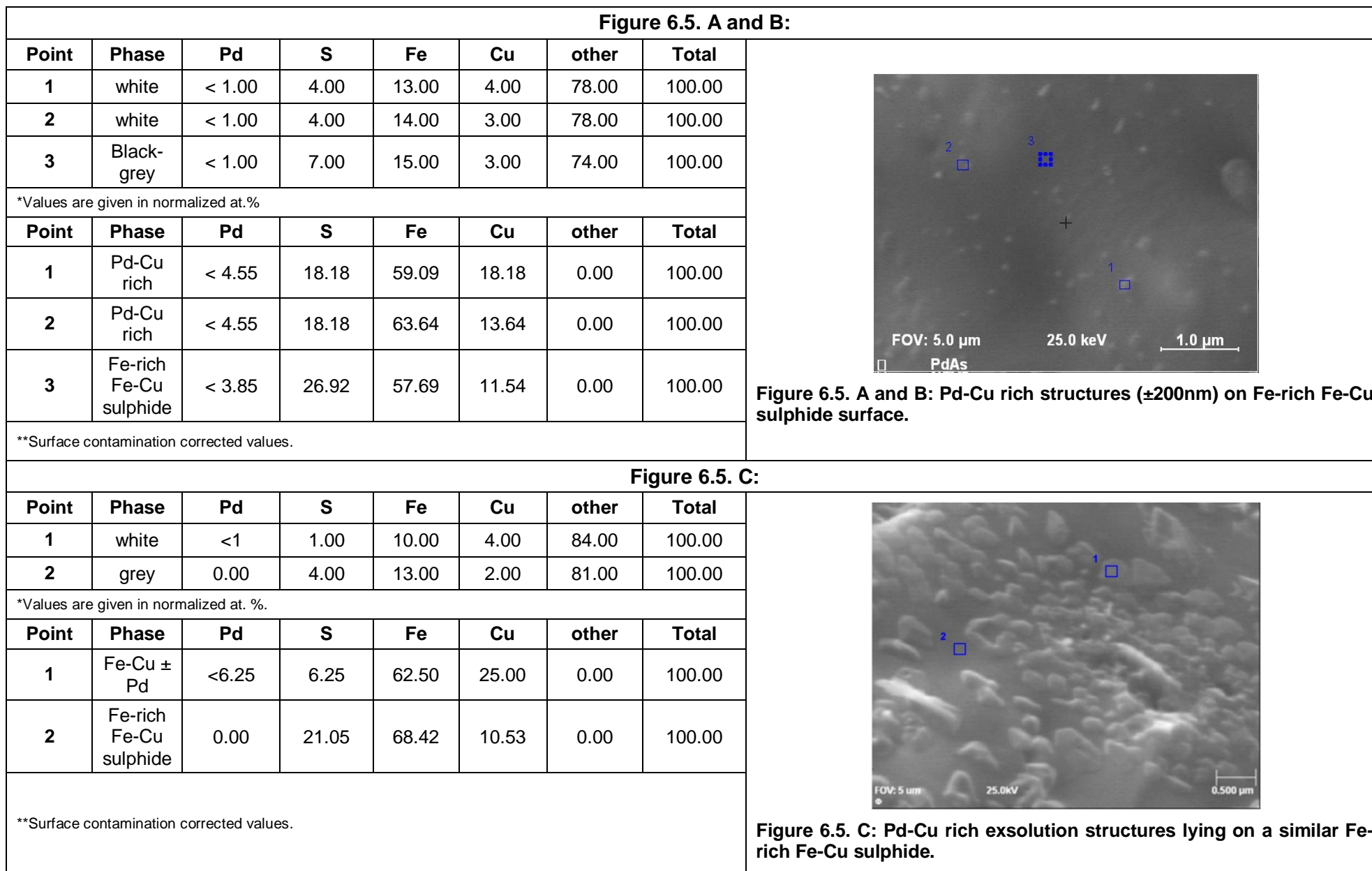
Figure 6.4. A-D: See following pages

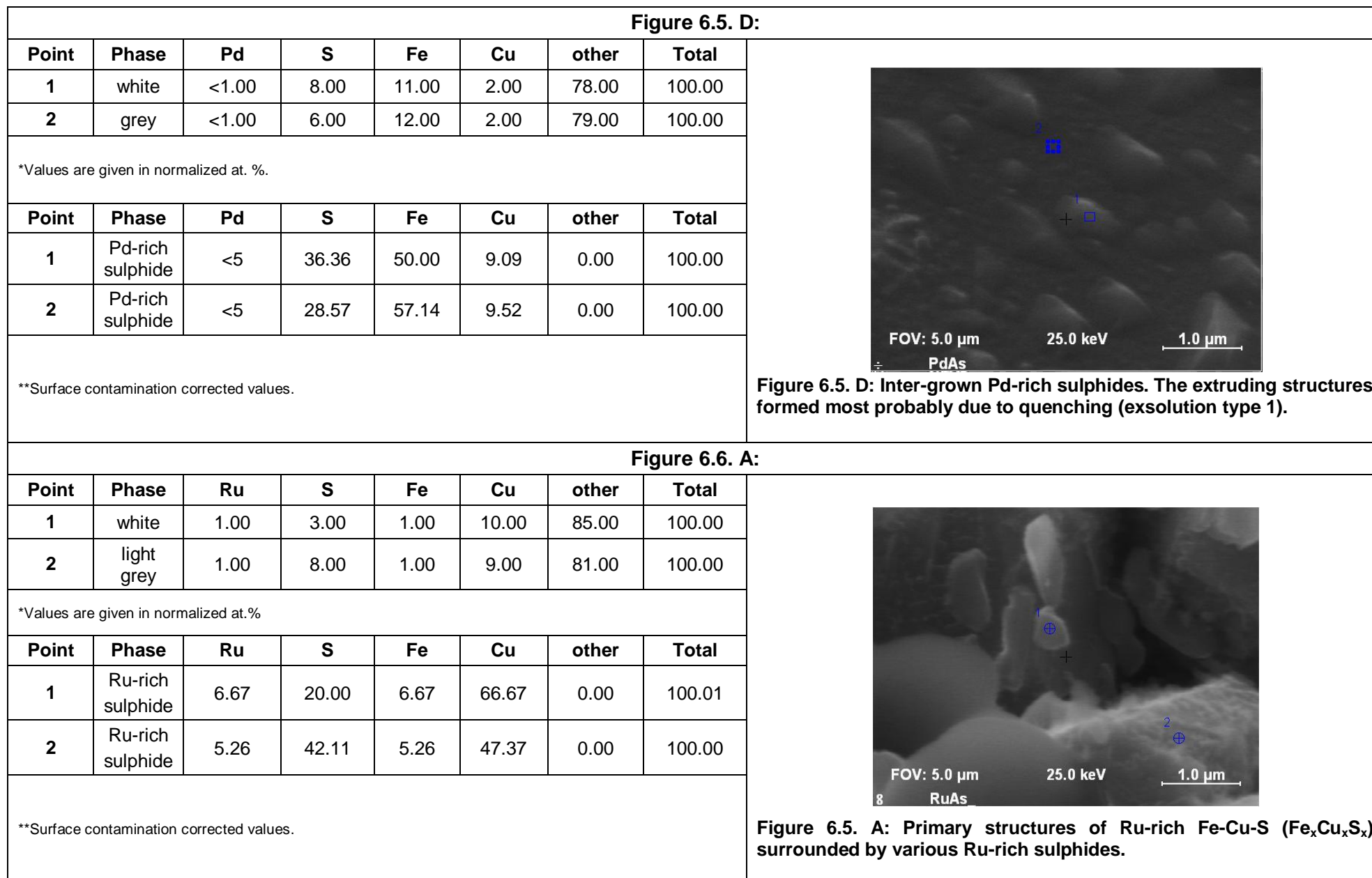
Table 6.4., 6.5., 6.6. and 6.7.:

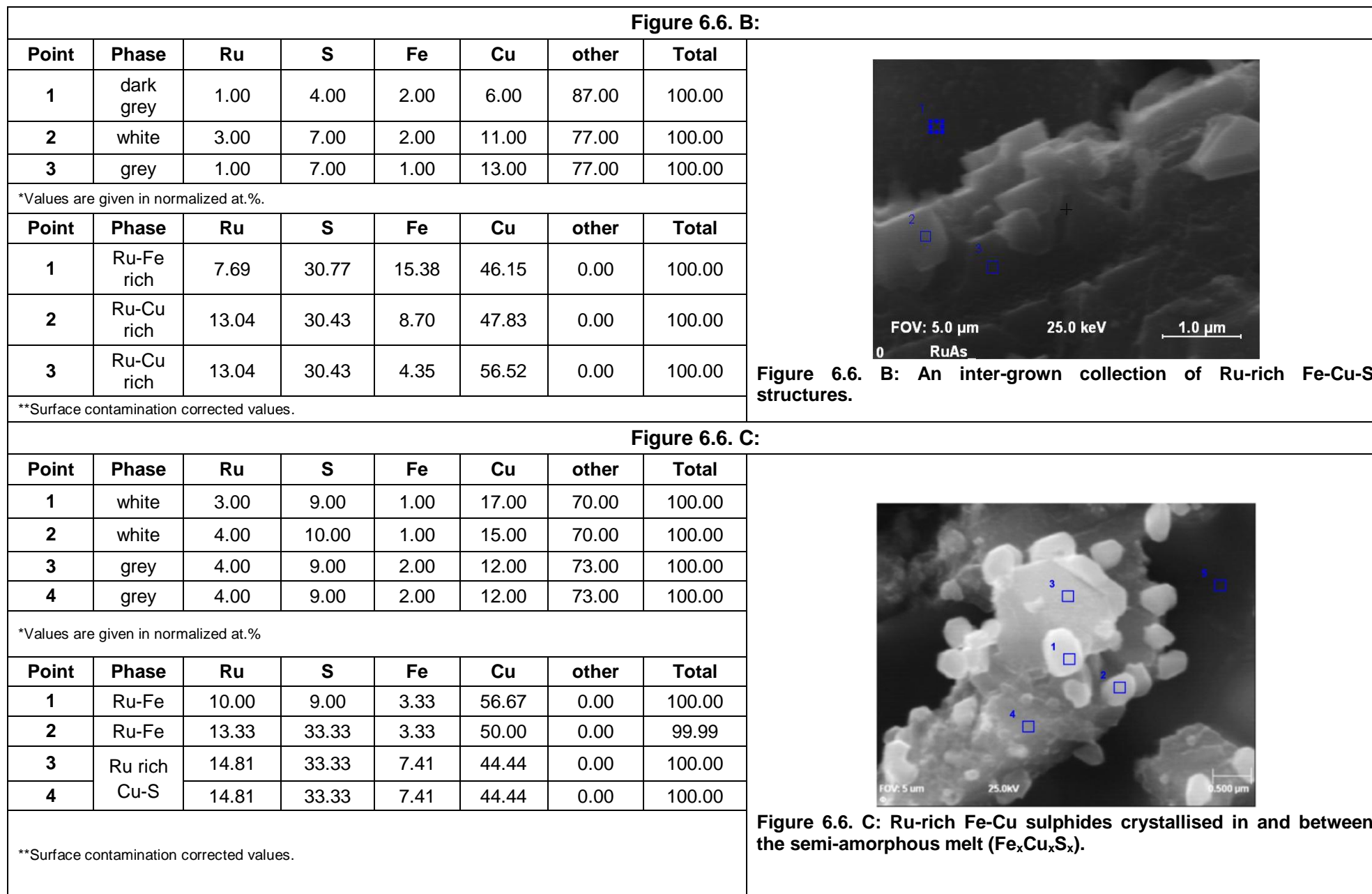
The average size, shape, classification and distribution of PGE-rich nano structures, larger than 100nm, measured in experiments A, B and C.

Composition	Size, nm					Avg. size nm
	1	2	3	4	5	
Experiment A: FAST						
Pt-rich Fe _x Cu _x S _x	300	500	450	250	500	400
Pt-Cu rich Fe _x Cu _x S _x	250	250	750	200	500	390
Average						395
Experiment B: FAST						
Pd-Cu rich Fe _x Cu _x S _x	120	120	250	250	200	188
Pd-Cu rich Fe _x Cu _x S _x	200	250	250	300	500	300
Pd-rich Fe _x Cu _x S _x	500	300	800	1200	1000	760
Average						420
Experiment C: FAST						
Ru-rich sulphide	600	1000	1200	500	1000	860
Ru-Fe rich Fe _x Cu _x S _x	800	600	550			650
Ru-Fe Cu _x S _x	600	500	500	600	300	500
Ru-rich Cu _x S _x	600					600
Average						650
Average A, B and C						±500









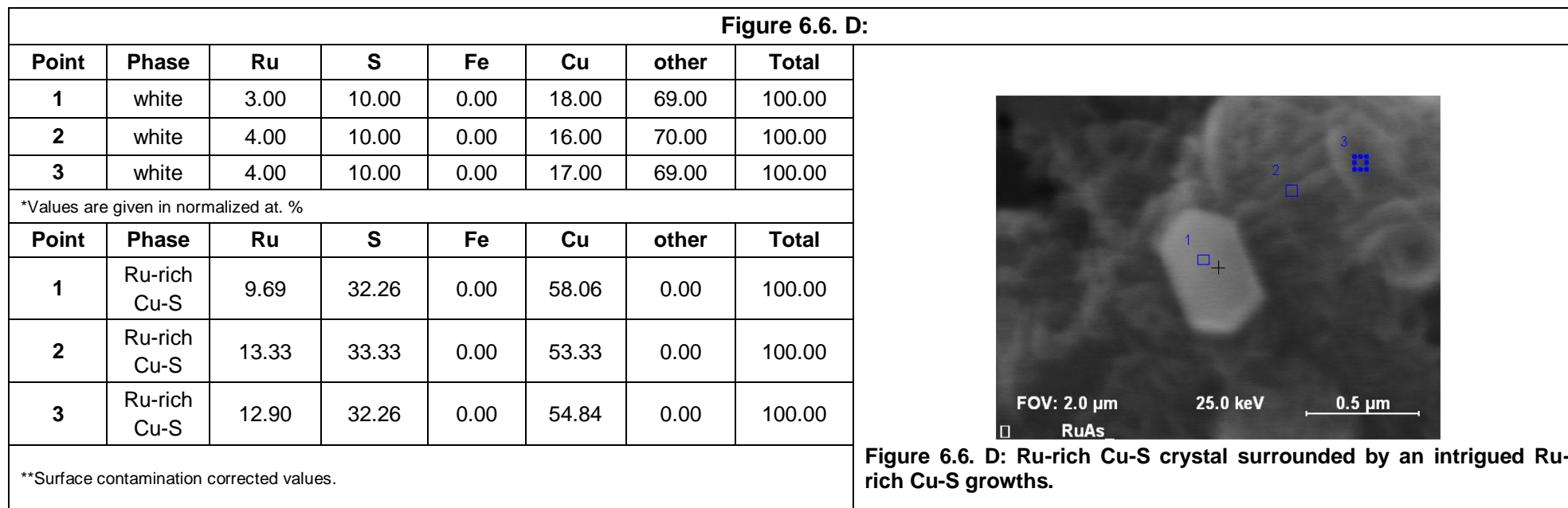


Table 6.9., 6.11. and 6.12.:

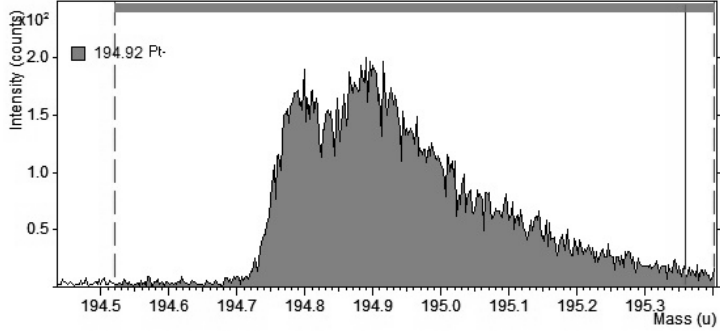
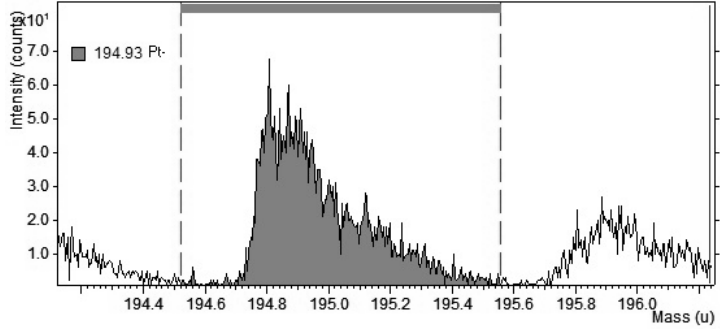
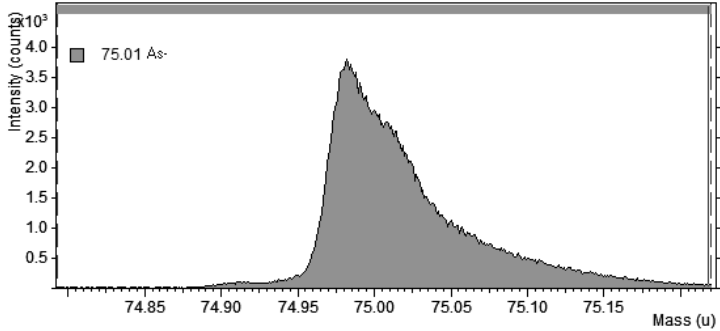
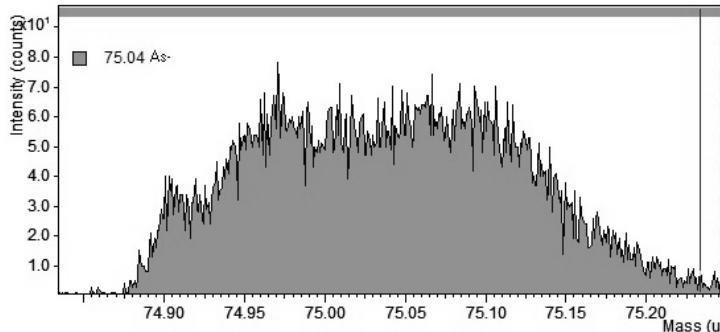
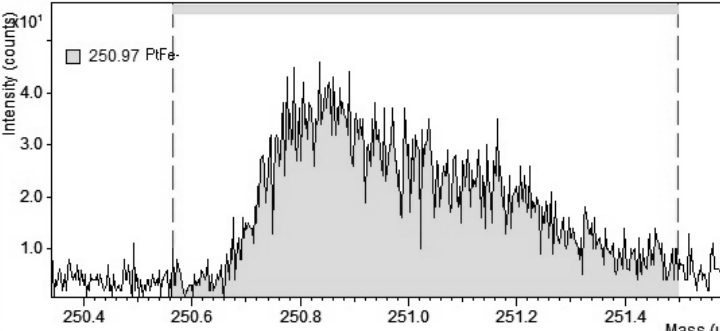
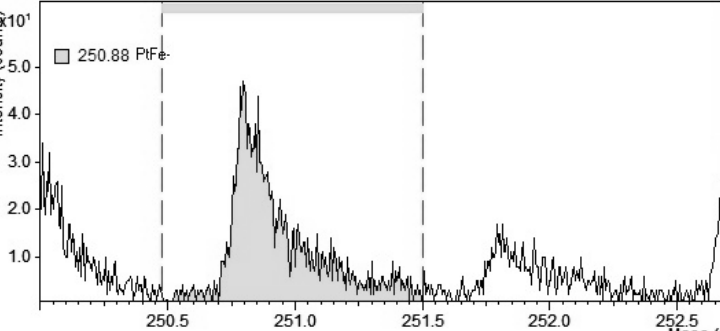
The size, morphology (shape), classification and distribution of PGE-rich nano structures, smaller than 100nm, measured with SAM and/or TOF-SIMS, in samples from experiment A, B and C.

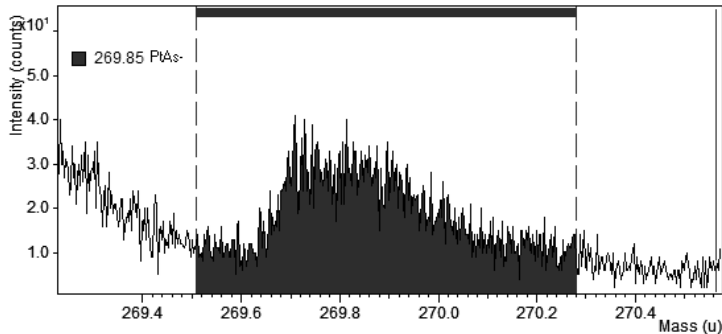
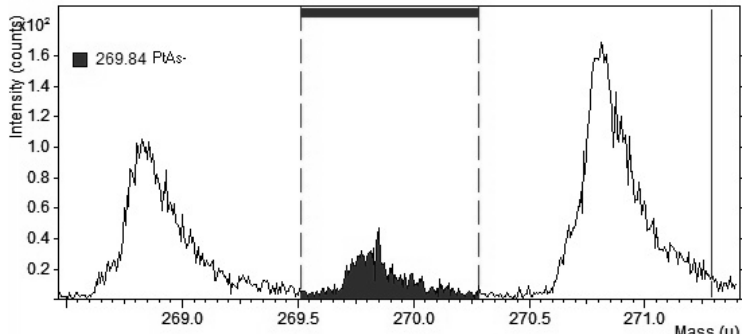
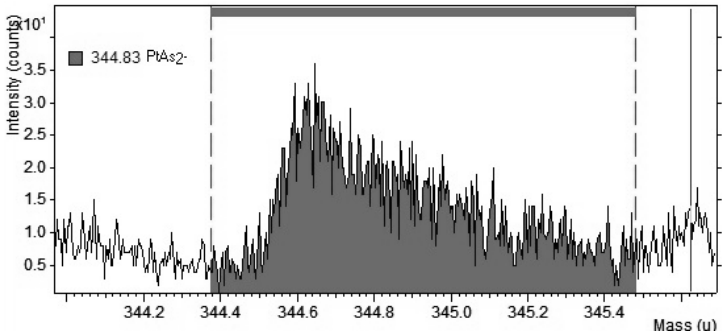
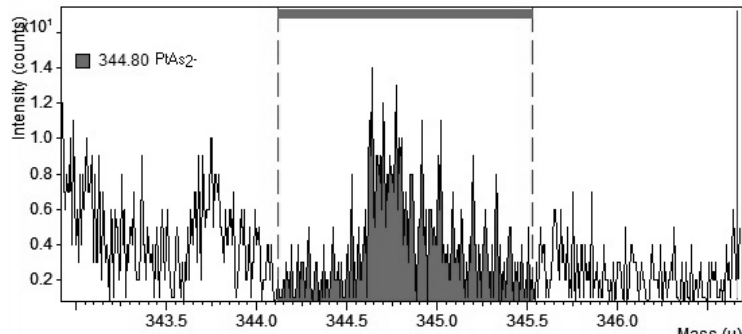
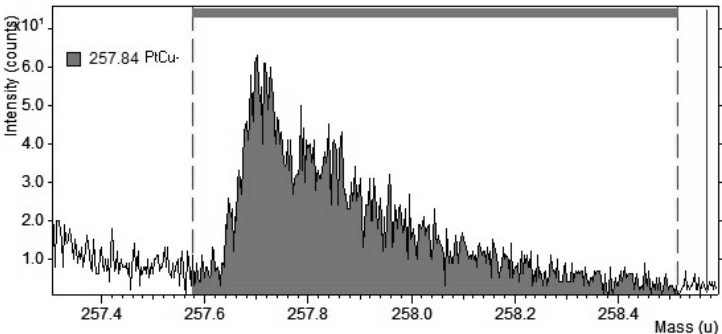
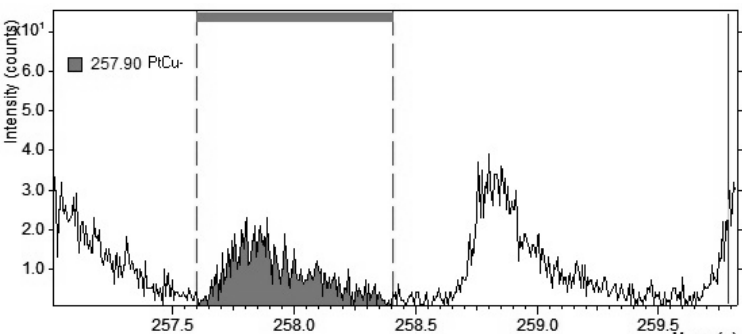
Composition	Size, nm					Avg. size nm
	1	2	3	4	5	
Experiment A: FAST						
Pt _x	70	100	60	50	80	70
Avg.						70
Experiment B: FAST						
Pd _x	70	45	55	70	45	55
Avg.						55
Experiment C: FAST						
Ru _x	110	80	120	90	100	100
Avg.						100
Avg. A, B and C						75
Experiment A: SLOW: No phases were picked-up by SAM						

Figure 6.7., 6.8. and 6.9.: See following pages

Table 6.10. and 6.13.: See following pages

Table 6.10.:

Before sputtering: Scan 1			After sputtering: Scan 2		
Ion	Mass	Spectrograph	Ion	Mass	Spectrograph
Pt	194.92		Pt	194.93	
As	75.01		As	75.04	
PtFe	250.97		PtFe	250.88	

Before sputtering: Scan 1				After sputtering: Scan 2			
Ion	Mass	Spectrograph		Ion	Mass	Spectrograph	
PtAs	269.85			PtAs	269.84		
PtAs ₂	344.83			PtAs ₂	344.80		
PtCu	257.84			PtCu	257.90		

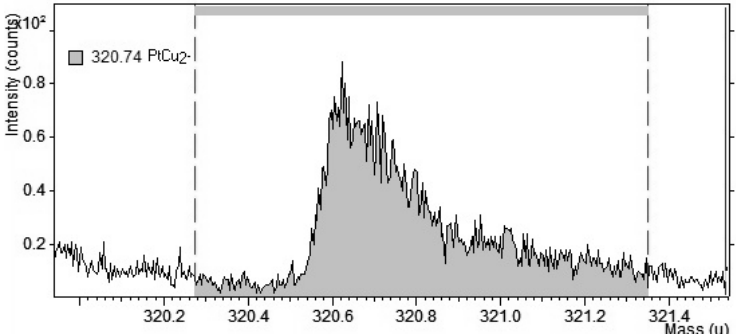
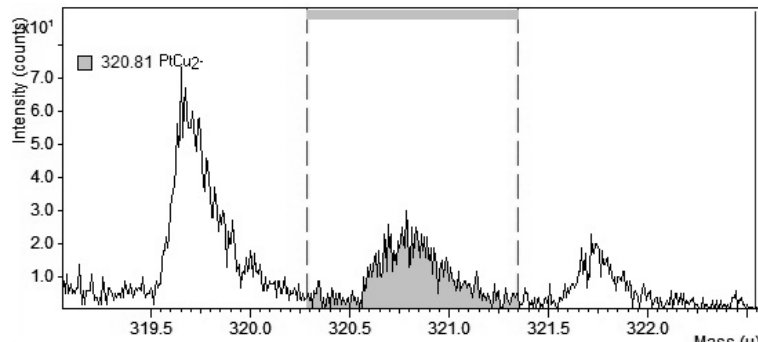
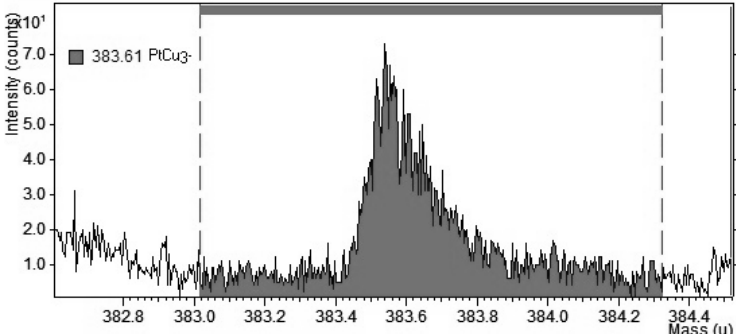
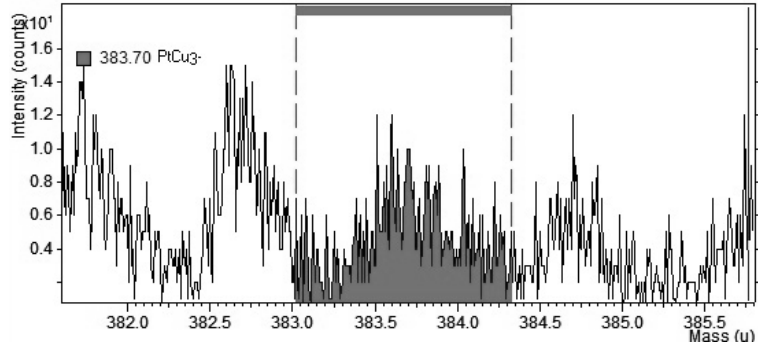
Before sputtering: Scan 1				After sputtering: Scan 2			
Ion	Mass	Spectrograph		Ion	Mass	Spectrograph	
PtCu ₂	320.74			PtCu ₂	320.81		
PtCu ₃	381.61			PtCu ₃	383.70		

Figure 6.7.:

Point	Phase	Pt	S	Fe	Cu	other	Total
1	white	3.00	8.00	16.00	19.00	47.00	100.00
2	grey	5.00	19.00	24.00	8.00	44.00	100.00

*Values are given in normalized at. %.

Point	Phase	Pt	S	Fe	Cu	other	Total
1	Pt _x Cu _x	5.66	15.09	30.19	35.85	0.00	100.00
2	Cu _x Fe _x S _x	8.93	33.93	42.86	14.29	0.00	100.00

**Surface contamination corrected values.

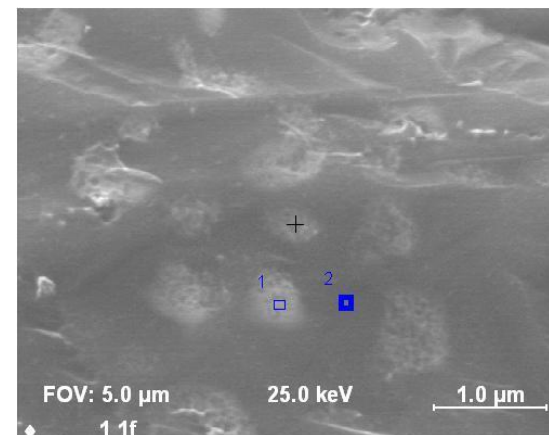


Figure 6.7.: Pt-rich patch-like features (avg. 70nm) lying on the melt surface.

Figure 6.8. A:

Point	Phase	Pd	S	Fe	Cu	other	Total
1	white	3.00	7.00	12.00	6.00	78.00	100.00
2	white	1.00	7.00	11.00	5.00	76.00	100.00

*Values are given in normalized at. %

Point	Phase	Pd	S	Fe	Cu	other	Total
1	Pd-rich	10.71	25.00	42.86	21.43	0.00	100.00
2	Pd-rich	4.17	29.17	45.83	20.83	0.00	100.00

**Surface contamination corrected values.

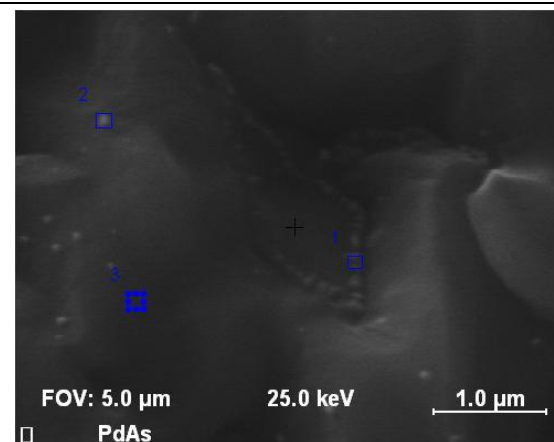


Figure 6.8. A: Pearls of Pd, 70-45 nm, on Fe-rich Fe-Cu-S (melt) phase.

Figure 6.8. B:

Point	Phase	Pd	S	Fe	Cu	other	Total
1	white	3.00	6.00	14.00	6.00	71.00	100.00
2	white	2.00	6.00	18.00	4.00	70.00	100.00
3	grey	<1.00	4.00	18.00	4.00	73.00	100.00

*Values are given in normalized at. %.

Point	Phase	Pd	S	Fe	Cu	other	Total
1	Pd-rich	10.34	20.69	48.28	14.81	0.00	100.00
2	Pd-rich	6.67	20.00	60.00	13.33	0.00	100.00
3	Fe _x Cu _x S _x	<3.70	14.81	66.67	20.69	0.00	100.00

**Surface contamination corrected values.

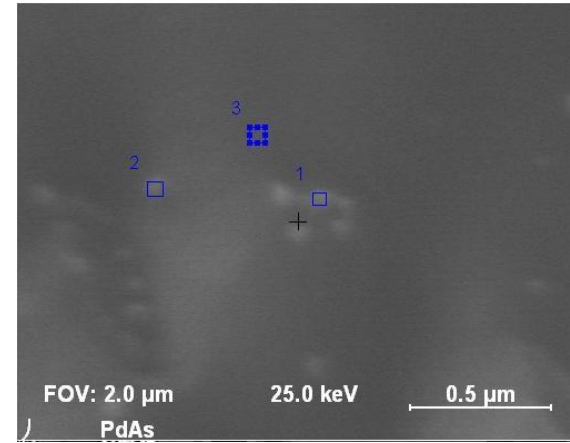


Figure 6.8. B: High density Pd-rich nano structures (55 nm) on a Fe-rich Fe-Cu-S (melt) phase.

Figure 6.9. A and B:

Point	Phase	Ru	S	Fe	Cu	other	Total
1	white	3.00	9.00	1.00	17.00	70.00	100.00
2	white	4.00	10.00	1.00	15.00	70.00	100.00
3	grey	4.00	9.00	2.00	12.00	73.00	100.00

*Values are given in normalized at. %.

Point	Phase	Ru	S	Fe	Cu	other	Total
1	Ru-rich	10.00	30.00	3.33	56.67	0.00	100.00
2	Ru-rich	13.33	33.33	3.33	50.00	0.00	100.00
3	(Ru,Fe) _x Cu _x S _x	14.81	33.33	7.04	44.44	0.00	100.00

**Surface contamination corrected values.

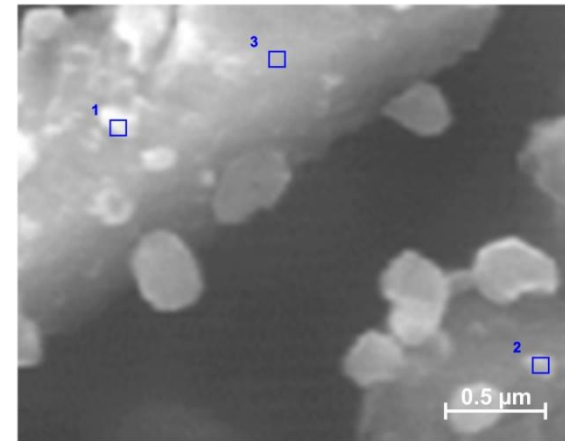
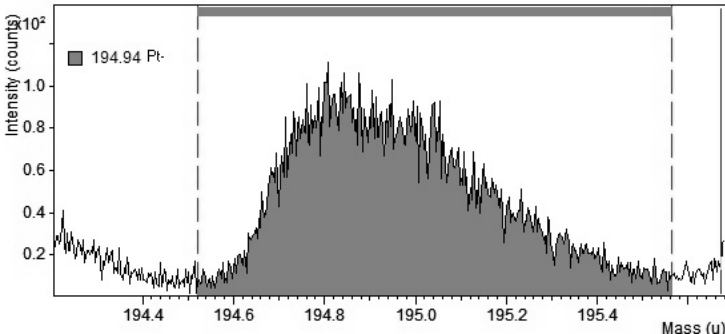
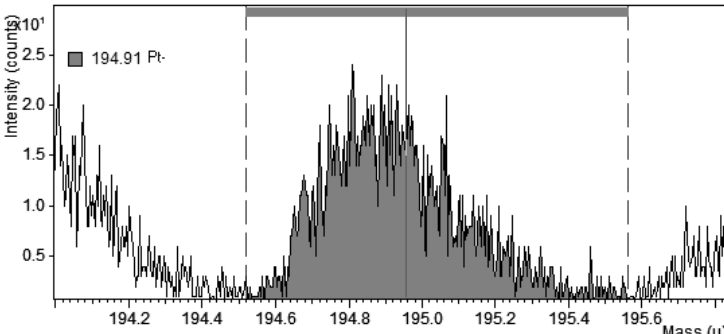
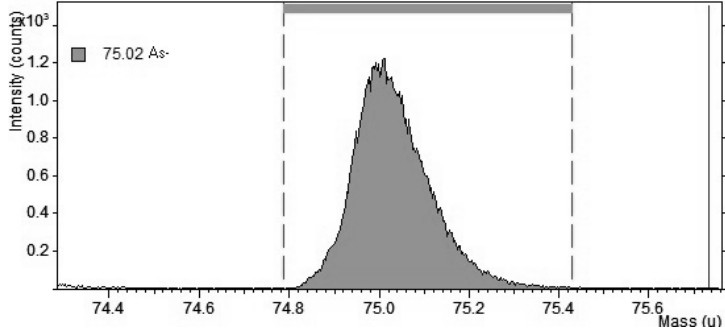
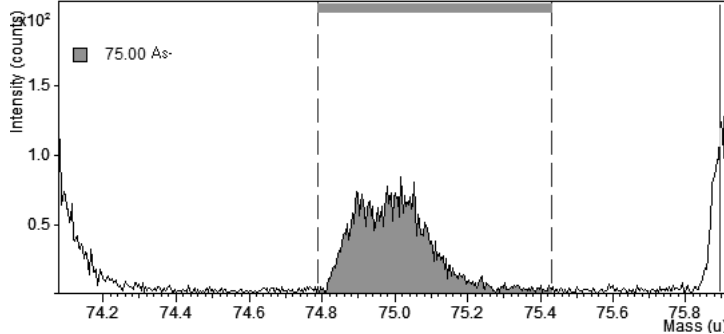
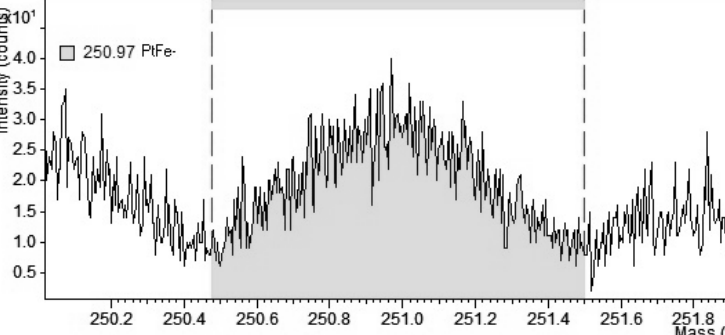
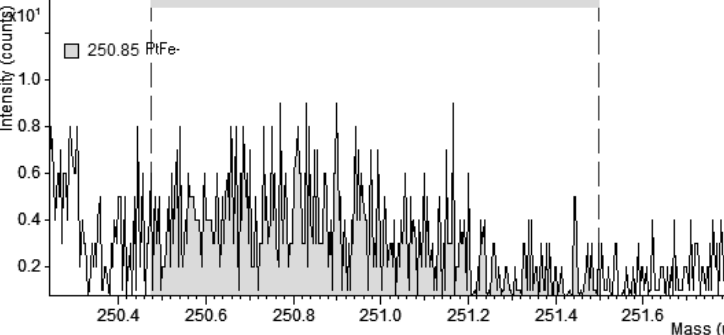
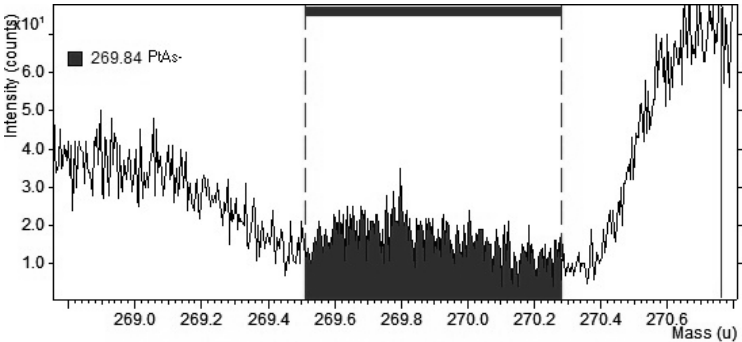
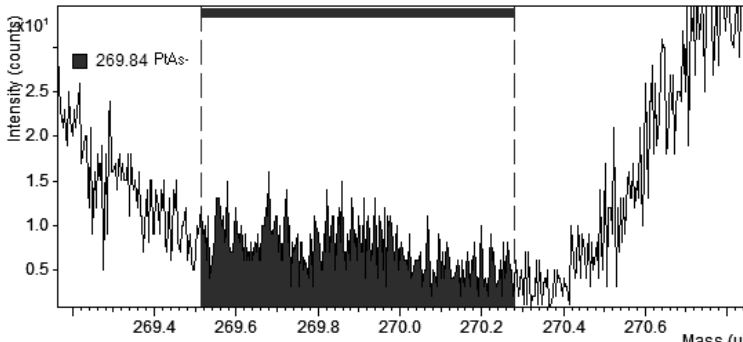
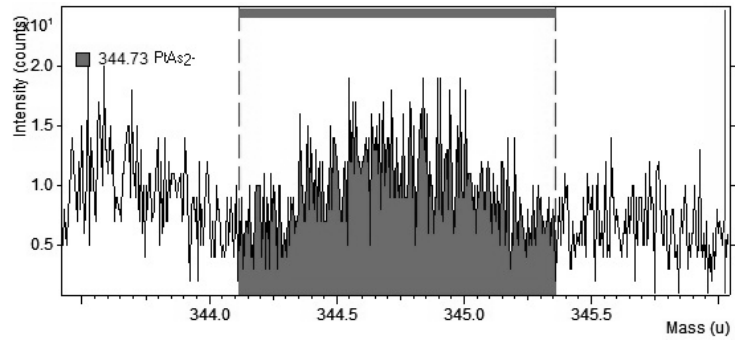
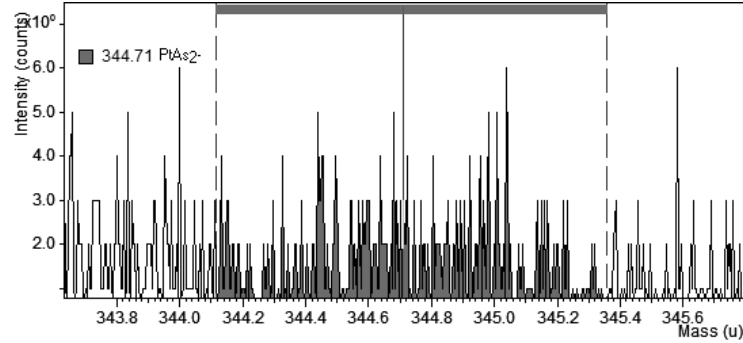
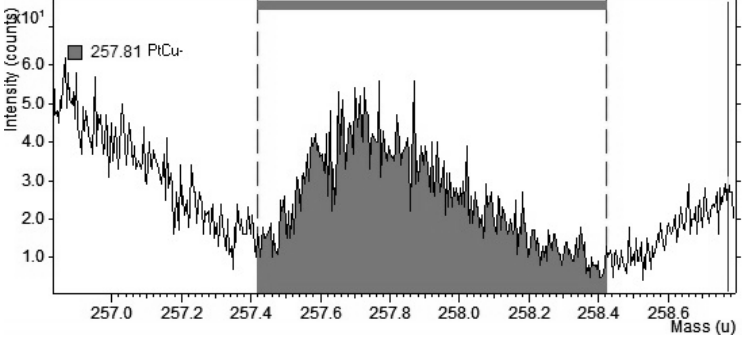
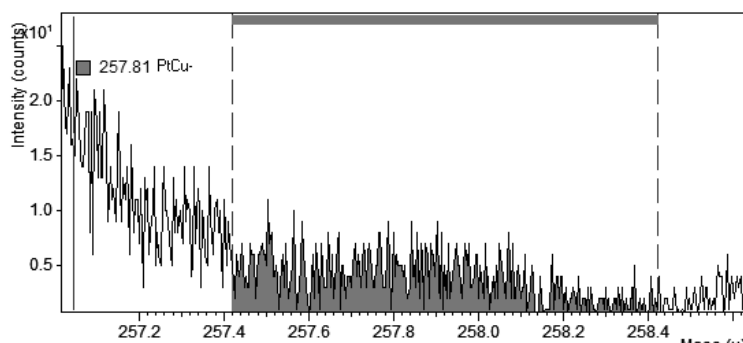
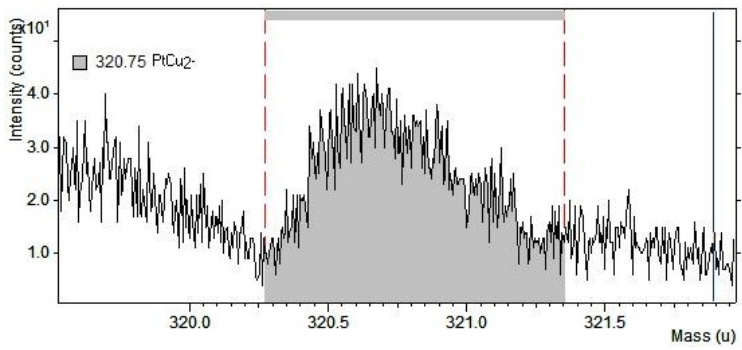
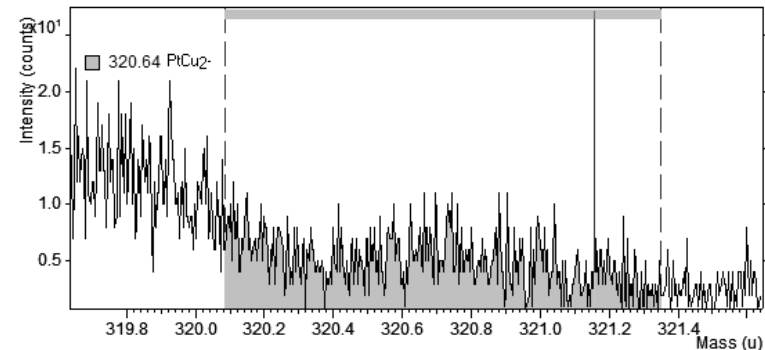
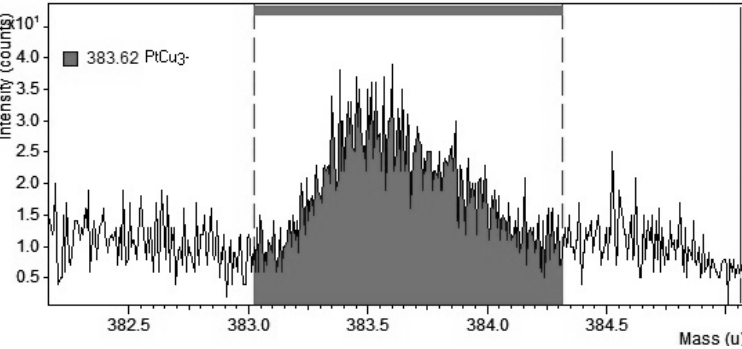
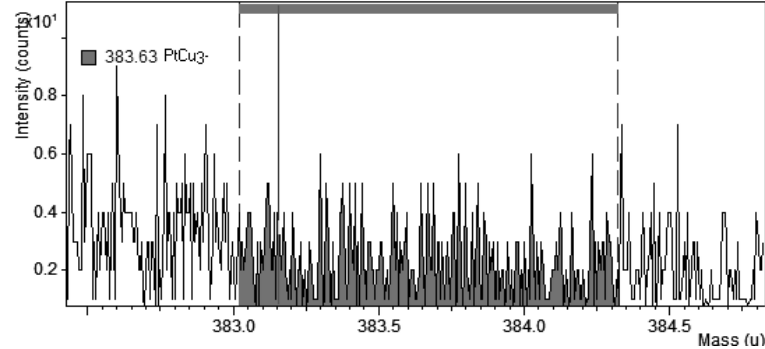


Figure 6.9. A and B: Ru-rich nano structures, ranging from 80-120nm, measured in samples from experiment C.

Before sputtering: Scan 1			After sputtering: Scan 2		
Ion	Mass	Spectrograph	Ion	mass	Spectrograph
Pt	194.94		Pt	194.91	
As	75.02		As	75.00	
PtFe	250.97		PtFe	250.85	

Before sputtering: Scan 1			After sputtering: Scan 2		
Ion	Mass	Spectrograph	Ion	mass	Spectrograph
PtAs	269.84		PtAs	269.84	
PtAs ₂	344.73		PtAs ₂	344.71	
PtCu	257.81		PtCu	257.81	

Before sputtering: Scan 1			After sputtering: Scan 2		
Ion	Mass	Spectrograph	Ion	mass	Spectrograph
PtCu₂	320.75		PtCu₂	320.64	
PtCu₃	383.62		PtCu₃	383.63	

Appendix F

Original publications formatted according to conference specifications.

List of documents attached:

1. Kennedy B and Tredoux M (2011) Investigation of the behaviour of platinum group elements (PGE), in synthetic sulphide systems, 23rd Colloquium of African Geology (CAG23) and YES, Johannesburg, South Africa: 8-14 January 2011, Abstract volume, 216 **p 153**
2. Kennedy B, Tredoux M, Ballhaus C, Helmy HM, Swart HC and Coetsee L (2011) Possible platinum group element (PGE) clusters in magmatic systems, using synthetic sulphide melts, 21st Goldschmidt Geochemistry Conference, Prague, Czech Republic: 14-19 Augustus 2011, abstracts published in Mineralogical Magazine, 75 (3), 1169 **p 154**
3. Kennedy B, Tredoux M, Ballhaus C, Helmy HM, Steyl G, Swart HC and Coetsee E (2011) The growth of PGE nano-structures in magmatic systems, using synthetic sulphide melts, 8th Annual Inkaba YeAfrica Workshop at GeoSynthesis 2011, Cape Town, South Africa: 28 August- 2 September 2011, Abstract volume **p 155**
4. Kennedy B, Tredoux M, Steyl G, Swart HC and Coetsee E (2012) A possible explanation for the PGE enrichment in the chromitites of ophiolite complexes, Ophiolites and related ore and industrial minerals Workshop, Trabzon, Turkey: 16-22 May 2012, Abstract volume, 16 **p 156**

5. Kennedy B, Tredoux M, Ballhaus C, Coetsee-Hugo E, Swart HC and Steyl G (2013) PGE nano structures in natural Ni-Cu-S systems, 6th Igneous and Metamorphic Petrology Study Group (IMSGS 6), Bloemfontein, South Africa: 21-23 January 2013, Abstract volume, 31 **p 157**

6. Kennedy, B., 2013, 'Bestudering van moontlike platinumgroepelement nanostrukture in monosulfiedsisteme deur middel van sintetiese sulfiedsmeltings', Suid- Afrikaanse Tydskrif vir Natuurwetenskap en Tegnologie 32(1), Art #415, 1 page. <http://dx.doi.org/10.4102/satnt.v32i1.415> **p 158**

7. Kennedy B, Tredoux M, Ballhaus C, Coetsee E and Steyl G (2013) The possible influence of PGE clusters on phase association in Ni-Cu-S deposits, as deduced from synthetic sulphide deposits, 12th SGA Biennial Meeting, Uppsala, Sweden: 12-15 August 2013, Abstract volume **p 159**

8. Kennedy B, Tredoux M, Ballhaus C, Coetsee-Hugo E and Steyl G (2013) Possible PGE nano structures, in magmatic systems, 23rd Goldschmidt Geochemistry Conference, Florence, Italy: 20-25 August 2013, abstract published in Mineralogical Magazine, 77 (5), 1447 **p 162**

INVESTIGATION OF THE BEHAVIOUR OF PLATINUM GROUP ELEMENTS (PGE), IN SYNTHETIC SULPHIDE SYSTEMS

Kennedy, B.¹ & Tredoux, M.²

1. Dept. of Geology, University of the Free State, Bloemfontein, R.S.A., kennedybia@gmail.com

2. Dept. of Geology, University of the Free State, Bloemfontein, R.S.A., mtredoux@ufs.ac.za

KEYWORDS: PGE, experimental petrology, PGE clusters, physical behaviour

The research aims to verify whether the binding mechanism of PGE in a magmatic environment is primarily a chemical or physical/-mechanical process. The existence of small Pt clusters (10-100 atoms) within a mono-sulphide phase would inevitably prove that an initial primary mechanical binding process is dominant and this possibility was investigated.

Several experiments were conducted using variable quantities and ratios of Pt, As, Cu and Fe to mimic the manner in which Pt binds in a high pressure, high temperature and highly reducing magmatic environment. The experiments were done using a silica-vacuum technique. The samples were cooled down at different tempos to ensure that various formation conditions were achieved. This was done to test if the same results (clusters) would be obtained in every case, for if so a physical model is very probable.

The charges were made into polished sections which were analysed using several analytical methods including ore-microscopy and SEM. It was found that the Pt forms Pt-As clusters within the mono-sulphide (crystalline) phase of both slowly and faster cooled monsters. The presence of the clusters (10-100 atoms) in the faster cooled monsters confirms that they must form as a primary phase. This behaviour cannot be explained by sub-solidus immiscibility properties as has been suggested as an explanation for the frequent presence of PGE minerals in base metal sulphide minerals (Tredoux et al).

Preliminary results seem to indicate that Pt as a proxy for the PGE forms clusters of about 10-100 atoms during the early stages of magma differentiation, probably due to their siderophile behaviour. The clusters can easily be taken up into an immiscible sulphide fraction or in oxide or silicate phases (L. Robb). This mechanism may explain the high enrichment of PGE in cumulus (olivine and chromite) phases of the Bushveld Igneous Complex.

2.

Possible platinum group element (PGE) clusters in magmatic systems, using synthetic sulphide melts

KENNEDY, B. ^{1*}, TREDoux, M. ¹, BALLHAUS, C. ², HELMY, H.M. ², SWART, H.C. ³ & COETSEE, L³

¹Department of Geology, University of the Free State, South Africa (*correspondence:kennedybia@gmail.com)

²Steinmann Institute, Universität Bonn, Bonn, Germany

³Department of Physics, NNSCF, University of the Free State, South Africa

The aim of the study is to verify whether or not the primary binding mechanism of PGE, in a magmatic environment, is a pure chemical or physical/- mechanical process. The monosulphide (mss) phases of temperature controlled synthetic melts were investigated for the existence of small Pt clusters or nano-structures (10-100 atoms). If such entities are found, they would point towards an initial physical mechanism as the dominant process during early magma differentiation.

Experiments were run with variable concentrations of Pt, As, Cu, S and Fe, chosen to mimic a natural Cu-Ni-S ± PGE system. Samples were cooled down rapidly (from 1050-25°C in a few seconds) and slowly (1050-400 °C over 48 hours).

Pt forms large heterogeneously distributed Pt-As_x and Pt- Fe_x phases (0.2-50 µm i.e. approximately 700-166666 atoms) within the melt phase of both slow and fast cooled samples. Results indicate that Pt needs a suitable anion like As, Fe or Cu to form a stable phase in a magmatic system. Pt-Cu_x phases (200-1000nm i.e. approximately 700-3333 atoms) in the mss phase of faster cooled samples confirm that some kind of clustering process is at work in Cu-Ni-S systems. Faster cooled samples show exsolution textures of Pt out of the mss phases into the melt phase (Cu_x-Fe_x-S_x).

While chemical behaviour may govern the secondary distribution of Pt-phases, clustering is potentially the primary (physical) mechanism. The clusters can easily be taken up into an immiscible sulphide, oxide or silicate phase. Clustering behaviour may explain the high enrichment of PGE in early cumulus phases (olivine and chromite) of the Bushveld complex.

Investigation of the growth of platinum group element nano-structures in synthetic sulphide melts

B. Kennedy¹, M. Tredoux¹, C. Ballhaus², H.M. Helmy², H.C. Swart³, E. Coetsee³, G. Steyl⁴

1. Geology Dept., University of the Free State, South Africa, kennedybia@gmail.com

2. Steinmann Institute for Mineralogy, Universität Bonn, Germany

3. Physics Dept., University of the Free State, South Africa

4. Chemistry Dept., University of the Free State, South Africa

The project is aimed at the verification of the primary binding mechanism of platinum group elements (PGE), in a magmatic environment, is either of a pure chemical or a mixed physical/mechanical process. The mono-sulphide (mss) phases of temperature controlled synthetic sulphide melts were investigated for the existence of small Pt clusters or nano-structures (<1000 atoms). The presence of such entities would point towards an initial primary physical mechanism as the dominant process during early magma differentiation, rather than a chemical one. Experiments were run with variable concentrations of Pt, As, Cu, S and Fe, chosen to mimic a natural magmatic Cu-Ni-S \pm PGE system. Some samples were quenched (from 1050°C-25°C in a few seconds) and others cooled slowly (1050°C-400°C over 48 hours). Determination of major elements and PGE concentration and distribution were investigated using SEM and SAM. Pt formed large heterogeneously distributed Pt-As_x and Pt-Fe_x phases (0.2-50 μ m, i.e. approximately 700-167000 atoms) within the melt phase of both slow and fast cooled samples. The Pt-phases showed various growth structures ranging from perfect isometric crystals to skeleton- and blob-like structures. Results indicated that Pt requires a suitable anion like As or a metal such as Fe or Cu to form a stable phase at magmatic temperatures. Fast and slow cooled samples both showed exsolution textures of Pt out of the mono-sulphide phase into the melt phase (Cu_x-Fe_x-S_x), possibly indicating a lack of primary chemical bonding in the solid phase. While chemical behaviour may govern the secondary distribution of Pt-phases, clustering is potentially the primary binding (physical) mechanism. The PGE clusters can easily be taken up into an immiscible sulphide, oxide or silicate phase. Clustering behaviour may explain the high enrichment of PGE in early cumulus phases (olivine and chromite) of the Bushveld complex, as crystals of these minerals might use the PGE clusters as nucleation points.

KEYWORDS: PGE, sulphide melts, PGE clusters, physical behaviour

A possible explanation for the PGE enrichment in the chromitites of ophiolite complexes

B. Kennedy¹, M. Tredoux¹, G. Steyl², H. Swart³ & E. Coetsee³

¹Dept. of Geology, University of the Free State, South Africa

²Dept. of Chemistry, University of the Free State, South Africa

³Dept. of Physics, University of the Free State, South Africa

Corresponding Author's e-mail address: kennedybia@gmail.com

The depleted mantle sections of ophiolite complexes host PGE-enriched chromitites, with concentrations up to economic levels in certain cases. The retention of the PGE in the mantle restite is difficult to explain by conventional chalcophile models. The aim of the study is to investigate to what extent 'cluster' behaviour might contribute to the enrichment process.

The siderophile IPGEs (Os, Ir, Ru) and Pt are more associated with chromite than with the more chalcophile PPGEs (Pd and Rh). The chromitites that remain in the depleted upper mantle are therefore enriched in IPGEs, and depleted in sulphides. Nevertheless, the available S and other ligands (e.g. As) apparently act as trapping agents for the IPGEs, causing enrichment in remaining oxide and silicate phases. The question is whether this entrapment is a purely chemical process (compatibility driven partitioning) or a more physical process. As no experiment data has yet proved that the extremely high sulphide coefficients ($>10^5$) which would be required for chemical partitioning can occur at geologically reasonable conditions, the possibility exists that the PGEs exist in a form which allows for physical inclusion in sulphide.

To test the hypothesis, experiments were conducted using a Fe-Cu-S system doped with Pt, Pd and Ru and variable amounts of As. The experiments were manipulated to form an mss (pyrrhotite) phase and a melt phase. Very small (10-1000 nm) entities, or clusters, in which the PGE are bonded to As or Fe or Cu, are present in the mss. This observation indicates that the PGE may form minerals, on a nano level, without sulphide saturation having been achieved.

Physio-chemical bonding mechanisms (involving large electron clouds, polarization effects and electron negativity) may play a much greater role on the atomic level (greater surface to volume ratios) than previously thought. The large electron clouds of the PGEs allow them to form sigma bonds with anions like As. These PGE-As clusters may associate with sulphide or be included in chromite, to later crystallize as PGMs.

PGE NANO STRUCTURES IN NATURAL Ni-Cu-S SYSTEMS

Kennedy, B¹ & Tredoux, M¹ & Ballhaus, C² & Steyl, G³ & Coetsee, E⁴

¹ Department of Geology, University of the Free State, Bloemfontein, South Africa;
kennedybia@gmail.com

² Steinmann Institute for mineralogy, University of Bonn, Bonn, Germany

³ Department of Chemistry, University of the Free State, Bloemfontein, South Africa

⁴ Department of Physics, University of the Free State, Bloemfontein, South Africa

Keywords: platinum group elements, clusters, experimental petrology, synthetic sulphide systems

The feasibility of cluster formation as the primary binding mechanism of platinum group elements (PGE) in a magmatic environment was investigated. Variable concentrations of As and PGE (Pt, Pd and Ru) were added to constant amounts of S, Cu and Fe. The experiments were manipulated to best present a natural Cu-Ni-S \pm PGE system. Samples were prepared using the silica-tube technique. The final products were investigated using scanning electron microscopy (SEM) and scanning auger microscopy (SAM). Preliminary results indicated that Pt formed agglomerations of about 10-100 atoms during the early stages of experiments, probably due to its siderophile behaviour. The existence of PGE clusters within a mono-sulphide phase would indicate that an initial primary physical (mechanical) binding process is more dominant during early crystallization than chemical association with sulphide bonds. This behaviour cannot be explained by sub-solidus immiscibility properties as has been suggested to account for the frequent presence of PGE in base metal sulphide minerals (BMS).

Bestudering van moontlike platinumgroepelement nanostrukture in monosulfiedsisteme deur middel van sintetiese sulfiedsmeltings

Studying possible platinum group element nanostructures in monosulphide systems by means of synthetic sulphide melts. Is the primary binding mechanism of platinum group elements (PGE) in a magmatic environment purely a chemical or both a physical and mechanical process? The presence of Pt nanostructures (< 1000 atoms) in monosulphide phases would point towards an initial primary physical mechanism as the dominant process during early magma differentiation.

Is die primêre bindingsmeganisme van die platinumgroepelemente (PGE) in 'n magmatiese stelsel 'n suiwer chemiese of 'n fisiochemiese of meganiese proses?

Die monosulfiedfases (mss [*mono-sulfide solid solution*] of Fe_xS) van temperatuurbeheerde eksperimente is ondersoek vir platinumnanostrukture (< 1000 atome). Die teenwoordigheid van platinumnanostrukture in die mss-fases sal bewys dat 'n fisiese meganisme eerder as 'n suiwer chemiese proses die primêre bindingskrag gedurende vroeë magmatiese differensiasie is.

'n Natuurlike Cu-Ni-S \pm PGE-magmatiese stelsel is deur middel van temperatuurbeheerde eksperimente nageboots. Die eksperimente bestaan uit 'n basiese Cu-Fe-S-mengsel met varieerbare konsentrasies Pt en As. Platinum is as analoog vir die platinumgroepelemente gebruik. Monsters is oor varieerbare tydgrepe verhit en afgekoel (van 1050 °C tot 25 °C binne enkele sekondes en geleidelik van 1050 °C tot 400 °C oor 'n tydperk van 48 uur). Die tydgrepe van formasie is gebruik om te bepaal of dieselfde resultate in verskillende omstandighede verkry word. Die afgekoelde monsters toon twee primêre fases: 'n monosulfiedfase (Fe_xS) en 'n smeltfase ($\text{Cu}_x\text{-Fe}_x\text{-S}_x$). In die smeltfase vorm Pt groot heterogeen verspreide Pt-As_x-en Pt-Fe_x-fases (0.2 μm – 50 μm of 700 atome – 167 000 atome). Geen Pt-strukture is tot dusver in die monosulfiedfase waargeneem nie.

Die gemete Pt-fases is heterogeen deur die stelsel versprei en wissel in grootte en vorm. Daar is geen korrelasie tussen die Pt-fases se vorm, grootte en konsentrasies Pt nie. Resultate toon dat Pt 'n an-ioon soos As, Fe of Cu nodig het om 'n stabiele fase in 'n magmatiese stelsel te vorm. Pt is onversoenbaar met S en sal dus nie met swaer bind nie. Eksperimente met ander PGE (Pd, Ru, Rh, Os en Ir) toon soortgelyke neigings.

Vinnig en stadig afgekoelde monsters wys *eksklusieteksture* van Pt en Cu uit die mss in die smeltfase ($\text{Cu}_x\text{-Fe}_x\text{-S}_x$). Hierdie tipe gedrag dui op 'n moontlike tekort aan primêre chemiese bindings in die soliede fase.

Chemiese gedrag mag dalk die sekondêre verspreiding van Pt-fases beheer, maar die formasie van platinumnanostrukture is hoofsaaklik 'n primêre bindingsmeganisme. Die PGE-nanostrukture kan maklik in 'n onversoenbare sulfied-, oksied- of silikaatfase opgeneem word. Die PGE-nanostrukture dien as nukliasie-groei-punte. Die nanostrukture mag dalk die hoë verryking van PGE in die vroeë kumulusfases (olivien en chromiet) van die Bosveld-stollingskompleks verklaar.

The possible influence of PGE clusters on phase associations in Ni-Cu-S deposits, as deduced from synthetic sulphide systems.

B. Kennedy, M. Tredoux

Department of Geology, University of the Free State, South Africa

C. Ballhaus

Steinmann Institute for mineralogy, University of Bonn, Germany

E. Coetsee

National Nano Surface Characterization Centre, Department of Physics, University of the Free State, South Africa

G. Steyl

Department of Chemistry, University of the Free State, South Africa

Abstract. Nano scale platinum phases (10-1000 nm) in a synthetic sulphide system were measured, by high resolution SAM and TOF-SIMS. These phases might contribute to the enrichment of PGE in incompatible sulphide phases in sulphur poor Ni-Cu deposits, like the Bushveld Complex. The starting powders were based on the composition the sulphide portion of a Cu-Ni-S melt. Ligands such as S, As, Fe and Cu appear to act as trapping agents for the PGE. Chemical behaviour may govern the secondary distribution of PGE phases but the "clustering" reported here is potentially a primary (physical) enrichment mechanism.

Keywords. Platinum-group elements, clusters, synthetic sulphide systems, experimental petrology

1 Introduction

The genesis of the highly PGE enriched ore layers of the Bushveld complex (BIC), is enigmatic. Most geochemical models, based on chalcophile principles cannot fully explain the over enrichment of PGM and Cr within the relatively small magma budget of the BIC. In this investigation, alternative models, such as the cluster model (Tredoux et al. 1995), were investigated, to explain the extreme PGE enrichment factors in these magmatic deposits.

The aim of the study was to verify if clusters do form in a magmatic environment and if so, to what extent may they contribute to the ore enrichment process.

2 Materials and methods

Samples were prepared using the dry reaction silica tube technique (Kullerud et al. 1969). The synthetic sulphide system consisted of a mixture of

S, Cu and Fe powders. The powders were doped with various concentrations of PGE and As, see Table 1.

Table 1. Outline of experiments

	Mixture mg	Exp.	PGE ppm	As ppm
S	358	1	300	280
Fe	480	2	40	30
Cu	174	3	300	0

As was chosen as stabilizing chalcogene ligand in all the experiments. Experimental conditions were manipulated to form a mono-sulphide (mss) or pyrrhotite (FeS) phase and melt phase ($\text{Fe}_x\text{Cu}_x\text{S}_x$). Pyrrhotite is one of the first ore minerals to crystallize in a magmatic environment and thus the ideal place to look for possible clusters.

Experiments were quick quenched from 900°C to room temperature. Other samples were slowly cooled from max temperatures to around 400°C.

Samples were analysed using ore-microscopy, XRD, SEM, SAM and TOF-SIMS.

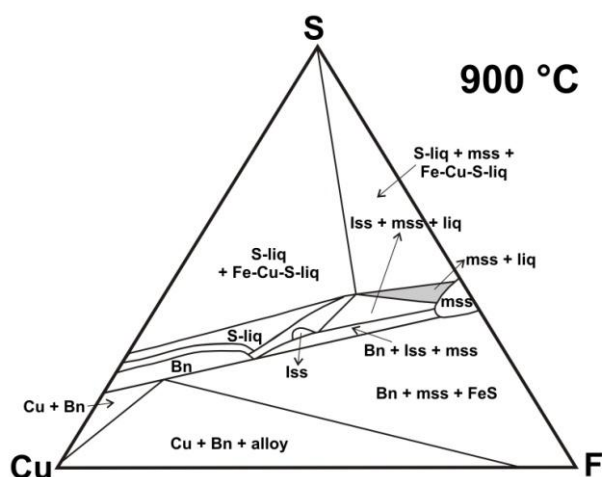


Figure 1. The phase diagram of the mss system at 900°C, adapted from Kullerud et al. 1969. The grey area indicates the starting concentration of the experiments.

3 Results

The quick quench samples showed two primary phases, an amorphous melt phase ($\text{Cu}_x\text{Fe}_x\text{S}_x$) and an mss or po (Fe_xS_x) phase with \pm PGMs. The slower cooled samples had a more complex mineralogy with mss, melt, bn, cpy and \pm PGMs.

Several quench and secondary PGE-Cu dominant exsolution textures were measured, on the mss and melt surfaces. The size of the PGE phases varied between 10-1000nm. Secondary structures and textures formed due to exsolution and segregation of elements, as the system moves to a final equilibrium state. The Cu-rich 'flowers' indicated that a vast concentration of Cu and PGE was present in the mss phase, at high temperatures.

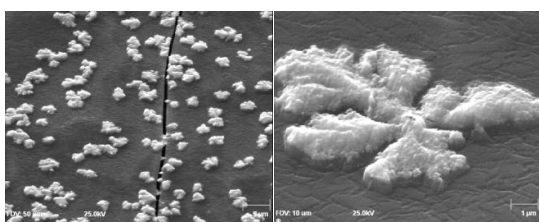


Figure 2. Secondary Pt-Cu exsolution phases (light grey) sitting on the mss surface (darker grey), measured with AES.

Nano scale entities (10-100nm), in which the PGE are bonded to As or Fe or Cu, were present in the mss and melt phases of the synthetic samples. This observation indicated that the PGE may form phases, on a nano level, without sulphide saturation having been achieved.

4 Discussion

The results indicated that PGE-ligand clusters, of 10-1000 nm, form due to the physio-chemical association of the PGE with chalcogene ligands, such as As, Fe and Cu.

The PGE-ligand clusters form due to the physio-chemical characteristics of the PGE. Their heavy electron-clouds, unfilled d-orbitals and huge surface areas may be the agents that prompt the PGE to nucleate and form clusters. Cluster formation does not seem to be dependent on the PGE concentration but on the availability of appropriate stabilising ligands or anions to form a phase.

The clusters are semi-stable to stable. The entities form during the early stages of magmatic differentiation. A fraction of the clusters are reabsorbed into the melt, while a fraction may act as nucleation points to form nano-crystals and minerals in the incompatible sulphide, spinel or silicate phases.

What makes the cluster model different is that it is based on nano scale driven processes and interactions. Elements exhibits vastly different chemical and physical characteristics and behaviour, then their bulk solid counterparts, between 10-100nm.

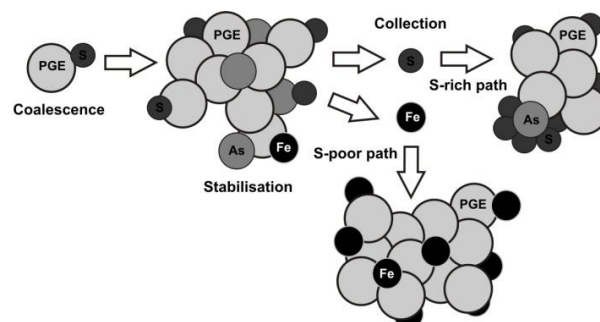


Figure 3. The cluster model, adapted from Tredoux et al. 1995

Physical or mechanical bonding (adsorption) is the primary binding mechanism. In an S-rich environment the PGE clusters are taken up in the sulphide melt and will precipitate as alloys, arsenides and tellurides. The fraction of PGE that is not removed will subsequently precipitate as sub-microscopic PGE minerals (PGM) in the BMS. In an S-poor environment the clusters can be stabilized by Fe or other chalcogene ligands such as Se, Cu, As, Bi, Te and Sb, to form metallic PGMs. The PGE clusters are physio-chemical ally relative incompatible with the major silicate minerals and will thus concentrate in the residual fluid, if not removed by one of the mechanisms mentioned above.

5 Conclusion

Ligand-mediated PGE cluster formation, in a magmatic environment, is driven by the isochemical (siderophile) characteristics of the elements, as appose to chemical (chalcophile) association with the mss. Clustering is a physical to physiochemical mechanism. Cluster behaviour cannot be explained by sub-solidus immiscibility properties as has been suggested as an explanation for the frequent presence of PGE minerals in base metal sulphide minerals.

We speculate that nano phase formation (clusters of 10-100nm) takes place before the exsolution of a mono sulphide melt from the magma, and before formal chemical bonding to

from PGMs. If this interpretation is correct, it might indicate that a physical enrichment process is at work during the early stages of magmatic differentiation.

Clustering is only one of several mechanisms that contribute to the PGE enrichment in S-poor PGE ore deposits, like the BIC. Other mechanisms like sulphide saturation, filter pressing, hiatus and the role of secondary fluids play vital roles in ore formation, distribution and concentration.

Acknowledgements

The authors would like to thank the Inkaba YeAfrica Research Programme, AEON and the NRF for funding the project.

Possible PGE nano structures, in magmatic systems

KENNEDY, B.^{1*} & TREDoux, M.¹ & BALLHAUS, C.² & COETSEE, E.³ & STEYL, G.⁴

1. Dept. of Geology, University of the Free State, South Africa, (*correspondence: kennedybia@gmail.com)

2. Steinmann Institute, University of Bonn, Germany

3. Dept. of Physics, University of the Free State, South Africa

4. Dept. of Chemistry, University of the Free State, South Africa

The retention of platinum-group elements (PGE) in the mantle restite is difficult to explain by conventional chalcophile models. PGE nano-structures (clusters of 10-100nm), might be the cause that magma can become enriched in PGE, during the early stages of magmatic differentiation. The study focused on the possible formation of these entities, in a magmatic system. If these entities do form, to what extent might they contribute to ore forming processes in ultra mafic deposits, like the Bushveld complex.

A synthetic sulphide system was used to replicate the sulphide portion of a Cu-Ni-S \pm PGE system. Sulphides are of the first ore minerals to crystallize in a magmatic environment and thus the ideal place to look for clusters. Experiments were run, using the dry powder silica charge technique. A base mixture of Cu, S and Fe, was doped with variable concentration of PGE (Pt, Pd and Ru) and As. As was chosen as stabilising chalcogene ligand. The systems were manipulated to form a mono sulphide- or pyrrhotite (Fe_xS_x) and a Cu-rich melt ($\text{Fe}_x\text{Cu}_x\text{S}_x$) phase.

Nano scale PGE-ligand phases, ranging from 10-1000 nm, were measured in the synthetic samples, with high resolution scanning auer microscopy (SAM). This might indicated that the PGE may form phases, on a nano level, without sulphide saturation having been achieved. The clusters form due to the physio-chemical association of the PGE with chalcogene ligands, such as As, Fe and Cu, before formal chemical bonding, to form PGMs. A fraction of the clusters are reabsorbed into the melt, while a fraction may act as nucleation points to form nano-crystals and minerals in the incompatible sulphide, oxide or silicate phases. The clusters form during the early stages of magmatic differentiation.

Chemical behaviour may govern the secondary distribution of PGE-phases, but clustering is potentially the primary (physical) enrichment mechanism. This behaviour cannot be explained by sub-solidus immiscibility properties as has been suggested to account for the frequent presence of PGE in base metal sulphide minerals.

Keywords: Platinum-group elements, clusters, nano structures, synthetic sulphide melt

Appendix G

Original publications formatted according to publication specifications.

List of documents attached:

9. Kennedy, B., Tredoux, M., Ballhaus, C., Coetsee-Hugo, E., Swart, H.C. and Steyl, G. (2014) Platinum cluster growth in a synthetic sulphide system, European Journal of Mineralogy, in press **p 164**

Platinum cluster growth in a synthetic sulphide system

B. Kennedy^{1*}, M. Tredoux¹, C. Ballhaus², E. Coetsee-Hugo³, H.C. Swart³, G. Steyl⁴

This paper reports on PGE cluster formation, in a high temperature synthetic magmatic Fe-Cu-S system. PGE clusters contribute to early enrichment processes. Pt was used as analogue for the PGE in synthetic sulphide experiments, based on a Cu-Ni-S sulphide portion of a natural PGE-containing melt.

A variety of Pt-rich and Pt-poor nano-structures were measured using scanning Auger microscopy (SAM). Primary and secondary nano phases could be distinguished. Several of the nano-structures could be reclassified as possible Pt-clusters. This notation was supported by Pt and Pt-ligand ion distribution measured with time of flight secondary ion mass spectrometry (TOF-SIMS).

It seemed possible that the cluster model, proposed to explain the enrichment of the PGE in sulphide poor magmatic systems such as the Bushveld complex (BIC), may be underlain by the presence of such pre-crystallization phases.

Key words: Platinum-group elements, clusters, BIC, experimental petrology, nano-structures

Appendix H

List of documents attached:

10. Extended summary in English **p 166**

11. Extended summary in Afrikaans **p 168**

Investigation of the possibility of platinum-group element clusters in magmatic systems, using synthetic sulphide melts

The origin and genesis of the PGE (Ru, Rh, Pd, Os, Ir and Pt) enriched Bushveld complex, remains a controversy. Geochemical models, based on chalcophile principles cannot fully explain the enrichment of platinum-group minerals (PGM) and the primary metal (PGE) concentration mechanism in these deposits. The cluster model, based on the physico-chemical properties of the PGE, may be of the key driving forces behind early PGE enrichment.

The cluster model hypothesises that the PGE may bond mechanically or physico-chemically to ligands (As, Fe and Cu) to form clusters or nano phases (10-100nm), before magmatic differentiation. A cluster is not a crystalline phase and does not represent a mineral. Clusters are semi-stable and may latch onto traditionally incompatible phases such as sulphides, silicate and oxides, causing enrichment. The aim of the study was to investigate if clusters can form in a magmatic environment and if so to what extent do clusters contribute to PGE enrichment.

A sulphide system was mimicked experimentally. Sulphides are of the first minerals to form in a magmatic system and more likely to carry PGE-clusters. Samples were prepared using the dry reaction silica tube technique. The experiments consisted of an S, Cu and Fe mixture doped with variable concentrations of PGE (Pt, Pd, Ru) and a chalcogene ligand (As). The samples were cooled at different rates to monitor the influence of external factors (time, chemistry, kinematic- and thermodynamic) on possible cluster formation.

The synthetic systems mss reacted successfully to form various Fe-Cu sulphides, a melt phase, PGM phases, associated textures and numerous PGE and non-PGE nano features. The non-PGE structures were a collection of Fe-Cu sulphides that formed either as primary structures or as secondary exsolutions. High temperature mss melts cannot be quenched and various secondary Fe-Cu-S phases will form as a result of rapid cooling. These phases showed no phase associations or orientations. The focus of the study however was on PGE-rich nano structures smaller than 100nm. These structures fall within the size range of clusters (10-100nm) and were a good indication whether clusters could form. The measured

nano structures (<100nm) differed in accordance to the PGE system (Pt or Pd or Ru) and allowed annealing time. These structures showed no distribution-, composition- of morphological trends.

Several of the measured nano structures were reclassified as potential PGE-clusters. It is possible that ligand-mediated PGE-cluster formation takes place, before the exsolution of mss melt from the magma and before formal chemical bonding, to form PGM. Cluster formation is driven by the isochemical (siderophile) characteristics of the elements, as appose to chemical (chalcophile) association with the mss.

If PGE-clusters did indeed form the following assumptions can be made 1) cluster formation is not dependent on the PGE concentration but the availability of appropriate trapping agents (ligand) or anions As, Cu or Fe. Nano phases formed without the melt being over-saturated in PGE. 2) Cluster formation is not a function of temperature. Nano structures were identified in systems that were quick quenched and slower annealed. However a large majority of these structures were lost over time and temperature change. The influence of the change in environment on nano phase formation is yet to be quantified. 3) The assortment of morphologies of measured nano structures (primary and secondary) confirmed that a variety of phase transitions and processes are present in natural magmatic systems. These nano entities have yet to be defined.

If this interpretation is correct, it might indicate that a physical enrichment process is at work during the early stages of magmatic differentiation. However clustering is only one of several mechanisms that may contribute to PGE enrichment of Bushveld-type deposits.

Onderzoek na die moontlikheid van platinumgroup element klusters in magmatiese stelsels, deur gebruik te maak van syntetiese sulfied smelte

Die oorsprong en verryking van platinum-group elemente (PGE) in die Bosveld kompleks bly 'n kontraversiële onderwerp. Die meerderheid verrykingsmodelle is gebaseer op chemiese (chalkofiele) beginsels. Die modelle kan nie die primêre verryking van PGE sonder twyfel verklaar nie. Die sleutel tot die verryking van PGE mag dalk lê in die metale se fisio-chemiese eienskappe en gedrag op nano vlak.

Die kluster model is gebaseer op die fisiese assosiasie van PGE met ligande (As, Fe en Cu) om PGE-klusters te vorm. Die klusters, tussen 10 en 100nm, vorm voor magmatiese differensiasie. Die semi stabiele klusters is nie 'n kristalyne fase of 'n mineraal nie. Die klusters verryk onversoembare fases, soos sulfied, oksied en silikaat fases, deur fisies aan die fases aan te heg soos klitsgras. Die uiteindelige doel van die studie was om te bepaal of klusters wel kan vorm in a magmatiese stelsel en indien dit moontlik is, wat is die invloed van die strukture op ertsverryking.

'n Sulfied smelt was eksperimenteel nageboots. Sulfides is van die eerste minerale om te vorm, in a magmatiese omgewing, en dus die eerste plek om te soek vir PGE-klusters. Die silikabuisie tegniek was gebruik om die sintetieses monsters voor te berei. Poeiers van Fe, Cu en S was verryk met verskillende konsentrasies van of PGE (Pt, Pd, Ru) en 'n chalkogeen ligand (As). Die bogenoemde tegniek laat toe om die monster teen verskillende tempos af te koel. Dit was belangrik om die invloed van eksterne faktore (tyd, chemiese, kinetiese en termiese) op kluster formasie te bepaal.

Die sintetiese stelsels het suksesvol gereageer om verskeie fases te form. Dit het ingesluit Fe-Cu sulfiedes, Fe-ryke smelt, PGM fases, verskeidenheid teksture en 'n versameling PGE-ryk en nie-PGE nano strukture. Die nie-PGE nano strukture was n versameling van Fe-Cu sulfiedes. Die strukture het geen voorkeur assosiasie of orientasie getoon met betrekking tot vorm, grootte en samestelling nie. Die fokus van die studie was op PGE-ryk nano strukture, kleiner as 100nm. Die strukture is die naaste aan klusters in grootte en samestelling en mag dalk as aanduiding gebruik word om te bepaal of klusters gevorm het. Die PGE-ryk nano strukture het 'n verskil getoon volgens PGE-stelsel en afkoelings venster. Die strukture het

geen verband getoon met betrekking tot verspeiding, komposisie of morfologiese patrone nie.

Verskeie van die geïdentifiseerde nano strukture kan geklassifiseer word as moontlike PGE-klusters. Ons spekuleer dat die ligand klusters vorm as gevolg van die isochemiese eienskappe van die PGE. Die klusters vorm voor die ontmenging van sulfiedsmelt van die magma af, en dus voor formele chemiese binding geskied.

Die volgende gevolgtrekkings kan gemaak word 1) die vorming van klusters was nie afhanklik van die aanvanklike konsentrasie van PGE nie, maar van die beskikbaarheid van ligande of anione, soos As, Cu en Fe. Nano strukture het steeds gevorm ongeag of die smelt PGE versadig was. 2) Kluster formasie was nie 'n funksie van temperatuur nie. Nano strukture is gemeet in stelsels wat vinnig en stadig afgekoel is. Alhoewel van die nano strukture verdwyn het in die afkoelings proses, het van die strukture behoue gebly. Die invloed op nano struktuur formasie as gevolg van omgewings veranderinge moet nog gekwantifiseer word. 3) Vanuit die verskeidenheid nano entiteite blyk dit dat daar verskeie oorgangs fases en prosesse, op 'n nano vlak plaasvind, wat nog onopgeteken is, in magmatiese stelsels.

As die intepretasie korrek is, is dit moontlik dat die PGE, gedurende die vroeë stadiums van magmatiese differensiasie, verryk kan word in PGE deur 'n fisiese proses. Klusters is net een van verskeie prosesse, in Bosveld kompleks tipe afsettings, wat bydrae tot die verryking van PGE.

Appendix I

1. platinum-group element (PGE)
2. cluster
3. nano structure
4. 10-100nm
5. mono-sulphide solid solution system (mss)
6. experimental petrology
7. primary physico-chemical enrichment process
8. thermodynamic constraints
9. ore enrichment process
10. Bushveld complex (BIC)